Functions of Histone Deacetylase 8 in Schwann cells during peripheral nervous system regeneration

Dissertation zur Erlangung des Grades Doktor der Naturwissenschaften

am Fachbereich Biologie der Johannes-Gutenberg-Universität Mainz

von
Nadège HERTZOG
geboren am 23.12.1994 in Porrentruy, Schweiz

Mainz, August 2024

Dekan:	Prof. Dr. Eckhard Thines Institut für Molekulare Physiologie Fachbereich Biologie
1. Bereichterstatter:	Prof. Dr. Claire Jacob Institut für Entwicklungs und Neurobiologie Fachbereich Biologie
2. Bereichterstatter:	Prof. Dr. Martin Heine Institut für Entwicklungs und Neurobiologie Fachbereich Biologie

Tag der mündlichen Prüfung: 16. Oktober 2024

Table of Contents

Zusammenfassung

Im Gegensatz zum Zentralnervensystem verfügt das periphere Nervensystem (PNS) über eine erstaunliche Regenerationsfähigkeit nach einer Schädigung. Schwann-Zellen (SZ), die myelinisierenden Gliazellen des PNS, sind hochgradig plastisch und reagieren auf Verletzungen, indem sie demyelinisieren und sich in Reparaturzellen umwandeln, die das axonale Nachwachsen fördern, Axone zu ihrem früheren Ziel zurückführen und dann die regenerierten Axone remyelinisieren. Die Umwandlung in Reparatur-SZ wird weitgehend durch den Transkriptionsfaktor c-Jun gesteuert. Die Mechanismen, die eine Hochregulierung von c-Jun nach einer Verletzung bewirken, sind jedoch nur teilweise bekannt.

In unserer Studie zeigen wir, dass die Ablation von Histondeacetylase 8 (HDAC8) in adulten SCs die c-Jun-Phosphorylierung und -Hochregulierung früh nach der Läsion erhöht und das Nachwachsen der sensorischen Axone sowie die Erholung der sensorischen Funktion beschleunigt. Nach der Läsion entsteht durch die Unterbrechung der Sauerstoffzufuhr ein hypoxisches Milieu, das bekanntermaßen die c-Jun-Phosphorylierung und -Expression hochreguliert und durch die Hochregulierung des Hypoxie-induzierbaren Faktors 1α (HIF1α) gekennzeichnet ist. Außerdem fanden wir heraus, dass HDAC8 die E3-Ubiquitin-Ligase TRAF7 stabilisiert, die HIF1α destabilisiert, was zu einer verzögerten Umwandlung in Reparatur-SZ führt. Unsere Studie unterstreicht die Funktion von HIF1α in SZ nach Verletzungen und zeigt, dass die Herunterregulierung von HDAC8 die Plastizität der SZ verbessert und die Regeneration der sensorischen Axone und die funktionelle Erholung durch die Stabilisierung von HIF1α fördert. Interessanterweise haben wir festgestellt, dass die Ablation von HDAC8 das Nachwachsen sensorischer Axone und die Wiederherstellung der sensorischen

Funktion fördert und dass HDAC8 nur in SZ nachgewiesen werden kann, die sensorischen Axone ummanteln. Dies deutet darauf hin, dass ein spezifischer Subtyp von SCs, die nur sensorische Axone ummanteln, mit HDAC8 als Marker identifiziert werden kann und dass die Umwandlung von SCs in Reparatur-SZ durch unterschiedliche Mechanismen in motorischen und sensorischen SZ gesteuert wird.

Summary

In contrast to the central nervous system, the peripheral nervous system (PNS) has an amazing regenerative capacity after lesion. Indeed, Schwann cells (SCs), the PNS myelinating glial cells, are highly plastic and react to injury by demyelinating and converting into repair cells that foster axonal regrowth, guide axons back to their former target, and then remyelinate the regenerated axons. The conversion into repair SCs is largely controlled by the transcription factor c-Jun. However, the mechanisms that induce c-Jun upregulation after injury are partially understood.

In our study, we show that ablating histone deacetylase 8 (HDAC8) in adult SCs enhances c-Jun phosphorylation and upregulation early after lesion and accelerates the regrowth of sensory axons and sensory function recovery. After lesion, the interruption of oxygen supply creates a hypoxic environment, which is known to upregulate c-Jun phosphorylation and expression and is characterized by hypoxia-inducible-factor 1α (HIF1α) upregulation. Additionally, we found that HDAC8 stabilizes the E3 ubiquitin ligase TRAF7, which destabilizes HIF1α, resulting in a delayed conversion into repair SCs. Our study emphasizes the function of HIF1α in SCs after injury and demonstrates that downregulating HDAC8 improves SC plasticity and promotes sensory axons regeneration and functional recovery by stabilizing HIF1α.

Interestingly, we found that HDAC8 ablation specifically promotes the regrowth of sensory axons and sensory function recovery and that HDAC8 is detected only in SCs ensheating sensory axons. This indicates that a specific subtype of SCs ensheating only sensory axons can be identified using HDAC8 as a marker and that the conversion of SCs into repair SCs is controlled by different mechanisms in motor and sensory SCs.

1 INTRODUCTION

1.1 Overview of the nervous system and the myelinating glial cells

The nervous system can be divided into two parts. The central nervous system (CNS) and the peripheral nervous system (PNS). The CNS is composed by the brain, the spinal cord, and the optic nerves (**Fig. 1a**). It acts as the master regulator of our body functions and integrates all the sensory afferences, processes them and elicits an accurate motor response. The PNS is divided into sensory, motor, and autonomic domains. The sensory nervous system allows the collection of environmental cues like touch, pain, temperature, or positional information from the skin, muscles, and viscera to transmit them to the CNS. Sensory neurons are pseudo-unipolar and organized into dorsal root ganglia (DRG), located along the spinal cord. DRG neurons project to their peripheral targets as well as to the CNS. The motor nervous system is composed of the projections of the spinal motoneurons, which innervate striated skeletal muscles via neuromuscular junctions. Each spinal nerve results of the fusion of the ventral root of the spinal cord, which contains the spinal motor neurons, and the dorsal root of the spinal cord, which contains the DRG sensory neurons. The sensory and motor spinal nerves constitute the somatic PNS, which is under voluntary control (Catala and Kubis, 2021) (**Fig. 1b**). Lastly, the autonomic nervous system comprises the sympathetic, parasympathetic, and enteric portions ensuring proper functions and homeostasis of the internal organs, blood vessels, and glands. The autonomic part of the PNS functions beyond voluntary control. The sympathetic and parasympathetic nervous systems contain afferent and efferent fibers that provide sensory and motor inputs to the CNS. While its afferent fibers travel directly along cranial and somatic PNS

fibers, the efferent fibers innervate their targets in a two-neuron way. Indeed, a preganglionic neuron arising from the lateral horn of the spinal cord forms a synapse with a postganglionic neuron in autonomic ganglia. The sympathetic neurons have cell bodies located in the lateral horns of the spinal cord and the presynaptic fibers exit the spinal cord between T1 and L2 spinal nerve roots, whereas the presynaptic fibers of the parasympathetic fibers exit the CNS as well as through the S2-4 nerve roots (Murtazina and Adameyko, 2023; Waxenbaum, Reddy and Varacallo, 2023) (Fig.1c).

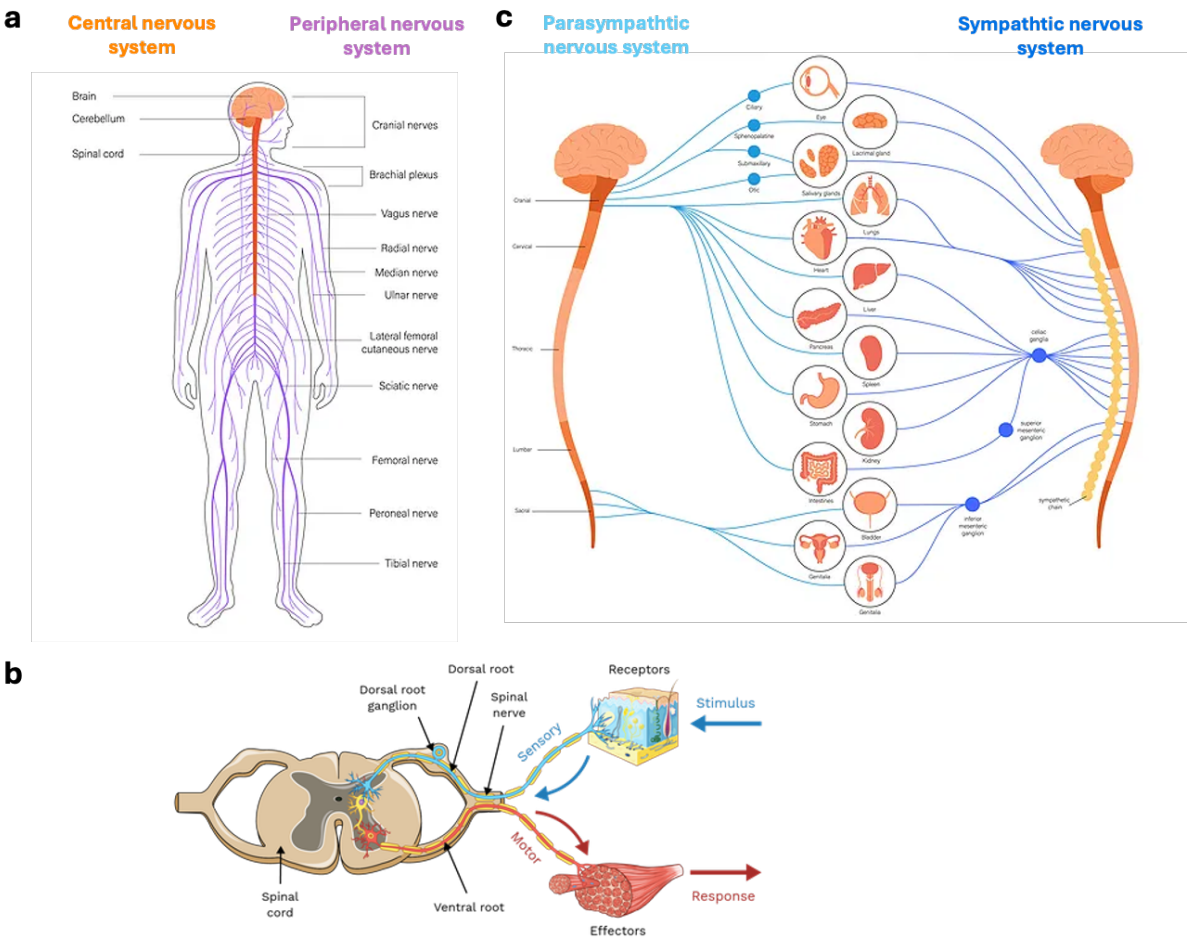

Figure 1. Overview of the nervous system. (a) Components of the central and peripheral nervous systems. (b) Afferent (sensory) and efferent (motor) nerve fibers of the spinal cord. Each sensory neuron has two projections: one projection with a sensory receptor in skin, muscle, or sensory organs and a second one that synapses with a neuron in the dorsal horn of the spinal cord. The cell bodies of motor neurons are located in the ventral grey matter of the spinal cord and project to muscle through the ventral root. Motor neurons can either be directly stimulated by a sensory neuron or indirectly by an interneuron in between. (c) Overview of the autonomic nervous system anatomy. Activation of the sympathetic nervous system promotes the "fight and flight" response, whereas the activation of the parasympathetic nervous system promotes the "rest and digest" processes. (*The pictures have been downloaded from https://macconcussion.com/dysautonomia-autonomic-nervous-system-ans-dysfunction-and-concussions/ for Fig. 1 (a) and (c) and from https://courses.lumenlearning.com/wm-biology2/chapter/sensory-somatic-nervous-system) for (b))*

During embryonic development, the nervous system develops from the central part of the ectoderm, called neuroectoderm, while the lateral regions of the ectoderm will give rise to the epidermis. In a process known as neurulation, the neuroectoderm folds to generate the neural tube, which is the primitive form of the CNS (**Fig. 2a**). On its side, the PNS will be generated by a population of cells, called neural crest cells, which arise from the dorsal part of the neural tube and migrate into the surrounding tissues. Neural crest cells give rise to different types of cells depending on the direction of their migration (Gammill and Bronner-Fraser, 2003). The neural crest cells that will form the PNS migrate first through the dorsal roots to form the DRG, peripheral nerves and the autonomic nervous system. Sensory neurons are the first to be specified, followed by Schwann cell precursors, satellite glial cells, and boundary cap cells. Satellite glial cells remain in the DRG and are tightly associated with neuron cell bodies, whereas Schwann cells precursors will migrate through the DRG to reach the peripheral nerve to myelinate peripheral axons (Jacob, 2015; Jessen and Mirsky, 2019). During a second wave of gliogenesis, boundary cap cells generate all the Schwann cells precursors located in the dorsal roots, a fraction of Schwann cell precursors in the ventral root as well as some satellite glial cells. In the embryo, boundary cap cells have a barrier function and prevent oligodendrocytes (OLs) and motor neurons migration into the PNS (Jacob, 2015) (**Fig. 2b**).

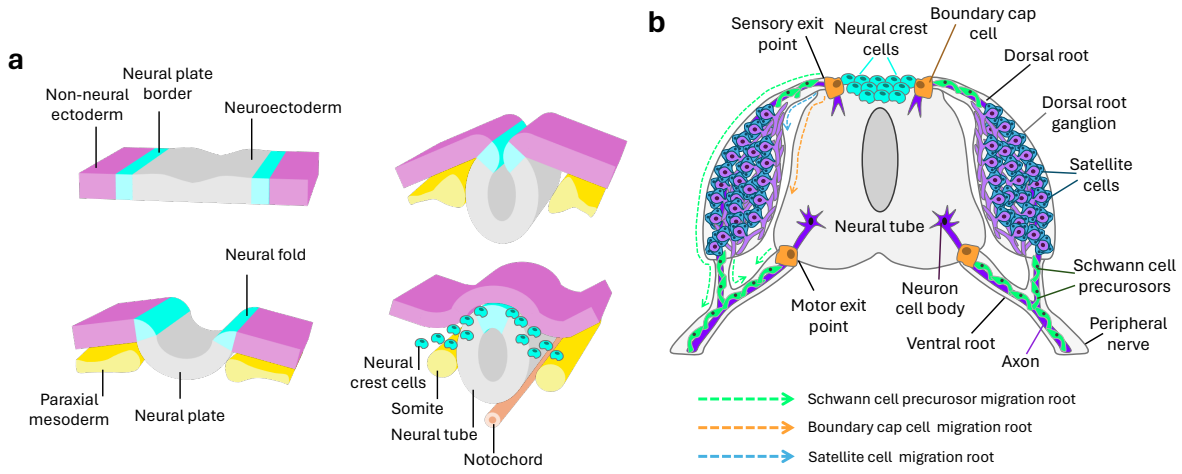

Figure 2. Embryonic development of Schwann cells. (a) Neurulation. During neurulation, the neural plat borders elevate, causing the neural plate to roll into the neural tube, which is the primitive form of the CNS. The PNS will be generated by neural crest cells, which delaminate from the neural folds of the dorsal neural tube. **(b) Localization and migration routes of peripheral glia**. Neural crest cells from the dorsal neural tube migrate through the dorsal roots, dorsal root ganglia and peripheral nerves to generate sensory neurons, Schwann cell precursors and satellite glial cells. Later, boundary cap cells located at the sensory and motor exit points generate all the Schwann cells precursors located in the dorsal roots, a fraction of Schwann cell precursors in the ventral root as well as some satellite glial cells. In the embryo, boundary cap cells have a barrier function and prevent oligodendrocyte and motor neuron migration into the PNS. (*Modified from Gammill and Bronner-Fraser, 2003; Jacob, 2015*).

The nervous system is not only composed of neurons but consists of an immense network of neurons and glial cells, whose interactions are crucial to ensure the proper transmission of information, nervous system integrity, development, and regeneration. Indeed, the ease with which we can perform our professional and everyday life tasks is disconcerting. We become conscious about it after our spinal cord or brain has been lesioned or over the time course of a demyelinating disease for example. This ease is the consequence of the high speed of nerve impulse conduction provided by what is called the myelin sheath. The myelin sheath is an extended and modified plasma membrane derived from glial cells that spirals around the nerve axon. It insulates the axons in such a way that action potential conduction is much more rapid than it would be without myelin. This type of axonal conduction is called saltatory nerve conduction. The myelin

sheath is also required to protect axon integrity (Brosius Lutz and Barres, 2014; Rasband and Macklin, 2012). Two different types of myelinating glial cells are described: the oligodendrocytes (OLs) in the CNS and the Schwann cells (SCs) in the PNS. Although they function in a similar way, they differ in certain points. Indeed, OLs derive from the neuroepithelium and wrap several axons thank to their extended processes, whereas neural-crest derived SCs are evenly spaced along the axon and spiral around one segment of a single axon (Brosius Lutz and Barres, 2014; Salzer, 2015) (**Fig. 3a-c**). OLs and SCs also differ in their regenerative capacities as SCs promote axonal regrowth and remyelination after nerve injury, whereas OLs do not provide any support for CNS axon repair. Indeed, the most sticking feature of SCs is the conservation of their embryonic plasticity in adult nerves. SCs can adopt a repair phenotype upon nerve injury and thus can assist PNS axon regrowth and remyelinate them. In contrast, the differentiation state of OLs is fixed and OLs do not acquire regeneration-supportive features and thus do not sustain CNS axon regrowth and cannot efficiently promote remyelination (Arthur-Farray et al., 2012; Brosius Lutz and Barres, 2014). This makes SCs a very interesting cell type to study as the understanding of SC molecular pathways sustaining PNS regeneration may be applied to OLs to improve CNS axon regeneration and remyelination (Duman et al., 2020; Nocera et al., 2023; Vaquié et al., 2018).

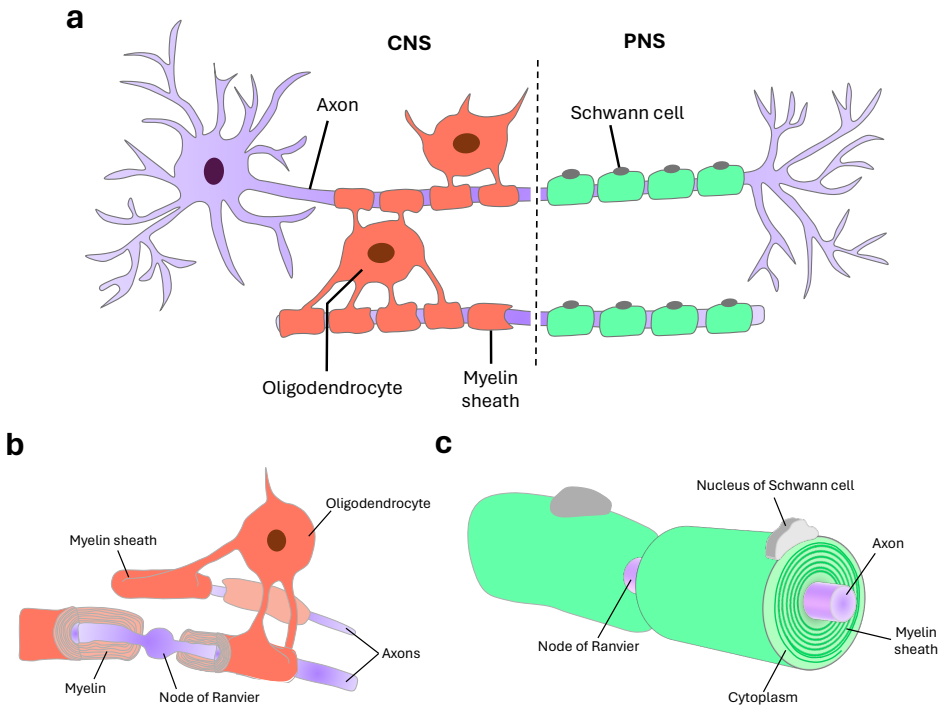

Figure 3. Comparison between central and peripheral myelination. (a) In the central nervous system, each oligodendrocyte can extend several cytoplasmic processes to form myelin around different axons. In the peripheral nervous system, each Schwann cell wraps numerous times around a single axon. **(b)** Depicted is one oligodendrocyte between two axons. **(c)** Compared to central axons, peripheral axons possess a thicker myelin sheath. (*Modified from Chen et al., 2021*).

1.2 Chromatin remodeling enzymes

In eukaryotic cells, DNA is wrapped around histone proteins which protect and organize the packed DNA in a dynamic structure called chromatin. The building units of chromatin are the nucleosomes. Each nucleosome consists of an octamer of four core histones (one H3/H4 tetramer and two H2A/H2B dimers) surrounded by 146 bp of DNA (Strahl and Allis, 2000). Transcriptional regulation is influenced by the level of chromatin compaction, which depends on covalent modifications of DNA and on post-translational modifications of histone tails. These modifications constitute the epigenetic code, which can adapt and respond to changes throughout the life of an organism. There are currently four main types of cytosine residue modifications in the DNA namely methylation,

hydroxy-methylation, formylation, and carboxylation. The factors responsible of DNA and histone modifications can be grouped into three classes: the writers, the erasers, and the readers. The writers encompass enzymes that add a chemical group to a nucleotide base or to specific amino acid residues on histone tails. The epigenetic marks laid down by the writers are not permanent and their removal is catalyzed by a group of enzymes called erasers, which relieve the effects of epigenetic marks on gene expression (Biswas and Rao, 2018). The two most studied epigenetic modifications are methylation and acetylation. Whereas both DNA and histones are subjected to methylation, only histones can be acetylated. Other histone modifications include phosphorylation, ubiquitination, sumoylation, ADP ribosylation, biotinylation, citrullination, to cite only few (Andrews, Strahl, and Kutateladze, 2016). On their side, the readers possess specialized domains which bind to and recognize specific epigenetic marks. The presence of readers is essential to mediate the effects of the epigenetic marks laid down by the writers. Among the numerous identified histone readers, we can mention the bromodomain proteins, which recognize and bind acetylated histones and the chromobarrel and chromodomain proteins which bind to lysine-methylated histones (Biswas and Rao, 2018).

Histone acetylation and deacetylation play a key role in regulating chromatin structure (de Ruijter et al., 2003). Histone acetyltransferases (HATs) add acetyl groups to lysine residues of histones, leading to chromatin decompaction and transcriptional activation. Conversely, histone deacetylases (HDACs) remove acetyl groups from histones, which results in chromatin condensation that limits DNA access for the transcriptional machinery. (de Ruijter et al., 2003; Duman and Martinez-Moreno, 2020; Hodawadekar and Marmorstein, 2007). In general,

HATs are known as transcriptional co-activators, whereas HDACs are rather considered as transcriptional co-repressors.

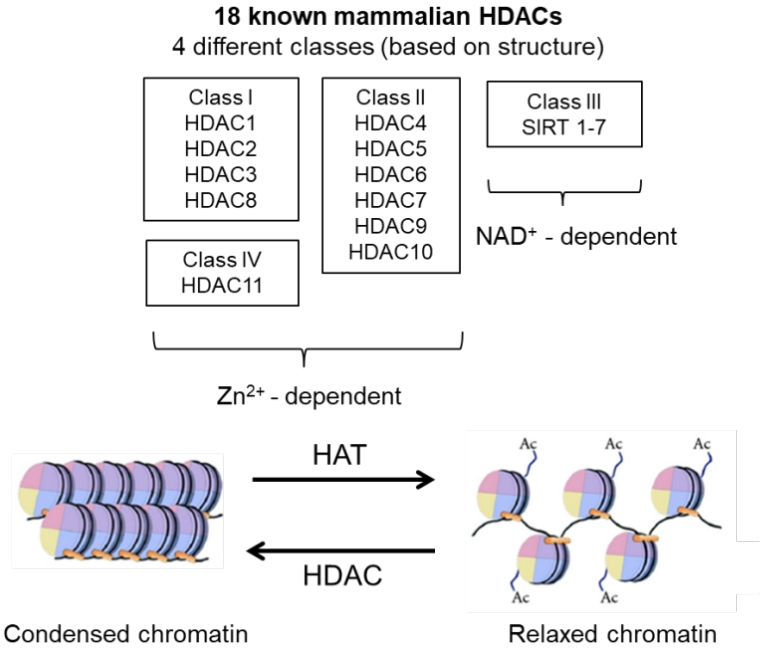

Figure 4. Histone acetyltransferases and histone deacetylases. HATs add acetyl groups to histones to relax chromatin and facilitate transcriptional initiation and elongation. Conversely, HDACs remove acetyl group to condense chromatin and prevent access for the transcriptional machinery. The four HDAC classes and their cofactors are depicted in the upper part of the figure. HAT, histone acetyltransferase. HDAC, histone deacetylase; HDAC1, histone deacetylase 1; HDAC2, histone deacetylase 2; HDAC3, histone deacetylase 3; HDAC4, histone deacetylase 4; HDAC5, histone deacetylase 5; HDAC6, histone deacetylase 6; HDAC7, histone deacetylase 7; HDAC8, histone deacetylase 8; HDAC9, histone deacetylase 9; HDAC10, histone deacetylase 10; HDAC11, histone deacetylase 11; NAD, nicotinamide adenine dinucleotide; SIRT, Sirtuin. *(Modified from de Ruijter et al., 2003; Rodd et al., 2012*).

However, HDACs also participate in transcriptional activation (Greer et al., 2015; Wang et al., 2009). Indeed, HDACs are required for efficient elongation of RNA polymerase II by facilitating the recruitment of elongation factors on acetylated promoters and enhancers (Greer et al., 2015). Furthermore, HDACs prevent histone hyperacetylation at active genes to avoid uncontrolled initiation of transcription and remove acetyl groups on inactive genes to prevent Pol II binding (Wang et al., 2009). HATs and HDACs do not bind DNA directly and thus

need a DNA-binding partner to modify histones. In addition, HATs and HDACs can acetylate and deacetylate non-histone proteins such as transcription factors and thus control the activity of the latter (Glozak et al., 2005; Jacob, 2017; Spange et al., 2009).

HATs are categorized into five different families depending on the functional and structural resemblance of their catalytic domain: Gcn5-related acetyltransferases (GNATs), the MYST (MOZ, Ybf2/Sas3, Sas2 and Tip-60)-related KATs, the p300/CBP HATs, the general transcription factor HATs, and the steroid/nuclear receptor co-activators (SRC/NCoA) HATs (Biswas and Rao, 2018).

The 18 known members of the HDAC family are subdivided into four different classes, based on their structure: class I, II and IV HDACs are Zn^{2+}-dependent and constitute the classical HDACs, whereas the class III is composed of the sirtuins and requires NAD^{+} to be active (de Ruijter et al., 2003) (**Fig. 4**).

Histone methyltransferases (HMTs) are classified into three families: the SET-domain-containing proteins and DOT1-like proteins, which methylate lysine (K) residues, and the protein arginine N-methyltransferases, which methylate arginine (R) residues. HMTs catalyse the transfer of up to three methyl groups on lysine residues, resulting in mono- (me1), di- (me2) and tri-methylated (me3) residues. These modifications lead to transcriptional activation or repression based on the location of the amino acid residues. In the case of arginine methyltransferases, the outcome also depends on the position of the methyl group on the target arginine residue. The active histone methylation marks are H3K4 H3K36, H3K79, H3R17, H3R26, H3R42, whereas methylation of H3K9 H3K27, and H4K20 are considered as repressive histone marks (Biswas and Rao, 2018; Duman et Martinez-Moreno, 2020, Pattaroni and Jacob, 2013).

Demethylation of lysine residues is carried out by two families of histone demethylases (HDMs): the amine oxidase and the Jumonji C (JmjC) domain-containing proteins. While the members of HDM families have been showed to remove methyl groups from lysine residues, very little is known about the removal of methyl groups from arginine residues. However, JMJD6 has recently been shown to catalyze the demethylation of arginine residues (Kwok et al., 2017).

The functions of chromatin remodeling enzymes in the context of SC development and PNS regeneration will be described in the different sections of this introduction.

1.3 Schwann cells: Origin and Development

Neural crest cells give rise to the PNS glia. This group of cells comprise non-myelinating and myelinating SCs, satellite glial cells in the ganglia, terminal SCs at the neuromuscular junction and enteric glial cells (Jessen and Mirsky, 2019).

In rodents, the development into mature SCs occurs through three major steps. The first one is the generation of highly proliferative SC precursors (SCPs) from neural crest cells, which can be observed in embryonic nerves at embryonic day (E) 12-13 in the mouse (E14-E15 in the rat). The second one is the transition from SCPs to immature SCs (iSCs) which are present in mouse nerves from E15-E16 (E17-E18 in the rat) until the perinatal period (Jessen and Mirsky, 2019). Finally, during a process called radial sorting, iSCs wrap numerous times around one big caliber axon in a 1:1 relationship and differentiate into pro-myelinating and further into myelinating SCs (Feltri et al., 2016; Jessen and Mirsky, 2019). Small caliber axons will associate with iSCs, which differentiate into Remak cells. The axons associated with Remak SCs (rSCs) are called Remak bundles (Jessen and

Mirsky, 2005a, Monk et al., 2015). Axons surrounded by Remark cells are not myelinated. In addition, some sensory postganglionic fibers of the autonomous nervous system are also surrounded by a single layer of SC cytoplasm and are not myelinated, whereas motor, preganglionic and big caliber sensory neurons are myelinated by SCs (Murtazina and Adameykto, 2023). An overview of SC developmental steps with their associated molecular markers is given in Figure 5.

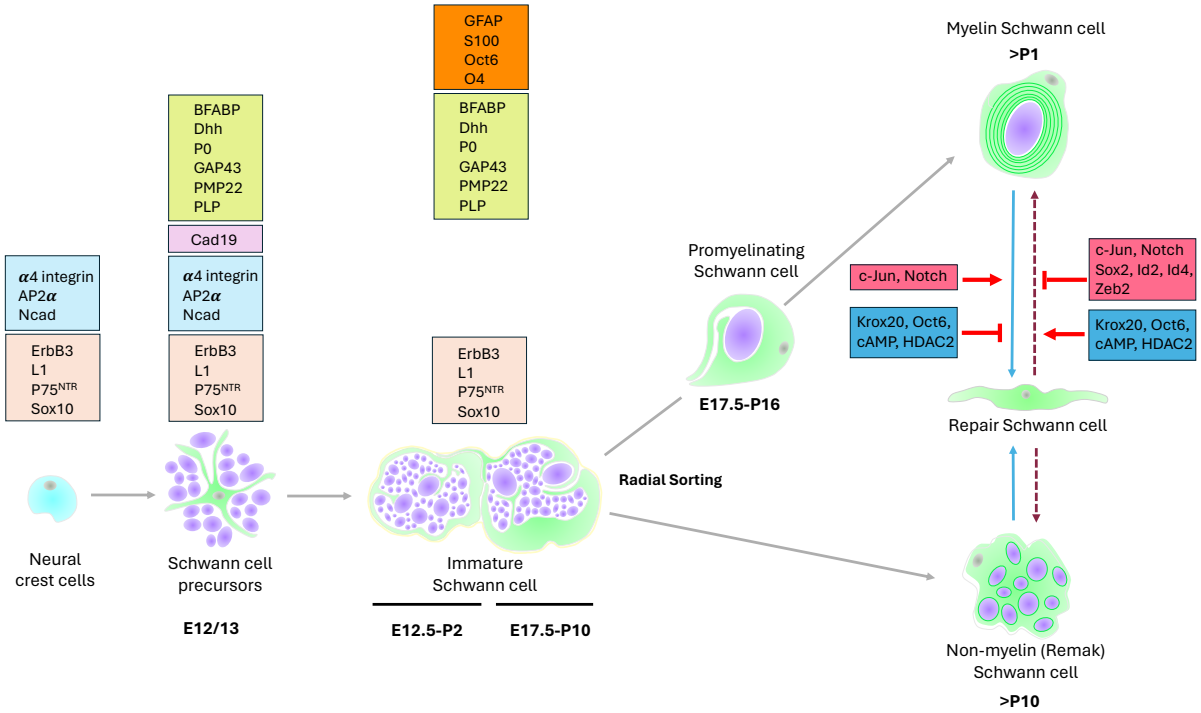

Figure 5. Overview of SC development and response to injury. Diagram of developmental and injury-induced transition of SCs. The molecular markers of each SC developmental stages are listed in the coloured boxes above the lineage drawing. Shared molecular profiles have the same color code. The positive and negative regulators of SC transition into repair SCs as well as in SC redifferentiation/remyelination are listed in the coloured boxes on the left and on the right of the double vertical arrows. Grey uninterrupted arrows indicate normal developmental stages, blue uninterrupted arrows indicate SC conversion into repair SCs, and red dotted arrows indicate repair SC redifferentiation into mature, myelinating or non-myelinating SCs. Embryonic day (E) and postnatal day (P) refer to mouse development**;** AP2-α, activator protein 2; BFABP, brain fatty acid-binding protein; cAMP, cyclic adenosine monophosphate; DHH, desert hedgehog; ErbB3, neuregulin receptor; GAP43, growth associated protein 43; Krox20, early growth response 2; L1, L1 adhesion molecule; N-cad, N-cadherin; Oct6, octamer-binding transcription factor 6; O4, lipid antigen; PLP, proteolipid protein; PMP22, peripheral myelin protein, 22-kDa22; P0, protein zero; $p75^{NTR}$, p75 neurotrophin

receptor; Sox2, SRY (sex determining region Y) box 2 Sox10, SRY box 10; Zeb2, Zinc finger E-box-binding homeobox 2. (*Modied from Jessen and Arthrur-Farraj, 2019; Jessen and Mirsky, 2005)*.

SC development is driven by the interplay of extracellular signals and intrinsic factors, that are tightly integrated by transcription factors and chromatin remodeling enzymes. Indeed, besides transcription factors, the epigenetic landscape plays a crucial role in governing the accessibility of the transcriptional machinery to specific DNA sequences. The central component of the transcriptional regulatory network controlling SC development is the HMG-domain transcription factor Sox10, whose expression extends from neural crest cells to mature SCs and is necessary for SC specification, terminal differentiation, myelin maintenance and SC homeostasis by cooperating with stage-specific transcriptional regulators (Fröb and Wegner, 2020; Sock and Wegner, 2019). The stage-specific cellular, transcriptional, and epigenetic mechanisms of SC development will be described in the following sections.

It is important to note that axons and SCs constantly interact and form a symbiotic relationship, which is required for normal development, maintenance, and function of the PNS. On one side, axonal signalling controls SCP survival and differentiation, iSC differentiation into myelin or Remak SCs as well as myelin sheath formation and maintenance (Jessen and Arthur-Farraj, 2019). On the other side, SCs determine axon diameter during PNS development and regulate the localization of ions channels along the axons (Fledrich et al., 2019). Furthermore, in the last years a strong and complex metabolic support of axons by SCs has been highlighted, independently of myelination itself (Bouçanova and Chrast; 2020).

1.3.1 Schwann cell precursors

Once neural crest cells have reached the mesenchyme, they undergo an important remodeling of their gene expression pattern and start to express SC-associated genes such as *P0*, *Pmp22, Plp* or *desert hedgehog* (*Dhh*), leading to the generation of SCPs. SCPs are proliferative cells which migrate along and are closely associated with the axons in the developing PNS nerves. Indeed, SCP survival, proliferation and migration rely on axonal signaling molecules. Among those, the axonal surface molecule neuregulin 1 (NRG1) type III and its receptor tyrosine kinase on SCs ErbB2/3 are of particular importance, as NRG1, ErbB2 or ErbB3 ablation in axons or SCs respectively, leads to depletion or absence of SCPs (Birchmeier and Nave, 2008; Birchmeier, 2009; Monk et al., 2015; Taveggia et al., 2010). By inducing ErbB3 expression on SCs, the transcription factor Sox10 renders SCs dependent on the presence of axonal NRG1 type III (Britsch et al., 2001; Sock and Wegner, 2019). Besides NRG1, developing axons also express Notch ligands which bind to Notch on SCPs. This results in the amplification of NRG1 signaling by increasing ErbB2 levels on SCPs and thus indirectly participates to the regulation of SCP survival. Interestingly, axon survival also relies on SCPs and iSCs, as a lack of PNS glial cells leads to motor and DRG neuron loss in later embryonic development. It thus appears that neuron and SCP survival seem to mutually depend on each other (Jessen and Mirsky, 2019; Woldeyesus et al., 1999).

So far, the molecular pathways that govern neural crest cell differentiation into SCPs have not been totally elucidated. However, histone deacetylase 1 and 2 (HDAC1/2) have been shown to be necessary for neural crest cell specification into SCPs (Jacob et al., 2014). This study shows that the transcription factor

Sox10 interacts with HDAC1/2 to induce Pax3 expression in the neural crest cells. Pax3 then synergizes with Sox10 to maintain high levels of Sox10. Subsequently, Sox10 indirectly activates the *Fabp7* promoter and interacts with HDAC1/2 to activate the *P0* promoter in neural crest cells. The activation of the two key lineage genes of peripheral glia, *Fabp7* and *P0*, is necessary for lineage progression. Sox10 is the only cell type-restricted transcription factor and is expressed at all stages of SC development. It is therefore of utmost importance for SC specification, myelination, and maintenance. Indeed, neural crest cells lacking Sox10 can generate DRG neurons but fail to generate the glial components (Britsch et al., 2001; Sonnenberg-Riethmacher et al., 2001; Wahlbuhl et al., 2012). At each SC developmental stage, Sox10 plays a specific role and requires physical interaction with stage-specific transcription factors or chromatin remodeling enzymes, posttranslational modifications, and change in cellular localization (Jacob, 2017; Sock and Wegner, 2019).

SCPs are intimately associated with large bundles of axons and surround them with their extended membranous processes. At this stage, the embryonic nerve is only composed of SCPs and axons and do not yet contain any connective tissue or blood vessels (**Fig. 6a**). Interestingly, SCPs are multipotent cells and are known to give rise not only to iSCs but also to mesenchymal cells giving rise to odontoblasts and tooth pulp cells, melanocytes, fibroblasts, enteric and parasympathetic ganglion neurons (Dyachuck et al., 2014; Espinosa-Medina et al., 2017; Uesaka et al., 2015). During their transition to iSCs, SCPs also generate fibroblasts that will remain within the nerve and secrete collagen that will progressively fill the extracellular space called endoneurial connective tissue. The latter will become vascularized upon iSC generation. Indeed, PNS nerves contain a non-negligeable amount of connective tissue and lineage tracing of

embryonic fibroblasts showed that these cells are linked cells expressing Dhh, a marker of SCPs (Jeagle et al., 2003; Joseph et al., 2004; Parmentier et al., 1999; Sharghi-Namini et al., 2006). In contrast to the CNS, which is protected by hard layers of connective tissue, the protective layers of peripheral nerves are softer and consist of the extracellular matrix (ECM) of the endoneurial tissue surrounding individual axon-SC units, of a cellular layer surrounding the different nerve branches called perineurium and, finally, of a collagenous layer called epineurium (Jessen and Mirsky, 2015).

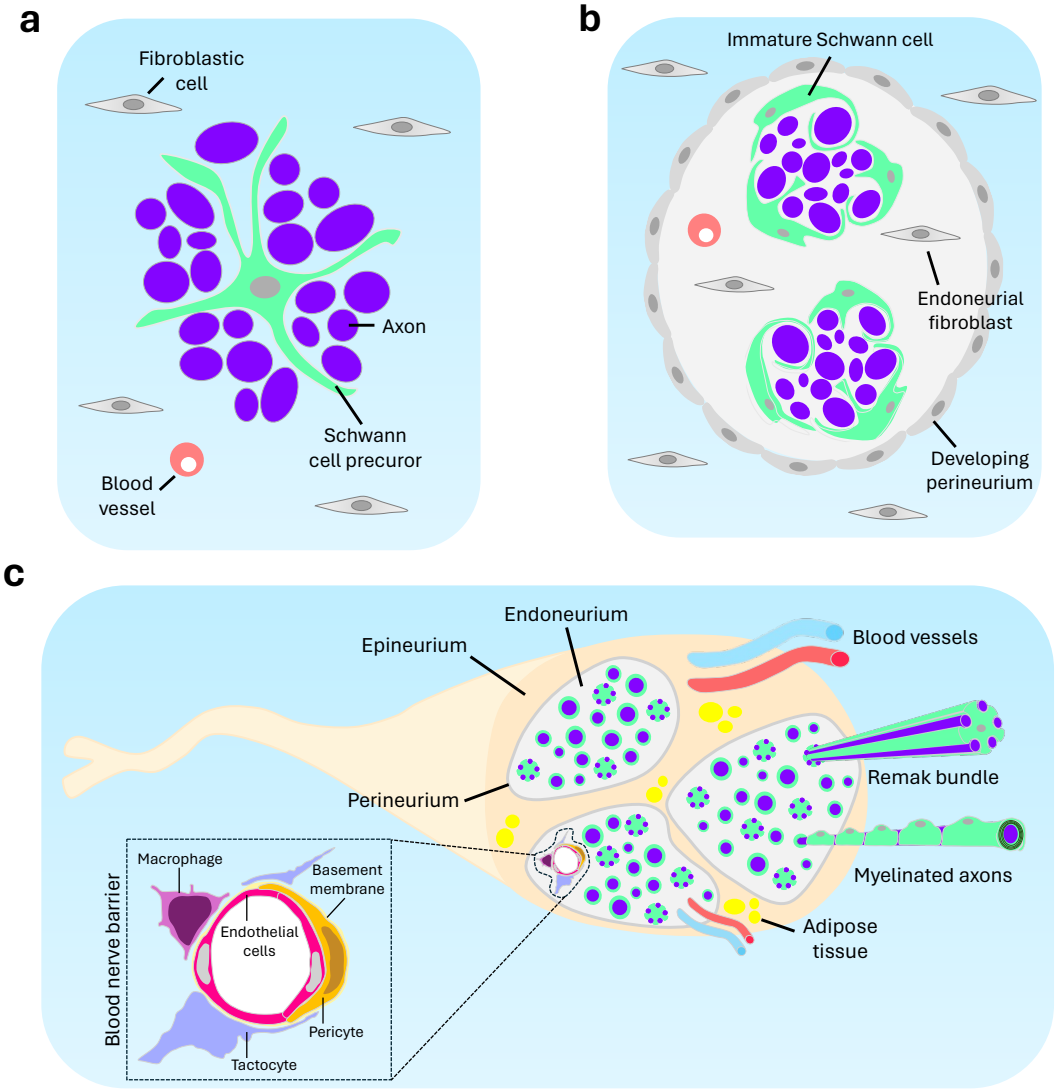

Figure 6. Structure and development of peripheral nerves. **(a) E14-E15 nerve**. At this stage, early nerves contain only SCPs associated with axons. **(b) E18-E19 nerve**. The developing perineurium defines the endoneurial space with several axon-SC families. The embryonic nerves now contain blood vessels, endoneurial fibroblasts and an extracellular matrix. **(c) Adult peripheral nerve**. Adult peripheral nerves are composed of several fascicules, each containing myelinated and non-myelinated axons**.** The endoneurium, perineurium and epineurium constitute the three protective layers of peripheral nerves. The blood-nerve barrier (BNB) consists of the perineurium and the endoneurial blood vessels. At the level of the endoneurial blood vessels (square inset), the BNB is defined by endothelial cells (ECs) tightly associated with pericytes, tactocytes, and macrophages. (*Adapted from Bosch-Queralt et al., 2022; Jessen and Mirsky, 2016; Malong et al.,2023*).

In addition of promoting axonal survival, SCPs also play a role in nerve fasciculation and formation of neuromuscular junctions. It has been shown that in nerves lacking PNS glia, axons can grow and migrate at early embryonic stages but are defasciculated distally and show an abnormal branching and inaccurate

localization of synaptic sites (Birchmeier, 2009; Lin et al., 2000; Morris et al., 1999; Woldeyesus et al., 1999; Wolpowitz et al., 2000).

1.3.2 Immature Schwann cells

The presence of iSCs extends until the perinatal period. iSCs serve as a pool to generate either myelinating or Remak cells. Therefore, their developmental potential is narrower than for SCPs. SCP lineage progression into iSCs is directly controlled by NRG1, yet several other positive or negative factors have been described. Among them, Notch signaling is another positive regulator of SCP/iSC transition by acting positively on NRG1 signaling. Indeed, inactivation of Notch signaling in SCs *in vivo* delays iSC appearance, whereas iSCs appear prematurely in mice overexpressing Notch (Woodhoo et al., 2009). Among the negative regulators, we can cite Endothelin and AP2α, which delay iSC generation when overexpressed in cultured SCPs (Brennan et al., 2000; Stewart et al., 2001).

The expression of myelin inhibitors in iSCs is timely controlled by the transcription factor Zeb2, both in myelinating SCs and during remyelination. Zeb2 has been found to downregulate the expression of *Hey2* and *Hes1*, which are downstream effectors of Notch signalling pathway, endothelin receptor B (Ednrb), c-Jun, and Sox2 (Quintes et al., 2016, Wu et al., 2016). These factors are known to maintain SCs in a proliferative and progenitor stage, thus preventing precocious differentiation. Moreover, Zeb2 silences the expression of these genes by recruiting the HDAC1/2-NuRD complex on their promoters (Wu et al., 2016). Indeed, genetic ablation of Zeb2 in SCs results in persistent elevation of Hey2, Edrnb and Sox2 levels together with a low expression of the promyelinating factors Sox10, Oct6 and Krox20, and SCs of Zeb2-deficient mice are arrested at the immature stage. Consequently, animals show axonal sorting

failure, myelination defects and motor deficits. Moreover, HDAC1/2, together with HDAC3 and Schwann cell factor 1, from a transcriptional repressor complex by binding on *Cyclin E* promoter, thereby arresting cell proliferation (Chittka et al., 2004).

iSCs differ from SCPs in several points. In contrast to SCPs, iSCs bypass axonal signaling dependance and use their own autocrine survival circuits by secreting survival factors like FGF, IGF or PDGF for example. This autocrine supporting loop is thought to maintain SC survival after nerve injury, while the axonal dependence of SCPs matches the number of axons and SCPs (Jessen and Mirsky, 2005). Additionally, iSCs stop migrating and start upregulating S100 and GFAP, while downregulating the SCP marker Cadherin 19 (**Fig. 5**).

The transition between SCPs and iSCs is characterized by drastic changes in the structure of the embryonic nerves, which constitutes an important step in PNS nerve organogenesis. iSCs surround smaller bundles of axons and promote the differentiation of the surrounding mesenchymal cells. Indeed, by secreting Dhh, iSCs induce mesenchymal cells differentiation into perineurial cells, from which the perineurium and epineurium arise. The latter structures fail to develop properly in mice carrying an inactive form of Dhh thus leading to severe nerve pathology (Parmentier et al., 1999; Umehara et al., 2000). Upon VEGF secretion, iSCs trigger arterial differentiation of endothelial cells (Monk et al., 2015; Mukouyama et al., 2005; Parmentier et al., 1999). Additionally, by communicating with endoneurial fibroblasts, iSCs also promote the deposition of basal lamina (Joseph et al., 2004). At this stage, the embryonic nerve consists of axon-SC families with vascularized connective tissue and a basal lamina around iSCs (**Fig. 6b**).

Around birth, iSCs extend radial lamellipodia into the axon bundles and sort out individual large caliber axons, destined to be myelinated, from small caliber axons which remain nonmyelinated in Remak bundles. This process is known as radial sorting (Feltri et al., 2016).

1.3.3 Radial sorting

In the rodent PNS, the process of radial sorting starts perinatally and proceeds until postnatal day 10 (P10). It leads to the acquisition of a proper axon-SC one-to-one relationship according to axonal size, and it is a prerequisite for successful SC differentiation into myelinating SCs.

The radial sorting process can be divided into several steps. At the start, axons of mixed calibers are separated in bundles surrounded by a family unit of three to eight iSCs that deposit a common basal lamina. Then, iSCs segregate axon bundles even further by extending long cellular processes called lamellipodia into the bundle and progressively select and bring large caliber axons towards the periphery of the bundle. iSCs surrounding single large-caliber axons then divide to match axon-SCs number and defasciculate. The defasciculation requires the formation of a new basal lamina and allows SCs to form a 1:1 relationship with axons. At this stage, iSCs differentiate into pro-myelinating (ProMy) SCs, which will initiate the myelination of large-caliber axons. As more and more large-caliber axons are sorted, concomitantly to SC proliferation, axon bundles become progressively smaller and end up containing only small-caliber axons (**Fig. 7**). The latter will be surrounded by Remak SCs and develop into Remak bundles, without myelin production (Feltri et al., 2016; Monk et al.,

2015). Radial sorting is determinant for the correct architecture and function of adult nerves, which will consist of 50% myelinating SCs in a 1:1 relationship with axons, 20% of Remak SCs associated with small-caliber axons, 8% of resident macrophages, 6% of endothelial cells (ECs), 1,5% of pericytes, and interestingly, 12.5% of a new population of cells in the endoneurium called tactocytes, which interact with the endothelial cells outside of their basal lamina and make multiple contacts along the length of endoneurial blood vessels, which consist mostly of small arterioles and capillaries. The endoneurium is protected by the blood-nerve barrier (BNB) at two levels: the perineurium and the endoneurial blood vessels. The BNB vascular unit around the endoneurial blood vessels is defined by ECs together with the closely associated pericytes inside the EC basal lamina as well as the associated tactocytes and macrophages located outside of the EC basal lamina. In contrast, epineurial blood vessels consist of larger blood vessels, mostly arterioles and venules, and do not have a barrier function (Malong et al., 2023; Stierli et al., 2018) (**Fig. 6c**).

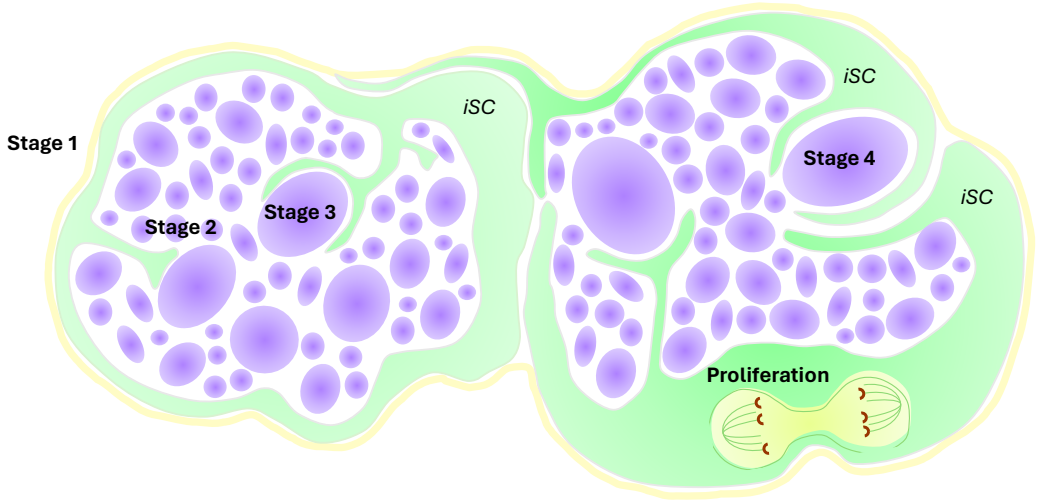

Figure 7. Schematic representation of the radial sorting process. At stage 1, axons of mixed calibers are grouped in bundles surrounded by iSCs, which produce the basal lamina (in yellow). At stage 2, iSCs extend lamellipodia into axonal bundles. During stage 3, large-caliber axons are sorted and segregated towards the periphery of the bundle. At stage 4, iSCs surrounding single large-caliber axons proliferate and separate from the bundle. (*Adapted from Feltri et al., 2016*).

Proper radial sorting requires a fine-tuned regulation of many different aspects. Among them, we can mention the regulation of ECM components deposition, SC cytoskeleton reorganization, SC-axon interactions, establishment of SC polarity between the basal lamina and axons, and cell cycle regulation (Feltri et al., 2016; Monk et al., 2015). Many molecules are required but the most important are components of the ECM and intracellular signaling pathways regulating cytoskeleton dynamics. Furthermore, the functions of transcriptional and epigenetics mechanisms have also been described. For example, deletion of the chromatin remodeling enzymes HDAC1/2 in mouse SCs delay radial sorting by affecting SC survival (Jacob et al., 2011).

An appropriate balance between proliferation and survival is crucial during radial sorting. Indeed, on one side, SCs need to generate enough daughter cells to segregate all large-caliber axons and on the other side, they need to exit the cell cycle to differentiate properly into myelinating or Remak SCs. *In vivo*, SC proliferation is triggered by axon-associated signals such as NRG1 and Notch, by

signals derived from the basal lamina such as laminin, the Rho GTPase cdc42 and focal adhesion kinase (FAK), by the components of the Hippo signaling pathway YAP and TAZ or by Gpr126 signaling pathway (Deng et al., 2017; Feltri et al. 2016; Monk et al., 2009, 2015; Poitelon et al., 2016). Among the molecules which promote cell cycle exit, we can cite the cyclin-dependent kinase inhibitor 1b, also called p27 (Li and al., 2011). Lastly, a balance between death and survival signals is also crucial to assure the control of iSC survival. Survival signals either come from axons (via NRG1) and from SC basal lamina (laminin). The only death signal which is acting in SC development is TGFβ. However, the function of TGFβ is contradictory since it has been shown to promote both SC proliferation and death. Currently, some studies suggest that TGFβ would promote the proliferation of SCs tightly associated with axons and trigger apoptosis in SCs with a less effective axon association (D'Antonio et al., 2006; Jessen and Mirsky, 2019).

1.3.4 Pro-myelinating Schwann cells

Once pro-myelinating SCs have sorted an axon segment, they begin the transition to wrapping and terminal differentiation. Terminal differentiation is characterized by SC basal lamina maturation, which drives the activation of Gpr126 and subsequent cAMP elevation. However, cAMP elevation always requires NRG1 signalling to insure proper terminal differentiation and vice versa. While the N-terminal fragment of Gpr126 is required for radial sorting, activation of the C-terminal fragment upon laminin binding results in cAMP accumulation, which is required for SC myelination. Both NRG1 signaling and cAMP elevation trigger Oct6 expression, a prerequisite for SCs to timely progress to the myelinating stage (Mogha et al., 2013; Monk et al., 2009, 2011). Oct6 is

expressed transiently in pro-myelinating SCs, with a peak at the transition to myelinating SCs, and decreases rapidly once myelination begins. Oct6 is the central target of Sox10 in the late iSCs, and its expression is induced by Sox10 binding on the *Oct6* SC-specific enhancer (SCE), together with Brg1-containing BAF chromatin remodeling complexes (Weider et al., 2012). Of note, Sox10 expression is further sustained by the recruitment of either Sox10 itself or NFkB, both in complex with HDAC1/2 and BRG1, on Sox10 promoter (Chen et al., 2011; Jacob et al., 2011). Interestingly, Jacob et al. (2011) found specific primary functions for HDAC1 and HDAC2. They demonstrated that HDAC1 controls SC survival by preventing precocious increase of active beta-catenin and that HDAC2 interacts with Sox10 to activate *Sox10*, *Krox20*, and *P0* transcription. Brn-2 is a close relative to Oct6 and is expressed with similar kinetics. While single Oct6 or Brn-2 null mice display a transient arrest at the promyelinating stage, the phenotype of double Oct6/Brn2 double mouse mutant is more severe, although myelination is not completely prevented (Jaegle et al. 2003). NRG1 signalling also upregulates the expression of several transcription factors necessary for myelination, like YY1 and NFATC3/4. Activation of the latter ultimately leads to Krox20 expression. NRG1 was also shown to activate mTOR signaling, whose functions in SC development and myelination have been highlighted (Norrmén et al., 2014). Recently, the E3 ubiquitin ligase Fbxw7 has been shown to regulate myelin gene expression and to prevent hypermyelination by suppressing mTOR signaling (Harty et al., 2019).

Upon Gpr126 and NRG1 signaling, Oct6, Brn-2, Sox10, and NFATC3/4 are all recruited to *Krox20* myelinating SC element (MSE) to activate Krox20 expression. NFATC3/4 form a complex with Sox10, and YY1 participates in the loop formation between *Krox20* promoter and *Krox20* MSE (He et al., 2010; Kao et al., 2009; Weinstraub et al., 2017). Induction of *Krox20* transcription also

requires HDAC1, HDAC2, Brg1-containing BAF complexes and the MED12 subunit of the Mediator complex. The latter has been shown to physically interact and collaborate with Sox10 on *Krox20* MSE (Jacob et al., 2011; Sock and Wegner, 2016; Vogl et al.,2013; Weider et al., 2012). A co-expression of Oct6 and Krox20 is observed during the initial myelination phase. However, Oct6 expression is rapidly turned off, at least in part by Krox20, as continuous Oct6 expression leads to hypomyelination and axonal loss (Ryu et al. 2007; Zorick et al., 1999). The transition from pro-myelinating SCs to myelinating SCs also requires the repression of negative regulators of myelination. Indeed, Gomis-Coloma et al. (2018) showed that cAMP elevation induces HDAC4 shuttling to SC nucleus, where it binds to the *c-Jun* promoter and interacts with the repressor complex NCoR1/HDAC3, resulting in *c-Jun* transcriptional repression and SC differentiation. The histone methyltransferase EZH2, by catalysing the tri-methylation of H3K27, inactivates the *p75kip2* promoter, thus preventing the expression of Hes5, an inhibitor of myelination (Heinen et al. 2012; Liu et al., 2006).

An additional layer of regulation is insured by non-coding RNAs (micro RNAs and long non-coding RNAs) at all stages of SC development, whose expression is mostly regulated by Sox10. The regulatory network thus reaches a higher degree of complexity, as microRNAs also control various transcription factors in addition to transcription factors and chromatin remodeling enzymes themselves (Svaren et al., 2014). Micro RNAs (miRNAs) are 21-23 nucleotides non-coding RNAs, which modulate gene expression by binding to the 3´-UTR of their target mRNA. Their role in SC biology has been highlighted in mice lacking essential enzymes for miRNA maturation like DiGeorge syndrome critical region 8 (DGCR8) or Dicer, whose PNS axons are severely hypomyelinated with SCs

expressing iSC markers (Pereira et al., 2010; Bremer et al., 2010). Among the miRNAs discovered in SCs, the Lin28B/let-7 axis is a critical driver of PNS myelination. Let-7 miRNA levels are inversely correlated to Lin28B, an antagonist of let-7. Mechanistically, let-7 miRNAs have been shown to promote Krox20 expression by inhibiting Notch signaling. Moreover, miR138 is induced at the myelination onset and has been predicted to repress *Sox2*, *c-Jun* and, *Cyclin D1* expression (Yun et al., 2010). Many other miRNAs have been found to regulate SC proliferation, migration, myelin maintenance and response to injury (Gu et al., 2015, Qian et al. 2016; Svaren et al., 2014; Yi et al., 2016).

In contrast to the ligand NRG1 type III on axons, its receptor ErbB2 on SCs is not rate limiting for myelination. In addition, NRG1 signaling instructs SCs for myelination and identify axons that have reached a diameter of around 1 µm (Fledrich et al., 2019; Michailov et al., 2004; Taveggia et al., 2005). The interaction between NRG1 type III on ErbB2/3 receptors on SCs activate different signaling cascades, especially MAPK/ERK and PI3K/AKT signaling cascades. MAPK/ERK overactivation can rescue the loss of NRG1/ErbB signaling. However, Akt overactivation or ablation of PTEN leads to hypermyelination and myelin pathology (Domènech-Estévez et al., 2016; Fledrich et al., 2019; Sheean et al., 2014). In contrast, Notch signaling acts as an inhibitory signal for myelination onset (Woodhoo et al., 2009).

Components of the ECM also play a role in the onset of myelination. Indeed, laminin 211 limits NRG1 type III signaling in small-caliber axons (Ghidinelli et al., 2017). Interestingly, the rigidity of the ECM or mechanical stimulation have been shown to modulate the Hippo pathway. When inactivated, the transcriptional co-activators YAP and TAZ are de-phosphorylated, enter the nucleus and co-activate the transcription factor TEAD1, resulting in *Krox20* and *Pmp22*

expression (Lopez-Anido et al., 2016; Poitelon et al., 2016). This suggests that mechanical stimuli can be integrated by SCs and participate in the control of myelination.

1.3.5 Myelinating Schwann cells

During terminal differentiation and initiation of the myelination program, pro-myelinating SCs wrap their membrane iteratively around the axonal segment to form the myelin sheath. Myelin growth demands the synthesis and assembly of a large amount of myelin components, requiring a tight coordination between protein translation, lipid biosynthesis, and their trafficking to maintain a proper myelin stoichiometry. Indeed, imbalances and impairment of myelin component synthesis can result in peripheral dysmyelinating or demyelinating neuropathies (Fledrich et al., 2012, 2018, Hertzog and Jacob, 2022). During maturation, SC cytoplasm is progressively extruded from the membrane to produce compact myelin between the abaxonal and adaxonal layers of the SC membrane. The stabilization of opposing membrane layers is initiated by myelin proteins. Indeed, compaction occurs via extracellular binding of P0 tetramers on opposing membrane surfaces. The cytoplasmic leaflets between the opposing membranes are then compressed via the electrostatic interactions between MBP and the cytoplasmic tail of P0. On electron microscopy images, compact myelin appears as a major dense line, with MBP as primary constituent (Muppirala et al., 2021; Salzer, 2015). Furthermore, SC wrapping requires an important and constant cytoskeletal remodeling, which is dependent on the recruitment and interaction of cytoskeleton modifiers with the ECM components (Muppirala et al., 2021). NRG1 signaling through PI3K/AKT pathway plays an important function in wrapping and myelin formation. Indeed, NRG1

signaling is known to promote myelination and to modulate the number of myelin wraps (Michailov, 2004; Taveggia et al., 2005). Interestingly, *in vitro* inhibition of AKT perturbed myelin formation without affecting terminal differentiation gene expression such as *Krox20* (Domènech-Estévez et al., 2016).

The transition between promyelinating SCs to myelinating SCs is controlled by several categories of signals. The first category comprises the signaling between axons and SCs, among which NRG1 and Gpr126 signaling are the most studied. The axonal control of myelination has been demonstrated already in the 1970s as axonal molecules were shown to be responsible for the acquisition of the SC myelinating phenotype (Weinberg and Spencer, 1975). Among the members of the NRG1 family, NRG1 type III has been identified as the molecule determining the myelinating phenotype and the fate of SC differentiation and regulates Sox10 and Krox20 expression. NRG1 type III is also required for the formation of Remak bundles, indicating that NRG1 signaling is required for the specification of both myelinating and nonmyelinating SCs (Fricker et al., 2009; Monk et al., 2015; Taveggia et al., 2005). NRG1 type III activity is controlled by post-translational modifications mediated by secretases. While the β-secretase BACE-1 acts as positive activator, the α-secretase ADAM17 acts as a negative regulator of NRG1 activity. Indeed, BACE-1 cleavage promotes myelination, whereas ADAM17 inhibits myelination (La Marca et al., 2011; Taveggia et al., 2005). After the extracellular cleavage, the transmembrane domain of NRG1 type III undergoes a proteolysis mediated by the y-secretase complex, triggering the expression of prostaglandine D2 (PGD2) synthase, catalyzing the production of PGD2, which then activates Gpr44 in SCs and promotes myelination. This pathway reinforces NRG1 type III signaling during development and may contribute to myelin maintenance in adulthood (Trimarco et al., 2014).

G-protein-coupled receptors are a family of cell surface receptors composed of 7 transmembrane domains and an N-terminal extracellular domain, with the ability to transduce signaling via heterodimeric G proteins. Gpr126 integrates signals from ECM molecules like laminin 211 and collagen IV, triggering an increase in cAMP levels and PKA activation to control different stages of SC development and myelination (Mogha et al. 2013; Monk et al., 2011; Peterson et al., 2015). Another GPCR implicated in PNS myelination is Gpr44, which activates the transcription factor NFATC4 (Trimarco et al., 2014). Interestingly, GPCR effectors modulate signals from other pathways. The best example is cAMP. Low levels of cAMP favor NRG1-induced cell proliferation and high levels of cAMP promote NRG1-induced SC differentiation. Additionally, Laminin 211-Gpr126 interactions suppress cAMP accumulation during radial sorting and promote cAMP accumulation at later developmental stages (Peterson et al., 2015; Monk et al., 2015).

The dependence of SCs on axonal signaling cues persists beyond the developmental period and is required for myelin maintenance during adulthood as well, however to a lesser extent. For example, conditional ablation of NRG1 in adult neurons leads to myelin alteration only after 22 weeks. In contrast, the axon-derived prion protein PrP^c is needed only for myelin maintenance. PrP^c acts upstream of Gpr126 in myelinating SCs, indicating that cAMP signaling is also required to preserve myelin integrity (Bremer et al., 2010; Fledrich et al., 2019; Küffer et al., 2016). Hence, the axonal signals directing SC development and myelination differ from the ones preserving myelin integrity. Similarly to the developmental period, SCs also provide essential support for axon integrity.

Several signaling pathways are activated downstream of NRG1 type III, including the PI3K/AKT pathway, the MEK/ERK pathway, and the phospholipase C-y Ca^{2+}

pathway. Of note, those pathways are commonly activated by different signaling molecules, indicating that they act as an integration center to control myelination. *In vivo*, PI3K/AKT pathway activation has been shown to initiate myelination and control myelin thickness, whereas MEK/ERK pathway was shown to regulate SC differentiation and myelin sheath thickness. Indeed, MEK-dependent phosphorylation of YY1 transcription factor is necessary for Krox20 activation and myelination (He et al., 2010). The omnipresence of NRG1 type III signaling at almost every SC developmental stage raised the question of how NRG1 type III can generate such a wide array of responses in SCs. The current consensus is that SCs respond to axonal NRG1 type III in a concentration-dependent manner. Another explanation would reside in the intersection of other signaling pathways with NRG1 signaling at each stage, so that the combination of different pathways would affect SC response to NRG1 signaling (Glenn and Talbot, 2013; Monk et al., 2015). Lastly, it has been shown, *in vitro*, that NRG1 activation leads to increased levels of intracellular Ca^{2+}, NFAT phosphorylation and nuclear translocation. NFATs then dimerize with Sox10 and activate *Krox20* and *P0* expression (Kao et al., 2009).

At later stages of SC development, Sox10 together with Krox20 are of paramount importance for SC terminal differentiation, myelination, and myelin maintenance. Indeed, numerous studies shed light on the synergistic activation of myelin protein genes such as *Mbp*, *P0* and *Cx32*, and lipid biosynthesis genes by Sox10 and Krox20, as well as co-occupancy on their regulatory regions (Bondurand et al, 2001; Denarier et al., 2005; Jang et al., 2009; Jones et al., 2007). Of note, the activation of lipid biosynthesis genes also relies on the binding of Srebp downstream of mTOR signaling, as well as RXRγ (LeBlanc et al., 2005; Srinivasan et al., 2012). In adult SCs, HDAC1 and HDAC2 act as co-factors

of Sox10 to activate the *P0* promoter and are required to maintain the integrity of the paranodes and nodes of Ranvier. Indeed, P0 levels are decreased by 50% in mice lacking HDAC1/2 in SCs and is accompanied by severe motor and sensory loss of function (Brügger et al., 2015). While HDAC1/2 expression is high in developing SCs, their expression levels are considerably decreased in mature myelinating SCs. Indeed, once developmental myelination is completed, SCs switch from a myelin biogenesis state to homeostasis state in adulthood. This transition is under the control of HDAC3, whose deletion maintains HDAC1/2 expression levels found in developing SCs, leading to hypermyelination and, consequently, to the development of peripheral neuropathies (Rosenberg et al., 2018). In the homeostatic state, continuous myelin gene expression is required but at lower levels to ensure myelin maintenance. Regulation of Krox20 levels in adult SCs is crucial for myelin integrity, as a misregulation of Krox20 expression leads to demyelination or hypermyelination. To maintain low Krox20 and Oct6 levels, repressive histone marks are added to *Krox20* MSE and *Oct6* SCE in the adult SC stage. Lastly, histone methylases have also been shown to regulate SC myelination. For example, the Polycom repressor complex 2 (PRC2) represses the *Igfbp2* promoter by catalyzing H3K27 tri-methylation, thereby dampening Akt-dependent myelination and preventing overmyelination (Ma et al., 2018).

The final integrators and responders of the different extracellular and intracellular cues are transcription factors and chromatin remodeling enzymes. Transcriptional changes are required to produce myelin proteins and lipids. The most important transcription factor necessary for SCP differentiation, SC maturation, myelination and myelin maintenance is Sox10 (Fröb and Wegner, 2020; Sock and Wegner, 2019).

SC terminal differentiation is always accompanied by inhibition of negative regulators of myelination such as c-Jun, Id2, Id4, Pax3, Sox2, and Notch signaling. These factors have the particularity of being expressed in iSCs, downregulated in mature SCs, and re-expressed in SCs after injury or in the case of some peripheral neuropathies. Several pathways and second messengers need to be tightly regulated during myelination. For example, the pro-myelinating PI3K/AKT pathway is counteracted by PTEN, whose activity is potentiated by Dlg1. Indeed, PTEN inactivation or ablation of Dlg1 lead to hypermyelination. Moreover, DDIT4 has been identified as a negative regulator of PNS myelination and loss of DDIT4 results in increased PI3K/AKT activity and hypermyelination (Goebbels et al., 2010; Noseda et al., 2013). At the transcriptional levels, the inhibition of negative regulators of myelination is achieved by the recruitment of the transcription factors Krox20, NAB1/2 and the chromatin remodeling complex NuRD on regulatory regions of *c-Jun*, *Id2* and *Id4* genes. NAB1/2 allows Krox20 to recruit the HDAC/NuRD complex. In support to a negative function of c-Jun on myelination is the cross-inhibitory relationship between c-Jun and Kox20 (Parkinson et al., 2004, 2008). The high mobility group (HMG) domain transcription factor Sox2 has also been shown to repress Krox20 expression and axon myelination in SC/DRG neuron co-cultures and impairs myelination *in vivo* (Le et al., 2005, Roberts et al., 2017). Such as for c-Jun, a cross-inhibitory relationship between Sox2 and Krox20 has been observed *in vitro*. In addition, mice with persistent *Sox2* expression in SCs show a hypomyelinating phenotype, increased number of unmyelinated axons and reduced levels of Krox20 and myelin proteins, resulting in impairment of sensory-motor function (Le et al., 2005; Parkinson et al., 2008; Roberts et al., 2017). Of note, c-Jun and Sox2 expressions are also downregulated by Zeb2 at this stage. Additionally, Krox20

also downregulates Notch-1 expression in SCs at the onset of myelination (Woodhoo et al., 2009). Lastly, the methyltransferase EZH2, one of the two methyltransferases found in the PRC2 complex, catalyzes the trimethylation of H3K27 on the promoter of injury-induced genes to prevent their inappropriate expression (Ma et al., 2015).

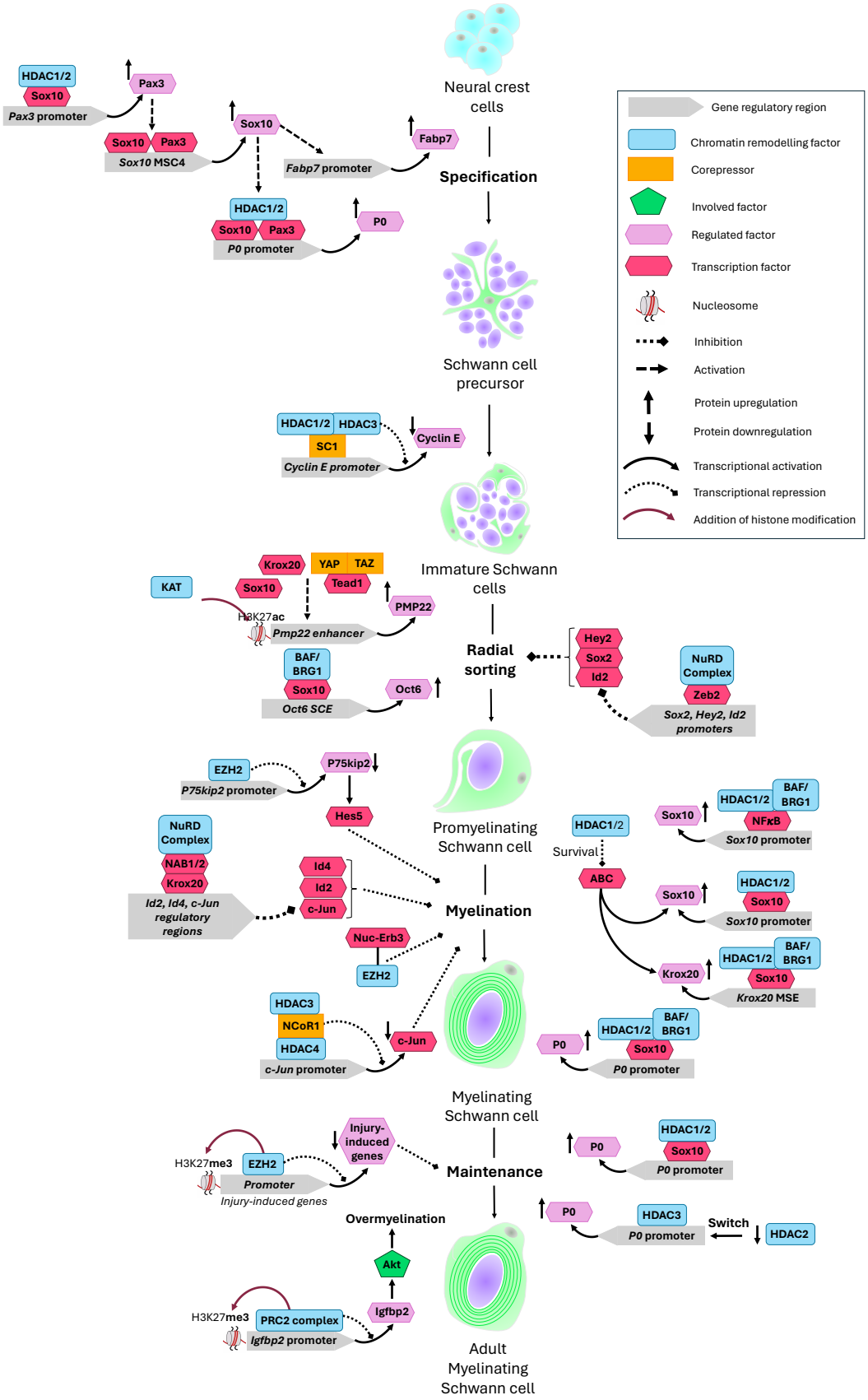
Neural crest cells
HDAC1/2
Sox10
Pax3 promoter
Pax3
Sox10
Pax3
Sox10 MSC4
Sox10
Fabp7 promoter
Fabp7
Specification
HDAC1/2
Sox10
Pax3
P0 promoter
P0
Schwann cell precursor
HDAC1/2
HDAC3
SC1
Cyclin E promoter
Cyclin E
Immature Schwann cells
Krox20
YAP
TAZ
Tead1
KAT
Sox10
H3K27ac
Pmp22 enhancer
PMP22
Radial sorting
Hey2
Sox2
Id2
NuRD Complex
Zeb2
Sox2, Hey2, Id2 promoters
BAF/ BRG1
Sox10
Oct6 SCE
Oct6
Promyelinating Schwann cell
EZH2
P75kip2 promoter
P75kip2
Hes5
NuRD Complex
NAB1/2
Krox20
Id2, Id4, c-Jun regulatory regions
Id4
Id2
c-Jun
Myelination
Nuc-Erb3
EZH2
HDAC3
NCoR1
HDAC4
c-Jun promoter
c-Jun
Myelinating Schwann cell
HDAC1/2
Survival
ABC
Sox10
HDAC1/2
BAF/ BRG1
NFκB
Sox10 promoter
Sox10
HDAC1/2
Sox10
Sox10 promoter
Krox20
HDAC1/2
BAF/ BRG1
Sox10
Krox20 MSE
P0
HDAC1/2
BAF/ BRG1
Sox10
P0 promoter
Maintenance
Injury-induced genes
H3K27me3
EZH2
Promoter
Injury-induced genes
P0
HDAC1/2
Sox10
P0 promoter
Overmyelination
P0
HDAC3
Switch
HDAC2
P0 promoter
Akt
Igfbp2
H3K27me3
PRC2 complex
Igfbp2 promoter
Adult Myelinating Schwann cell
Gene regulatory region
Chromatin remodelling factor
Corepressor
Involved factor
Regulated factor
Transcription factor
Nucleosome
Inhibition
Activation
Protein upregulation
Protein downregulation
Transcriptional activation
Transcriptional repression
Addition of histone modification

Figure 8. Histone modifications and histone modifiers in SC development and maintenance. Schematic representation of chromatin-remodeling enzymes and associated mechanisms regulating SC development and maintenance. ABC, active β-catenin; ac, acetyl group; Akt, murine thymoma viral oncogene homolog 1; BAF, Barrier-to-autointegrated factor; BRG1, Brahma-related gene 1; c-Jun, c-Jun proto-oncogene; EZH2, Enhancer of zeste homolog 2; Fabp7, Fatty acid binding protein 7; HDAC1, histone deacetylase 1; HDAC2, histone deacetylase 2; HDAC3, histone deacetylase 3; HDAC4, histone deacetylase 4; Hes5, transcriptional repressor Hairy Enhancer of Split 5; Hey2, Hairy/enhancer-of-split related with YRPW motif protein 2; Id2, DNA binding protein inhibitor 2; Id4, DNA binding protein inhibitor 4; IGFBP2, Insulin-like growth factor binding protein 2; KAT, histone methyltransferase; Krox20, early growth response 2; me, methyl group; NAB1/2, NGF1-A (Nerve growth factor-induced protein A) binding factor ½; NCoR1, Nuclear receptor corepressor 1; NFkB, Nuclear factor kappa-light-chain-enhancer of activated B cells; NuRD, Nucleosome remodeling and deacetylase; Oct6, Octamer-binding transcription factor 6; P0, Myelin protein zero; p75kip2, Cyclin-dependent kinase inhibitor p75; PRC2, Polycomb repressive complex 2; Pax3, Paired box gene 3; PMP22, Peripheral myelin protein 22-kDa; SC1, Schwann cell factor 1; SCE, Schwann cell specific enhancer; Sox2, SRY (sex determining region Y) box 2; Sox10, SRY (sex determining region Y) box 10; TAZ, Transcriptional co-activator with PDZ binding motif; TEAD1, TEA domain transcription factor 1; YAP, Yes-associated protein; Zeb2, Zinc finger E-box-binding homoebox 2. (*Modified and adapted from Duman and Martinez-Moreno, 2022; Jacob, 2017).*

1.3.6 Nonmyelinating Schwann cells

The PNS comprises several classes of nerve fibers associated with nonmyelinating SCs (NMSCs): the C fiber nociceptors, the postganglionic sympathetic and parasympathetic fibers, and the motor nerve terminals at the neuromuscular synapses. NMSCs are themselves divided into three classes: the Remak SCs ensheathing small-caliber axons, the perisynaptic SCs at the neuromuscular junctions (NMJs), and the terminal SCs associated with cutaneous sensory end organs like Pacini or Meissener corpuscles (Monk et al., 2015). Of note, perisynaptic and terminal SCs also derive from iSCs.

Remak SCs enwrap between one and fifty axons of either sensory C-fibers or postganglionic sympathetic and parasympathetic fibers into single bundles, with the number of axons per bundle varying along the same nerve and in different nerves. It has been shown that a single Remak SC can surround axons that respond differently to given growth factors, thereby highlighting a critical

function of Remak cells in the trophic and metabolic support of axons (Beirowski et al., 2014, Monk et al., 2015). Remak cells share some markers with iSCs such as NCAM1 and GFAP but more specific Remak SCs markers, ApoD and SMOC2 have recently been identified at the transcript level (Wolbert et al., 2020). The exact mechanism by which iSCs differentiate into Remak SCs is still under investigation. However, sensory axon NRG1 type III expression is necessary for Remak SC generation (Bosch-Queralt et al., 2022; Fricker et al., 2009; Taveggia et al., 2005).

Terminal SCs do not wrap axons but rather extend processes toward them and cover the entire synapse. Usually, three to five cells are found in close contact with both the pre- and postsynaptic NMJ components. Terminal SCs ensure synapse formation, refinement, and axon pathfinding during development, functional maintenance, and proper re-innervation of NMJs after injury (Bosch-Queralt et al., 2022; Kang et al., 2014; Monk et al., 2015; Smith et al., 2013). In addition, terminal SCs bear neurotransmitter receptors at their surface, whose activation triggers a Ca^{2+} wave in SCs, thereby modulating synaptic transmitter release (Bosch-Queralt et al., 2022; Ko and Robitaille 2015).

At the epidermis-dermis junction, terminal SCs and Remak fibers form a 1:1 relationship but only the Remak fibers extend through the dermis. Terminal SCs in the skin are thought to preserve nerve terminals and provide innervation of sensory end organs. For instance, terminal SCs-derived NGF allows continuous axon sprouting and growth, which are characteristic of sensory fibers in the skin (Diamond et al., 2012; Monk et al., 2015). Terminal SCs thus actively take part in the modulation of sensory responses in the skin. Furthermore, their role in

wound healing of the skin has recently been highlighted (Bosch-Queralt et al., 2022; Johnston et al., 2013; Parfejevs et al., 2018; Rinwa et al., 2021).

1.4 Peripheral nerve injury and regeneration

In response to a lesion, PNS neurons and SCs undergo extensive changes in their differentiation state and in their gene expression distal to the injury. On the one hand, PNS neurons switch from a cell-cell signaling function to a growth-competent phenotype. On the other hand, SCs temporarily abandon their axonal ensheathment and myelin maintenance function to acquire a phenotype supporting regeneration. These cells, called repair SCs, differ from other cells of the SC lineage (Jessen and Mirsky, 2016). Thus, peripheral nerves owe their regenerative capacities to the flexible differentiation phenotype of both neurons and SCs. In contrast, the regenerative capacity of the CNS is a lot lower, due to some extent to a lower capacity of CNS neurons to regrow, and mostly to the absence of repair cells in the CNS. indeed, OLs do not reprogram into repair cells and provide no helpful support. Instead, a CNS lesion is followed by the formation of a glial scar and retention of myelin debris, which are deleterious for axonal regrowth (Jessen and Mirsky, 2016; Brosius Lutz and Barres, 2014).

1.4.1 The neuron response to injury

During development, the formation of synapses progressively decreases axon growth competence and directs its functions into transmitting information and signal integration. However, after an injury, axons recapitulate some of the developmental processes and switch from an electrically transmitting state back to an electrically silent, growth-competent state (Mahar and Cavalli, 2018;

Quadrato et al., 2013). The presence of an injury is conveyed from injury site to the cell soma by retrograde axonal signaling occurring in two phases. The early and rapid signaling phase results from ion flux changes. A damage to the axonal membrane triggers massive ion influx and opening of voltage-dependent sodium channels, leading to the inversion of the Na+/Ca2+ exchange pump. This, together with the Ca^{2+} release from intracellular stores, generates a Ca^{2+} wave that propagates along the axon (Rishal and Fainzilber, 2014). Interestingly, it has been shown that the Ca^{2+} wave triggers phosphorylation and nuclear export of HDAC5 in a PKCμ-dependent manner. HDAC5 export increases histone H3 acetylation levels, thus priming chromatin for subsequent transcriptional changes (Cho et al., 2013).

The late signaling phase occurs by dynein-mediated retrograde transport. The dual leucin zipper kinase (DLK) is locally activated by phosphorylation after injury and binds together with JNK and JIP3 on dynein. The retrograde transport of this complex to the cell soma allows the phosphorylation and activation of the transcription factors c-Jun, STAT3 and ATF3 as well as their translocation to the nucleus, which ultimately leads to the transcription of regeneration associated genes (RAGs). Of note, STAT3 is locally translated in axons and phosphorylated after lesion (Ben-Yaakov et al., 2012). Beside the DLK-JNK-JIP3-mediated activation of transcription factors, the second signaling phase is also characterized by retrograde transport of transcription factors bearing a nuclear localization signal (NLS) upon direct binding to importin-α isoform. It has been shown that the levels of importin-β isoform are increased after injury by local translation of importin-β mRNA and that binding of importin-β to importin-α increase the affinity of importin-α for the NLS of the transcription factor (Hanz et al., 2003; Perry and Fainzilber, 2009). The intermediate filament vimentin has also been shown to be locally translated and cleaved after injury. Vimentin

fragments possess a NLS and interact directly with importin-β and phosphorylated ERK (pERK), allowing the nuclear translocation of pERK. In addition, the presence of vimentin in this complex prevents ERK dephosphorylation (Perlson et al., 2005).

Neuronal activation after injury involves massive changes in the gene transcription profile of neurons. RAG genes include the immediate-early genes c-Jun and JunD, as well as constitutive transcription factors such as CREB, STAT3, ATF3, Sox1 and SMAD1 (Abe and Cavalli, 2008). Among them, c-Jun is the central component of the RAG network since it is required for the initiation of the additional transcriptional changes. Thus, c-Jun is not only crucial for the acquisition of the repair phenotype in SCs but also for neuronal plasticity after lesion to promote neurite outgrowth (Raivich et al., 2004).

In the distal stump, the axonal transport of Nicotinamide mononucleotide adenylyltransferase 2 (NMNAT2) in the distal part is interrupted after lesion and the remaining NMNAT2 pool is degraded. Consequently, the conversion of Nicotinamide mononucleotide (NMN) to Nicotinamide adenine dinucleotide (NAD) by NMNAT2 is prevented, leading the NMN accumulation in the distal stump. NMN then binds to Sterile alpha and TIR motif containing 1 (SARM1) octamer, inducing a conformational change promoting its activation. SARM1 has been identified and described as a protein promoting degradation of injured axons and is an essential effector of Wallerian degeneration (Arthur-Farraj and Coleman, 2021; Osterloh et al., 2012). Indeed, the activated form of SARM1 generates cyclic ADP-ribose (cADPR) from NAD as well as other products from NAPD or nicotinic acid such as nicotinic acid adenine dinucleotide phosphate (NAADP) and 2´-phospho-cyclic ADP-ribose (cADPRP), leading to calcium

accumulation, generation of reactive oxygen species and ATP decline, which promote axonal degeneration (Arthur-Farraj and Coleman, 2021).

1.4.2 The Schwann cell response to injury

In the CNS, once OLs have myelinated neurons, they remain in a post-mitotic state. New OLs are produced throughout life from a pool of progenitor cells known as OL progenitor cells (OPCs) to replace OLs, to myelinate new axon segments or for remyelination following demyelination events. In contrast, the adult PNS is a more quiescent tissue and both PNS homeostasis and regeneration do not rely on a specific stem cell population. Indeed, myelinating SCs do not turn over in adult nerves and Remak cell turnover rate is extremely slow (72 months). However, both mSCs and Remak SCs can adopt a repair phenotype as well as the acquisition of proliferative and migratory features after injury (**Fig. 5**). Repair SCs are the central orchestrators of the regenerative response. Indeed, they control the blood-nerve barrier breakdown and allow the influx of inflammatory cells, they clear the nerve environment from axon and myelin debris, and guide and support axonal regrowth back to their former targets. Repair SCs retain features of the SC lineage and can redifferentiate into either myelinating or Remak cells once regeneration is complete, independently of their phenotype (mSCs or Remak SCs) before lesion (Cattin and Llylod, 2016; Jessen and Mirsky, 2016; Stierli et al., 2018).

It has long been thought that SCs were de-differentiating after lesion, retrieving iSC characteristics. However, it is now proved that the acquisition of the repair phenotype involves both the loss of SC differentiation features as well as the activation of a set of repair-supportive genes and phenotypes that are not observed during SC development. In fact, the simultaneous loss of differentiation features and activation of regeneration-supportive features have

also been observed in other cell types in mammals (skin, liver, pancreas) or in amphibians (limb or pigmented cells in the newt), for example. This type of cell conversion is rather defined as transdifferentiation or direct (lineage) reprogramming (Jessen and Mirsky, 2016; Sisakhtnezhad and Martin, 2012). Indeed, a comparison between iSCs and repair SCs reveal several differences. First, repair SCs show a different expression profile and transcriptional controls than iSCs. For example, expression of c-Jun and c-Jun target genes such as GDNF, Oligodendrocyte transcription factor 1 (Olig 1), Sonic Hedgehog (Shh) and artemin occur *de novo* after injury and serve as repair SC markers. Those genes are only a small fraction of the genes that are up-regulated after injury, as over a hundred of genes are up-regulated after lesion (Arthur-Farraj et al.,2012; Balakrishnan et al., 2016; Bosse et al., 2006; Yi et al., 2017). Second, in contrast to iSCs, repair SCs elicit a local innate immune response in the distal stump to attract and activate macrophages and other immune cells (Gaudet et al., 2011). Third, repair SCs can degrade their own myelin sheath after lesion by activating a special form of autophagy called myelinophagy. Fourth, repair SCs are morphologically distinct from iSCs as they adopt an elongated, bipolar shape to form regeneration tracks and iSCs lack such a guidance function. Those four aspects are discussed in more details in the section below.

Axons can be interrupted by either nerve crush or nerve cut. After nerve crush, the basal lamina tubes surrounding the axon/SC units remain intact and axons lie within their native basal lamina sheath as they elongate into the distal stump. The SC response to injury can be divided into two steps. The first one consists of downregulating the expression of pro-myelinating and myelin genes like *Krox20*, enzymes of the cholesterol synthesis, and genes coding for myelin structural proteins such as P0, MBP, MAG or periaxin. At the same time, repair SCs upregulate the expression of some iSC genes, including Neural cell adhesion

molecule (NCAM), p75 neurotrophin receptor (p75NTR) and glial fibrillary acidic protein (GFAP). The second one is the acquisition of the repair program, a set of phenotypes observed neither in mature myelinating SCs, nor in developing nerves (Jessen and Mirsky, 2008; Mirsky et al., 2008).

Repair SCs start expressing neurotrophic factors and surface proteins whose functions are to promote axonal survival and elongation. Among them, we can cite glial cell-derived neurotrophic factor (GDNF), artemin, brain-derived neurotrophic factor (BDNF), neurotrophin-3 (NT-3), nerve growth factor (NGF). Repair SCs also upregulate N-CAM and N-cadherin, which allow axon migration at the SC surface (Arthur-Farraj et al., 2012; Napoli et al., 2012).

An innate immune response is then activated in the distal stump and is characterized by increased production of cytokines by SCs, including tumor necrosis alpha (TNFα), interleukin-1α (IL-1α), leukemia inhibitory factor (LIF), and monocyte chemotactic protein 1 (MCP-1). In this way, SCs can interact with immune cells and recruit macrophages to the distal stump. In addition of providing a second source of cytokines, the recruited macrophages promote vascularization, co-operate with SCs to remove myelin and axonal debris, thereby generating a growth-promoting environment together with SCs (Tofaris et al., 2002).

Repair SCs adopt an elongated and bipolar morphology and slightly overlap to form cords called bands of Büngner inside the basal lamina tubes. These structures are essential to guide regrowing axons back to their previous targets. The conversion of myelinating and Remak SCs into repair SCs includes a 2-to-3-fold increase in cell length, i.e. 7-to-10 times longer than iSCs. Although myelin and Remak cells have very different morphologies, they give rise to repair cells with a comparable general appearance and branching pattern as well as overlapping size range. Around 50% of Remak-derived repair SCs display

between 2 and 3 long branches, oriented parallel to the cell axis, whereas iSCs are unbranched. In contrast, myelinating SC-derived repair SCs are even longer than Remak SC-derived repair SCs and around 30% of myelinating SC-derived repair cells are branched. SC elongation is reversible and repair SCs shorten to 1/7 of their length during the remyelination phase. Indeed, lineage tracing analysis revealed that both myelinating and Remak cells in uninjured nerves convert into repair SCs in injured nerves and that repair SCs convert back to either myelinating or Remak SCs after nerve regeneration (Gomez-Sanchez et al., 2017; Stierli et al., 2018). It has been hypothesized that this massive increase in length can provide a safety to ensure the formation of bands of Büngner in the absence of SC proliferation, as axonal regrowth is unaffected when proliferation is prevented in SCs (Atanasoski et al., 2001; Gomez-Sanchez et al., 2017). However, myelinating SCs in regenerated nerves are only 150-µm long, about 75% shorter in length than myelinating SCs in uninjured nerves and correspond to SC length when they start myelinating axons during development (Gomez-Sanchez et al., 2017; Hildebrand et al., 1985). However, during development, SCs progressively elongate to match the increase in axonal length, a process not observed during remyelination, suggesting that the initial length is optimal to start myelination or remyelination (Court et al., 2004; Gomez-Sanchez et al., 2017).

Lastly, repair SCs have been shown to degrade their own myelin by activating a special form of autophagy known as myelinophagy. Indeed, SCs themselves degrade around 50% of their own myelin during the first 5 to 7 days following injury (Perry et al., 1995). To this end, SCs activate an actin-dependent process resulting in the division of their myelin sheath into small oval-shaped fragments, which will be further reduced in size and delivered to lysosomes for digestion. Of note, activation of myelinophagy is part of the normal generation of repair

SCs since mice with genetic ablation of autophagy function in SCs show a reduced expression of the repair SC markers GDNF, Shh, Olig 1 and Artemin, as well as a different expression profile of the normally down-regulated and up-regulated genes in repair SCs at 5 days post injury compared to control mice (Gomez-Sanchez et al., 2015). At the molecular level, SC myelinophagy occurs in an mTOR-independent form of autophagy, whereas the autophagic process in response to starvation is mTOR-dependent (Gomez-Sanchez et al., 2015; Jessen and Mirsky, 2016; Jung et al., 2011). Instead, myelinophagy is driven by the JNK/c-Jun pathway since autophagic flux is massively reduced in c-Jun cKO animals or in WT animals treated with a JNK inhibitor (Gomez-Sanchez et al., 2015). Surprisingly, SCs also clear myelin debris by phagocytosis. Indeed, after lesion SCs upregulate Axl and Mertk, two members of the TAM phagocytic receptor family, which are both necessary for myelin clearance (Brosius Lutz et al., 2017). Later, in the distal stump, myelin clearance is dominated by the influx of monocyte-derived macrophages, recruited by the variety of chemokines and cytokines, notably CCL2, released by SCs. SCs seem sufficient to attract monocyte-derived macrophages, as SCs constitutively activating ERK signaling attract macrophages even in the absence of lesion (Napoli et al., 2012). In addition, fibroblasts secrete CSF1, which is thought to target macrophages to repair SCs (Groh et al., 2012). However, the small population of nerve-resident macrophages also proliferates, phagocytoses myelin debris, and contribute to the early inflammatory response after lesion, before the massive macrophage influx. Resident macrophages may also account for the cytokine secretion triggering hematogenous macrophage infiltration (Klein and Martini, 2016; Müller et al., 2001, 2003). Beside macrophages, neutrophils also take part in myelin removal during Wallerian degeneration, as neutrophil depletion substantially inhibits myelin clearance *in vivo* and neutrophil recruitment has

been shown to compensate for the absence of macrophages (Lindborg et al., 2017). Recently, it has been shown that SCs actively take part into axon disintegration. Indeed, placenta growth factor (PIGF) released by injured axons activates and upregulates VEGFR1 in Schwann cells, which in turn activates Pak1. Upon Pak1 activation, SCs form constricting actomyosin spheres along distal cut axons, leading to their disintegration (Vaquié et al., 2018). Altogether, SCs and macrophages allow axonal and myelin debris clearance and remodeling of the tissue to create a growth-promotive environment. Upon arrival at the neuromuscular junction, regenerating motor axons follow the processes that terminal SCs extended within the old synaptic site during denervation, allowing precise reinnervation (Kang et al., 2014). Once axons have reinnervated their targets, repair SCs re-ensheath or remyelinate axons by reverting to their differentiated and myelinating phenotypes.

After a nerve cut, the connective tissue and basal lamina sheaths are interrupted, and both the proximal and distal stumps need to be re-attached for regeneration to occur. In that case, a tissue bridge will form between the two ends, through which SC cords, emanating from both stumps, migrate directionally along fibroblasts and blood vessels. This results in the formation of cellular conduits along which regrowing axons are guided through the tissue bridge towards the distal stump. Two days after transection, the proximal and the distal stumps are rejoined by the tissue bridge, and repair SCs can already be observed at the tips of both nerve stumps. Five days after transection, SCs from both stumps have migrated into the bridge as discrete SC cords, which eventually join in the middle of the bridge. Axons emanate from the proximal stump and elongate along SC cords. Seven days after transection, the whole bridge is filled with SC cords and axons travelling to the distal stumps.

Interestingly, the two major cell types present in the bridge five days after transection are fibroblasts and SCs, grouped into discrete clusters (Min et al., 2021). Indeed, it has been shown *in vitro* that fibroblasts sort SCs into clusters by repulsing SCs and by switching SC behavior from repulsive to attractive. This is mediated, *in vivo* and *in vitro*, by the binding of ephrin-B ligands on fibroblasts to EphB2 receptors on SCs, inducing posttranslational modifications and stabilization of the transcription factor Sox2, resulting in the relocalization of N-cadherin in SCs to cell-cell junctions as well as an increase of N-cadherin at the protein level, but not at the mRNA level. The relocalization of N-cadherin results in SC sorting into organized cords, along which axons can migrate directionally. Indeed, when EphB2 receptor signaling is inhibited *in vivo*, axonal regrowth appears disorganized, with shorter and fragmented axons regrowing in different directions (Cattin and Llyod, 2016; Parinello et al., 2010).

The guidance of axons through the length of the nerve bridge confers a specialized function to bridge SCs, which is not observed in repair SCs in the distal stump. While EphB2 receptors and Sox2 are expressed in dedifferentiated SCs in both the bridge and the distal stump, N-cadherin expression is restricted to SC cords in the nerve bridge, where SCs are in contact with fibroblasts. This indicates that SCs in the nerve bridge (bSCs) have distinct molecular signatures than SCs in the distal stump (dSCs). Additionally, the isolation of pure SC populations from different parts of the nerve after lesion using a FACS-based approach followed by RNA-sequencing showed that the reprogrammed state is not homogenous throughout the injured nerve and that the microenvironment modulates the SC transcriptome. Indeed, the number of differentially regulated genes between dSCs and bSCs is as important as between dSCs and intact, differentiated SCs. Interestingly, genes essential to the repair program such as genes involved in inflammation, immune signaling, ECM production are

downregulated in bSCs compared to dSCs. In contrast, bSCs upregulate genes involved in cell division and growth and have a more pronounced epithelial to mesenchymal transition (EMT) signature than dSCs, with more EMT genes highly expressed in bSCs compared to dSCs. These differences are already observed when SCs invade the bridge and persist until the bridge is fully invaded by SCs. This indicates that bSCs constitutes a subpopulation of SCs with a reduced repair ability but an increased proliferative potential and differentiation capacity toward the mesenchymal lineage. Furthermore, it has been shown that bSC reprogramming into invasive mesenchymal-like cells is triggered by the release of TGFß by fibroblasts and endothelial cells in the nerve bridge, allowing bSC invasion into the wound. In addition, TGFß potentiates EphB2 receptor-dependent cell sorting by maintaining high N-cadherin levels in bSCs. Overall, SC reprogramming requires both the activation of cell-intrinsic transcriptional programs and cell extrinsic signals from the microenvironment, which allow SCs to acquire specific functions in a context-dependent manner. Indeed, bSCs and dSCs are two distinct cell populations with a specific transcriptome and repair features (Clements et al. 2017). In addition, repair SCs have been shown to be more closely related to embryonic stem cells than to neural crest cells and that the acquisition of the mesenchymal traits can be added to the molecular features of repair SCs (Clements et al., 2017).

The SC cords are however unable to migrate directly through the matrix of the bridge and need to move along the surface of the blood vessels. Blood vessels are formed within the bridge at around 3 days post transfection from both stumps and provide directionality as well as a preferred substrate for SC migration. The interactions between SCs and endothelial cells are direct, due to the thin and discontinuous basement membrane, and the migration motions that are driven by actin-dependent forward protrusions and actomyosin-

dependent contraction of the rear of the cells. Interestingly, SC-endothelial cell interactions are thought to be non-molecular, with the blood vessels providing a frictional and discontinuous surface allowing SCs to gain sufficient traction and force to migrate. Initially, the nerve bridge, composed of matrix and inflammatory cells, is not vascularized, and hypoxic. Hypoxia is sensed by macrophages, which represent 98% of hypoxic cells within the bridge. In response to hypoxia, macrophages upregulate HIF1α expression, leading to the secretion of VEGFA which results in the recruitment and proliferation of endothelial cells and thus angiogenesis. VEGFA has been shown to be both necessary and sufficient to induce bridge vascularization and SC migration (Cattin et al., 2015; Cattin and Llyod, 2016; Krock et al., 2011).

An overview of the SC response to injury and peripheral nerve regeneration after lesion is depicted in Figure 9.

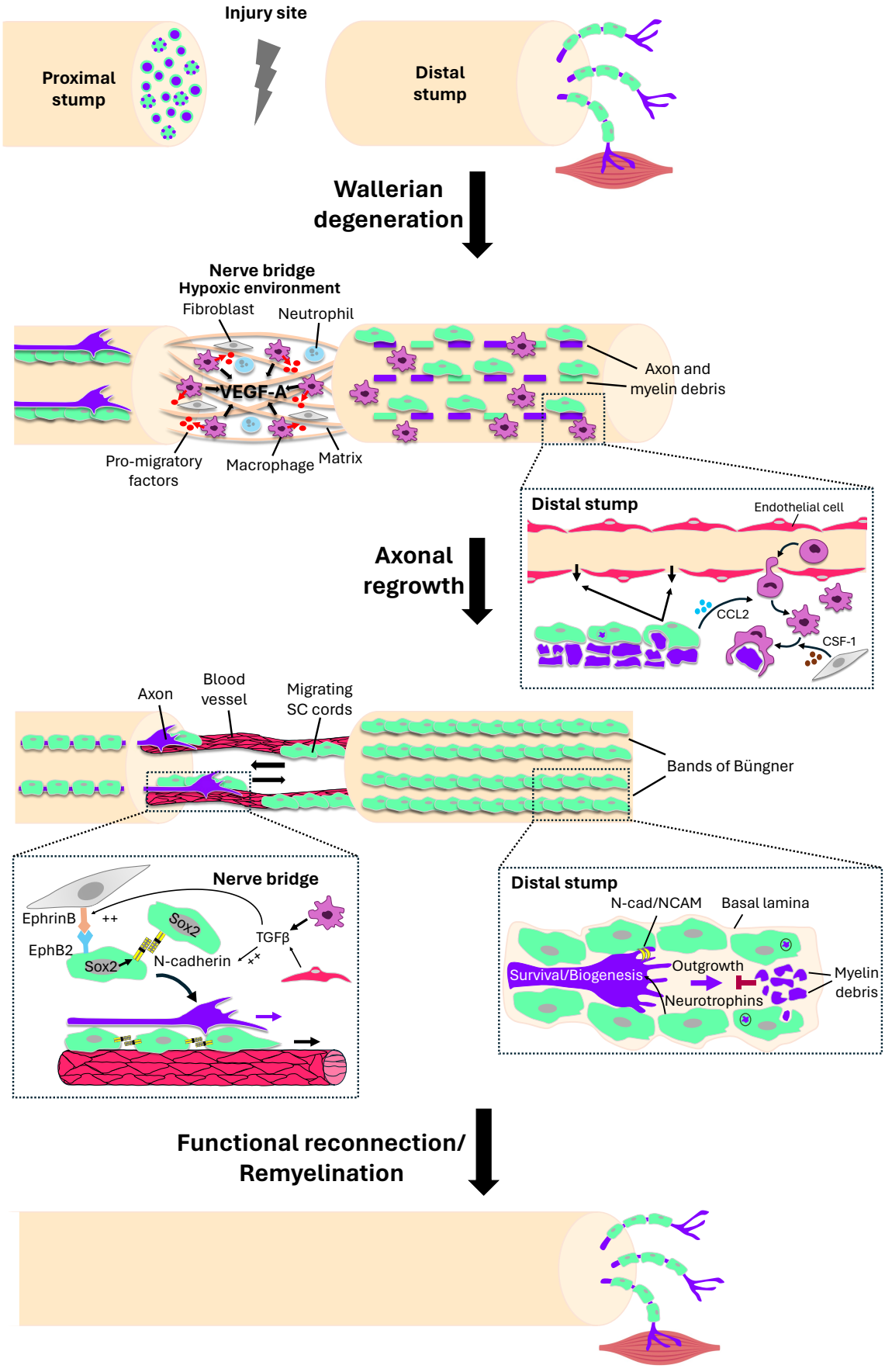
Injury site
Proximal stump
Distal stump
Wallerian degeneration
Nerve bridge
Hypoxic environment
Fibroblast
Neutrophil
VEGF-A
Axon and myelin debris
Pro-migratory factors
Macrophage
Matrix
Distal stump
Endothelial cell
CCL2
CSF-1
Axonal regrowth
Axon
Blood vessel
Migrating SC cords
Bands of Büngner
Nerve bridge
EphrinB
++
EphB2
Sox2
Sox2
TGFβ
N-cadherin
Distal stump
N-cad/NCAM
Basal lamina
Survival/Biogenesis
Outgrowth
Neurotrophins
Myelin debris
Functional reconnection/ Remyelination

Figure 9. Overview of the stages of peripheral nerve regeneration after lesion. Representation of SC response occuring after injury in both the nerve bridge and the distal stump, as well as the interactions between repair SCs and the nerve microenvironment until functional reconnection and SC remyelination. CCL2, C-C motif chemokine ligand 2 ; CFS-1, Colony stimulating factor 1 ; EphB2, Ephrin B2 receptor ; N-cad, N-cadherin ; NCAM, Neural cell adhesion molecule ; Sox2, SRY (sex determining region Y) box 2 ; TGFβ, Transforming growth factor beta ; VEGF-A, Vascular endothelial growth factor A. (*Modified and adapted from Cattin and Llyod, 2016*).

1.4.3 The special role of c-Jun

c-Jun expression is absent in SCPs, upregulated in iSCs but downregulated during postnatal development. Low c-Jun levels are detectable in both Remak and adult myelinating SCs of uninjured nerves. Despite being upregulated in iSCs (Jessen and Mirsky, 2008), c-Jun has not been shown to be essential for SC development and myelin maintenance. However, c-Jun levels are rapidly and extensively increased after nerve injury with an 8-to-10-fold increase at the mRNA level and an increase of up to 40-fold at the protein level (Norrmén et al., 2018). In this condition, c-Jun has been shown to be of paramount importance for successful axonal regeneration and functional recovery after lesion. Indeed, the absence of c-Jun specifically in SCs impedes both SC conversion into repair SCs and the downregulation of myelin proteins. c-Jun upregulation occurs already a few hours after lesion and is required for the suppression of *P0*, *Mbp* and *Krox20* expression. Of note, a cross-inhibitory relationship exists between c-Jun and Krox20 (Parkinson et al., 2008). In mice lacking c-Jun specifically in SCs, SCs distal to the injury fail to upregulate the expression of neurotrophic factors, leading to substantial neuronal death. SCs also fail to activate the myelinophagy program and do not adopt the typical narrow and rod-like morphology of normal repair SCs, leading to structural disorganization of the regeneration tracks (Arthur-Farraj et al., 2012). However, the absence of c-Jun does not totally inactivate the immune response. Macrophage invasion is reduced at the injury site, but cytokine expression normally takes place and macrophages number is not much

affected in the distal stump. Other pathways than c-Jun trigger the immune response after injury. Among them, the extracellular signal-regulated protein kinases 1 and 2 (ERK1/2)-mitogen-activated protein kinase (MAPK) signaling pathways is activated after injury and has been shown to activate the expression of the macrophage attractive molecule MCP-1 (Fischer et al., 2008). Other MAPK signaling pathways such as p38 and JNK have also been shown to promote SC conversion into the repair phenotype and the Notch signaling pathway accelerates SC demyelination, even in the absence of lesion (Boerboom et al., 2017; Woodhoo et al., 2009). A still opened and unanswered question is what triggers c-Jun expression after injury. This question can be partially answered by the study of Norrmén et al (2018), in which they showed that mTORC1 is transiently and robustly reactivated after injury in repair SCs and is necessary for prompt myelin clearance, SC conversion into the repair phenotype and accurate remyelination by promoting timely c-Jun upregulation at the transcriptional but also post-transcriptional levels by increasing c-Jun translation rate.

Interestingly, c-Jun is also upregulated, however to a lesser extent, in SCs in different neuropathic conditions and rather has a neuroprotective role. For example, in a mouse model of Charcot-Marie-Tooth disease type 1A (CMT1A), downregulating c-Jun expression results in distal sensory axonopathy and deterioration of the sensory-motor performance. These observations indicate that a moderate c-Jun elevation is compatible with SC differentiation and does not trigger demyelination. Indeed, mice overexpressing 5 to 8-fold c-Jun specifically in SCs have normal myelin sheath and no impairment of sensory-motor function (Hantke et al., 2014; Jessen and Mirsky 2016; Jessen and Mirsky, 2022; Klein et al., 2014).

1.4.4 Chromatin remodeling enzyme and histone modifier functions during peripheral nerve regeneration

In the context of peripheral nerve injury, SCs are profoundly reprogrammed and are characterized by the downregulation of pro-myelinating factors as well as the upregulation of different transcription factors and molecules providing repair-supportive capacities to SCs. SCs react dynamically to environmental cues by rapidly changing their expression profile and identity. This complex and massive change in gene expression not only involves transcriptional pathways but is also tightly controlled at the chromatin level by epigenomic pathways, whose functions in PNS and CNS development, injuries and diseases have recently gained more and more interest (reviewed in Duman et Martinez-Moreno, 2020; Gomez-Sanchez et al., 2022; Hertzog and Jacob, 2023; Lu et al., 2019; Shukla and Tekwani, 2020). The functions of the chromatin remodeling complexes and miRNAs in repair SCs are illustrated in Figure 10. Their functions during SC remyelination will be described in section 1.6.

1.4.4.1 Chromatin remodeling enzymes

After injury, the promoter of injury-induced genes loses the repressive histone mark H3K27me3 and acquires the active promoter mark H3K4me3. The trimethylation of H3K27 is catalyzed by the polycomb repressive complex 2 (PRC2) and inactivation of PRC2 in sciatic nerves leads to premature and increased activation of repair genes (Ma et al., 2015). Additionally, more than 4000 injury-induced enhancers acquire the active enhancer mark H3K27ac, whereas H3K27 is deacetylated at enhancers of positive regulators of myelination. Moreover, enhancers of injury genes are enriched in c-Jun binding motifs. Altogether, the demethylation of H3K27, the trimethylation of H3K4 and the deacetylation of H3K27 lead to the expression of repair genes such as *Shh*

and *Gdnf*, thereby promoting axonal regrowth (Hung et al., 2015; Ma et al., 2015; Ma and Svaren, 2016).

In the acute phase of injury, the SUMOylated form of HDAC2 recruits Sox10 and two H3K9 demethylases, JMJD2C and KDM3A, to de-repress and activate *Oct6* SCE, resulting in Oct6 expression. Oct6 is transiently expressed during myelination and is known to promote timely expression of the pro-myelinating factor Krox20 (Jeagle et al., 1996; Ryu et al., 2007). The expression of Oct6 early after injury prevents c-Jun upregulation and thus delays SC conversion into repair SCs and axonal regrowth (Brügger et al., 2017). At a later stage, repair SCs upregulate the H3K27me3 demethylase JMJD3, which demethylates the *p19Arf* and *p16Ink4a* promoters, leading to the activation of the *Ink4a/Arf* locus that prevent SC overproliferation and potentially tumor formation (Gomez-Sanchez et al., 2013).

1.4.4.2. MicroRNAs

Regulation of gene transcription can also occur through non-coding RNAs. Among them, miRNAs repress gene expression post-transcriptionally by binding to the 3´-UTRs of their target genes and promote mRNA degradation or inhibition of protein translation (O´Brien et al.,2018).

The role of microRNAs (miRNAs) during SC development is already well established and several miRNAs are under the control of Sox10 (Bremer et al., 2010; Gokey et al., 2012; Pereira et al., 2010). The relevance of miRNAs for SC response to peripheral nerve injury has also been highlighted (Adilakshmi et al., 2012; Gokey et al., 2012).

Indeed, several miRNAs have been shown to control either the positive or the negative regulators of myelination. For example, miR-138 and miR-79 bind to *c-*

Jun and *Sox2* promoter and promote c-Jun and Sox2 expression after injury (Adilakshmi et al., 2012). Interestingly, Arthur-Farray et al. found that c-Jun regulates the expression of several miRNAs in repair SCs. Indeed, after injury, miR-21 and miR-34 are expressed at lower levels in c-Jun-null nerves compared to control nerves, whereas miR-96, miR-124, miR-183 and miR-204 are expressed at higher levels in c-Jun-null nerves. However, the functions of the latter miRNAs in SCs after injury are still unknown. This study also identified several differentially expressed long-noncoding RNAs (lncRNAs) in repair SCs, whose functions still need to be defined (Arthur-Farray et al., 2017). miRNA binding sites have been identified on *Krox20* MSE, whose expression is totally inhibited at 48 hours post injury (hpl) (Adilakshmi et al., 2012). miRNAs have also been shown to regulate chromatin accessibility by forming epigenetic silencing complexes (Morris et al., 2004). In repair SCs, miR-709 forms a silencing complex together with AGO-1 on the *Krox20* MSE at regions enriched in the repressing histone mark H3K27me3 (Adilakshmi et al., 2012). Lastly, Martinez-Moreno et al. identified a lncRNA antisense to the promoter of *Krox20* (Erg2-AS-RNA), whose expression increases during the first 12 hpl and is part of a chromatin remodeling complex acting on *Krox20* promoter. Indeed, Erg2-AS-RNA sequentially recruits AGO1, AGO2 and the methyltransferase EZH2 at 48 hpl, leading to trimethylation of H3K27 and *Krox20* silencing (Martinez-Moreno et al., 2017).

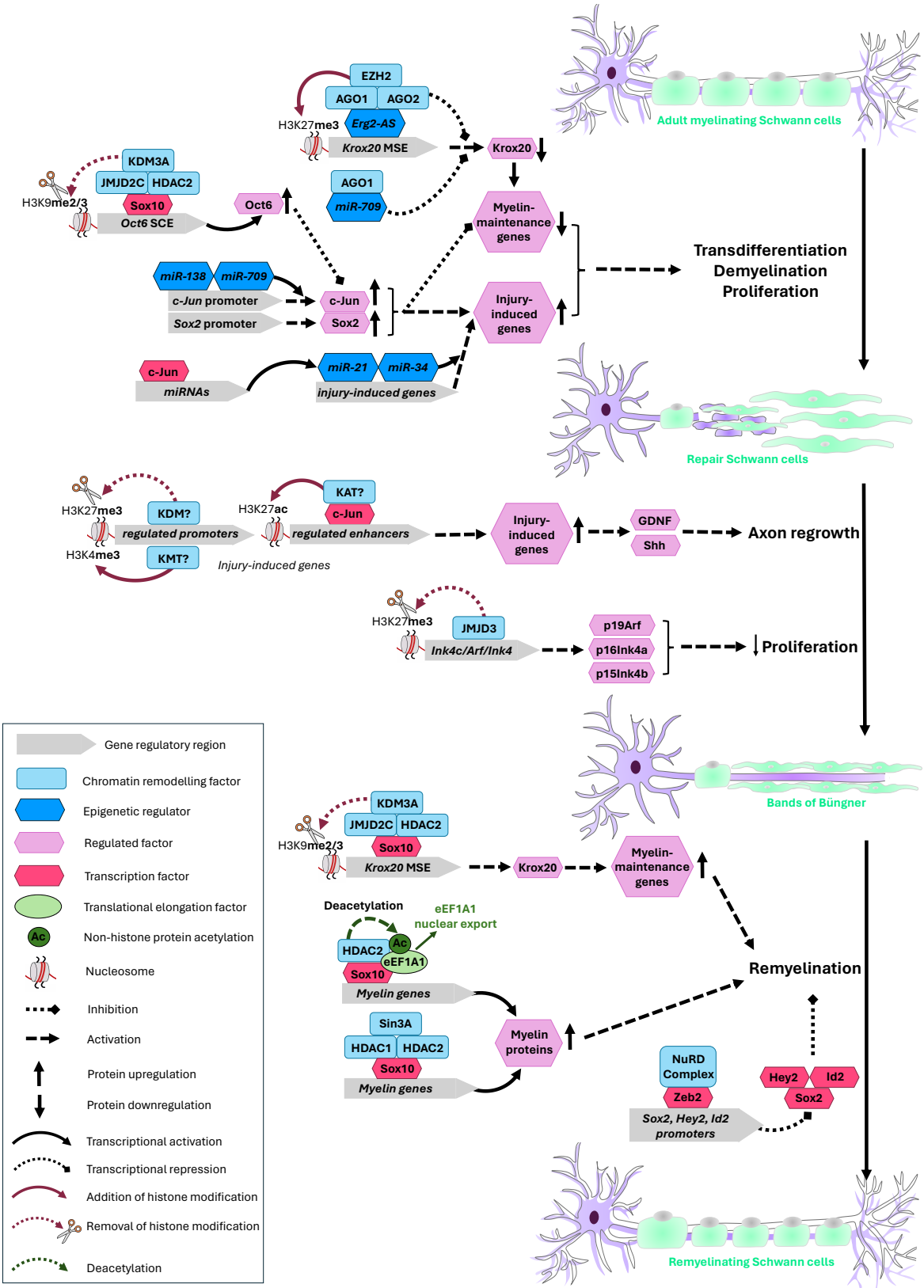
EZH2
AGO1
AGO2
H3K27me3
Erg2-AS
Krox20 MSE
Krox20
Adult myelinating Schwann cells
KDM3A
JMJD2C
HDAC2
H3K9me2/3
Sox10
Oct6 SCE
Oct6
AGO1
miR-709
Myelin-maintenance genes
Transdifferentiation
Demyelination
Proliferation
miR-138
miR-709
c-Jun promoter
Sox2 promoter
c-Jun
Sox2
Injury-induced genes
c-Jun
miRNAs
miR-21
miR-34
injury-induced genes
Repair Schwann cells
H3K27me3
KDM?
H3K4me3
KMT?
regulated promoters
H3K27ac
KAT?
c-Jun
regulated enhancers
Injury-induced genes
Injury-induced genes
GDNF
Shh
Axon regrowth
H3K27me3
JMJD3
Ink4c/Arf/Ink4
p19Arf
p16Ink4a
p15Ink4b
Proliferation
Bands of Büngner
KDM3A
JMJD2C
HDAC2
H3K9me2/3
Sox10
Krox20 MSE
Krox20
Myelin-maintenance genes
Deacetylation
eEF1A1
nuclear export
HDAC2
Ac
eEF1A1
Sox10
Myelin genes
Remyelination
Sin3A
HDAC1
HDAC2
Sox10
Myelin genes
Myelin proteins
NuRD Complex
Zeb2
Sox2, Hey2, Id2 promoters
Hey2
Id2
Sox2
Remyelinating Schwann cells
Gene regulatory region
Chromatin remodelling factor
Epigenetic regulator
Regulated factor
Transcription factor
Translational elongation factor
Ac
Non-histone protein acetylation
Nucleosome
Inhibition
Activation
Protein upregulation
Protein downregulation
Transcriptional activation
Transcriptional repression
Addition of histone modification
Removal of histone modification
Deacetylation

Figure 10. Histone modifications and histone modifiers in SCs after lesion. Schematic representation of chromatin-remodeling enzymes and associated mechanisms regulating SC conversion into repair SCs and SC remyelination. ac, acetyl group ; AGO1, Argonaute protein 1; AGO2, Argonaute protein 2; Arf, ADP-ribosylation factor; c-Jun, c-Jun proto-oncogene; eEF1A1, eukaryotic elongation factor 1 alpha 1; Erg2-AS, non-coding RNA antisense to the promoter of Egr2; GDNF, Glial cell line-derived neurotrophic factor; HDAC1, histone deacetylase 1; HDAC2, histone deacetylase 2; Hey2, Hairy/enhancer-of-split related with YRPW motif protein 2; Id2, DNA binding protein inhibitor 2; IGFBP2, Insulin-like growth factor binding protein 2; Ink4, inhibitor of cyclin-dependent kinase 4; Ink4c, inhibitor of cyclin-dependent kinase 4c; JMJD2C, Jumonji C domain-containing protein D2C; JMJD3, Jumonji C domain-containing protein D3; KAT, histone acetyltransferase; KDM, histone demethylase; KMT, histone methyltransferase; Krox20, early growth response 2; me, methyl group; MSE, myelinating SC element; miR, microRNA; NuRD, Nucleosome remodeling and deacetylase; Oct6, Octamer-binding transcription factor 6; P0, Myelin protein zero; p15Ink4b, cyclin-dependent kinase 4 inhibitor B; p16Ink4a, cyclin-dependent kinase inhibitor 2 A; p19Arf, tumor suppressor ARF; SCE, SC specific enhancer; Shh, Sonic hedgehog; Sin3a, suppressor interacting 3a; Sox2, SRY (sex determining region Y) box 2; Sox10, SRY (sex determining region Y) box 10; Zeb2, Zinc finger E-box-binding homoebox 2 (*Modified and adapted from Duman et al., 2020 ; Duman and Martinez-Moreno, 2020 ; Jacob, 2017 ; Zhang et al., 2022)*.

1.5 Maintenance of the repair phenotype

Maintenance and survival of repair SCs are a prerequisite for a successful nerve regeneration. Unfortunately, the regeneration capacity fades with age and in the context of chronic nerve injury. This problematic is relevant for the regeneration failure occurring in larger mammals and in humans since the longer the distal SCs remain without axonal contact, the more they lose their repair-supportive capacities, together with a large-scale SC death (Höke et al., 2006; Sulaiman and Gordon, 2009). Indeed, the lesion can be localized very proximally, thus requiring axons to grow over a very long distance at a relatively low speed. Therefore, deciphering the mechanisms behind the phenotypic instability of the repair SCs will improve the clinical outcome of both the young and the elderly population after nerve damage. Interestingly, the decrease in the regenerative capacity is not due to age-dependent changes in neurons, as no difference in the intrinsic growth capacity of neurons has been found in aged animals compared to young animals (Kang and Lichtman, 2013; Painter et al., 2014). Rather, it is restrained by SCs, which fail to activate the repair phenotype

rapidly and successfully (Painter et al., 2014, 2017). Consequently, the aged PNS shows delayed axonal degeneration and myelin clearance defect after injury. Indeed, aged axons extend as fast as young axons but must slow down and navigate around a lot of remaining myelin debris, thereby affecting the speed of axonal regeneration (Kang and Lichtman, 2013). Furthermore, aged repair SCs secrete less growth factors and immunomodulating cytokines, leading to macrophage recruitment delay (Painter et al., 2014; Scheib and Höke, 2016). The work of Scheib and Höke also pointed to alterations of the phagocytic activity of both aged repair SCs and macrophages as well as an overall altered immune response in aged animals after lesion. While young animals upregulate both pro- and anti-inflammatory cytokines, aged animals show muted cytokine responses (Scheib and Höke, 2016). The presence of debris within the nerve impairs axonal migration and it has been found that the poorer regeneration in aging animals is in part due to the inefficient debris clearance resulting from the inefficient SC reprogramming after lesion (Kang and Lichtman, 2013). Interestingly, the microenvironment of uninjured old sciatic nerve is pro-inflammatory. Indeed, transcriptome analysis of SCs revealed higher expression of genes involved in SC conversion into repair SCs and higher expression of macrophages markers, together with reduced levels of myelination-associated genes in old animals compared to young animals. In old animals, an overshooting and persisting macrophage infiltration occurs in later phases of regeneration after lesion together with a higher and prolonged cytokine expression compared to young animals. Treating mice with low doses of acetylsalicylic acid (ASA) downregulated cytokines levels, reduced macrophages number and improved remyelination (Büttner et al., 2018). In the context of chronic denervation, distal nerves gradually lose their repair supportive capacity due to death of chronically denervated SCs as well as the loss of SC repair-supportive features over time

(Benito et al., 2017; Wagstaff et al., 2021). Besides the deregulated immune response in aged animals, regeneration inefficiency can also be explained by the reduced c-Jun activation in aged animals, which never reaches the levels observed in young animals after lesion. Indeed, in aged animals, c-Jun activation is delayed, whereas it occurs already within the first 24 hours after lesion in young animals. In addition, many c-Jun-controlled genes are deregulated in aged animals, suggesting defects in the transcriptional machinery (Painter et al., 2014, 2017; Wagstaff et al., 2021). During long-term denervation, c-Jun levels fail to be maintained, irrespective of age. Restoring c-Jun levels to similar levels as in young animals after lesion is sufficient to restore efficient nerve regeneration in aged mice as well as in the context of chronic denervation (Wagstaff et al., 2021). Similarly to rodents, c-Jun and $p75^{NTR}$ levels are also upregulated in human SCs after lesion and decline during long-term denervation, demonstrating that chronic denervation in humans also results in a deterioration of repair SC functions (Wilcox et al., 2020). Interestingly, Sonic Hedgehog (Shh) expression is strongly upregulated in SCs only after injury and mice lacking Shh in SCs show decreased c-Jun and phospho-c-Jun levels. The Shh-dependent enhancement of c-Jun after injury is likely to be mediated by an autocrine Shh signaling loop, as SCs are the major source of Shh in nerves. Indeed, blocking the cellular response to Shh results in decreased c-Jun and phospho-c-Jun levels. Therefore, the failure of maintaining high c-Jun levels in aged mice or during chronic injury may be due to the failure of SCs to establish or maintain the autocrine Shh signaling loop (Arthur-Farraj et al., 2012; Lin et al., 2015; Wagstaff et al., 2021). In addition to c-Jun, STAT3 is the second transcription factor in SCs with selective functions only in SCs of injured nerves. Like c-Jun, STAT3 is not required for SC development and myelination. However, STAT3 is required for both short- and long-term SC survival as well as for the

maintenance of the repair SC phenotype after injury. Indeed, levels of the key repair SC markers c-Jun, Olig1, and Shh as well as the axonal growth-promoting factors GDNF and BDNF are reduced in STAT3cKO mice at 8 weeks post injury compared to control animals, whereas short-term denervated cells and functional recovery are normal in STAT3cKO mice. Thus, in contrast to c-Jun, STAT3 is not essential for the acquisition of the repair phenotype early after lesion. However, STAT3 is required for a functional autocrine survival signaling in denervated SCs and the defective autocrine survival loop observed in STAT3cKO SCs contributes to the loss of SCs during chronic denervation (Benito et al., 2017). Altogether, these findings suggest that targeting the SC autocrine-survival loop, c-Jun, STAT3 as well as modulating the immune response could help improving functional recovery in both young and old individuals after a severe nerve injury.

1.6 Schwann cell remyelination

Although the molecular mechanisms of myelination have been extensively investigated, the remyelination process is less documented and differs to some extent to the myelination process. Indeed, remyelination occurs faster than myelin formation during development and the myelin sheath is thinner after lesion (Strassart et al., 2018). In addition, while some factors are only required during developmental myelination, others are only required for axon remyelination. The molecular mechanisms of factors implicated in both processes have mostly been studied during development. However, their functions and mechanisms may differ during remyelination. Despite these differences, some molecular programs remain unchanged between developmental myelination and remyelination, as exemplified by the expression

pattern of Sox10, Oct6, Krox20 or Zeb2 and subsequent transcriptional activation of myelin genes (reviewed in Jacob, 2017; Sock and Wegner, 2019)

1.6.1 Transmembrane proteins, proteases, and secretases

The communication between axons and SCs is critical for SC differentiation during development and for myelin maintenance, as axons provide signals for SCs to differentiate. In addition, axo-glia communication is critical for nerve repair. Indeed, the correct re-establishment of axon-SC contact allows repair SCs to re-differentiate and remyelinate axons (Strassart and Woodhoo, 2021).

One of the most studied transmembrane molecules so far during SC development and regeneration is Neuregulin-1(NRG1). NGR1 belongs to the epidermal growth factor (EGF)-like growth factors and bind to the ERBB tyrosine kinase receptors on SCs. This interaction activates several signal transduction pathways like PI3K-Akt, MEK/ERK and Calcineurin, which modulate the activation of pro-myelinating factors and thus myelin gene transcription. NRG1 exists in different isoforms, including NRG1-type I and NRG1-type III, which have been detected in the PNS. NRG1-type III is expressed on PNS axons and is required for SC proliferation and differentiation. Later, NRG1-type III regulates the myelination fate of SCs as well as myelin thickness (reviewed in Nave and Salzer, 2006). Axonal NRG1 has been shown to regulate the rate of axonal regeneration and remyelination. Indeed, genetic ablation of NRG1 in axons leads to severe hypomyelination and slower axonal regrowth two months after injury. However, while remyelination is almost absent until 8 weeks post lesion, axons are fully remyelinated after 12 weeks. In contrast to its function during development, NRG1 does not determine the myelinating fate of axons after lesion, indicating that NRG1 may control developmental myelination and

remyelination in a different manner. Indeed, while the developmental phenotype of a lack of NRG1 is not compensated, axonal remyelination occurs after lesion in mice in which NRG1 has been ablated in the adulthood (Fricker et al., 2011, 2013). However, in the two studies both NRG1-type I and III were ablated. Thus, the specific role of each isoform during remyelination cannot be precisely determined. In contrast, Strassart et al. observed complete remyelination in mice overexpressing either NRG1-type I or NRG1-type III. In addition, these findings indicate that while axonal NRG1-type III regulates both developmental myelination and remyelination, axonal NRG1-type I acts only during remyelination. Indeed, NRG1-type I is not required during development, as axons of mice overexpressing NRG1-type I do not show myelination defects (Michailov et al., 2004; Strassart et al., 2013). Interestingly, Strassart et al. found that NRG1-type I mRNA is upregulated in SCs 24h after injury and during the first two weeks after injury, when SCs start to re-differentiate and remyelinate axons. In vitro and in vivo experiments demonstrated that axonal NRG1-type III signalling to SCs via the ERBB receptor and subsequent ERK1/2 pathway repress NRG-1 type I expression in myelinating SCs. After lesion, when SCs loose contact with axons, NRG1-type I is re-expressed by SCs and acts in an autocrine or paracrine way on SCs to promote remyelination and functional recovery by inducing Krox20 expression. Consistently, remyelination in mice lacking NRG1-type I in SCs is strongly impaired. Furthermore, overexpressing axonal NRG1-type I in these mice did not improve remyelination. These results indicate that SC-derived NRG1-type I drives remyelination until they regain axonal contact and SC-derived NRG1-type I cannot be substituted by axonal NRG1-type I. Finally, mice lacking NRG1-type I in embryonic SCs do not show myelination defects, indicating that SC-derived NRG1-type I is not required for developmental myelination (Stassart et al., 2013).

These findings make NRG-1 a very interesting target to improve remyelination. Indeed, administration of NRG1-type III and type I enhanced nerve regeneration and modulation of NRG1 activity or expression has shown very promising results in animal models of CMT1A and CMT1B (Fledrich et al., 2014; Scapin et al., 2019).

During development, NRG1-type III activity is modulated by extracellular cleavage regulated by secretases localized in axons. While B-amyloid precursor protein-cleaving enzyme 1 (BACE1) cleaves and activates NRG1-type III and enhances myelination, A Disintegrin and Metalloprotease 17 (ADAM17) inhibits NRG1 activity and impairs myelination (reviewed in Pellegatta and Taveggia, 2019). BACE1 is expressed by motor and sensory DRG neurons and regulates the myelination process and myelin sheath thickness during PNS development. BACE1 also affects remyelination, as the ablation of BACE1 delays but does not prevent remyelination (Hu et al., 2006, 2008). Interestingly, SC and axonal BACE1 are highly expressed after injury and are both required for optimal remyelination. Moreover, since NRG1-type I and BACE1 are expressed in SCs after nerve injury, it is possible that BACE1 promotes remyelination by cleaving NRG1-type I, thereby releasing the soluble form of NRG1-type I to produce the autocrine signalling. Of note, both NRG1-type I and III bear BACE1 cleavage sites (Hu et al., 2008, 2015). Furthermore, while dispensable for myelin development, ADAM19 acts as a timer for axon remyelination by activating Krox20 expression in SCs via the PI3K-Akt pathway, thereby promoting SC redifferentiation (Wakatsuki et al., 2009). Indeed, mice lacking ADAM19 show fewer remyelinated axons and thinner myelin sheaths. These observations make BACE1 and ADAM19 interesting candidates to modulate NRG1 activity and improve remyelination, both after injury and in the context of inherited peripheral neuropathies.

Another interesting transmembrane receptor for peripheral nerve remyelination is the transmembrane receptor $p75^{NTR}$, which regulates fibrinolysis after nerve injury. After lesion, fibrin accumulates in the nerve and triggers SC de-differentiation. Simultaneously, $p75^{NTR}$ is induced and downregulates myelin genes via ERK1/2 phosphorylation. Later, tissue plasminogen activator (tPA) promotes fibrin clearance by activating plasmin. However, p75NTR downregulates tPA and blocks fibrin degradation (Akassoglou et al., 2002; Sachs et al., 2007; Tomita et al., 2007). Recently, Pellegatta et al., found that the absence of ADAM17 in SCs impairs fibrinolysis and remyelination after lesion by accumulation of unprocessed p75NTR and subsequent downregulation of tPA expression. In this study, the authors discovered a new function for ADAM17 as well as a different molecular mechanism. Indeed, in contrast to its function during remyelination, ADAM17 regulates developmental myelination by modulating the NRG1-ErbB axis. Furthermore, while ADAM17 acts as a negative regulator of myelination, it acts as a positive regulator of remyelination (Pellegatta et al., 2022).

Lastly, the G protein-coupled receptor Gpr126 has been shown to be crucial for initiation of SC myelination, axon regeneration and remyelination. Grp126 signals by the second messenger cAMP and induces Oct6 expression. Indeed, SCs lacking Grp126 do not express Oct6 and Krox20 and are arrested at the pro-myelinating stage. However, the ligand activating Grp126 remains unknown. Consistent with its crucial role in developmental myelination, the ablation of Grp126 in SCs of adult mice severely impairs remyelination after sciatic nerve crush injury. In addition, Grp126 is also needed for chemokine secretion by SCs and subsequent macrophage recruitment, for myelin clearance and axonal regrowth. These findings highlight distinct roles for Grp126 in SCs after nerve damage. While Grp126 is needed autonomously in SCs for proper remyelination,

it acts in a non-autonomous way for myelin clearance and axon regeneration. It would be interesting to know whether Grp126 functions in nerve regeneration also require cAMP elevation (Mogha et al., 2013, 2016; Monk et al., 2009, 2011).

1.6.2 Transcription factors

Remyelination of regenerated axons requires the redifferentiation of repair SCs and thus the downregulation of negative regulators of myelination and the upregulation of positive regulators of myelination, as observed during developmental myelination (Jessen and Mirsky, 2016).

Two major negative regulators of myelination are c-Jun and Sox2. c-Jun expression is low during SC development and myelin maintenance and is not required in both processes. In contrast, it is highly expressed after injury. c-Jun is considered as the key transcription factor controlling SC reprogramming into repair SCs and is both necessary and sufficient for the establishment of a regeneration-supportive environment. Indeed, c-Jun regulates the expression of several genes implicated in the regeneration process. In addition, c-Jun is necessary for neuron survival, axonal regrowth, repair SC morphology and the structure of the regeneration tracks (Arthur-Farraj et al., 2012; Fontana et al., 2012; Parkinson et al., 2008). In support with a negative function of c-Jun on myelination is the cross-inhibitory relationship between c-Jun and Krox20 (Parkinson et al., 2008). Consistently, remyelination in mice mildly overexpressing c-Jun in SCs (c-Jun$^{OE/-}$) is delayed to two weeks after injury together with a transient decreased in Krox20 levels. By 10 weeks after injury, axon myelination was similar to control animals, but with a thinner myelin sheath. In c-Jun$^{OE/-}$ mice, developmental myelination is also delayed, and adult nerves present a thinner myelin sheath than control animals. In contrast, in

adult nerves of mice highly overexpressing c-Jun (c-Jun $^{OE/OE}$), myelination is inhibited, and nerves are severely hypomyelinated. These observations indicate that c-Jun exerts its effects on myelination in a dose-dependent manner (Fazal et al, 2017). Recently, Kim et al. showed that c-Jun O-linked N-acetylglucosaminylation (O-GlcNAc) at multiple sites reduces c-Jun transcriptional activity and promotes remyelination after lesion. Indeed, in mice lacking O-GlcNAc transferase in SCs (OGT-SCKO), c-Jun levels and activity are constantly elevated and SCs failed to timely downregulate the injury program, thus preventing SCs redifferentiation and remyelination. c-Jun activity depends on its phosphorylation levels and c-Jun also regulates its own transcription (Angel et al., 1988; Shaulian and Karin, 2001). The authors found that O-GlcNAc decreases c-Jun activity and transcriptional activity by interfering with c-Jun phosphorylation (Kim et al., 2018). Furthermore, while SC myelination is not affected during development in the OGT-SCKO, myelin maintenance is defective and leads to demyelinating neuropathy (Kim et al., 2016).

The high mobility group (HMG) domain transcription factor Sox2 has also been shown to repress Krox20 expression and axon myelination in SCs/DRG co-culture and impairs myelination in vivo (Le et al., 2005; Roberts et al., 2017). Indeed, mice with persistent Sox2 expression in SCs show a hypomyelinating phenotype, increased number of unmyelinated axons and reduced levels of Krox20 and myelin proteins, resulting in impairment of sensory-motor function. Although Sox2 is important for the formation of SC regeneration cords and thus for correct axon pathfinding after nerve transection, a prolonged Sox2 expression after lesion leads to hypomyelination, reduced number of remyelinated axons, decreased P0 levels and poor functional recovery (Parinello et al., 2010; Roberts et al., 2017).

The expression of myelin inhibitors is timely controlled by the transcription factor Zeb2, both in myelinating SCs and during remyelination. Zeb2 has been found to downregulate the expression of *Hey2*, a downstream effector of Notch signalling pathway, endothelin receptor B (*Ednrb*) and *Sox2* (Quintes et al., 2016; Wu et al., 2016). Moreover, Zeb2 silences the expression of these genes by recruiting the HDAC1/2-NuRD complex on their promoters (Wu et al., 2016). Indeed, genetic ablation of Zeb2 in SCs results in persistent elevation of Hey2, EDNRB and Sox2 levels together with a low expression of the promyelinating factors Sox10, Oct6 and Krox20, and SCs of Zeb2-deficient mice are arrested at the immature stage. Consequently, animals show axonal sorting failure, myelination defects and motor deficits. Zeb2 is also required for SC redifferentiation after lesion. Indeed, in conditionally inducible Zeb2 KO mice (Zeb2KO), Krox20 levels fail to be upregulated, while Sox2, Id2 and Hey5 levels remain high, even beyond four weeks post injury. Therefore, only a few axons of Zeb2KO mice are remyelinated, and functional recovery is severely impaired. However, the early steps of SC reprogramming are not affected by the absence of Zeb2, and c-Jun levels remain unaffected in Zeb2KO mice during developmental myelination and after lesion. Thus, Zeb2 is required for repair SCs to re-differentiate and remyelinate axons after lesion by timely repressing myelination inhibitors. Taken together, the results of both studies indicate that Zeb2 may represent a secondary inhibitory axis, working in concert with transcriptional activators for the activation of the myelination program (Brinkmann and Quintes, 2017; Quintes et al., 2016; Wu et al., 2016).

Recent studies also highlighted the two paralogous effectors of the Hippo pathways YAP and TAZ as important factors for SC remyelination after lesion (Grove et al., 2020; Jeanette et al., 2021). In myelinating developing SCs, YAP and TAZ recruit TEAD1 on regulatory regions of promyelinating genes in concert

with Sox10, and SCs lacking both YAP and TAZ fail to myelinate axons (Deng et al, 2017; Grove et al., 2017; Poitelon et al., 2016). Moreover, the lack of YAP and TAZ in SCs leads to failure of SC redifferentiation and remyelination after lesion and to impaired functional recovery in conditional inducible YAP/TAZ knock-out mice (YAP/TAZ iDKO) (Grove et al., 2020; Jeanette et al., 2021). While YAP/TAZ are not required for SC reprogramming and axonal regrowth, they are required during SC redifferentiation (Grove et al., 2020; Jeanette et al., 2021). Indeed, YAP/TAZ ablation after SC reprogramming also decreases the number of remyelinated axons and myelin thickness and maintains c-Jun expression until 60 days post injury (Jeanette et al., 2021). Since YAP/TAZ regulate Krox20 levels during SC myelination and Krox20 represses c-Jun expression (Deng et al., 2017; Grove et al., 2017; Parkinson et al., 2008), the sustained c-Jun expression in YAP/TAZ KO mice may be explained by the incapacity of YAP/TAZ to upregulate Krox20. These results are also in accordance with the remyelination delay observed in c-Jun$^{OE/-}$ mice (Fazal et al., 2017). In contrast, Grove et al. did not report any change in c-Jun expression in crushed nerves.

After nerve damage, nuclear factor kB (NF-κB) transcription factor is activated by phosphorylation, leading to nuclear localization and gene regulation. Morton et al. found that the nuclear, active form of NF-κB modulates axonal regeneration and remyelination rate after injury. Indeed, the i*n vivo* inactivation of NF-kB results in a delayed axonal remyelination at 4 weeks post injury, which normalizes at 8 weeks post injury. However, the downstream NF-kB target genes in SCs during the regeneration process are still unknown (Morton et al., 2012). While NF-κB activation is required for timely remyelination, its activation is dispensable for developmental myelination (Morton et al., 2013). This contrasts with the crucial role of NF-kB for *in vivo* myelination found by Chen et al. In their

study, the authors showed that HDAC1/2 deacetylate and recruit NF-kB to the *Sox10* promoter and by doing so, induces myelination (Chen et al., 2011).

1.6.3 Chromatin remodeling enzymes

The investigations on epigenetic modifier functions after peripheral nerve injury is a recent and very promising research field. The phenotypic switches occurring in SCs during peripheral nerve regeneration and remyelination requires a fine-tuned regulation of gene transcription, which is provided by epigenetic regulation and chromatin remodeling complexes. Among those, histone deacetylases have been extensively studied. These enzymes can also deacetylate non-histone targets such as transcription factors or function as a protein bridge to recruit other chromatin remodeling enzymes (Seto and Yoshida, 2014). Some members of the HDAC family can functionally compensate, and therefore double (in the case of HDAC1 and HDAC2) and triple (in the case of HDAC4, 5 and 7) ablations have been used in the studies presented below (Gomis Colona et al., 2018; Jacob et al., 2011; Velasco-Aviles, Patel et al., 2022).

The two class I HDACs HDAC1 and HDAC2 (HDAC1/2) control SC specification, myelination, survival, and myelin maintenance (Brügger et al., 2015; Chen et al., 2011; Jacob et al., 2014; Jacob et al., 2011). In postnatal SCs, Sox10 recruits HDAC1/2 to regulatory regions of *Sox10*, *Krox20* and *P0* genes and deletion of HDAC1/2 in iSCs leads to developmental arrest at the promyelinating stage, followed by SC apoptosis. During regeneration, HDAC2 is sequentially recruited to the *Oct6* SCE and *Krox20* MSE together with Sox10 and two demethylases JMJD2C and KDM3A to derepress and thus activate *Oct6* and *Krox20* expression, respectively. While activation of *Oct6* expression early after lesion impedes early

c-Jun upregulation and thus delays SC conversion into repair SCs, and slows down axonal regrowth, the activation of *Oct6* and *Krox20* expression at a later stage after lesion promotes remyelination. Consistently, ablation of HDAC1/2 in SCs improves axonal regeneration but impairs remyelination. Interestingly however, a 3-day short-term treatment with an HDAC1/2 inhibitor early after lesion does not impair remyelination and promotes functional recovery (Brügger et al., 2017). Recently, Duman et al. (2020) identified eEF1A1 as the HDAC2 deacetylation target allowing the formation of the HDAC2/Sox10 remyelination complex. The authors found that the acetylated form of eEF1A1 translocates to the nucleus and drags Sox10 out of the nucleus to target it to proteasomal degradation. Therefore, by deacetylating eEF1A1, HDAC2 prevents the cytoplasmic relocalization of Sox10 and its degradation. Consistently, a short treatment with the HDAC2 activator theophylline just before the start of remyelination leads to increased Sox10 levels and to increased activation of its target genes, increased myelin thickness and improved sensory and motor function recovery (Duman et al., 2020). Importantly, the myelin sheath of mice treated with theophylline after injury has a similar thickness than the uninjured animal and thus allows full remyelination (Duman et al., 2020).

While HDAC1/2 act positively on the myelination program, the class I histone deacetylase 3 (HDAC3) impairs myelination (He et al., 2018; Rosenberg et al, 2018). Indeed, mice treated with an HDAC3 inhibitor or conditionally lacking HDAC3 in SCs show increased expression of promyelinating factors, myelin genes and myelin thickness during PNS maintenance or after injury. Treatment with and HDAC3 inhibitor also improves sensory-motor recovery in both young and aged mice after lesion (Rosenberg et al, 2018, He et al., 2018). Since regeneration capacity is known to decline with age (Jessen and Mirsky, 2019), these results encourage the use of HDAC3 inhibitors in young and old patients

after injury or in the context of demyelinating diseases. However, starting the treatment already at one day post injury in the study of He et al. (2018) seems contradictory with effects of HDAC3 on remyelination. It would be interesting to start the treatment at a later time point after lesion, when remyelination normally occurs. Two different mechanisms have been proposed to explain HDAC3 function. He et al. found that HDAC3 represses myelination by antagonizing NRG1-PI3K-Akt signalling. Moreover, HDAC3 simultaneously inactivates promyelinating programs and, by recruiting p300, activates myelination inhibitory programs, through activation of the transcription factor TEAD4. Interestingly, two negative regulators of myelination targeted by HDAC3, *Pten* and *Dlg1*, are also inhibitors of PI3K-Akt signalling. This indicates that the repressive effect of HDAC3 on NRG1-PI3K-AKT signalling may be indirect (He et al., 2018). In contrast, Rosenberg et al. propose that HDAC3 allows the switch from the adult biogenic state to the homeostatic state, during which myelin protein synthesis rate decreases to levels needed to maintain myelin sheath innntegrity during adulthood (Rosenberg et al., 2018). Additional studies will be necessary to clarify HDAC3 functions.

The class II histone deacetylases HDAC4, 5 and 7 are also implicated in SC myelination and remyelination. During myelination onset, HDAC4 is phosphorylated, translocates to the nucleus, and represses c-Jun expression by recruiting the NcoR1-HDAC3 complex on the *c-Jun* promoter (Gomis Colona et al., 2018). In the absence of HDAC4/5 and 7 in SCs, remyelination is delayed and reaches normal levels only late after injury. This can be explained by the prolonged c-Jun and c-Jun target genes expression, leading to the incapacity of SCs to redifferentiate on time. Accordingly, the levels of Krox20, myelin proteins and enzymes involved in lipid biosynthesis were decreased when remyelination is normally active in control animals. Furthermore, HDAC4 has been shown to

be enriched on *c-Jun*, *Gdnf*, *Runx2* and *Sox2* promoters. The authors concluded that class II HDACs are needed to repress negative regulators of myelination and activate myelin gene expression. Whether HDAC4 interacting partners during remyelination are the same as during myelination remains to be determined (Velasco-Aviles, Patel et al., 2022).

Recently, the chromatin regulator suppressor interacting 3a (Sin3a) has been found to be essential for SC myelination and myelin regeneration. Sin3a is a scaffold protein that interacts with HDAC complexes and act both as a transcriptional activator or repressor (Kadam and Mittal, 2013). Sin3a follows the same expression pattern as Krox20 after nerve injury, and *in vivo* Sin3a knock-down specifically in SCs decreases myelin protein levels and myelin thickness after lesion. The authors found that Sin3a forms a complex with HDAC1/2 and cooperates with Sox10 to regulate the myelination program (Zhang et al., 2022). The mechanisms of chromatin remodeling enzymes in the context of SC remyelination are summarized in Figure 10.

1.6.4 MicroRNA

In 2011, Viader et al. pointed to the regulatory function of miR-140 for SC remyelination after lesion through regulation of Krox20 levels. Indeed, miR-140 levels are downregulated early after lesion and re-expressed at the pre-injury levels when SCs redifferentiate. The authors found that miR-140 targets *Krox20* 3´-UTR and downregulates Krox20 and myelin protein levels in SCs *in vitro*. Additionally, overexpression of miR-140 in SCs co-cultured with DRG neurons inhibits myelination. It would be very interesting to further investigate the relevance of miR-140 for remyelination *in vivo*, by using mice conditionally lacking miR-140 in SCs (Viader et al, 2011).

Another miRNA, miR-30c, promotes remyelination in injured sciatic nerves. miR-30c expression is downregulated immediately in rat sciatic nerves and gradually increases until 28 days post lesion. Injection of miR-30c agomir early after lesion in injured rat sciatic nerves increases P0 and MAG protein levels and myelin thickness. However, miR-30c agomir was already injected at day 1 and day 7 post injury. As mentioned for HDAC3 inhibitor, injection at day 1 seems too early to promote remyelination. It would be interesting to see the effects on remyelination with a first injection at day 7 and a second one at day 14. *In vitro* microarray analysis in SCs identified several miR-30c candidate target genes, yet the validation of miR-30c direct target genes needs to be experimentally conducted (Yi et al., 2017).

Recently, miR-29a-3p has been found to repress PMP22 expression and delay remyelination after injury. Indeed, injection of miR-29a-3p mimic in rat after injury results in reduced myelin sheath thickness and impairs electrophysiological parameters and functional recovery (Shen et al., 2022). Since PMP22 gene duplication and overexpression cause Charcot-Marie-Tooth disease type 1A (CMT1A), miR-29a-3p may represent a novel therapeutic approach to normalize PMP22 levels in CMT1A patients (Fridman and Saporta, 2021).

2 MATERIAL AND METHODS

2.1 Statistical analyses

For each data set presented, experiments were performed at least three times independently or with at least three animals and p values were calculated in Microsoft Excel (Mac version 16.34) using two-tailed (black asterisks) or one-tailed (gray asterisks) Student's t-tests. P values: *<0.05, **<0.01, ***<0.001, data are presented as mean values ± SEM. For data sets obtained using animals or their tissues, three to seven animals were used per group and tissues of each animal were processed independently. For data sets obtained using cells, three to ten independent experiments were conducted and analyzed. Sample size was determined by the minimal number of animals or individual experiment required to obtain statistically significant results and increased in some cases to improve confidence in the results obtained. No animal or data point was excluded from the analysis.

2.2 Animals

2.2.1 Mouse strains

To identify HDAC8 functions during regeneration after lesion in adult mice, we ablated HDAC8 in adult SCs by crossing either tamoxifen-inducible P0CreERT2 or PLPCreERT2 mice with the HDAC8-loxP line, in which exon 4 of *hdac8* gene is flanked by two *loxP* sites (**Fig. 11a**). Exon 4 codes for the acetyl-transferase domain of HDAC8. CreERT2 is a fusion protein consisting of the Cre recombinase fused to the ligand-binding domain of the human oestrogen receptor. In the latter, the G400V/M543A/L544A triple mutation prevents binding of β-oestradiol and allows the recombinase to be activated upon injection of 4-

hydroxy (OH)-tamoxifen. In these mouse lines, CreERT2 is expressed in the cytoplasm and is bound to Hsp90. Upon administration, Tamoxifen binds to the ERT2 domain and displaces Hsp90. This binding allows the translocation of CreERT2 into the nucleus, where it induces recombination of the floxed exon (Leone et al., 2003) (**Fig. 11b**).

When expressed under the control of the *P0* promoter, CreERT2 is expressed only in SCs. However, when expressed under the control of the *PLP* promoter, CreERT2 is expressed in SCs but also in oligodendrocytes (Leone et al., 2003). We chose to use the PLPCreERT2 line for experiments requiring only sciatic nerves collection, whereas behavioural tests and subsequent molecular analyses were performed with P0CreERT2 line. Indeed, since CreERT2 is expressed in oligodendrocytes and SCs in the PLPCreERT2 line, a lack of HDAC8 in oligodendrocytes could have an undesirable effect on CNS function and could potentially influence the results of the behavioural tests.

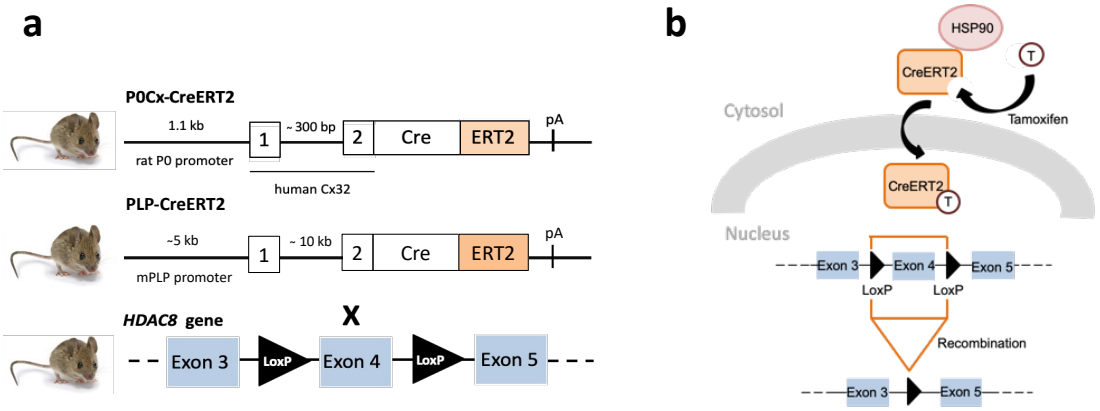

Figure 11. Generation of HDAC8 KO mice inducible by Tamoxifen (a). Tamoxifen-inducible P0-CreERT2 or PLP-CreERT2 line is crossed with HDAC8-loxP line, in which exon 4 of *hdac8* gene is flanked by two loxP sites. **(b)** Translocation of CreERT2 into the nucleus upon Tamoxifen injection. The cell type-specific, Tamoxifen-mediated translocation of CreERT2 into the nucleus allows the recombination between the two loxP sites. CreERT2, Cre recombinase - estrogen receptor T2; HDAC8, Histone deacetylase 8; Hsp90, Heat shock protein 90; P0, Protein zero; PLP, Proteolipid protein (*Modified from Leone et al., 2003 ; Parkitna and Engblom, 2012*).

Mice homozygous for floxed *Hif1α* allele (The Jackson Laboratory, Strain # 007561) were crossed with *Plp*-CreERT2 mice. To ablate HDAC8 or HIF1α in adult SCs, three- to four-month-old adult mice received daily injections of 2 mg tamoxifen (Sigma) for five consecutive days. As control mice, Cre-negative littermates of HDAC8 or HIF1α knockout mice were used. The preparation of Tamoxifen is described in Table 1. Genotypes were determined by PCR on genomic DNA. The different mice lines used in the study are listed in Table 2. Stratified random allocation in blocks with gender and age as strata was used. Analysis of the raw data was done at least twice by different researchers, independently. All mice used in this study were from mixed strains backcrossed to C57BL/6 J. Mice were housed in a standard mouse facility with controlled temperature (22 ± 2°C) and humidity (45 ± 10%) in individually ventilated cages containing sawdust bedding, a plastic cylinder and 2 paper tissues on the floor, food pellet and water ad libitum. Light cycle: 12:12 h. This study complies with all relevant ethical regulations concerning animal use, which was approved by

the Veterinary office of the Canton of Fribourg, Switzerland, the Veterinary office (Landesuntersuchungsamt) of Rheinland-Pfalz, Germany, and the Veterinary office (Landesdirektion) in Sachsen, Germany.

Plp-CreERT2 and *P0*-CreERT2 mice have been used in collaboration with Dr. Ueli Suter (ETH Zürich, Switzerland).

Table 1. Tamoxifen preparation

Reagent	*Amount*	*Final concentration*
Tamoxifen	400mg	20mg/ml
Ethanol	2ml	10%
Sunflower oil	18ml	90%
Weight Tamoxifen directly in a falcon tube. Add ethanol and sunflower oil directly on top. Wrap the falcon tube in aluminum foil and mix 1h on a rotating wheel at RT. Aliquot and store at -20°C		

Table 2. Mouse strains

Name	*Background*	*Source*	*Genotyping /Primers*	*References*
Wild type	C57BL/6N	Jackson Laboratory		Strain #:005304
Hdac8 flox	C57BL/6NTac Hdac8tm1a(EUCOMM)Wtsi	EMMA	HDAC8_F (54) HDAC8_R (55)	Strain # EM:05717
Hif1α flox	B6.129 Hif1atm3Rsjo/J	Jackson Laboratory	Performed by collaborators	Strain # 007561
P0Cx-CreERT2	C57BL/6.DBA/2F1 Tg(Mpz-cre/ERT2)2Ueli	Ueli Suter Swiss Federal Institute of Technology, ETH, Zürich, Switzerland	P0Cre-up (271) P0Cre-lo (272)	Leone et al., 2003

PLP-CreERT2	C57BL/6.DBA/2F1 Tg(Plp1-cre/ERT2)1Ueli	Ueli Suter Swiss Federal Institute of Technology, ETH, Zürich, Switzerland	PLPCre-up (269) PLPCre-lo (270)	Leone et al., 2003
DhhCre	FVB(Cg) Tg(DhhCre)1Mejr /J	Dies Meijer, Erasmus University Medical Center, Rotterdam, Netherlands	DhhCre-for (267) DhhCre-rev (268)	Jeagle et al., 2003
R26R-EYFP	B6.129X1 Gt(ROSA)26Sortm 1(EYFP)Cos/J	Jackson Laboratory		Strain #:006148

2.2.2 Utilized transgenes

The mouse strains listed in Table 2 were crossed to generate either conditional or conditional and inducible knock-out mice. Of note, both Hif1α $^{fl/fl}$; PLP$^{wt/wt}$ and Hif1α $^{fl/fl}$; PLP$^{creERT2/wt}$ mice samples were kindly provided by Ruth Stassart and Robert Fledrich from the Paul-Flechsig-Institute of Neuropathology, Leipzig University, Leipzig, Germany

The following genotypes used in this study are listed in Table 3.

Table 3. Utilized transgenes

Name	*Internal denomination*	*Mutation (grade) 1*	*Mutation (grade) 2*	*Mutation (grade) 3*
Hdac8$^{fl/fl}$; PLP$^{wt/wt}$; Rosa26-EYFP $^{fl/fl}$	Hdac8 fl/fl	Hdac8 (fl/fl)	Rosa26STOP floxEYFP (fl/fl)	
Hdac8 $^{fl/fl}$; P0$^{wt/wt}$; Rosa26-EYFP $^{fl/fl}$	Hdac8 fl/fl	Hdac8 (fl/fl)	Rosa26STOP floxEYFP (fl/fl)	
Hdac8 $^{fl/fl}$; Dhh$^{wt/wt}$;	Hdac8 fl/fl	Hdac8 (fl/fl)		
Hdac8 $^{fl/fl}$; PLP$^{creERT2/wt}$; Rosa26-EYFP $^{fl/fl}$	Hdac8 fl/fl PLPCre+	Hdac8 (fl/fl)	PLP (creERT2/wt)	Rosa26STOP floxEYFP (fl/fl)
Hdac8 $^{fl/fl}$; P0$^{creERT2/wt}$; Rosa26-EYFP $^{fl/fl}$	Hdac8 fl/fl P0Cre+	Hdac8 (fl/fl)	P0 (creERT2/wt)	Rosa26STOP floxEYFP (fl/fl)
Hdac8 $^{fl/fl}$; Dhh$^{cre/wt}$	Hdac8 fl/fl DhhCre +	Hdac8 (fl/fl)	Dhh (cre/wt)	
Hif1α $^{fl/fl}$; PLP$^{wt/wt}$	Hif1α fl/fl	Hif1α (fl/fl)		
Hif1α $^{fl/fl}$; PLP$^{creERT2/wt}$	Hif1αfl/fl PLPCre+	Hif1α (fl/fl)	PLP (creERT2/wt)	

2.3 Genotyping

2.3.1 DNA extraction

Ear, tail, or toe biopsies were lysed overnight in 100µl TE-lysis buffer (see section 2.23.1.2) supplemented with Proteinase K at 55°C at 900 rpm. The day after, Proteinase K was inactivated by heating the samples to 95°C for 1min. Samples were then centrifuged at 13'000 rpm for 1min, cooled down at RT and either directly used for genotyping or store at -20°C.

2.3.1 Polymerase chain reaction setup

2.3.2.1. List of genotyping primers

Table 4. Genotyping primers

Mice strain	*Primer name*	*Sequence in 5´→3´direction*
HDAC8 fl/fl	HDAC8_F (54)	CACCAAGGAGAGGCAAGAGG
	HDAC8_R (55)	TTTGTCAGTTTGTCACACGAGATG
PLPCreERT2	PLPCre-up (269)	CACTCTGTGCTTGGTAACATGG
	PLPCre-lo (270)	TCGGATCCGCCGCATAACC
P0CreERT2	P0Cre-up (271)	CTGCACAGACATGAGACCATAGG
	P0Cre-lo (272)	TCGGATCCGCCGCATAACC
DhhCre	DhhCre for (267)	ATACCGGAGATCATGCAAGC
	DhhCre rev (268)	GGTGGTGTGGTAGAGCAGGT
Cre unspecific	Cre-up (22)	ACCAGGTTCGTTCACTCATGG
	Cre-lo (23)	AGGCTAAGTGCCTTCTCTACA
R26R-EYFP	R26R-F (24)	AAAGTCGCTCTGAGTTGTTAT
	R26R-R (25)	GCGAAGAGTTTGTCCTCAACC

All primers were produced by Microsynth AG

2.3.2.2 List of Master Mix

Table 5. HDAC8 master mix

PCR reaction setup component	*Volume*	*Final concentration*
Nuclease-free dH_2O	18.25µL	
10x Taq polymerase buffer	2.5µL	1X
10µM Forward primer	1.25µL	0.5µM
10µM Reverse primer	1.25µL	0.5µM
10mM dNTPs	0.5µL	0.2mM
Taq polymerase	0.25µL	
Template	1µL	Variable

Table 6. PLP-CreERT2, P0Cx-CreERT2, DhhCre master mix

PCR reaction setup component	*Volume*	*Final concentration*
Nuclease-free dH_2O	15.785µL	
10x Taq polymerase buffer	2.5µL	1X
10µM Forward primer	2.5µL	1µM
10µM Reverse primer	2.5µL	1µM

10mM dNTPs	0.5µL	0.2mM
Taq polymerase	0.125µL	
Template	1µL	Variable

Table 7. Cre unspecific master mix

PCR reaction setup component	*Volume*	*Final concentration*
Nuclease-free dH_2O	9.34µL	
5x Green Go Taq® buffer	6µL	1X
1µM Forward primer	6µL	0.2µM
1µM Reverse primer	6µL	0.2µM
10mM dNTPs	0.66µL	0.22mM
WT Taq polymerase	1µL	Variable (depend on the lot -> homemade Taq Polymerase
Template	1µL	Variable

Table 8. R26R-EYFP master mix

Component	*Volume*	*Final concentration*
Nuclease-free dH_2O	18.9µL	
5x Green Go Taq® buffer	6µL	1X
20µM Forward primer	1.5µL	1µM
20µM Reverse primer	1.5µL	1µM
10mM dNTPs	0.6µL	0.2mM
WT Taq polymerase	0.5µL	Variable (depend on the lot -> homemade Taq Polymerase
Template	1µL	Variable

2.3.3 Polymerase chain reaction cycling conditions

Table 9. HDAC8 PCR cycle

Step	*Degree*	*Time*	*Cycles*
Initial denaturation	94°C	5 min	1x
Denaturation	94°C	30 sec	35x
Primer annealing	60°C	30 sec	35x
Elongation	68°C	30sec	35x
Final elongation	68°C	5 min	1x

Table 10. P0Cx-CreERT2 PCR cycle

Step	*Degree*	*Time*	*Cycles*
Initial denaturation	94°C	3 min	1x
Denaturation	94°C	1 min	2x
Primer annealing	62°C	1 min	2x
Elongation	68°C	1 min	2x
Denaturation	94°C	30 sec	33x
Primer annealing	62°C	30 sec	33x
Elongation	68°C	45 sec	33x
Final elongation	68°C	5 min	1x

Table 11. PLP-CreERT2 PCR cycle

Step	*Degree*	*Time*	*Cycles*
Initial denaturation	94°C	2 min	1x
Denaturation	94°C	30 sec	35x
Primer annealing	54°C	45 sec	35x
Elongation	68°C	45sec	35x
Final elongation	68°C	5 min	1x

Table 12. DhhCre PCR cycle

Step	*Degree*	*Time*	*Cycles*
Initial denaturation	94°C	2 min	1x
Denaturation	94°C	45 sec	35x
Primer annealing	53°C	30 sec	35x
Elongation	68°C	1 min	35x
Final elongation	68°C	5 min	1x

Table 13. Cre and R26R-EYFP PCR cycle

Step	*Degree*	*Time*	*Cycles*
Initial denaturation	94°C	3 min	1x
Denaturation	94°C	1 min	35x
Primer annealing	57°C	1 min	35x
Elongation	72°C	1 min	35x
Final elongation	72°C	5 min	1x

2.3.4 Agarose gel electrophoresis

DNA samples were separated by length using gel electrophoresis. A 2% agarose gel was prepared by mixing 3g of agarose with 150mL of 1X TAE buffer (see section 2.23.1.2). The solution was heated in a microwave until the agarose was dissolved. The solution was then poured into a horizontal gel chamber and combs were added. Once the gel was polymerized, samples were mixed with 5µL of 6X Orange gel loading dye (when needed), 3.3µL of SyBrGreen and loaded to the gel, next to the DNA ladder, whose preparation is described in Table 4. The gel was run between 80 to 100mV for 30 to 45 min. PCR products were visualized with a transilluminator (IO Rodeo). The size of the PCR bands is referenced in Table 5.

Table 14. DNA ladder preparation

Reagent	*Amount*	*Final concentration*
1mg/ml 1kb Plus DNA Ladder	150µL	125µg/mL
6X Purple gel loading dye	200µL	1X
dH_2O	850µL	
Mix reagents until dH_2O and store at 4°C for few days. Before loading, add 6µL of SyBrGreen		

Table 15. PCR products for genotyping

Basepairs	*Allel*
670bp	HDAC8 floxed
410bp	HDAC8 wt
800bp	P0Cx-CreERT2
500bp	PLP-CreERT2
389bp	DhhCre
200bp	Cre unspecific
260bp	R26R-EYFP

2.4 Surgical procedures

For all surgical procedures, isoflurane (3% for induction, 1.5-2% for narcosis during the operation, Isofluoran, CP Pharma) was used for anesthesia. For analgesia, 0.1 mg/kg body weight buprenorphine (Richter) was administered by i.p. injection 1 h before surgery and every four hours until the evening on the day of surgery. The following day, 1 mL agarose gel containing 0.027 mg/ml buprenorphine was given twice (morning and evening). The mice were placed on a heat pad during the entire procedure until waking up from anaesthesia. To prevent dehydration of the eyes, a carbomer liquid eye gel (Lacryvisc, Alcon) was used preoperatively. Mice were shaved at the height of the hip for sciatic nerve crush lesion and the field of operation was cleaned and disinfected. Sciatic nerve crush lesions were carried out on three- to four-month-old adult mice (males and females) as follows (by the procedure described in Brügger et al., 2017): An incision was made at the height of the hip and the sciatic nerve was exposed on one side. The nerve was crushed (5 times for 10 sec with crush forceps: Ref. FST 00632-11). The wound was closed using Histoacryl Tissue Glue (BBraun). After the operation, mice were wrapped in paper towels until recovery from anaesthesia. After surgery, both the crushed sciatic nerve and the contralateral sciatic nerve were collected for different purposes (**Fig. 12a-b**)

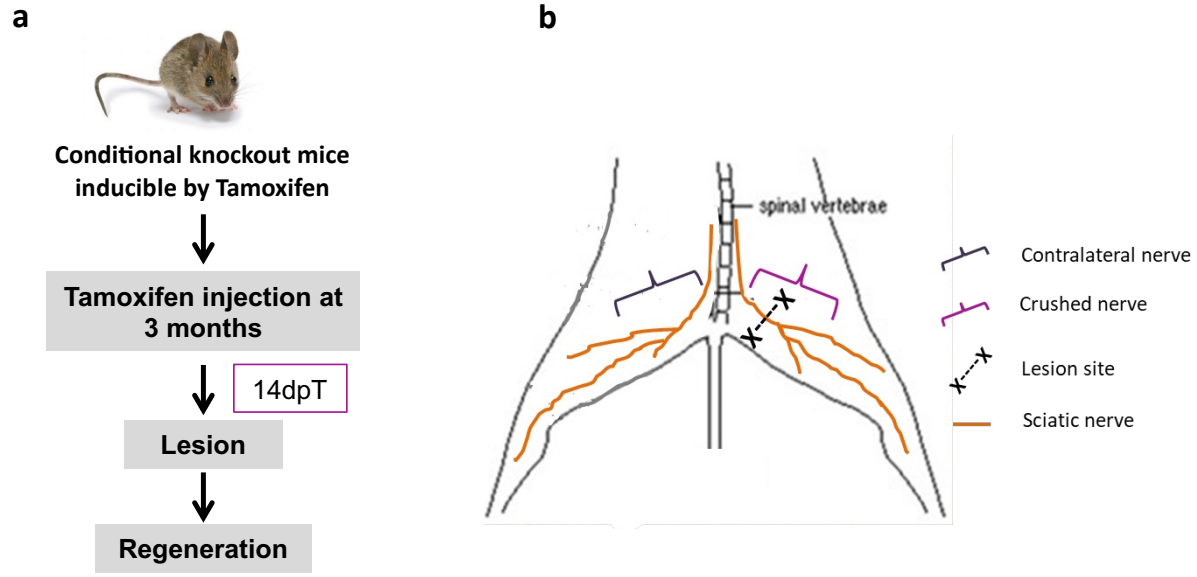

Figure 12. Experimental set-up to study the regeneration process after sciatic nerve crush. **(a)** Experimental paradigm. Adult, conditional HDAC8KO mice are injected with Tamoxifen for 5 consecutive days. At 14 days post Tamoxifen (dpT), sciatic nerve is crushed and collected at different time-points after lesion to study the regeneration process. **(b)** Schematic representation of crushed and contralateral mouse sciatic nerve. The contralateral intact nerve is used as internal control.

2.5 Functional recovery experiments

Recovery of motor function was tested at 12, 19 and 30 dpl using the Rotarod test and the inverted grid test. For the Rotarod test, mice were placed four times on the Rotarod apparatus at a fixed speed of 15 revolutions per minute to test balance and motor coordination, at 12, 19 and 30 dpl. The duration of each trial was limited to 1200 sec. Latency to fall from the rotating beam was recorded and the average of the four trials was used for quantification. For the inverted grid test, mice were placed on a cage grid, that was slowly inverted and observed for 30 sec. The test was stopped if the animal fell. For each animal, the average count of grabs and missed steps as well as the average time the animals stayed attached to the inverted grid among the four trials were calculated as described (Tillerson et al., 2001, 2003). All trials were video recorded for accurate analysis. For both tests, mice were first trained three times and trials were separated by a 30 min recovery period. Recovery of sensory function was tested at 12, 19 and

30 dpl by toe pinch test: each toe of the rear foot on the right side (lesioned side) was pinched with equal pressure applied by the same experimenter using flat tip forceps. Immediate withdrawal was recorded as functional sensitivity of the pinched toe. In case no toe exhibited sensitivity, the same test was applied to toes of the contralateral side (uninjured side), which always resulted in immediate withdrawal.

2.6 List of constructs

Table 16. List of constructs

Name	*Reference*
HDAC8 shRNA	Sigma, TRCN00000877999
TRAF7 shRNA	Sigma, TRCN0000302734
HIF1α shRNA	Sigma, TRCN0000232221
Ctrl shRNA (pLKO.1-puro)	Sigma, SHC001
pGL3-basic-c-Jun promoter	Claire Jacob, Johannes-Gutenberg University, Mainz, Germany
pGL3-basic	Promega, E1715
pSV-beta-Galactosidase	Promega, E1081
pCEP4F-HDAC8-FLAG	Kind gift from Dr. Edward Seto
pLenti-C-mGFP	Origene, PS100071
pCXN2-Flag-TRAF7	Kind gift from Dr. Huanjie Yang
pCXN2-Flag	Kind gift from Dr. Huanjie Yang
pCXN2-Flag-TRAF7-small-isoform	Nadège Hertzog and Claire Jacob, Johannes-Gutenberg University, Mainz, Germany

2.7 Cloning

2.7.1 Cloning of pGL3-basic-c-Jun promoter

The *c-Jun* promoter-luciferase construct was generated by PCR on mouse genomic DNA: a 2.5 kb fragment corresponding to the mouse *c-Jun* promoter (-1702/+781: 94939678-94942161 Mus musculus strain C57BL/6J chromosome 4, GRCm39) was inserted into the pGL3-Basic vector (Promega) between Mlu I and Bgl II restriction sites. The construct was verified by sequencing.

2.7.2 Cloning of pCXN2-Flag-TRAF7-small-isoform

We generated pCXN2-Flag-TRAF7-small-isoform construct by PCR using primers listed in Table and in Figure 13a. To this end, the NCBI entry of *Traf7* human gene (NM_032271.3), the NCBI entry predicting the sequence of the small TRFA7 isoform (>XR_007064922.1) as well as the sequence of the pCXN2-Flag-TRAF7 plasmid were used as reference to design the primers (**Fig. 13a**). The primers details for cloning and sequencing of pCXN2-Flag-TRAF7-small-isoform are listed in Table 17.

a

ATGAGCTCAGGCAAGAGTGCCCGCTACAACCGCTTCTCCGGGGGGCCCAGCAATCTTCCCACCCCAGACGTCACCAC
AGGGACCAGAATGGAAACGACCTTCGGACCCGCCTTTTCAGCCGTCACCACCATCACAAAAGCTGACGGGACCAGCA
CCTACAAGCAGCACTGCAGGACACCCTCCTCCTCCAGCACCCTTGCCTACTCCCCGCGGGACGAGGAGGACAGCATG
CCCCCCATCAGCACTCCCCGCCGCTCCGACTCCGCCATCTCTGTCCCTCCCTGCACTCAGAGTCCAGCATGTCTCT
GCGCTCCACATTCTCACTGCCCGAGGAGGAGGAGGCCGGAGCCACTGGTGTTTGCGGGAGCAGCCCTCGGTGAAGC
TGTGCTGTCAGCTCTGCTGCAGCGTCTTCAAAGACCCCGTGATCACCACGTGTGGGCACACGTTCTGTAGGAGATGC
GCCTTGAAGTCAGAGAAGTGTCCCGTGGACAACGTCAAACTGACCGTGGTGGTGAACAACATCGCGGTGGCCGAGCA
GATCGGGGAGCTCTTCATCCACTGCCGGCACGGCTGCCGGGTAGCGGGCAGCGGGAAGCCCCCCATCTTTGAGGTGG
ACCCCCGAGGGTGCCCCTTCACCATCAAGCTCAGCGCCCGGAAGGACCACGAGGGCAGCTGTGACTACAGGCCTGTG
CGGTGTCCCAACAACCCAGCTGCCCCCCGCTGCTCAGGATGAACCTGGAGGCCCACCTCAAGGAGTGCGAGCACAT
CAAATGCCCCCACTCCAAGTACGGGTGCACGTTCATCGGGAACCAGGACACTTACGAGACCCACCTGGAGACTTGCC
GCTTCGAGGGCCTGAAGGAGTTTCTGCAGCAGACGGATGACCGCTTCCACGAGATGCACGTGGCTCTGGCCCAGAAG
GACCAGGAGATCGCCTTCCTGCGCTCCATGCTGGGAAAGCTCTCGGAGAAGATCGACCAGCTAGAGAAGAGCCTGGA
GCTCAAGTTTGACGTCCTGGACGAAAACCAGAGCAAGCTCAGCGAGGAGCCTCATGGAGTTCCGGCGGGACGCATCCA
TGTTAAATGACGAGCTGTCCCACATCAACGCGCGGCTGAACATGGGCATCCTAGGCTCCTACGACCCTCAGCAGATC
TTCAAGTGCAAAGGGACCTTTGTGGGCCACCAGGGCCCTGTGTGGTGTCTCTGCGTCTACTCCATGGGTGACCTGCT
CTTCAGTGGCTCCTCTGACAAGACCATCAAGGTGTGGGACACATGTACCACCTACAAGTGTCAGAAGACACTGGAGG
GCCATGATGGCATCGTGCTGGCTCTCTGCATCCAGGGGTGCAAACTCTACAGCGGCTCTGCAGACTGCACCATCATT
GTGTGGGACATCCAGAACCTGCAGAAGGTGAACAGCATCGGGGCCGAGCAACCCGGTGTGCACGCTGGTCTCCTC
ACACAACGTGCTCTTCAGCGGCTCCCTGAAGGCCATCAAGGTCTGGGACATCGTGGGCACTGAGCTGAAGTTGAAGA
AGGAGCTCACAGGCCTCAACCACTGGGTGCGGGCCCTGGTGGCTGCCCAGAGCTACCTGTACAGCGGCTCCTACCAG
ACAATCAAGATCTGGGACATCCGAACCCTTGACTGCATCCACGTCCTGCAGACGTCTGGTGGCAGCGTCTACTCCAT
TGCTGTGACAAATCACCACATTGTCTGTGGCACCTACGAGAACCTCATCCACGTGTGGGACATTGAGTCCAAGGAGC
AGGTCCGACCCTCACGGGCCACGTGGCACCGTGTATGCCCTGGCGGTCATCTCGACGCCAGACCAGACCAAAGTC
TTCAGTGCATCCTACGACCGGTCCCTCAGGCTCGGAGTATGGACAACATGATCTGCACGCAGACCCTGCTGCGTCA
CCAGGGCAGTGTCACCGCGCTGGCTGTGTCCCGGGCCGACTCTTCTCAGGGGCTGTGGATAGCACTGTGAAGGTTT
GGACTTGCTAA

b

Primer A : TRAF7-ORF-Fw-XhoI (with 6 bases before XhoI site)

5'-TAAGCA*CTCGAG*ATGAGCTCAGGCAAGAGTGCCCGC-3'

Primer New B : Small-Traf7-Rv (part annealing to fragment 2 + part annealing to fragment 1)

5'-CGCTGTAGAGTTTGCACCCACACCTTGATGGTCTTG-3'

Primer New C : Small-Traf7-Fw (part annealing to fragment 1 + part annealing to fragment 2)

5'-CAAGACCATCAAGGTGTGGGTGCAAACTCTACAGCG-3'

Primer New D : TRAF7-ORF-Rv-NotI (with 6 bases before Not1)

5'-TAATTA*GCGGCCGC*TCATGGGCCCGGATGGTGTTCAC-3'

Figure 13. Primer A-D used for cloning of TRAF7 small isoform and alignment with coding sequence from human TRAF7 of the pCXN2-TRAF7-FLAG plasmid. (a) coding sequence of *Traf7* human gene. **(b)** Primers used to clone the TRAF7 small isoform. Colour codes for **a** and **b** as following: Sequence of primer A complementary to the CDS region (green), sequence complementary to fragment 1 (AB) (yellow), sequence complementary to fragment 2 (CD) (light blue), sequence added to primers B and

C to be 36nt long and have a similar Tm as primers A and D (grey), STOP codon (red), the two bases from the sequence to be removed that are kept to stay in frame after the deletion (dark blue), and sequence that will be deleted (bolt and italics). (reference sequence from NM_032271.3)

The small isoform of TRAF7 consists of two parts of the TRAF7 sequence. Consequently, a sequence localized in the middle of the *Traf7* CSD (in italic and bolt in Figure 13a) had to be deleted (**Fig. 13b**). Fragments AB (bp 1 to bp 1266) and CD (bp 1346 to 1436) were aligned into the final product AD in a second PCR (**Fig. 14b**).

The Primer A has a restriction site for the restriction enzyme Xho1 and binds to the beginning of the TRAF7 sequence (bp 1 to bp 1266), while primer New B anneals at the end of fragment 1 (AB). The AB PCR thus generates the fragment AB. Primer New D has a restriction site for the restriction enzyme Not1 and binds to the end of the CSD for the TRAF7 short isoform (bp 1346 to 1436), while primer New C anneals at the beginning of fragment 2 (CD). The CD PCR thus generates fragment CD (**Fig. 14a**). Primers New B and New C bind at either side of the region to be deleted (depicted in orange in Figure 14a). In this way, they prevent its incorporation in fragments AB and CD. The complementary sequences of primers New B and New C (blue and yellow arrows in Figure 14a) allow the generation of complementary sequences on AB and CD fragments. The latter can then hybridize during the second round of PCR. The final product AD consists of the CSD of the TRAF7 small isoform and is generated by using fragments AB and CD as template with the Primers A and New D (**Fig. 14b**).

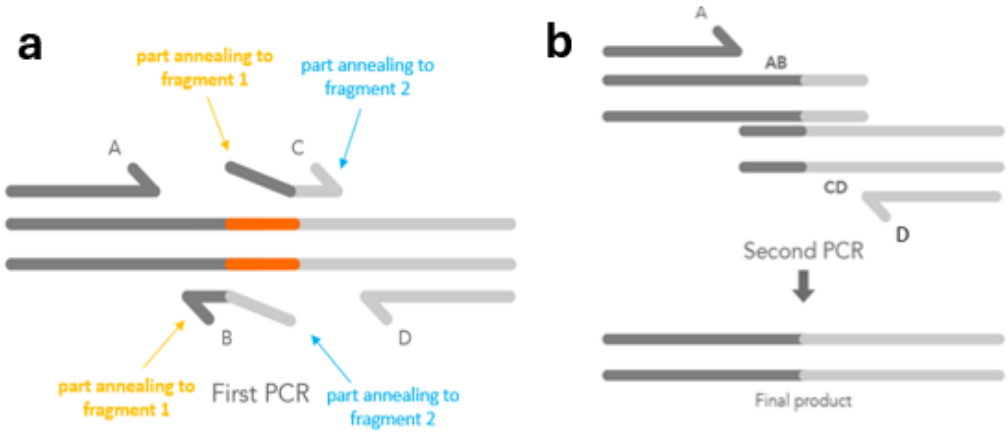

Figure 14. Illustration of primer extension for deletion (a) The Primer A binds to the beginning of the DNA sequence, while primer New B anneals at the end of fragment 1 (AB). The AB PCR thus generates the fragment AB. Primer New D binds to the end of the DNA sequence, while primer New C anneals at the beginning of fragment 2 (CD). The CD PCR generates fragment CD. Primers New B and New C bind at either side of the region to be deleted (in orange). In this way, they prevent its incorporation into fragments AB and CD. The complementary sequences of primers B (blue arrow) and C (yellow arrow) allow the generation of complementary sequences on AB and CD fragments. **(b)** AB and CD fragments hybridize during the second round of PCR. The final product AD is generated by the Primers A and D (Illustration from https://eu.idtdna.com/pages/education/decoded/article/methods-for-site-directed-mutagenesis and modified by Nadège Hertzog).

Table 17. Primers for cloning and sequencing of pCXN2-Flag-TRAF7-small-isoform construct

Target	*Primer name*	*Sequence in 5´→3´direction*
TRAF7-ORF-Fw-XhoI	Primer A (279)	TAAGCACTCGAGATGAGCTCAGGCAAGAGTGCCCGC
Small-Traf7-Rv	Primer New B (280)	CGCTGTAGAGTTTGCACCCACACCTTGATGGTCTTG
Small-Traf7-Fw	Primer New C (281)	CAAGACCATCAAGGTGTGGGTGCAAACTCTACAGCG
TRAF7-ORF-Rv-NotI	Primer New D (282)	TAATTAGCGGCCGCTCATGGGCCCGGATGGTGTTCAC
TRAF7-small isoform	TRAF7-small sequencing-Fw (285)	TTGTGCTGTCTCATCATTTTGG
TRAF7-small isoform	TRAF7-small sequencing-Fw_2 (287)	ACAACGTCAAACTGACCGTGG
TRAF7-small isoform	TRAF7-small sequencing-Fw_3 (288)	AGTTTCTGCAGCAGACGGATG

All primers were produced by Microsynth AG

The PCR reactions was carried out according to protocol provided by Phusion High-Fidelity DNA Polymerase (Thermo Fischer). Briefly, for the generation of fragments AB, CD and AD, the PCR cycle was designed as described in Table 18.

Table 18. PCR cycle to generate products AB, CD, and AD

Step	*Degree*	*Time*	*Cycles*
Initial denaturation	98°C	30 sec	1x
Denaturation	98°C	5 sec	30x
Primer annealing	72°C	30 sec	30x
Elongation (AB) and (AD)	72°C	30 sec	30x
Elongation (CD)	72°C	15 sec	30x
Final elongation	72°C	5 min	1x

Each PCR product was purified using the Nucleospin Gel and PCR clean up kit according to the manufacturer recommendations (Macherey-Nagel, #740609.50). The product AD and the pCXN2-FLAG-TRAF7 plasmid were then double digested using the restriction enzymes Xho1/Not1 by following the recommendations provided by New England Biolabs, purified, ligated in a 3:1 ratio using the T4 DNA ligase according to the manufacturer recommendations (New England Biolabs), and then transformed into competent *E.coli*. The enzymes and buffers used for the generation of pCXN2-Flag-TRAF7-small-isoform listed in Table 19. The construct was verified by sequencing.

Table 19. List of enzymes used for the generation of pCXN2-Flag-TRAF7-small-isoform construct

Product name	*Reference*
Phusion™ High-Fidelity DNA Polymerase (and 5X Phusion™ HF Buffer)	Thermoscientific, F530S (and F518L)
Not1 restriction enzyme	New England Biolabs, R0189S
Xho1 restriction enzyme	New England Biolabs, R0146S
NEBuffer™ r3.1	New England Biolabs, B7203S
T4 DNA ligase (and 10X T4 DNA Ligase buffer)	New England Biolabs, M202 (and B202S)

2.8 *E.Coli* calcium chloride competent cell protocol

A single *E.Coli* colony was inoculated into 5mL LB and grown overnight at 37°C. The next morning, 1mL of the culture was inoculated into 100mL of LB (see section 2.23.3) and incubated at 37°C for 3 h. Bacteria were then incubated on ice for 10 min and centrifuged for 3 min at 6000 rcf. The pellet was then gently resuspended in 10mL of sterile, cold 0.1M $CaCl_2$ solution, incubated on ice for 20 min, and centrifuged again for 3 min at 6000 g. The pellet was then resuspended in 5 ml of sterile, cold 0.1M $CaCl_2$ solution containing 15% glycerol, aliquoted in microcentrifuge tubes and stored at -80°C.

2.9 Transformation of Competent *E.Coli*

Chemical competent *E.Coli* were thawed on ice and 0.2µL of 14.3M β-mercaptoethanol were added to 100µL of competent *E.Coli*. Bacteria were mixed gently and incubated on ice for 10 min and gently swirled every 2 min. 50ng of plasmid were added and incubated on ice for 30 min. Then, bacteria were heat-shocked at 42°C for 45 min and incubated on ice for 2min. 900µL of LB (see section 2.23.3) were then added to the bacteria and incubated at 37°C

for 1h on a shaking platform at 225-25 rpm. 200µl of transformation product were plated on a LB agar plate containing the selective antibiotic (see section 2.23.3).

2.10 Plasmid preparation from bacteria

For MiniPrep, a single bacteria colony was picked using a sterile pipet tip, inoculated in 5mL LB (see section 2.23.3) supplemented with the selective antibiotic, and incubated for 12 to 18 h at 37°C on a shaking platform at 225-250 rpm. The next morning, bacteria were pelleted at 10'000 rcf for 10 min and subjected to plasmid preparation according to the manufacturer's recommendations (Macherey-Nagel, #740588.50). Plasmids were eluted in nuclease-free dH_2O and stored at -20°C. MiniPrep DNA was checked by restriction digestion and sequencing (StarSeq, Mainz).

For MaxiPrep, a single bacteria colony was picked using a sterile pipet tip, inoculated in 3ml LB supplemented with the selective antibiotic, and incubated for 12 to 18 h at 37°C on a shaking platform at 225-250 rpm. The next morning, 300µL of the preculture were added to 300mL LB with the selective antibiotic and incubated for 12 to 18h at 37°C at 225-250 rpm. When a glycerol stock was used, the preculture step was omitted and 1ml of the glycerol stock was directly added to 300µL LB with the selective antibiotic. The day after, bacteria were pelleted at 10'000 rcf for 15 min and subjected to plasmid preparation according to the manufacturer's recommendations (Macherey-Nagel, #740424.10). Plasmids were eluted in nuclease-free dH_2O and stored at -20°C.

For both MiniPrep and MaxiPrep protocols, 500µL of the overnight culture were mixed with 500µL of glycerol and stored at -80°C. The DNA concentration was determined using NanoDrop 100 Spectrophotometer (Thermo Scientific).

2.11 qRT-PCR

Isolation of RNA was carried out using Trizol reagent (Invitrogen) and cDNA was produced using SuperScript II Reverse Transcriptase (Thermo Scientific), according to the manufacturers' recommendations. Quantitative real-time PCR analyses were performed with an ABI 7000 Sequence Detection System (Applied Biosystems) using FastStart SYBR Green Master (Roche), according to the manufacturer's recommendations. A dissociation step was added to verify the specificity of the products formed. Primer sequences, master mix and qRT-PCR cycle are described in Tables 20, 21, and 22 respectively.

Table 20. Real-time quantitative PCR primers

Target	*Primer name*	*Sequence in 5´→3´direction*
c-Jun gene rat	rat *c-Jun* forward (151)	CACCTCCGAGCCAAGAACTC
	rat *c-Jun* reverse (152)	CTGGACTGGATGATCAGGCG
Gapdh gene rat	rat *Gapdh* forward (147)	GTATCCGTTGTGGATCTGACAT
	rat *Gapdh* reverse (148)	GCCTGCTTCACCACCTTCTTGA

All primers were produced by Microsynth AG

Table 21. Gapdh and c-Jun master mix

PCR reaction setup component	*Volume*	*Final concentration*
Nuclease-free dH_2O	10.75µL	
2X SYBR Green Master Mix (Fast Start)	12.5µL	1X
10µM Forward primer	0.375µL	0.15µM
10µM Reverse primer	0.375µL	0.15µM
cDNA	1µL	Variable

Taq polymerase and dNTPs are included in SYBR Green Master Mix

Table 22. Real-time quantitative PCR cycle for Gapdh and c-Jun

Step	*Degree*	*Time*	*Cycles*
Initial denaturation	95°C	10 min	1x
Denaturation	95°C	15 sec	45x
Primer annealing	60°C	60 sec	45x
Elongation	72°C	60 sec	45x

2.12 Primary rat Schwann cell cultures

Purified primary rat SC cultures were derived from P2 Wistar rat sciatic nerves, as previously described in Jacob et al., 2008. SCs were then purified by sequential immunopanning in plastic dishes coated with a Thy1.1 antibody (Dong et al., 1997). Identity and purity were checked for each primary preparation by immunofluorescence of SC-specific markers (Sox10, Oct6, Krox20, P0, MAG). SCs were grown in proliferation medium: DMEM containing 10% FBS (Gibco), 1:500 penicillin/streptomycin (Invitrogen), 4 µg/ml crude GGF (bovine pituitary extract, Bioconcept), and 2 µM forskolin (Sigma) (see section 2.23.2.2), at 37°C and 5% CO2/95% air. SC culture protocol mimicking SC demyelination and conversion into repair cells that occur after a PNS lesion was as follows (previously described in Brügger et al., 2017): SCs were first growth-arrested for 8 to 15 h in differentiation medium (DM): DMEM/F-12 (Gibco) containing 0.5% FBS (Gibco), 1:500 penicillin/streptomycin (Invitrogen), 100

µg/ml human apo-transferrin (Sigma), 60 ng/mL progesterone (Sigma), 1 µg/mL insulin (Sigma), 16 µg/mL putrescin (Sigma), 400 ng/mL L-thyroxin (Sigma), 160 ng/mL selenium (Sigma), 10 ng/mL triiodothyronine (Sigma) and 300 µg/mL bovine serum albumin (Sigma) (see section 2.23.2.2). Then 1 mM dbcAMP (Sigma) was added to induce differentiation and cells were incubated in this medium for another 3 days. The medium was then changed to DM only without dbcAMP, and RSCs were incubated in this medium for 3 days (differentiation mimicking adult SC stage). To mimic SC conversion into the repair phenotype, cells were then changed to proliferation medium and incubated in this medium for 1 day.

To inhibit HDAC8, 1µM, 10µM or 100µM PCI-34051 (HDAC8 inhibitor, Selleckchem), 30µM or 90µM 1-Naphthohydroxamic acid (HDAC8 inhibitor, MedChemExpress) or their vehicle were added in conditions mimicking the conversion into the repair phenotype at the time of change to proliferation medium.

To inhibit JNK, 1 µM JNK-IN-8 (JNK inhibitor, MedChemExpress) or its vehicle were added to rat SCs in conditions mimicking the conversion into the repair phenotype the day before and at the time of change to proliferation medium for 24 h.

To mimic hypoxia, 250µM $CoCl_2$ was added to SCs in conditions mimicking the conversion into the repair phenotype 8h after the change to proliferating medium and incubated for 16h. To induce hypoxia, RSCs were incubated in a hypoxic incubator (CO_2-Incubator C16, Labotect) in conditions mimicking the conversion into the repair phenotype, at the time of change to proliferation medium and for 16 h at 5%CO_2 and 1%O_2/94%N_2. We thank Dr. Regnier-Vigouroux (JGU Mainz, Germany) for access to the hypoxia incubator.

To inhibit the proteasome, 20µM MG-132 (proteasome inhibitor, Hycultec) or its vehicle were added to rat SCs in conditions mimicking the conversion into the repair phenotype for 4 to 8 h.

HEK293T cells were obtained from ATCC and cultured in DMEM containing 10% FCS (Gibco) and 1:500 penicillin/streptomycin (Invitrogen) (see section 2.23.2.2) on poly-D-lysine (Sigma)-coated dishes.

Mycoplasma contamination was not tested in primary rat SCs or in HEK293T cells, because of the low incidence of mycoplasma contamination in primary cells, and because mycoplasma contamination results in inefficiency of transfection, which we did not observe in our primary rat SCs or in HEK293T cells.

2.13 Generation and use of lentiviruses

To produce lentiviral particles, HEK293T cells (ATCC) were co-transfected with each lentiviral construct: HDAC8 shRNA (TRCN00000877999), TRAF7 shRNA (TRCN0000302734), HIF1α shRNA (TRCN0000232221) or control shRNA (SHC001), together with the packaging constructs pLP1, pLP2 and pLP/VSVG (Invitrogen), using Lipofectamine 2000 (Invitrogen), according to the recommendations of the manufacturer (ViraPower Lentiviral Expression Systems Manual). Lentiviruses were added to primary rat SCs in DM and incubated for two days. Then, infected cells were selected by adding 2 µg/ml puromycin (Sigma) in DM for two days, before adding proliferating medium. HDAC8 shRNA, TRAF7 shRNA, HIF1α shRNA and control shRNA lentiviral constructs were purchased from Sigma-Aldrich.

2.14 Transfection

Confluent primary rat SCs were transfected either in differentiating conditions or in conditions mimicking the conversion into the repair phenotype at the time

of change to proliferation medium with Fugene 6 (Promega) at 5:1 ratio Fugene 6:DNA, according to the manufacturer's recommendations, with the following modifications: the DNA was incubated in OptiMEM (Gibco) for 5 min at room temperature (RT) before addition of Fugene 6. The mix Fugene 6:DNA was then incubated for 30 min at RT before being added to the cells.

2.15 Luciferase gene reporter assay

Confluent primary rat SCs previously infected in differentiating conditions with HDAC8 shRNA or control shRNA in 12-well plates were transfected in conditions mimicking the conversion into the repair phenotype at the time of change to proliferation medium with Fugene 6 (Promega) at 3:1 ratio Fugene 6:DNA, according to the manufacturer's recommendations, with the following modifications: the DNA was incubated in OptiMEM (Gibco) for 5 min at RT before addition of Fugene 6. The mix Fugene 6: DNA was then incubated for 30 min at RT before being added to the cells. Eight hours after transfection, 250µM $CoCl_2$ or vehicle (H_2O) were added to the cells for 16 h. Cells were lysed 24 h after transfection in 110µL Reporter Lysis Buffer (Promega) and assayed for luciferase activity. Forty microliters of lysate were subjected to two consecutive injections of each 25µL luciferase substrate and values were recorded after an integration time of 2 and 10 sec, respectively. Efficiency of transfection was evaluated by measuring beta-galactosidase activity of a co-transfected beta-gal construct (Promega). Primary rat SCs were co-transfected with 1µg of the luciferase construct pGL3b-c-Jun promoter or empty pGL3b (Promega), and 300 ng beta-gal construct (Promega). Luciferase activity was first normalized to beta-galactosidase activity and then normalized to the empty pGL3b luciferase control (transfected at the same ratio Fugene 6: DNA). For beta-galactosidase activity, we followed the instructions of the manufacturer (Promega). Briefly,

50µL Assay Buffer 2x was added to 50µL lysate, and beta-galactosidase activity was recorded after a 15-20 min incubation time at 37°C. Endogenous beta-galactosidase activity (as determined from cells only transfected with overexpressing construct at the same ratio Fugene 6: DNA) was subtracted.

2.16 Western blot analysis

For all Western blots and immunoprecipitations on mouse sciatic nerve lysates, we collected the injured sciatic nerve from the lesion site to around 12mm distal to the lesion site (region where the nerve splits into the three branches of tibial, sural, and common peroneal nerves). We collected the same region of the contralateral nerve as internal control for each animal. After perineurium removal, sciatic nerves were frozen in liquid nitrogen, pulverized with a chilled mortar and pestle, lysed in radioimmunoprecipitation assay (RIPA) buffer (see section 2.23.1.2) for 30 min on ice, and centrifuged to pellet debris. Supernatants were collected.

Cells were washed once in PBS, lysed in RIPA buffer for 15 min on ice, and centrifuged to pellet debris. Sciatic nerves and cell lysates were submitted to SDS-PAGE and analyzed by Western blotting.

Primary and secondary antibodies used for Western blot are listed in Tables 23 and 24 respectively.

Table 23. Western blot primary antibodies

Name of Antibody	*Host species*	*Dilution*	*Reference*
Anti-HDAC8	rabbit	1:1000	Santa Cruz Biotechnology, cat. # sc-11405, lot # D0715
Anti-HDAC1	rabbit	1:1000	GeneTex, cat. # GTX100513, lot # 39471
Anti-HDAC2	mouse	1:1000	Sigma, cat. # H2663, lot # 092M4824V
Anti-HDAC3	rabbit	1:1000	GeneTex, cat. # GTX109679, lot # 39974

Anti-Oct6	rabbit	1:2000	Kind gift from Dr. Dies Meijer, University of Edinburgh
Anti-Krox20	rabbit	1:500	kind gift from Dr. Dies Meijer, University of Edinburgh
Anti-Sox10	mouse	1:1000	Abcam, cat. # ab216020, lot #GR3272630-2
Anti-Mpz	chicken	1:5000	Aves Labs, cat. # PZO, lot # PZO877982
Anti-MBP	rat	1:750	Bio-Rad, cat. # MCA409S, lot # 158446
Anti-c-Jun	rabbit	1:1000	Cell Signaling, cat. #9165, lot # 13
Anti-phospho-c-Jun	rabbit	1:1000	Cell Signaling, cat. #3270, lot # 5)
Anti-TRAF7	rabbit	1:1000	Proteintech, cat. # 11780-1-AP, lot # 00047291
Anti-TRAF7	rabbit	1:1000	ABclonal, cat. # A3095, lot # 5500008204
Anti-HIF1α	rabbit	1:1000	Novus Biological, cat. # NB100-479, lot # D108267-1
Anti-HIF1α	mouse	1:500	&D Systems, cat. # MAB1536, lot # KRK0521051
Anti-VHL	rabbit	1:1000	ABclonal, cat. # A0377, lot # 5500020894
Anti-Ubiquitin (P4D1)	mouse	1:1000	Cell Signaling, cat. # 3936, lot # 19
Anti-phospho-JNK1/JNK2	rabbit	1:1000	Invitrogen, cat. # 44-682G, lot # 2465206
Anti-GAPDH	mouse	1:5000	GeneTex, cat. # 28245, lot # 822203823
Anti-β-Actin	mouse	1:5000	Sigma, cat. # A5441, lot # 122M4782
Anti-α-Tubulin	mouse	1:5000	Sigma, cat. # T9026, lot # 000241529
Anti-Lamin A/C	mouse	1:1000	Sigma, cat. # SAB4200236, lot # 055M4822V
Anti-eEF1A1	rabbit	1:5000	Abcam, cat. # ab157455, lot #GR231741-10

Table 24. Western blot secondary antibodies

Name of Antibody	*Host species*	*Dilution*	*Reference*
Anti-rabbit (IgG) HRP	goat	1:10000	Jackson ImmunoResearch, cat. # 111-036-047
Anti-mouse (IgG) HRP	goat	1:10000	Jackson ImmunoResearch, cat. # 115-036-072
Anti-chicken (IgY) HRP	rabbit	1:10000	Jackson ImmunoResearch, cat. # 303-035-008

2.17 Immunoprecipitation

For non-denaturing IPs, tissues or cells were processed as described in the Western blot section in RIPA buffer (see section 2.23.1.2) supplemented with protease inhibitor cocktail (Thermo Scientific). Lysates were pre-cleared for 1 h at 4°C with 30µL protein A/G PLUS agarose beads (Santa-Cruz Biotechnology). Antibodies were conjugated to 30µL of agarose beads for 2 h at 4°C on a rotating platform. Then, 1mL of cleared lysate was rotated for 2 h at 4°C with immunoprecipitating antibodies conjugated to the beads.

For denaturating IPs, tissues or cells were lysed in denaturing buffer (see section 2.23.1.2), boiled for 5 min at 95°C, and mixed with 9 volumes of RIPA buffer (see section 2.23.1.2). Lysates were homogenized with a 20-gauge needle attached to a sterile plastic syringe, pre-cleared for 1 h at 4°C with 30µL of agarose beads and rotated overnight at 4°C with immunoprecipitating antibodies. The day after, 30uL of agarose beads were added and samples were further rotated at 4°C for 2 h.

Two to six micrograms of the antibodies listed in Table 25 were used per nerve or per $1x10^7$ cells:

Table 25. List of antibodies used for Immunoprecipitation

Name of Antibody	*Host species*	*Reference*
Anti- HIF1α	mouse	R&D Systems, cat. # MAB1536, lot # KRK0522111
Anti- HIF1α	rabbit	Novus Biological, cat. # NB100-479, lot # D108267-1
Anti-HDAC8	sheep	R&D Systems, cat. # AF4359, lot # CAKS0120091
Normal Goat IgG control	goat	R&D Systems, cat. # AB-108-C, lot # ES41160812
Anti-Flag	mouse	Sigma, cat. # F1804, lot # SLBM0089V
Anti-GFP	rabbit	Abcam, cat. # ab290, lot # GR3431263-1)

Rabbit anti-GFP, mouse anti-Flag and goat anti-IgG antibodies were used as control IPs.

Immunoprecipitates were pelleted, washed four times with RIPA buffer, eluted in 40 µL of Laemmli buffer and incubated at 75°C for 10 min. Analysis was done by Western blot.

2.18 Subcellular fractionation

Cytoplasmic and nuclear fractions were obtained by following the protocol of Senichkin et al., 2021. For fractionation on sciatic nerve lysates, we collected the injured sciatic nerve from the lesion site to around 12 mm distal to the lesion site (region where the nerve splits into the three branches of tibial, sural, and common peroneal nerves). We collected the same region of the contralateral nerve as internal control for each animal. After perineurium removal, sciatic nerves were pulverized with a chilled mortar and pestle and lysed in hypotonic buffer (see section 2.23.1.2) supplemented with 0.5mM DTT, 0.5mM PMSF and protease inhibitor (Thermo Scientific) for 30 min on ice.

Cells were harvested by trypsination, resuspended in PBS, centrifuged at 500 rcf for 3 min at 4°C and resuspended in hypotonic buffer for 3 min on ice. Then, Nonidet P-40 (NP-40) was added to a final concentration of 0.1% and the lysates were further incubated for 3 min and centrifuged at 1000 rcf for 3 min at 4°C. The supernatant (cytoplasmic fraction) was centrifuged a second time at 15000 rcf for 3 min at 4°C to pellet remaining debris. The pellet (nuclear fraction), was resuspended in isotonic buffer (see section 2.23.2.1) supplemented with 0.5mM DTT, 0.5mM PMSF and protease inhibitor on ice for 10 min, and centrifuged at 1000 rcf for 3 min at 4°C. The pellet was then resuspended in RIPA buffer containing 1% SDS, 1% sodium deoxycholate, 1% NP-40 and protease inhibitor (Thermo Scientific) (see section 2.23.1.2) for 30 min and centrifuged at 2000 rcf for 3 min at 4°C. Supernatants were collected.

2.19 Immunofluorescence and imaging

Mouse sciatic nerves were fixed in situ with 4% PFA for 10 min, dissected, embedded in PolyFreeze (Sigma), and frozen at −80°C. Sciatic nerve cryosections (5-µm thick) were first incubated with acetone for 10 min at −20°C, washed in PBS, blocked for 30 min at RT in blocking buffer with either BSA or Donkey serum (see section 2.23.1.2), and incubated with primary antibodies overnight at 4°C in blocking buffer. Sections were then washed 3 times in blocking buffer and secondary antibodies were incubated for 1 h at RT in the dark. Sections were washed again, incubated with DAPI for 5 min at RT, washed and mounted in Citifluor (Agar Scientific).

Cells were washed with PBS, fixed for 10 min with 4% PFA at RT, washed again in PBS, blocked, incubated with antibodies, DAPI, and mounted as described above.

For whole-mount sciatic nerve staining, nerves were processed as described in Dun et al., 2015) with the following modifications: the perineurium was fully removed after 5 h fixation in 4% PFA and each nerve branch was separated from one another.

The primary and secondary antibodies used for Immunofluorescence are listed in Tables 26 and 27 respectively.

Table 26. Immunofluorescence primary antibodies

Name of Antibody	*Host species*	*Dilution*	*Reference*
Anti-HDAC8	sheep	1:200	R&D Systems, cat. # AF4359, lot # CAKS0120091
Anti-TRAF7	rabbit	1:200	ABclonal, cat. # A3095, lot # 5500008204
Anti-c-Jun	rabbit	1:200	Cell Signaling, cat. #9165, lot # 13
Anti-phospho-c-Jun	rabbit	1:800	Cell Signaling, cat. #3270, lot # 5
Anti-F4/80	rat	1:200	GeneTex, cat. # GTX26640, lot # 821401311
Anti-NFM	chicken	1:1000	GeneTex, cat. # GTX85461, lot # 822102296
Anti-Stathmin 2	rabbit	1:1000	Novus Biologicals, cat. # NBP1-49461, lot # D-1
Anti-Stathmin 2	goat	5µg/µl	Origene, cat. # TA318234
Anti-GAP43	rabbit	1:500	Abcam, cat. # ab75810, lot #GR3299539-7

Table 27. Immunofluorescence secondary antibodies

Name of Antibody	*Host species*	*Dilution*	*Reference*
Anti-rabbit (IgG) Alexa Fluor 488	Donkey	1:500	Jackson ImmunoResearch, cat. # 711-545-152
Anti-rabbit (IgG) Cy3	Donkey	1:500	Jackson ImmunoResearch, cat. # 711-165-152
Anti-goat (IgG) Cy3	Donkey	1:500	Jackson ImmunoResearch, cat. # 705-165-147
Anti-sheep (IgG) Alexa Fluor 488	Donkey	1:500	Jackson ImmunoResearch, cat. # 713-546-147

Anti-chicken (IgY) Alexa Fluor 647	Donkey	1:500	Jackson ImmunoResearch, cat. # 703-605-155
Anti-Rat (IgG) Alexa Fluor 647	Donkey	1:500	Jackson ImmunoResearch, cat. # 712-605-153

Photos were acquired using a Visitron VisiScope spinning disk confocal system CSU-W1. Fiji (version 2.9.0) and Adobe Photoshop (CC 20.0.4 Release) were used to process images. z-series projections (stated in the figure legends) are shown. Axonal regrowth was measured using NeuronJ software (ImageJ plugin freely available online with a user manual: http://www.imagescience.org/meijering/software/neuronj/). Parameters used were the same as described in the method validation article (Meijering et al., 2004). Neurite appearance: Bright, Hessian smoothing scale: 2.0, Cost weight factor: 0.7, Snap window size: 9 x 9, Path-search window size: 2,500 x 2,500, Tracing smoothing range: 5, Tracing subsampling factor: 5, Line width: 1.

2.20 Electron microscopy

Mice were killed with 150 mg/kg pentobarbital i.p. (Esconarkon; Streuli Pharma AG) and sciatic nerves were fixed *in situ* with 4% paraformaldehyde (PFA) and 3% glutaraldehyde in 0.1M phosphate buffer, pH 7.4 (see section 2.23.1.2). Fixed tissues were post-fixed in 2% osmium tetroxide, dehydrated through a graded acetone series as described in Benninger et al., 2006 and embedded in Spurr's resin (Electron Microscopy Sciences). Semithin sections were stained with 1% Toluidine blue for analysis at the light microscope, and ultrathin sections (70-nm thick) were cut as described in Benninger et al., 2006. All analyses were done at 5 mm distal to the lesion site. No contrasting reagent was applied. Images were acquired using a Philips CM 100 BIOTWIN equipped with a Morada side mounted digital camera (Olympus).

2.21 Mass spectrometry analysis

Protein samples eluted from the beads in 1X Laemmli sample buffer were heated for 10 min at 75°C, treated with 1 mM DTT, and alkylated using 5.5mM iodoacetamide for 10 min at RT. Samples were fractionated on 4-12% gradients gels and proteins were in-gel digested with trypsin (Promega) into four fractions per sample. Tryptic peptides were purified by STAGE tips and LC-MS/MS measurements were performed on a QExactive HF-X mass spectrometer coupled to an EasyLC 1200 nanoflow-HPLC (all Thermo Scientific) as described in Kaeser-Pebernard et al., 2022. MaxQuant software (version 1.6.2.10) (Cox and Mann, 2008) was used for analyzing the MS raw files for peak detection, peptide quantification and identification using a full length Uniprot mouse database (version April 2016). Carbamidomethylcysteine was set as fixed modification and oxidation of methionine was set as variable modification. The MS/MS tolerance was set to 20 ppm and four missed cleavages were allowed for Trypsin/P as enzyme specificity. Based on a forward-reverse database, protein and peptide FDRs were set to 0.01, minimum peptide length was set to seven, and at least one unique peptide per protein had to be identified. The match-between run option was set to 0.7 minutes. MaxQuant results were analysed using Perseus software (version 1.6.2.10) (Tyanova et al., 2016).

2.22 Data availability

All relevant data are available from the authors. The mass spectrometry proteomics data have been deposited to the ProteomeXchange Consortium via the PRIDE [1] partner repository with the dataset identifier PXD046582. Reviewer account details: Username: reviewer_pxd046582@ebi.ac.uk; Password: 99F8fDcq

2.23 Stock solutions, buffers, and media

All stock solutions, buffers and media were prepared in sterile conditions or were sterilized by autoclaving or by filtration.

2.23.1 Stock solutions and buffers for molecular biology, biochemistry, immunofluorescence, and electron microscopy

2.23.1.1 Stock solutions

Table 28. Stock solutions

Reagent	*Amount*
0.1M EGTA, pH 8.0	
EGTA	3.8g
Make up to 80ml with dH_2O, adjust pH to 8.0 and complete up to 100ml with dH_2O. Store at 4°C.	
0.5M EDTA, pH 8.0	
EDTA	93.05g
Make up to 400mL with dH2O, adjust the pH to 8.0 using NaOH. Make up to 500mL with dH2O.	
10% Ammonium persulfate	
APS	100mg
dH_2O	1mL
Vortex to dissolve. Store at 4°C for up to three weeks.	
10% SDS	
SDS	50g
Make up to 500mL with dH_2O, shake carefully by heating the solution to 37°C, store at RT to avoid precipitation.	
100mM PMSF	
PMSF	0.174g
Make up to 10mL with ethanol. Aliquot and store at -20°C.	
1M DTT	
DTT	1.5g

Make up to 100mL with dH_2O. Aliquot and store at -20°C. It is rather recommended to prepare the required amount of 1M DTT at the last moment.	
1M KCl	
KCl	7.46g
Make up to 100mL with dH_2O.	
1M $MgCl_2$	
$MgCl_2*6H_2O$	20.33g
Make up to 100mL with dH_2O.	
1M Na_2HPO_4	
$Na_2HPO_4*7H_2O$	268.07g
Make up to 1L with dH_2O.	
1M NaH_2PO_4	
$NaH_2PO_4*2H_2O$	156.01g
Make up to 1L with dH_2O.	
4% PFA	
PFA	40g
Make up to 800mL with PBS. Dissolve on stir plate at 60°C. Adjust pH to 7.4 and complete up to 1L with PBS. Aliquot and store at -20°C.	

EM fixative solution		*Final concentration*
PFA	40g	4%
0.1M phosphate buffer	880mL	
25% Glutaraldehyde solution	120mL	3%
Dissolve PFA in phosphate buffer on a stir plate at 60°C. Cool down to RT and add glutaraldehyde. Aliquot and store at -20°C.		

2.23.1.2 Buffers

Table 29. Buffers

Reagent	*Amount*	
0.1M Phosphate buffer, pH7.4		
1M Na_2HPO_4	77.4mL	
1M NaH_2PO_4	22.6mL	
Make up to 1L with dH_2O. Do not adjust pH.		
0.5M Tris pH 6.8		
Tris base	30.25g	
Make up to 400ml with dH_2O, adjust pH to 6.8 and complete up to 500ml with dH2O. Store at 4°C.		
1M Tris pH 8.3		
Tris base	60.5g	
Make up to 400mL with dH_2O, adjust pH to 8.3 and complete up to 500mL with dH2O. Store at 4°C.		
1.5M Tris pH 8.8		
Tris base	90.75g	
Make up to 400mL with dH_2O, adjust pH to 8.8 and complete up to 500mL with dH2O. Store at 4°C.		
1X Phosphate buffer saline (PBS), pH7.4		*Final concentration*
Na_2HPO4	1.14g	8mM
KH_2PO_4	0.2g	1.5mM
NaCl	8g	137mM
KCl	0.2g	2.7mM
Make up to 800mL with dH_2O, adjust pH to 7.4 and complete up to 1L with dH_2O.		
4% Stacking gel (based on making 1 gel)		
40% acrylamide	0.5mL	
0.5M Tris-HCl, pH 6.8	1.25mL	
dH_2O	3.125mL	
10% SDS	50µL	
10% APS	40µL	
TEMED	5µL	

Add APS and TEMED at the last moment for polymerization.	
6% Stacking gel (based on making 1 gel)	
40% acrylamide	0.75mL
1.5M Tris-HCl, pH 8.8	1.25mL
dH_2O	2.9mL
10% SDS	50µL
10% AP	45µL
TEMED	3.75µL
Add APS and TEMED at the last moment for polymerization.	
8% Stacking gel (based on making 1 gel)	
40% acrylamide	1mL
1.5M Tris-HCl, pH 8.8	1.25mL
dH_2O	2.65mL
10% SDS	50µL
10% APS	45µL
TEMED	3.75µL
Add APS and TEMED at the last moment for polymerization.	
10% Stacking gel (based on making 1 gel)	
40% acrylamide	1.25mL
1.5M Tris-HCl, pH 8.8	1.25mL
dH_2O	2.40mL
10% SDS	50µL
10% APS	45µL
TEMED	3.75µL
Add APS and TEMED at the last moment for polymerization.	
12% Stacking gel (based on making 1 gel)	
40% acrylamide	1.5mL
1.5M Tris-HCl, pH 8.8	1.25mL
dH_2O	2.15mL

10% SDS	50µL	
10% APS	45µL	
TEMED	3.75µL	
Add APS and TEMED at the last moment for polymerization.		
14% Stacking gel (based on making 1 gel)		
40% acrylamide	1.75mL	
1.5M Tris-HCl, pH 8.8	1.25mL	
dH_2O	1.9mL	
10% SDS	50µL	
10% APS	45µL	
TEMED	3.75µL	
Add APS and TEMED at the last moment for polymerization.		
50x TAE buffer, pH8.3		*Final concentration*
Tris base	242g	2M
glacial acetic acid	57.1mL	1M
0.5M EDT	100ml	50mM
Make up to 1L with dH_2O, without adjusting pH. Use at a concentration of 1X.		
Blocking solution for IHC/IF with BSA		*Final concentration*
BSA	200mg	20g/L
Triton-X-100	30µL	0.30%
Make up with PBS to 10mL. Vortex well to dissolve. Store at 4°C.		
Blocking solution for IHC/IF with Donkey serum		*Final concentration*
Donkey serum	500µL	5% v/v
Triton-X-100	30µL	0.30%
Make up with PBS to 10mL. Vortex well to dissolve. Store at 4°C.		
Blocking solution for whole sciatic nerve staining		*Final concentration*
PTX	90mL	90%
FBS	10mL	10%
Mix well. Store at 4°C.		
Blocking solution for WB		*Final concentration*
Non-fat milk powder	10g	50g/L

10X TBS	20mL	10%
Tween 20	200µL	0.10%
Make up to 200mL with dH_2O. Dissolve Tween20 on a stir plate. Store at 4°C.		
Denaturing buffer, pH 7.4		*Final concentration*
Tris-HCl	0.157g	10mM
SDS	1g	1% w/v
Make up to 80mL with dH_2O, adjust pH to 7.4. Add and dissolve SDS and complete up to 100mL with dH_2O. Store at RT.		
Hypotonic buffer for subcellular fractionation		*Final concentration*
Tris-HCl	0.315g	20mM
1M KCl	1mlL	10mM
1M $MgCl_2$	200µL	2mM
0.1M EGTA	500µL	1mM
Make up to 80mL, adjust pH to 7.4 and complete up to 100mlLwith dH_2O. Store at 4°C. Add 0.5mM DTT and 0.5mM PMSF at the last moment.		
Isotonic buffer for subcellular fractionation		*Final concentration*
Tris-HCl	0.315g	20mM
KCl	1.119g	150mM
1M $MgCl_2$	200µL	2mM
0.1M EGTA	500µL	1mM
Make up to 80mL, adjust pH to 7.4 and complete up to 100mL with dH_2O. Store at 4°C. Add 0.5mM DTT and 0.5mM PMSF at the last moment.		
Laemmli buffer (4X)		*Final concentration*
SDS (Sodium Dodecyl Sulfate)	1g	100mg/mL
0.5M Tris-HCl	3.75mL	187.5mM
Glycerol	3mL	30% w/v
14.3M β-Mercaptoethanol	300µL	429mM
Bromophenol blue	10mg	1mg/mL
Make up with dH_2O to 10mL. Mix on a stir plate. Aliquot and store at -20°C. Use at a final concentration of 1X.		
PTX (PBS-Triton-X 100)		*Final concentration*
PBS	100mL	99%
Triton-X-100	1mL	1%
Mix well on a stir plate. Store at 4°C.		

RIPA lysis buffer		*Final concentration*
Tris-HCl	0.788g	10mM
NaCl	4.383g	150mM
NaF	1.05g	50mM
Na_3VO_4	0.09g	1mM
EDTA (Disodium Ethylene Diamine Tetra-Acetate)	0.19g	1mM
Sodium deoxycholate	2.5g	0.5% w/v
NP-40	2.5mL	0.5% w/v
Make up to 500mL with dH_2O, adjust pH to 7.4. Store at 4°C.		
RIPA lysis buffer for subcellular fractionation		*Final concentration*
RIPA lysis buffer	To 50mL	
NP-40	250µL	1%
10% SDS	150µL	1%
Sodium deoxycholate	250mg	1%
Dissolve on a stir plate. This buffer is single use and cannot be stored at 4°C otherwise SDS will precipitate.		
Running buffer (10X)		*Final concentration*
Tris base	30g	250mM
Glycine	144gr	1.92M
SDS	10g	10g/L
Make up to 1L with dH_2O and use at a final concentration of 1X.		
TBS (10X)		*Final concentration*
Tris base	24.2g	201.6mM
NaCl	80g	1.37M
Make up to 800mL with dH_2O, adjust pH to 7.6 and complete up to 1L. Use at a final concentration of 1X. Store at 4°C.		
TBST (1X)		*Final concentration*
10X TBS	100mL	10%
Tween20	1mL	0.10%
Make up to 1L with dH_2O. Dissolve Tween20 by mixing on a stir plate. Store at 4°C.		
Transfer buffer (10X)		*Final concentration*

Tris-HCl	30.3g	190mM
Glycine	144g	1.92M
Make up to 800mL with dH_2O, adjust pH to 8.3 and complete up to 1L with dH_2O. Use at a final concentration of 1X by adding 100mL of the 10X solution, 200mL Methanol and 700mL dH_2O. Store the 1X solution at 4°C.		
Tris-EDTA lysis buffer		*Final concentration*
0.5M EDTA	2mL	2mM
1M KCl	24.9mL	50mM
1M Tris, pH 8.3	5mL	10mM
NP-40	2.25mL	0.45% w/v
Tween 20	2.25mL	0.45% w/v
Make up to 500mL with dH_2O. Store at 4°C.		

2.23.2 Stock solutions and media for cell culture

2.23.2.1 Stock solutions

Table 30. Stock solutions for media and cell culture

Reagent	*Amount*	
1-Naphthohydroxamic acid stock solution		*Final concentration*
1-Naphthohydroxamic acid	10mg	100mM
DMSO	0.5342mL	
Dissolve in 1-Naphthohydroxamic acid in DMSO by vortexing. Aliquot and store at -80°C.		
50mM Tris buffer, pH 9.5		
Tris base	3.029g	
Make up to 400mL with dH_2O, adjust pH to 9.5 and complete up to 500mL with dH_2O. Store at 4°C.		
Bovine pituitary extract stock solution		*Final concentration*
Bovine pituitary extract	14mg	2mg/mL
dH_2O	7mL	
Dissolve the bovine pituitary extract in sterile dH_2O. Aliquot and store at -20°C.		
Bovine Serum Albumin (BSA) stock solution		*Final concentration*
BSA	3g	30mg/mL

dH_2O	10mL	
Dissolve BSA in dH_2O in a water bath at 37°C. Mix well and aliquot and store at -20°C.		
$CoCl_2$ stock solution		*Final concentration*
$CoCl_2*6H_2O$	1.19g	1M
dH_2O	5mL	
Dissolve in dH_2O by vortexing. Store at 4°C. At the time of use, dilute 1:100 in dH_2O, filter sterilize using 0.2µm filter and apply to your cells at the desired concentration (50µM to 250µM).		
Dibutyryl cAMP sodium salt (dbcAMP) stock solution		*Final concentration*
dbcAMP (dibutyryl cyclic adenosine monophosphate)	25mg	100mM
PBS	5.087mL	
Dissolve dbcAMP in PBS. Aliquot and store at -20°C.		
Forskolin stock solution		*Final concentration*
Forskolin	10mg	10mM
DMSO	2.44mL	
Dissolve the Forskolin in DMSO. Aliquot and store at -20°C.		
HDAC8-IN-1 stock solution		*Final concentration*
HDAC8-IN-1	5mg	10mM
DMSO (Dimethylsulfoxide)	1.4476mL	
Dissolve in HDAC8-IN-1 in DMSO by vortexing. Aliquot and store at -80°C.		
Human Apo-transferrin stock solution		*Final concentration*
Apo-transferrin (human)	100mg	20mg
dH_2O	5mL	
Dissolve human Apo-transferrin in sterile dH_2O. Aliquot and store at -20°C.		
Insulin stock solution		*Final concentration*
Insulin	50mg	2mg/ml
37% HCl (=12M HCl)	2.075mL	1M
dH_2O	22.925mL	
JNK-IN-8 stock solution		*Final concentration*
JNK-IN-8	10mg	10mM
DMSO	1.9701mL	
Dissolve in JNK-IN-8 in DMSO by vortexing. Aliquot and store at -80°C.		

L-thyroxin sodium salt stock solution		*Final concentration*
L-thyroxin sodium salt pentahydrate	1mg	0.1 mg/mL
dH_2O	10mL	
Dissolve L-thyroxin in dH_2O. Aliquot and store at -20°C.		
MG-132 stock solution		*Final concentration*
MG-132	10mg	20mM
DMSO (Dimethylsulfoxide)	1.051mL	
Dissolve in MG-132 in DMSO by vortexing. Aliquot and store at -80°C.		
PCI-34051 stock solution		*Final concentration*
PCI-34051	10mg	10mM
DMSO	3.3447mL	
Dissolve in PCI-34051 in DMSO by vortexing. Aliquot and store at -80°C.		
Progesterone stock solution		*Final concentration*
Progesterone	100mg	1mg/mL
Ethanol	100mL	
Dissolve Progesterone in ethanol on stir plate. Aliquot and store at -20°C.		
Putrescine stock solution		*Final concentration*
Putrescine	160mg	16mg/mL
dH_2O	10mL	
Dissolve Putrescine in dH_2O. Aliquot and store at -20°C.		
PX-478 stock solution		*Final concentration*
PX-478	5mg	60mM
DMSO	211.43µL	
Dissolve in PX-478 in DMSO by vortexing. Aliquot and store at -80°C.		
Sodium selenite stock solution		*Final concentration*
Sodium Selenite	1g	50mg/mL
dH_2O	20mL	
Dissolve Sodium selenite in dH_2O. Aliquot and store at -20°C.		
Triiodothyronine (T3) stock solution		*Final concentration*
T3	2g	200µg/mL
Ethanol	10mL	
Dissolve Triiodothyronine in 10ml ethanol. Aliquot and store at -20°C.		

2.23.2.2 Cell culture media

Table 31. Cell culture media

Reagent	*Amount*	
HEK medium (50mL)		*Final concentration*
DMEM	45mL	
FBS	5mL	10%
Penicillin/Streptomycin	0.1mL	0.20%
Filtrate and store at 4°C.		
OX-7 hybridoma medium (50mL)		*Final concentration*
RPMI	45mL	
FBS	5mL	10%
Penicillin/Streptomycin	0.1mL	0.20%
100mM sodium pyruvate	500µL	1mM
50mM β-Mercaptoethanol	50µL	5µM
Filter and store at 4°C.		
Rat Schwann Cells Differentiation Medium (50mL)		*Final concentration*
DMEM/F12	48.973mL	
FBS	250µL	0.50%
Penicillin-Streptomycin	100µL	0.20%
20mg/mL Human Apo-transferrin	250µL	100µg/mL
60µg/mL Progesterone (*stock at 1mg/ml at -20°. Add 60µl of 1mg/ml solution in 1ml EtOH to reach 60ug/ml*)	50µL	60ng/mL
2mg/mL Insulin	25µL	1µg/mL
16mg/mL Putrescine	50µL	16µg/mL
0.1mg/mL L-thyroxin	200µL	400ng/mL
160µg/ml Sodium Selenite (*stock at 50mg/ml at -20°. Add 3.2µl of 50mg/ml solution in 1ml dH_2O to reach 160ug/ml*)	50µL	160mg/mL
200µg/mL T3	2.5µL	10ng/mL

300mg/mL BSA	50µL	300µg/mL
Filtrate, aliquot, and store at -20°C.		
Rat Schwann Cells Growth Medium (50mL)		*Final concentration*
DMEM	45mL	
FBS	5mL	10%
Penicillin/Streptomycin	0.1mL	0.20%
2mg/mL Bovine pituitary extract	100µL	4µg/mL
10mM Forskolin	10µL	2µM
Filtrate and store at 4°C. Add Bovine pituitary extract and forskolin at the time of use and filtrate again.		

2.23.3 Stock solutions and media for bacteria

Table 32. Stock solutions and media for bacteria

Reagent	*Amount*	
0.1M $CaCl_2$		
$CaCl_2$*$6H_2O$	2.19g	
Make up to 100mL with dH_2O.		
Ampicillin sodium salt stock solution		*Final concentration*
Ampicillin sodium salt	500mg	50mg/mL
dH_2O	10mL	
Dissolve Ampicillin with dH_2O. Filter-sterilize using 0.2µm cellulose acetate filter. Aliquot and store at -20°C.		
LB (Luria-Bertani) Broth		*Final concentration*
LB Broth (Miller)	20g	20g/L
dH_2O	1L	
Dissolve LB Broth in dH_2O. Autoclave.		
LB Agar (for 10 Petri dishes)		*Final concentration*
LB Broth (Miller)	4g	2%
Agar	3g	1.50%
dH_2O	200mL	

Add LB Broth and Agar in a 1L bottle. Add dH_2O. Boil and dissolve the powders in the microwave. Cool the mixture down and add the antibiotics Poor 10mL of LB Agar per plate and let polymerize. Dry the Petri dishes in an incubator at 37°C.

2.24 List of chemicals, reagents, and kits

Table 33. List of chemicals, reagents, and kits

Product name	*Reference*
1-Naphthohydroxamic acid (HDAC8 inhibitor)	MedChemExpress, HY-130538
β -Galactosidase Enzyme Assay System	Promega, E2000
β-Mercaptoethanol	Alfa Aesar, A15890
Acetone	Roth, #5025.2
Acrylamide/Bisacrylamide solution (40%, 37.5:1)	Thermo Scientific Chemicals, #15433569
Agar	Sigma, A5306
Agarose	Sigma, A9539
APS	Sigma, #215589
Ampicillin	Sigma, A9518
Apo-transferrin (human)	Sigma, T2036
Bovine pituitary extract	Corning, #734-1311
Bromophenol blue	Amresco, #0449
BSA	Sigma, A7030
Buprenorphin	Buprenovet multidose, VetViva Richter, #18760711
$CaCl_2*2H_2O$	Merck, A862982 824
Citifluor™ AF1, Mounting Medium	Science services, E17970-100
$CoCl_2*6H_2O$	Sigma, C8661
DAPI	Sigma, D9542

DC Protein Assay Reagents Package	BioRad, #500-0116
dbcAMP	Sigma, D0627
DER 736 (Diglycidylether of polypropyleneglycol)	Electron Microscopy Sciences, #13000
S-1 Dimethtylaminoethanol	Electron Microscopy Sciences, #13300
DMEM	Gibco, #11594446
DMEM/F12	Sigma, D8062
DMSO	Acros Organics, ACR.39760.1000
DNA Ladder (1kb PLUS)	New England Biolabs, N3200S
dNTPs	Sigma, dNTP100-1kt
Donkey serum	Biozol, END9010-10
DTT	Roth, #6908.1
EDTA	Sigma, E9884
EGTA	Sigma, E3889
ERL 4221	Electron Microscopy Sciences, #15004
Ethanol (absolute)	Fisher Scientific, #15612540
FBS	Gibco, #10270-106, lot 2096981
Forskolin	Sigma, F6886
Fugene® 6 Transfection Reagent	Promega, E2693
Gel loading dye (orange)	Roth, HP04.1
Gel loading dye (purple)	New England Biolabs, B7024S
Glacial acetic acid	Sigma, A6283
Glutaraldehyde	Sigma, G5882
Glycerol	Fischer Bioreagents, BP229-1
Glycine	Roth, #3790.4
5X Green GoTaq® Reaction buffer	Promega, M7911
HCl (32%)	Roth, X896.2
HDAC8-IN-1 (HDAC8 inhibitor)	MedChemExpress, HY-111342

Histoacryl Tissue Adhesive	Praxis Dienst, #126137
Insulin	Sigma, I1882
Isofluoran	CP Pharma, #1214
JNK-IN-8 (JNK inhibitor)	MedChemExpress, HY-13319
KCl	Sigma, P9541
KH_2PO_4	Roth, P018.2
Lacryvisc (eye ointment)	Alcon, #768499540343
LB Broth	Sigma, L3022
Lipofectamine™ 2000 Transfection Reagent	Thermofisher, #11668019
L-thyroxine	Sigma, T1775
Luciferase Assay System	Promega, E1500
Methanol	Roth, AE17.2
MG-132 (proteasome inhibitor)	MedChemExpress, HY-13259
$MgCl_2*6H_2O$	Roth, #2189.1
Molecular Biology Grade dH_2O	HyClone, GE Healthcare Life Sciences, SH30538.2
NaCl	Roth, #3957.2
NaF	Sigma, #201154
$Na_2HPO_4*7H_2O$	Sigma, #431478
$NaH_2PO_4*2H_2O$	Sigma, #71505
NaOH	Sigma, #1.37020
Na_3VO_4	Sigma, #567540
Non-fat milk powder	Rapilait, Migros (Switzerland)
NP-40	Sigma, #74385
NSA	Electron Microscopy Sciences, #19050
NucleoBond Xtra Maxi EF	Macherey-Nagel, #740424.10
NucleoSpin Gel and PCR Clean-up	Macherey-Nagel, #740609.50

NucleoSpin Plasmid	Macherey-Nagel, #740588.50
OptiMEM	Gibco, #31985-070
Osmium Tetroxide	Elektron Technology, AGR1016
PFA	Sigma, P6148
PCI-34051 (HDAC8 inhibitor)	Selleckchem, S2012
Penicillin/Streptomycin	Sigma, P4333
Pentobarbital	Esconarkon; Streuli Pharma AG
Phenol:Chloroform:Isoamyl Alcohol 25:2	Sigma, P2069
PMSF	Roth, #6367.1
Poly-D-lysine hydrobromide	Sigma, P647
Precision Plus protein All Blue Prestained Protein Standards	BioRad, #1610393
Progesterone	Sigma, P8783
Propanol	Roth, #6752.5
Protease and Phosphatase Inhibitor, EDTA-free (100X)	Thermoscientific, #78443
Protein A/G PLUS-Agarose	Santa Cruz Biotechnology, sc-2003
Proteinase K	Sigma, P2308
Puromycin	Sigma, P8833
Putrescine dihydrochloride	Sigma, P5780
PX-478 (HIF1α inhibitor)	MedChemExpress, HY-10231
Random Primers	Promega, C1181
Reporter lysis buffer, 5X (luciferase assay)	Promega, E3971
RNase H (*E.Coli*)	Promega, M4280
RNasin Recombinant Ribonuclease Inhibitor	Promega, N2511
RPMI	Gibco, #1153586

SDS	Roth, CN30.3
Sodium chloride physiological solution	Sigma, #07982-100TAB-F
Sodium deoxycholate	Sigma, D6750
sodium pyruvate	Sigma, S8636
Sodium selenite	Sigma, S5261
Sunflower oil	Rewe, Germany
SuperScript™ Reverse Transcriptase (supplied with 5X First-Strand Buffer and 0.1M DTT)	Thermofisher, #18080044
SuperSignal™ West Pico PLUS Chemiluminescent Substrate	Thermofischer, #345778
SYBR Green Staining Reagent DNA Free	VWR, APLIA8511.100625
SYBR Green Master Mix (Fast Start)	Roche, #04 673 492 001
Tamoxifen	Sigma, T5648
Taq DNA polymerase (and 10X ThermoPol buffer) for genotyping	New England Biolabs, M0267S (and B9004S)
TEMED	Sigma, T9281
T3	Sigma, T2752
TRI Reagent (Trizol)	Sigma, T9424
Tris base	Roth, A411.1
Tris-HCl	Sigma, T3252
Triton-X-100	Fischer Scientific, #10254640phys
Trypsin-EDTA (0.25%)	Sigma, T4049
Tween-20	Sigma, P1379
Wonder Taq Polymerase	Home-made production. The construct was a kind gift from Dr. Alessandro Puoti, University of Fribourg, Fribourg, Switzerland

3. Aims and brief description of the results

The relevance of chromatin remodeling enzymes in SC biology is now well documented. Among them, class I HDACs have been extensively studied. Indeed, our previous studies on HDAC1/2 have shown that HDAC1/2 are essential for the specification of the SC lineage, SC myelination, and for the maintenance of paranodes and nodes of Ranvier (Brügger et al., 2015; Chen et al., 2011; Jacob et al., 2011). Additionally, HDAC1/2 have been shown to slow down axonal regrowth after injury but to promote remyelination (Brügger et al., 2017; Duman et al., 2020). In parallel, other research groups found that HDAC3 affects SC myelination, myelin maintenance, and remyelination after lesion (He et al., 2018; Rosenberg et al., 2018). Recently, two studies revealed that class II HDACs also influence SC myelination and remyelination process after lesion (Gomis-colona et al., 2018; Velasco-Aviles, Patel et al., 2022).

The aims of my thesis were to investigate the functions of the last member of the class I HDACs, namely HDAC8, in the context of SC development, maintenance and PNS regeneration after injury.

To study the functions of HDAC8 in SCs during postnatal development, we generated SC-specific knockout mice by crossing mice expressing floxed *Hdac8* with mice expressing Cre recombinase under the control of the *Dhh* promoter, which becomes active at E 12.5 after SC lineage specification. Sciatic nerves were collected for molecular and morphological analysis at different time points after birth. Our analyses as well as behavioral tests at different time points after birth did not reveal defects in SC development or impairments in motor and sensory functions in HDAC8 knockout mice.

In the context of myelin maintenance and regeneration, we generated SC-specific knockout mice by crossing mice expressing floxed *Hdac8* with mice

expressing the tamoxifen-inducible CreERT2 recombinase under control of either the (OL and SC)-specific *Plp* promoter or SC-specific *P0* promoter. We collected sciatic nerves at 3- and 6-months post tamoxifen treatment and analyzed the morphology of the nerves by electron microscopy. We did not find any morphological alterations, indicating that HDAC8 is not required for the maintenance of myelin integrity. To confirm our conclusions, we will also collect sciatic nerves of HDAC8 KO mice at 12 months after tamoxifen treatment.

To analyze the functions of HDAC8 in SCs during regeneration, we collected sciatic nerves at key time points after lesion in control animals and found that HDAC8 levels were strongly upregulated after injury, suggesting potential important functions of HDAC8 during PNS regeneration. In a first step, we collected sciatic nerves of control and HDAC8 KO mice for molecular and morphological analyses. Additionally, we also performed behavioral tests to assess sensory and motor function recovery after lesion as well as whole nerve immunofluorescence to measure axonal regrowth in HDAC8 KO mice compared to control animals.

In a second step, I aimed at elucidating the mechanisms of action of HDAC8 first *in vitro,* by using purified primary rat SCs to mimic SC conversion into repair SCs, and *in vivo* using HDAC8 KO mice.

In summary, we found that HDAC8 ablation in SCs specifically promotes the regrowth of sensory axons and sensory function recovery and that HDAC8 is detected only in SCs ensheating sensory axons. Mechanistically, HDAC8 stabilizes the E3 ubiquitin ligase TRAF7, leading to faster degradation of HIF1α, a factor that promotes c-Jun phosphorylation and upregulation during hypoxia. Consequently, HDAC8 delays both c-Jun and phospho-c-Jun upregulation after lesion, which slows down SC conversion into repair SCs.

My last objective in the context of PNS regeneration was to determine whether the modulation HDAC8 activity using a specific activator or inhibitor could increase regeneration efficiency *in vitro*, using DRG explant cultures in microfluidic chambers, or in *vivo*. We found that HDAC8 stabilizes TRAF7 independently of its deacetylase activity. It was therefore not possible to assess a potential increase in regeneration efficiency in mice treated with an HDAC8 inhibitor compared to vehicle-treated mice.

4. RESULTS – HDAC8 control hypoxia-induced conversion of sensory Schwann cells into repair cells

AUTHORS

Nadège Hertzog[1,2], Mert Duman[1,2†], Maëlle Bochud[2†], Valérie Brügger-Verdon[2†], Maren Gerhards[1], Felicia Schön[1], Franka Dorndecker[1], Robert Fledrich[3], Ruth Stassart[3], Devanarayanan Siva Sankar[2], Jörn Dengjel[2], Sofía Raigón López[1], Claire Jacob[1,2*]

AFFILIATION

[1]Institute of Developmental Biology and Neurobiology, Faculty of Biology, Johannes Gutenberg University Mainz, Mainz, Germany

[2]Department of Biology, University of Fribourg, Fribourg, Switzerland

[3]Paul-Flechsig-Institute of Neuropathology, Leipzig University, Leipzig, Germany

[†]Contributed equally to this work

AUTHOR CONTRIBUTIONS

NH and CJ conceived and designed the experiments. NH, MD, MB, VB, MG, FS, FD, RF, RS, DSS and SRL performed the experiments. NH, MB, DSS, JD and CJ analyzed the data, NH and CJ wrote the manuscript. All authors commented on the manuscript.

DECLARATION OF INTEREST

The authors declare no competing interest.

4.1 Abstract

After a traumatic injury, the peripheral nervous system (PNS) can efficiently regenerate. This is primarily due to the high plasticity of Schwann cells (reviewed in Nocera and Jacob, 2020), the myelinating glia and the main glial cell type of the PNS. Indeed, SCs react rapidly to a traumatic injury of the PNS by actively demyelinating and converting into repair cells that secrete neurotrophic factors which promote axonal regrowth, and form bands of Büngner that guide axons back to their former target (Jessen and Arthur-Farraj, 2019). SCs then remyelinate or re-ensheath regenerated axons, which leads to successful functional recovery (Nocera and Jacob, 2020; Sock and Wegner, 2019). In some cases, however, when the injury has created a large gap between axons and their target or in aged individuals, target re-innervation and functional recovery can partially or completely fail (Jessen and Mirsky, 2019). Understanding the molecular mechanisms that control SC plasticity after injury has the potential to

reveal drug targets for increasing SC plasticity and thereby accelerating axonal regrowth and remyelination efficiency.

The transcription factor c-Jun, which is rapidly upregulated in SCs after a PNS injury, is widely recognized as a master inducer of the SC demyelination process and conversion into repair cells and is critical for axonal regrowth after injury (Arthur-Farraj et al., 2012; Fazal et al., 2017; Gomez-Sanchez et al., 2015; Jessen and Mirsky, 2022). Interestingly, c-Jun expression levels in SCs after a PNS lesion are lower in aged individuals compared to young adults, and restoring c-Jun levels in aged individuals leads to axonal regeneration of similar efficiency as in young adults[9]. Although the functions and target genes of c-Jun have been extensively studied in SCs after injury, the mechanisms that control c-Jun upregulation remain partially understood. Wagstaff et al. (2019) showed an involvement of Sonic Hedgehog signaling in maintaining high c-Jun levels at 7 days post sciatic nerve cut lesion, but not at earlier time points. We have previously shown that the two highly homologous class I histone deacetylases 1 and 2 (HDAC1/2) are critical in SCs for the remyelination process after a PNS injury (Brügger et al., 2017; Duman et al., 2020). However, we also showed that HDAC2 is upregulated too early in SCs after injury, already 1 day after a sciatic nerve crush lesion. Indeed, HDAC2 upregulation following injury leads to precocious upregulation of the transcription factor Oct6, which in turn counteracts c-Jun upregulation in SCs, thereby slowing down axonal regrowth. We also demonstrated that a short treatment with an HDAC1/2 inhibitor following a PNS injury accelerates axonal regrowth and functional recovery without impairing remyelination (Brügger et al., 2017). These findings indicate that the regeneration process after a PNS injury is not optimal and can be improved. Other members of the HDAC family have also been described to be involved in the regeneration process of the PNS after injury (Duman and

Martinez-Moreno, 2020; Gomez-Sanchez et al., 2022; Jacob, 2017). Indeed, HDAC3, another class I HDAC, has been reported to prevent precocious remyelination after lesion (He et al., 2018), while members of class II HDACs have been shown to be involved in the remyelination process (Velasco-Aviles, Patel et al., 2022).

A PNS lesion abruptly interrupts oxygen supply and therefore creates a hypoxic environment (Cho et al., 2015). Hypoxia is known as a strong inducer of c-Jun phosphorylation and upregulation (Chang et al., 2014; Laderoute et al., 2002; Minet et al., 2001). Indeed, *hypoxia*-inducible factor 1-alpha (HIF1α), a transcription factor that is rapidly targeted to the proteasome and degraded in the cell cytoplasm under normoxic conditions, is instead rapidly upregulated in hypoxic conditions by inhibition of its degradation (reviewed in Jiang et al., 2021). Under hypoxia, HIF1a upregulation can promote c-Jun-N-terminal kinases (JNK) activation (Comerford et al., 2004; Minet et al., 2001) and both HIF1a and phosphorylated JNK translocate to the cell nucleus (Flores et al., 2019; Jiang et al., 2021; Schödel et al., 2019), which leads to JNK-dependent c-Jun phosphorylation and to the activation of *c-Jun* transcription (Laderoute et al., 2002; Minet et al., 2001) and c-Jun stabilization (Musti et al., 1997). The mechanisms regulating HIF1α stabilization and degradation have been extensively studied (Jiang et al., 2021; Yu et al., 2001), particularly in cancer cells (Kaelin et al., 2022; Pugh et al., 2003; Wicks et al., 2022). However, they remain partially understood and little is known about HIF1α regulation in SCs. Here, we show that HDAC8, a member of the class I HDAC family of proteins whose functions in SCs remained so far unreported, counteracts the stabilization of HIF1a in SCs, thereby slowing down HIF1α -dependent c-Jun phosphorylation and upregulation, axonal regrowth, and functional recovery after injury. Unexpectedly, we found that HDAC8 regulates this mechanism specifically in SCs

ensheathing sensory axons, thereby specifically controlling the regrowth of sensory axons and the recovery of sensory function.

4.2 Ablation of HDAC8 in adult Schwann cells accelerates myelin clearance, regrowth of sensory axons and sensory function recovery after injury

We found that after a sciatic nerve crush lesion, HDAC8 expression is upregulated in peripheral nerves distal to the lesion site (**Fig. 15a**) and is exclusively or in major part found in the cell cytoplasmic compartment, until at least 12 days post lesion (dpl) (**Fig. 15b**). To test for a potential function of HDAC8 in SCs during the regeneration process after lesion, we ablated HDAC8 specifically in adult SCs. To this aim, we crossed *Hdac8* floxed mice with mice expressing the tamoxifen-inducible CreERT2 recombinase under control of the *Plp* promoter (HDAC8 KO) that is active in SCs (and oligodendrocytes) and used *Plp*-CreERT2-negative littermates as control mice. To induce HDAC8 ablation, we injected 2 mg tamoxifen per day for five consecutive days. Control mice received tamoxifen injections simultaneously to HDAC8 KO mice. Mice were submitted to a sciatic nerve crush lesion two weeks after tamoxifen injections, where HDAC8 was efficiently ablated in SCs (**Fig. S1a**). Surprisingly, the regeneration process after lesion was not impaired by the ablation of HDAC8, but instead was accelerated. Indeed, we found by electron microscopy that myelin debris were cleared faster and more axons per surface area, including Remak axons, had regrown at 12 dpl (**Fig. 15c**) in HDAC8 KO compared to control mice. To test for a potential improvement in functional recovery, we crossed *Hdac8* floxed mice with mice expressing the tamoxifen-inducible CreERT2 recombinase under control of the *P0* promoter (also called thereafter HDAC8 KO, only used for functional recovery experiments) that is active only in SCs and used *P0*-CreERT2-

negative littermates as control mice. Here again, mice were submitted to a sciatic nerve crush lesion two weeks after tamoxifen injections, where HDAC8 was also efficiently ablated in SCs (**Fig. S1b**). We found that sensory function recovery was faster in HDAC8 KO mice (**Fig. 15d**). However, motor function recovery (**Fig. 15d**) and remyelination (**Fig. S2a-b**) were comparable in both HDAC8 KO and control mice and we did not detect compensatory expression of HDAC1, HDAC2 or HDAC3 (**Fig. S2b**), the other members of class I HDACs. We then carried out whole-nerve stainings for Stathmin-2 (STMN2, also called SCG10) and growth-associated protein 43 (GAP43) in sciatic nerves of HDAC8 KO and control mice at 3 dpl. STMN2 is a highly selective marker of regrowing axons that preferentially labels sensory axons after sciatic nerve injury, while GAP43 is a general marker of regrowing axons (Shin et al., 2014). Consistent with faster sensory function recovery, we found that STMN2-labeled axons had regrown over a longer distance at 3 dpl in sciatic nerves of HDAC8 KO mice compared to control mice (**Fig. 15e**), whereas we could not detect a significant difference for GAP43-labeled axons (**Fig. S3**). We thus asked whether HDAC8 is specifically expressed in SCs associated with sensory axons, which could potentially explain why HDAC8 ablation has a specific effect on the regrowth and functional recovery of sensory axons. To answer this question, we co-stained HDAC8 with STMN2 that preferentially labels sensory axons and Neurofilament that labels all axons. Indeed, SCs expressing high levels of HDAC8 were associated with STMN2-positive axons, whereas SCs associated with STMN2-negative axons (Neurofilament-positive) did not express HDAC8 or at very low level (**Fig. 15f** and **Fig. S4**). Of note, HDAC8 was also expressed in some axons (**Fig. 15f**). Taken together, our results identify HDAC8 as a specific marker of SCs associated with sensory axons in adult sciatic nerves and show that the ablation of HDAC8 in SCs

promotes myelin debris clearance, regrowth of sensory axons and sensory function recovery.

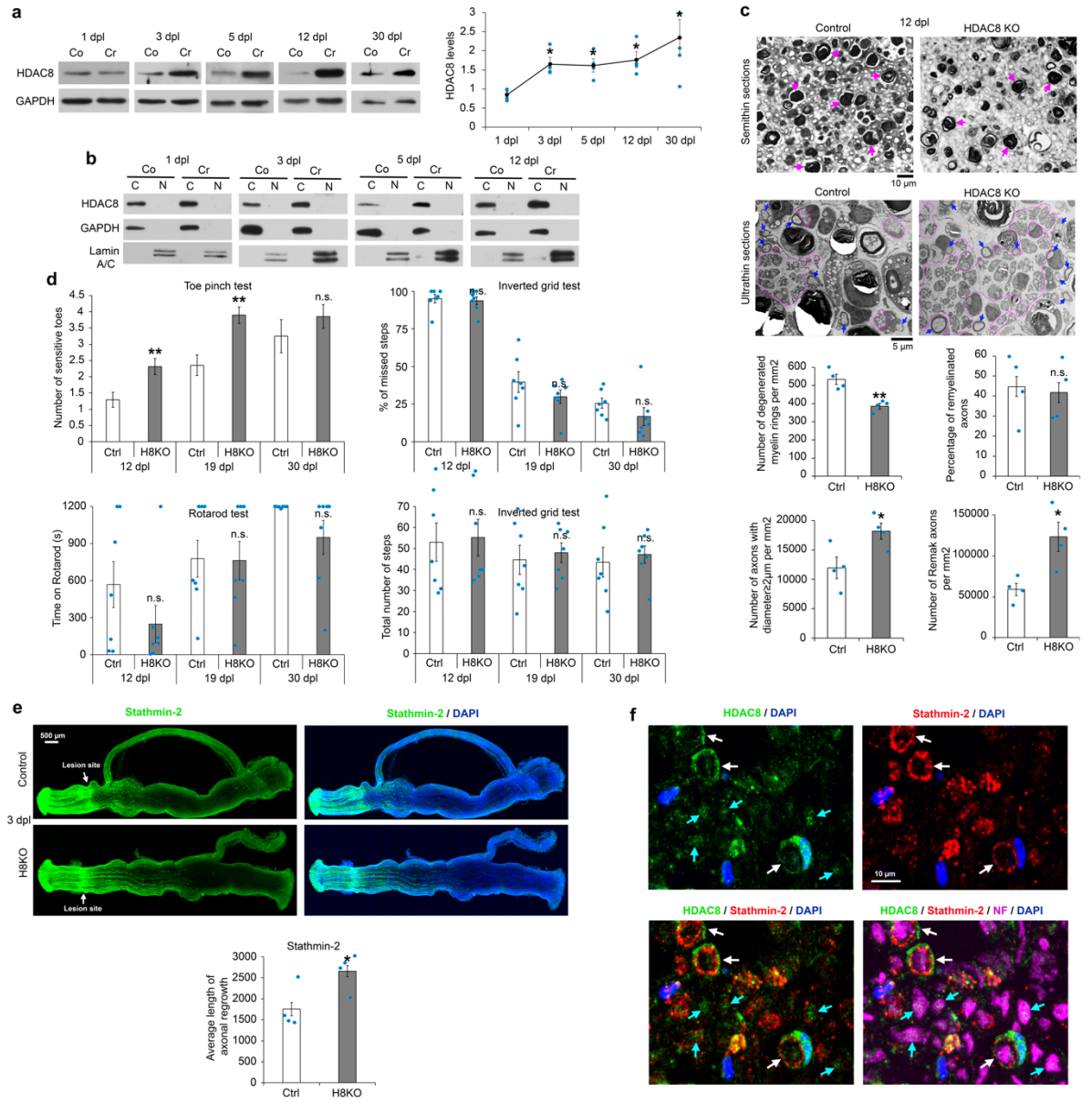

Figure 15. HDAC8 ablation in SCs promotes the regeneration of sensory axons and sensory function recovery. (**a**) HDAC8 Western blot and quantification normalized to GAPDH at 1, 3, 5, 12 and 30 dpl, showing upregulation of HDAC8 starting from 3dpl in crushed compared to contralateral sciatic nerves of wild type (WT) adult mice. Paired two-tailed Student's t-tests, p value: *<0.05, values=mean, error bars=s.e.m., n=4 (1, 3, 5, 12 dpl) or 5 (30 dpl) animals per group. (**b**) HDAC8 Western blot after subcellular fractionation of cytoplasmic (C) and nuclear (N) fractions of crushed (Cr) and contralateral (Co) sciatic nerves of adult mice at 1, 3, 5 and 12 dpl. GAPDH and Lamin A/C are used as markers of the cytoplasmic and nuclear fractions, respectively, and show the efficiency of the fractionation. Three WT mice per time point were used and representative images are shown. (**c**) Semithin (upper panel) and ultrathin (lower panel) cross-sections of HDAC8 KO (H8KO) and Control (Ctrl) sciatic nerves of adult mice at 12 dpl, and graphs showing the number of degenerated myelin rings per mm^2, the

percentage of remyelinated axons, the number of axons with diameter ≥ 2 µm per mm^2, and the number of Remak axons per mm^2. Unpaired two-tailed Student's t-tests, p values: *<0.05, **<0.01, values=mean, error bars=s.e.m., n=4 animals per group. On the upper panel, magenta arrows point to degenerated myelin rings. On the lower panel, blue arrows indicate remyelinated axons, and the areas surrounded by a pink line show Remak axons. (**d**) Graphs representing the performance of HDAC8 KO and Control mice at the Toe pinch test, Rotarod test and Inverted grid test. Unpaired two-tailed (Toe pinch test) or one-tailed (Rotarod test and Inverted grid test) Student's t-tests, p values: **<0.01, values=mean, error bars=s.e.m., n=12 (Toe pinch test), 7 (Rotarod test) and 7 (Inverted grid test) animals per group. (**e**) Whole sciatic nerve immunofluorescence of Stathmin-2 (green, marker of sensory regenerative fibers) and DAPI labeling (blue, nuclei) and quantification of axonal regrowth at 3 dpl showing longer regrowth in HDAC8 KO compared to Control nerves. Unpaired two-tailed Student's t-tests, p value: *<0.05, values=mean, error bars=s.e.m., n=4 animals per group, 45 to 76 regrowing axons measured and counted per animal. (**f**) Co-immunofluorescence of HDAC8 (green), Stathmin-2 (red) and Neurofilament (NF, magenta, general axonal marker) and DAPI labeling (blue) in a sciatic nerve cross-section of WT mice at 1 dpl. Three animals were used, and a representative image is shown. White arrows point to HDAC8-positive SCs surrounding Stathmin-2-positive axons, and blue arrows indicate HDAC8-positive axons (NF-positive).

4.3 HDAC8 ablation in Schwann cells enhances hypoxia-induced c-Jun phosphorylation and upregulation

Molecularly, we found that the levels of c-Jun (**Fig. 16a-b**) and phosphorylated c-Jun (**Fig. 16b**) were increased in SCs of HDAC8 KO compared to control mice, already at 1 dpl. c-Jun expression levels remained increased in SCs of HDAC8 KO mice until at least 3 dpl and returned to control levels at 5 dpl (**Fig. 16a**). Oct6 expression levels in SCs were not affected by the ablation of HDAC8 (**Fig. S5**), indicating that the mechanisms underlying c-Jun upregulation in HDAC8 KO SCs are different than the mechanisms responsible for c-Jun upregulation in HDAC1/2 KO SCs (Brügger et al., 2017).

To elucidate these mechanisms, we used purified primary rat SCs cultured under conditions that mimic the conversion into the repair SC phenotype occurring after a peripheral nerve lesion, where myelin proteins are downregulated and c-Jun upregulated (Brügger et al., 2017; Duman et al., 2020; Monje et al., 2010). To downregulate HDAC8 in primary SCs, we used a lentiviral vector carrying a highly efficient HDAC8-specific shRNA (**Fig. S6a**). HDAC8 downregulation in SCs

led to increased levels of c-Jun and phosphorylated c-Jun compared to levels in SCs transduced with a lentiviral vector carrying a non-targeting control shRNA (**Fig. S6b**), an effect that was however more significant under hypoxic conditions, either by incubation in a hypoxia chamber (**Fig. 16c-d**) or incubation with cobalt chloride ($CoCl_2$) which mimics hypoxic conditions (**Fig. 16e-f**). Hypoxia is known as a robust inducer of c-Jun expression and phosphorylation and occurs after a peripheral nerve injury (Babetto et al., 2020; Chang et al., 2014; Cho et al., 2015; Laderoute et al., 2002, 2004; Minet et al., 2001). Additionally, we show that knocking out HIF1a specifically in adult SCs by crossing *Plp*-CreERT2 mice with *Hif1α* -floxed mice and inducing *Hif1α* recombination by tamoxifen injections, such as described above for *Hdac8* recombination, leads to reduced c-Jun upregulation after lesion (**Fig. S7**). For these reasons, we carried out our cell cultures under hypoxia and tested whether hypoxia is involved in HDAC8-mediated regulation of c-Jun expression and phosphorylation after injury. In addition to increased c-Jun protein levels, we found that HDAC8 downregulation in primary SCs led to increased *c-Jun* mRNA levels under hypoxic conditions (**Fig. 16g**), but only to a trend under normoxia (**Fig. S6c**). Consistently, HDAC8 downregulation resulted in increased activation of the *c-Jun* promoter under hypoxic conditions (**Fig. 16h**), but not under normoxia (**Fig. S6d**). These results indicate that HDAC8 counteracts c-Jun upregulation and phosphorylation, particularly under hypoxic conditions.

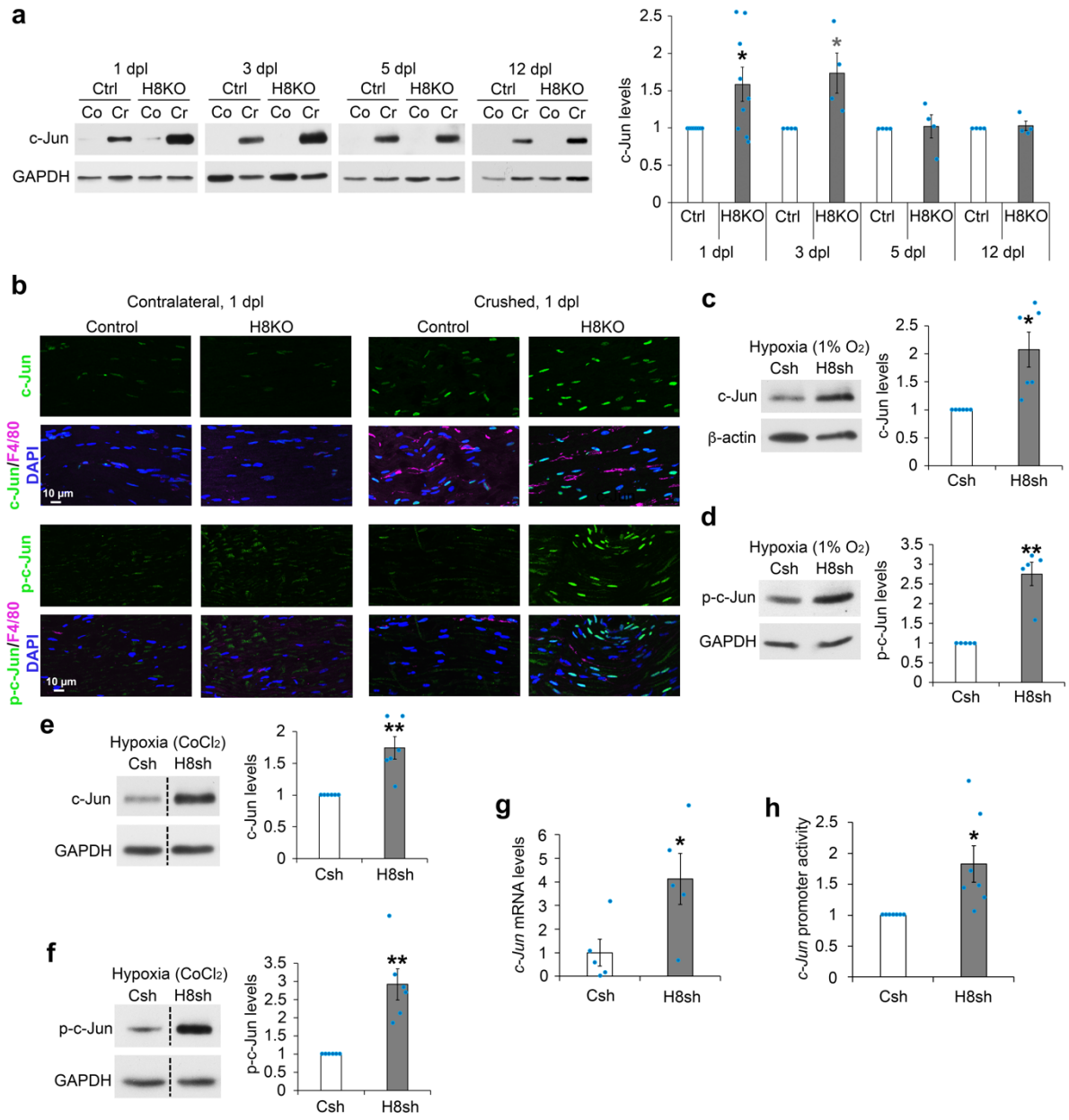

Figure 16. Ablation of HDAC8 in SCS leads to increased levels of c-Jun and phospho-c-Jun. (**a**) c-Jun Western blot and quantification normalized to GAPDH at 1, 3, 5 and 12 dpl, showing increased c-Jun levels at 1 and 3 dpl in crushed sciatic nerves of HDAC8 KO mice compared to Control mice. Paired two-tailed (1 dpl) or one-tailed (3, 5, and 12 dpl) Student's t-tests, p value: *<0.05, values=mean, error bars=s.e.m., n=9 (1 dpl) or 4 (3, 5, and 12 dpl) animals per group. (**b**) Co-immunofluorescence of c-Jun (green, upper panels) or phospho-c-Jun (p-c-Jun, green, lower panels) and F4/80 (magenta, marker of macrophages), and DAPI labeling (blue, nuclei) in longitudinal sections of crushed and contralateral HDAC8 KO and Control sciatic nerves at 1 dpl. Three animals per group were used and representative images are shown. (**c**, **d**, **e**, **f**) Western blot of c-Jun (c, e) or phospho-c-Jun (d, f) in primary rat SCs cultured under conditions mimicking the conversion into the repair phenotype in hypoxia (c, d : in hypoxic chamber for 16 h ; e, f : $CoCl_2$ for 16 h), and quantification normalized to GAPDH showing that prior downregulation of HDAC8 by shRNA (H8sh) leads to increased c-Jun and phospho-c-Jun levels compared to cells incubated with a control shRNA (Csh). The dashed lines indicate that samples were run on the same gel but not on consecutive lanes. Paired two-tailed Student's t-tests, p values: *<0.05, **<0.01, values=mean, error bars=s.e.m., n=6 (c, e, f) independent experiments per group. (**g**) Quantification of *c-Jun* mRNA levels by qRT-PCR in primary rat SCs cultured as in above (c, d), showing

increased *c-Jun* expression in cells where HDAC8 was downregulated by shRNA compared to cells incubated with a control shRNA. Unpaired two-tailed Student's t-tests, p values: *<0.05, values=mean, error bars=s.e.m., n=5 independent experiments per group. (**h**) Quantification of *c-Jun* promoter activity by luciferase gene reporter assay in cells cultured as above (c, d, g), showing higher activity when HDAC8 was downregulated by shRNA compared to cells incubated with a control shRNA. Paired two-tailed Student's t-tests, p values: *<0.05, values=mean, error bars=s.e.m., n=7 independent experiments per group.

Hypoxia leads to the stabilization of HIF1α and its translocation to the nuclear compartment (Jiang et al., 2021 and **Fig. S8**). Consistent with HDAC8 cytoplasmic localization in contralateral and crushed sciatic nerves of adult mice (Fig. 15b), we found that HDAC8 is exclusively localized in the cytoplasm of primary rat SCs cultured under conditions mimicking the conversion into the repair phenotype in normoxia or hypoxia (**Fig. 17a**). HDAC8 downregulation increased HIF1α levels under normoxic (**Fig. 17b**) and hypoxic (**Fig. 17b-c**) conditions, and HIF1α downregulation by shRNA (**Fig. S9**) reduced c-Jun expression and phosphorylation (**Fig. 17d-e**). We hypothesized that HDAC8 promotes HIF1α degradation. Indeed, when we inhibited the proteasome by a treatment with the proteasome inhibitor MG-132, HIF1α levels were no longer increased in cells where HDAC8 was downregulated compared to controls (**Fig. 17f**). Taken together, these data indicate that the increased levels of HIF1α in SCs mediated by HDAC8 downregulation are due to the protection of HIF1α from proteasomal degradation. Under normoxia, the Von Hippel-Lindau (VHL) tumor suppressor interacts with HIF1α and recruits a protein complex with E3 ubiquitin ligase activity that induces HIF1α ubiquitination and subsequent targeting to the proteasome (Kaelin et al., 2022). However, expression levels of VHL were increased in normoxic conditions in SCs where HDAC8 was downregulated by shRNA (**Fig. S10**), probably to compensate the increased levels of HIF1α, as previously shown (Karhausen et al., 2005; Turcotte et al., 2004), suggesting that HDAC8 regulates HIF1α stability by a VHL-independent mechanism. Consistent with our cell culture findings, we show that HIF1α levels are increased in sciatic

nerves of HDAC8 KO mice compared to control mice already at 1 dpl (**Fig. 17g**), indicating that HDAC8 KO SCs can rapidly upregulate HIF1α after injury. Interestingly, we identified this early increase of HIF1α levels in the cytoplasmic compartment (**Fig. 17g**), while nuclear levels of HIF1α were not affected (**Fig. S11**), indicating that HIF1α -dependent regulation of c-Jun expression and phosphorylation at 1dpl is mediated by a mechanism occurring in the cytoplasm. Similarly, at an early time point of hypoxia in rat SCs, the increase of HIF1α levels due to HDAC8 downregulation occurred in the cytoplasm (**Fig. 17h**), whereas no HIF1α was detected in the nucleus (data not shown). Several studies have also reported high levels of HIF1α in the cytoplasmic compartment while nuclear levels remained low (Baba et al., 2010; Kubis et al., 2005; Wu et al., 2021), suggesting a function of HIF1α in the cytoplasm. c-Jun is phosphorylated by JNK and in turn phosphorylated c-Jun dimerizes with ATF-2 to activate c-Jun expression (Herdegen et al., 1997). In addition, the JNK pathway is known to mediate various hypoxia-induced cellular processes (reviewed in Tam and Law, 2021). We found that in SCs cultured under hypoxic conditions, HIF1α downregulation by shRNA led to decreased activation of JNK (**Fig. 17i**), and JNK inhibition completely abrogated the increase of c-Jun phosphorylation and partly prevented c-Jun upregulation mediated by HDAC8 downregulation (**Fig. 17j-k**). Taken together, our data indicate that the ablation or downregulation of HDAC8 in SCs leads to HIF1α - and JNK-dependent c-Jun phosphorylation and upregulation.

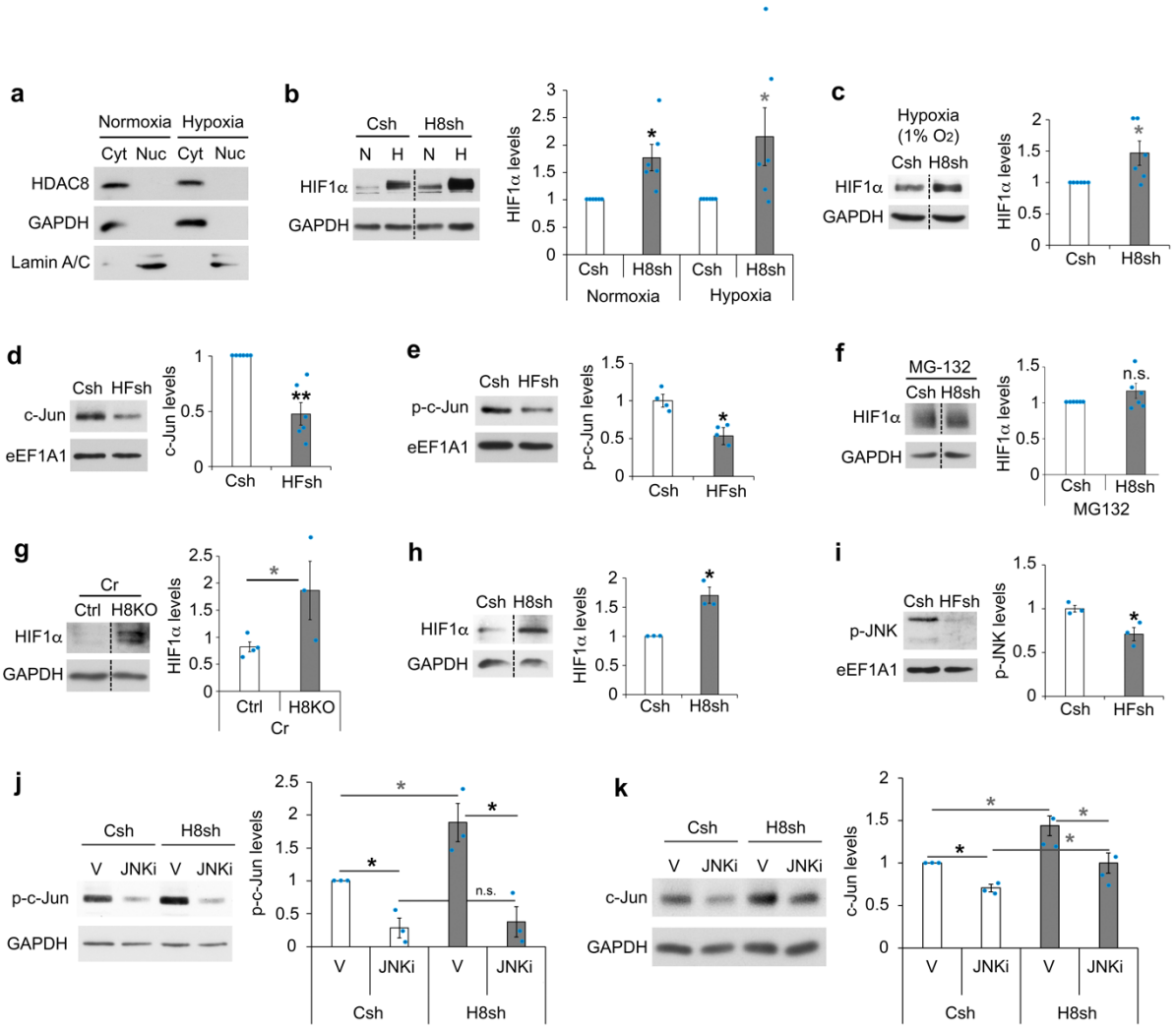

Figure 17. HDAC8 ablation activates a HIF1α/JNK/c-Jun axis. (**a**) HDAC8 Western blot after subcellular fractionation of cytoplasmic (Cyt) and nuclear (Nuc) fractions of rat SCs cultured under normoxia or hypoxia ($CoCl_2$ for 16 h) in conditions mimicking the conversion into the repair phenotype. GAPDH and Lamin A/C, used as markers of the cytoplasmic and nuclear fractions, respectively, show fractionation efficiency. Three independent experiments have been carried out and representative images are shown. (**b**, **c**) HIF1α Western blot on lysates of rat SCs cultured under the same conditions as above (a) in normoxia (N) or hypoxia (H) induced by $CoCl_2$ (b) or by incubation in a hypoxia chamber (c) for 16 h, and quantification normalized to GAPDH showing that the downregulation of HDAC8 by shRNA (H8sh) leads to increased HIF1α levels compared to cells incubated with a control shRNA (Csh). Paired two-tailed (Normoxia) or one-tailed (Hypoxia) Student's t-tests, p values: *<0.05, values=mean, error bars=s.e.m., n=6 independent experiments per group. (**d**, **e**, **i**) c-Jun (d), phospho-c-Jun (p-c-Jun, e) and phospho-JNK (p-JNK, i) Western blots on lysates of rat SCs cultured under the same conditions as above (a) in hypoxia ($CoCl_2$ for 16 h), and quantification normalized to eEF1A1 showing decreased levels of c-Jun, p-c-Jun and p-JNK when HIF1a was downregulated by shRNA (HFsh) compared to cells incubated with a control shRNA (Csh). Unpaired two-tailed Student's t-tests, p values: *<0.05, **<0.01, values=mean, error bars=s.e.m., n= 6 (c-Jun), 4 (p-c-Jun) or 3 (p-JNK) independent experiments per group. (**f**) HIF1α Western blot on lysates on rat SCs cultured as above (a) under normoxia and incubated with the proteasome inhibitor MG-132 for 4 h, and quantification normalized to GAPDH showing no significant difference (n.s.) of HIF1α levels in cells where HDAC8 was downregulated by shRNA (H8sh) compared to cells incubated with the control shRNA (Csh). Paired one-tailed Student's

t-test, n.s.=non-significant, values=mean, error bars=s.e.m., n=6 independent experiments per group. (**g**) HIF1α Western blot on lysates of crushed sciatic nerves (Cr) of HDAC8 KO (H8KO) and control (Ctrl) mice at 1 dpl after subcellular fractionation (the cytoplasmic fraction is shown), and quantification normalized to GAPDH and to levels in contralateral nerves showing increased HIF1α levels in H8KO compared to Ctrl. Unpaired one-tailed Student's t-tests, p value: *<0.05, values=mean, error bars=s.e.m., n=4 (Ctrl) or 3 (H8KO) animals per group. For nuclear fractions and contralateral nerve lysates, see Figure S10. (**h**) HIF1α Western blot on lysates of rat SCs cultured under the same conditions as above (a) under hypoxia (hypoxic chamber for 5 hours) after subcellular fractionation (the cytoplasmic fraction is shown), and quantification normalized to GAPDH showing higher levels of HIF1α in cells where HDAC8 was downregulated by shRNA (H8sh) compared to cells incubated with a control shRNA (Csh). Paired two-tailed Student's t-tests, p values: *<0.05, values=mean, error bars=s.e.m., n=3 independent experiments per group. (**j**, **k**) Phospho-c-Jun (p-c-Jun, j) or c-Jun (k) Western blots on lysates of rat SCs cultured under the same conditions as above (a) in hypoxia and where cells were either incubated with a HDAC8 shRNA (H8sh) or a control shRNA (Csh) lentivirus, and quantification normalized to GAPDH showing that treatment with a highly specific JNK inhibitor (JNKi) totally prevents c-Jun phosphorylation (j) and partially prevents c-Jun upregulation (k) mediated by HDAC8 downregulation, compared to vehicle-treated cells (V). Paired (comparison to Csh-V) or unpaired two-tailed (black asterisks) or one-tailed (grey asterisks) Student's t-tests, p values: *<0.05, n.s.=non-significant, values=mean, error bars=s.e.m., n= 3 independent experiments per group. Dashed lines indicate that samples were run on the same gel but not on consecutive lanes.

4.4 HDAC8 regulates TRAF7 expression to promote HIF1a degradation and to prevent c-Jun phosphorylation

To understand how HDAC8 regulates HIF1a stabilization, we first asked whether HDAC8 deacetylase activity is involved in this function. We tested 2 different HDAC8 specific inhibitors, PCI-34051 and 1-Naphthohydroxamic acid, at different concentrations. None of the two HDAC8 inhibitors was able to increase HIF1a levels, c-Jun expression, or phosphorylated c-Jun levels in SCs (**Fig. S12a-c**), indicating that these effects are independent of HDAC8 deacetylase activity. HDAC8 has been previously shown to have in some instances deacetylase-independent functions, including acting as a scaffold for protein complexes or preventing the degradation of its binding partners (Durst et al., 2003; Gao et al., 2009; Lee et al., 2006). To identify HDAC8 putative binding partners, we immunoprecipitated HDAC8 in unlesioned mouse sciatic nerves and at 1 day post sciatic nerve crush lesion and used a non-targeting IgG as immunoprecipitation control. We then analyzed co-immunoprecipitated

proteins by mass spectrometry. We found 9 interesting, significantly enriched terms among which “Ubiquitin conjugation” showed the highest number of matching proteins (**Fig. 18a** and Table S1). Among the putative binding partners of HDAC8 with a function in ubiquitin conjugation, we focused on tumor necrosis factor receptor-associated factor 7 (TRAF7) that is localized in the cytoplasmic compartment in both primary rat SCs (**Fig. 18b**) and adult sciatic nerves (**Fig. 18c**) such as HDAC8, possesses a RING domain with E3 ligase activity and can therefore mediate ubiquitination (Bouwmeester et al., 2004; Zotti et al., 2017). Our mass spectrometry analyses indicated TRAF7 as a putative binding partner of HDAC8 in both unlesioned nerves and nerves at 1 day post sciatic nerve crush lesion (Table S1). We first confirmed that TRAF7 co-immunoprecipitated with HDAC8 in primary rat SCs (**Fig. 18d**). We used two different TRAF7 antibodies, which both detected three to four bands in primary rat SCs and in mouse sciatic nerves, two-three ranging from around 65 to 75 kDa and one shorter around 50 kDa (**Fig. 18b-c**). Multiple isoforms of TRAF7 ranging from 65 to 75 kDa are commonly described. In addition, the NCBI database describes a shorter predicted isoform of 50 kDa (accession number: XR_007064922.1) that contains the RING finger domain with E3 ubiquitin ligase activity, the TRAF-type Zinc finger domain and the coiled-coil domain, but only one truncated WD40 repeat domain instead of the 7 WD40 repeat domains found in the longest TRAF7 isoform (Zotti et al., 2017). To test whether all bands detected by the TRAF7 antibodies are isoforms of TRAF7, we downregulated TRAF7 in primary rat SCs by using a lentivirus carrying a specific TRAF7 shRNA targeting a sequence common to all TRAF7 isoforms. Indeed, all four bands were downregulated (**Fig. 18e**), indicating that they correspond to four different isoforms of TRAF7. Among these four isoforms, we found that the shorter isoform co-immunoprecipitated with HDAC8 (**Fig. 18d**). Interestingly, in primary rat SCs

where HDAC8 was downregulated by shRNA, expression of the shorter TRAF7 isoform was significantly decreased while expression of the longest isoform was increased (**Fig. 18f**). In sciatic nerves, we found that TRAF7 is expressed in all SCs (**Fig. 18g**), while as described above, HDAC8 is present only in sensory SCs and in axons. Consistent with our cell culture findings, the short TRAF7 isoform was downregulated in HDAC8 KO nerves, while the long TRAF7 isoform was upregulated (**Fig. 18h**). Of note, the short TRAF7 isoform was also downregulated in crushed nerves of Control mice at 1 dpl compared to contralateral nerves, but not further downregulated in crushed nerves of HDAC8 KO mice compared to their contralateral nerves (**Fig. 18h**). This suggests that TRAF7 short isoform is completely downregulated already in SCs of contralateral nerves of HDAC8 KO mice and can therefore not be further downregulated. The remaining expression of TRAF7 short isoform is thus likely to be due to expression in non-sensory SCs. These results indicate that HDAC8 differentially regulates TRAF7 isoforms by stabilizing the short isoform and in contrast destabilizing the long isoform. We then asked whether TRAF7 is involved in HDAC8-dependent degradation of HIF1α and subsequent effects on c-Jun regulation. We found that TRAF7 downregulation by shRNA in primary rat SCs led to increased HIF1α levels in normoxic conditions (**Fig. 18i**) and increased c-Jun levels in hypoxic conditions (Fig. 18j), similar to the effects of HDAC8 downregulation. In addition, by co-immunoprecipitation we show that the short TRAF7 isoform interacts with HIF1α in primary rat SCs (**Fig. S13** and **Fig. 18k**) and that HIF1α ubiquitination is decreased in SCs where TRAF7 is downregulated by shRNA (**Fig. 18l**). However, in contrast to HDAC8 downregulation, we found that TRAF7 downregulation led to decreased levels of phosphorylated c-Jun in normoxia and has no effect on HIF1α and phospho-c-Jun levels in hypoxia (**Fig. S14a-b**). It has been previously shown that TRAF7 can promote JNK

phosphorylation (Bouwmeester et al., 2004; Scudiero et al., 2012; Xu et al., 2004), which in turn increases HIF1α levels and phosphorylates c-Jun (Comerford et al., 2004; Sala et al., 2018; Tam et al., 2020; Zeke et al., 2016). Indeed, we show in primary rat SCs that TRAF7 downregulation leads to decreased phospho-JNK levels in normoxia but not in hypoxia (**Fig. S12c**). It is highly likely that this effect is due to the downregulation of the long TRAF7 isoforms that contain WD40 repeats because TRAF7 is known to promote JNK phosphorylation by interacting with MEKK3 through its WD40 repeat domains (Gao et al., 2009; Zotti et al., 2017). As mentioned above, the short TRAF7 isoform contains only one truncated WD40 repeat domain and it was shown that a mutant of TRAF7 missing the WD40 repeat domains cannot interact with MEKK3 and that the long TRAF7 isoform cannot promote JNK phosphorylation in the absence of MEKK3 (Bouwmeester et al., 2004). Since HDAC8 stabilizes the short TRAF7 isoform but destabilizes the long TRAF7 isoform (**Fig. 18f**), we conclude that HDAC8 downregulation leads through the upregulation of the long TRAF7 isoform to increased phospho-JNK levels, inducing increased phospho-c-Jun levels and consequently increased c-Jun levels, and through the downregulation of the short TRAF7 isoform to increased HIF1α levels, resulting in JNK-dependent increase of phospho-c-Jun and c-Jun levels and to JNK-independent increase of c-Jun levels. Consistently, we show here that overexpression of TRAF7 (long and short isoforms) reverted the increase of HIF1α and c-Jun but not of phospho-c-Jun levels mediated by HDAC8 downregulation through shRNA (**Fig. 18m-p**). Of note, all four TRAF7 isoforms were overexpressed by transfection of a construct carrying the longest isoform, indicating that the isoforms detected by Western blot result either from post-translational modifications of the long isoform or potentially also from mRNA heterosplicing, a mechanism that has been recently described (Top et al., 2021).

Taken together, these data show that HDAC8 oppositely regulates the short and the long TRAF7 isoforms, which leads to TRAF7-induced ubiquitination and degradation of HIF1α and slows down JNK phosphorylation, c-Jun phosphorylation, and c-Jun upregulation in hypoxic conditions (**Fig. 19**).

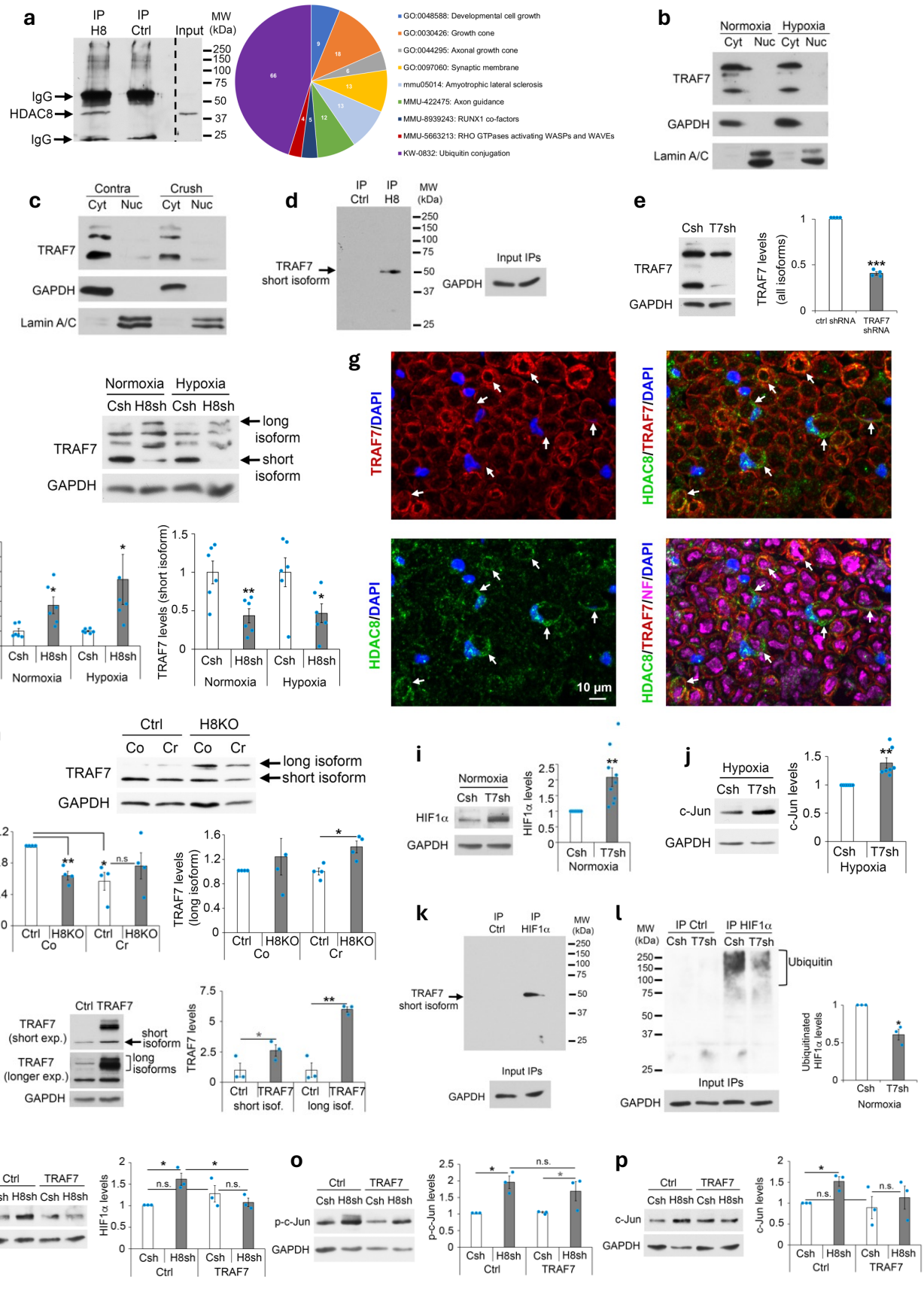
a
IP H8
IP Ctrl
Input
MW (kDa)
250
150
100
75
50
37
25
IgG
HDAC8
IgG
GO:0048588: Developmental cell growth
GO:0030426: Growth cone
GO:0044295: Axonal growth cone
GO:0097060: Synaptic membrane
mmu05014: Amyotrophic lateral sclerosis
MMU-422475: Axon guidance
MMU-8939243: RUNX1 co-factors
MMU-5663213: RHO GTPases activating WASPs and WAVEs
KW-0832: Ubiquitin conjugation
b
Normoxia
Hypoxia
Cyt Nuc Cyt Nuc
TRAF7
GAPDH
Lamin A/C
c
Contra
Crush
Cyt Nuc Cyt Nuc
TRAF7
GAPDH
Lamin A/C
d
IP Ctrl
IP H8
MW (kDa)
TRAF7 short isoform
Input IPs
GAPDH
e
Csh T7sh
TRAF7
GAPDH
TRAF7 levels (all isoforms)
ctrl shRNA
TRAF7 shRNA
***
f
Normoxia
Hypoxia
Csh H8sh Csh H8sh
TRAF7
long isoform
short isoform
GAPDH
TRAF7 levels (long isoform)
TRAF7 levels (short isoform)
Csh H8sh Csh H8sh
Normoxia
Hypoxia
g
TRAF7/DAPI
HDAC8/TRAF7/DAPI
HDAC8/DAPI
HDAC8/TRAF7/NF/DAPI
10 µm
h
Ctrl
H8KO
Co Cr Co Cr
TRAF7
long isoform
short isoform
GAPDH
TRAF7 levels (short isoform)
TRAF7 levels (long isoform)
Ctrl H8KO Ctrl H8KO
Co
Cr
i
Normoxia
Csh T7sh
HIF1α
GAPDH
HIF1α levels
Csh T7sh
Normoxia
j
Hypoxia
Csh T7sh
c-Jun
GAPDH
c-Jun levels
Csh T7sh
Hypoxia
k
IP Ctrl
IP HIF1α
MW (kDa)
TRAF7 short isoform
Input IPs
GAPDH
l
MW (kDa)
IP Ctrl
IP HIF1α
Csh T7sh Csh T7sh
Ubiquitin
Input IPs
GAPDH
Ubiquitinated HIF1α levels
Csh T7sh
Normoxia
m
Ctrl TRAF7
TRAF7 (short exp.)
TRAF7 (longer exp.)
short isoform
long isoforms
GAPDH
TRAF7 levels
Ctrl TRAF7 short isof.
Ctrl TRAF7 long isof.
n
Ctrl
TRAF7
Csh H8sh Csh H8sh
HIF1α
GAPDH
HIF1α levels
n.s.
Csh H8sh Csh H8sh
Ctrl
TRAF7
o
Ctrl
TRAF7
Csh H8sh Csh H8sh
p-c-Jun
GAPDH
p-c-Jun levels
n.s.
Csh H8sh Csh H8sh
Ctrl
TRAF7
p
Ctrl
TRAF7
Csh H8sh Csh H8sh
c-Jun
GAPDH
c-Jun levels
n.s.
Csh H8sh Csh H8sh
Ctrl
TRAF7

Figure 18. HDAC8 interacts with and regulates TRAF7 to control HIF1α levels and JNK activation. (a) GO analysis (selection of process relevant terms and enrichments compared to the whole genome as background) of HDAC8 putative binding partners after immunoprecipitation (IP) of HDAC8 (H8) on lysates of crushed and contralateral mouse sciatic nerves at 1 dpl and analysis of binding partners by mass spectrometry. As negative control, an IP with a non-targeting IgG was carried out on the same lysates as the HDAC8 IP. A representative IP and Western blot (carried out 3 times on independent samples) on similar samples (lysates of adult mouse sciatic nerves) with the same antibodies show the efficiency of the HDAC8 IP. (**b**, **c**) TRAF7 Western blot after subcellular fractionation of cytoplasmic (Cyt) and nuclear (Nuc) fractions of (b) rat SCs cultured under normoxia or hypoxia ($CoCl_2$ for 16 h) in conditions mimicking the conversion into the repair phenotype or (c) crushed (Crush) and contralateral (Contra) mouse sciatic nerves at 1 dpl. GAPDH and Lamin A/C, used as markers of the cytoplasmic and nuclear fractions, respectively, show the efficiency of the fractionation. (b) Three independent experiments have been carried out and (c) three animals have been used, and representative images are shown (b, c). (**d**) IP HDAC8 (H8) or control IP (Ctrl, IgG) and Western blot of TRAF7 in lysates of rat SCs cultured under the same conditions as above (b) in normoxia. The GAPDH input shows equal amount of lysates used for IP HDAC8 and control IP. Three independent experiments have been carried out and representative images are shown. (**e**) TRAF7 and GAPDH (loading control) Western blots in lysates of rat SCs cultured as above (b) in normoxia and incubated with lentiviruses carrying either a TRAF7 shRNA (T7sh) or a control shRNA (Csh), showing that all bands detected by the TRAF7 antibody are downregulated by the TRAF7-specific shRNA, and quantification normalized to GAPDH showing decreased levels of TRAF7 (all isoforms) in cells where TRAF7 was downregulated. Paired two-tailed Student's t-tests, p value: ***<0.001, values=mean, error bars=s.e.m., n=4 independent experiments per group. (**f**) TRAF7 Western blot in lysates of cells cultured as above (b) in normoxia and hypoxia and incubated with lentiviruses carrying either an HDAC8 shRNA (H8sh) or a control shRNA (Csh), and quantification normalized to GAPDH showing decreased levels of the short TRAF7 isoform and increased levels of the longest TRAF7 isoform in cells where HDAC8 was downregulated. Unpaired two-tailed Student's t-tests, p values: *<0.05, **<0.01, values=mean, error bars=s.e.m., n=6 independent experiments per group. (**g**) Co-immunofluorescence (z-series projection of confocal stacks) of TRAF7 (red), HDAC8 (green) and Neurofilament (NF, magenta, axonal marker), and DAPI labeling (blue, nuclei) in cross-section of adult mouse sciatic nerve showing TRAF7 expression in all SCs (rings surrounding axons). Three WT mice were used for this experiment and representative images are shown. (**h**) TRAF7 Western blot in lysates of HDAC8 KO (H8KO) and control (Ctrl) crushed (Cr) and contralateral (Co) mouse sciatic nerves at 1 dpl, and quantification normalized to GAPDH showing decreased levels of the short TRAF7 isoform and increased levels of the long TRAF7 isoform in H8KO nerves. Paired (comparison to Ctrl-Co) or unpaired two-tailed Student's t-tests, p values: *<0.05, **<0.01, n.s.=non-significant, values=mean, error bars=s.e.m., n=4 animals per group. (**i**, **j**) Western blot of HIF1α (i) or c-Jun (j) in lysates of rat SCs cultured as above (b) in normoxia (i) or hypoxia (j) and incubated with lentiviruses carrying a TRAF7 shRNA (T7sh) or a control shRNA (Csh), and quantification normalized to GAPDH showing increased levels of HIF1α and c-Jun in cells where TRAF7 was downregulated. Paired one-tailed (i) or two-tailed (j) Student's t-tests, p values: *<0.05, **<0.01, values=mean, error bars=s.e.m., n=9 (i) or 7 (j) independent experiments. (**k**) IP HIF1α or control IP (Ctrl, Flag antibody) and Western blot of TRAF7 in lysates of rat SCs cultured under the same conditions as above (b) in normoxia and incubated for 8 h with the proteasome inhibitor MG-132. Three independent experiments have been carried out and representative images are shown. (**l**) Denaturing IP of HIF1α and control IP (Ctrl, GFP antibody) and Western blot of ubiquitin (P4D1) in lysates of SCs transduced with TRAF7 shRNA (T7sh) or control shRNA (Csh) lentivirus and cultured as above (b) in normoxia and incubated for 8 h with MG-132, and quantification of ubiquitinated HIF1a levels in lysates of cells transduced with T7sh lentivirus compared to Csh lentivirus. Paired two-tailed Student's t-tests, p value: *<0.05, values=mean, error bars=s.e.m., n=3 independent experiments. In k and l, the GAPDH input shows same amount of lysates used for IPs. (**m**) TRAF7 Western blot on lysates of rat SCs transfected with a TRAF7-expressing

construct or with a Flag-expressing construct as control (Ctrl), and quantification normalized to GAPDH showing that all four TRAF7 isoforms are overexpressed by transfection of the cDNA of the longest TRAF7 isoform. Unpaired two-tailed (long isoforms) or one-tailed (short isoform) Student's t-tests, p values: *<0.05, **<0.01, values=mean, error bars=s.e.m., n=3 independent experiments. (**n**, **o**, **p**) Western blots of HIF1α (n), c-Jun (o) or phospho-c-Jun (p-c-Jun, p) on lysates of rat SCs cultured as above (b) under hypoxia and incubated with lentiviruses carrying a HDAC8 shRNA (H8sh) or a control shRNA (Csh) and subsequently transfected with a TRAF7-overexpressing construct or a Flag-expressing construct as control (Ctrl), and quantification normalized to GAPDH showing that TRAF7 overexpression by transfection reverts the increase of HIF1α (n) and c-Jun (o) but not of p-c-Jun (p) levels mediated by HDAC8 downregulation. Paired (comparison to Ctrl-Csh) or unpaired two-tailed (black asterisks) or one-tailed (grey asterisks) Student's t-tests, p values: *<0.05, n.s.=non-significant, values=mean, error bars=s.e.m., n=3 independent experiments.

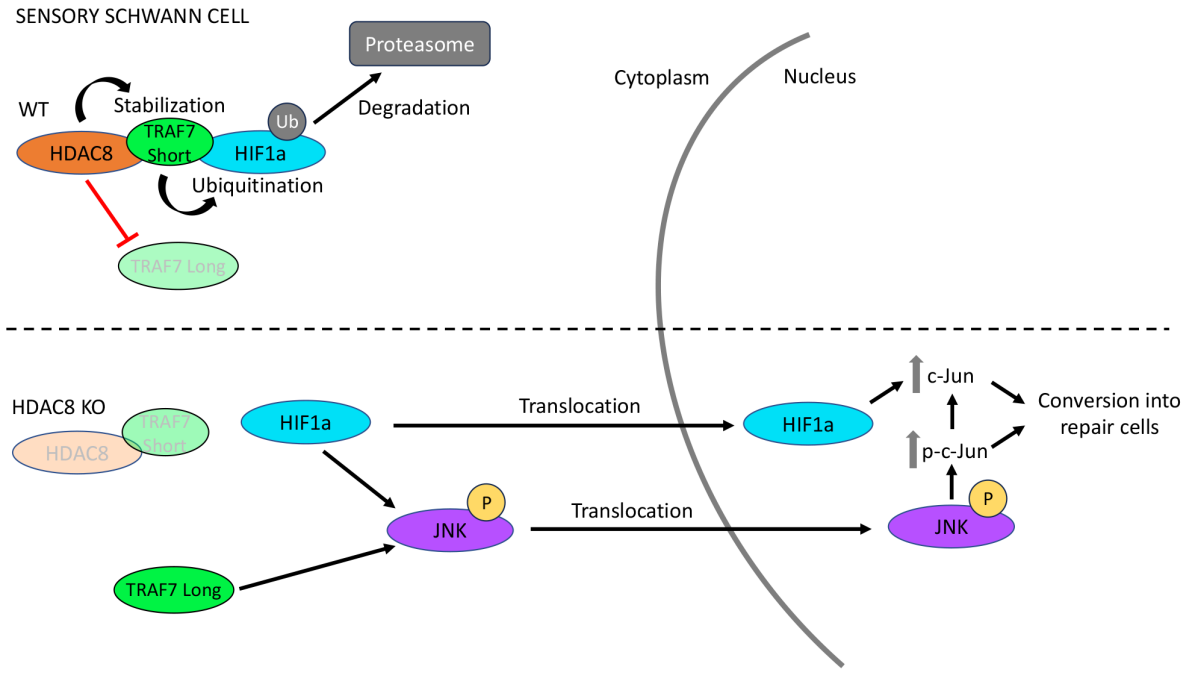

Figure 19. Mechanism of action of HDAC8 in SCs after injury. In WT SCs, HDAC8 interacts with and stabilizes TRAF7 short isoform, at the expense of TRAF7 long isoform; in turn, TRAF7 short isoform interacts with HIF1α and ubiquitinates it to target it to the proteasome for degradation. In the absence of HDAC8, TRAF7 short isoform is degraded, which leads to increased HIF1α levels. In parallel, TRAF7 long isoform is stabilized. Both HIF1α and TRAF7 long isoform increase the levels of phosphorylated JNK, HIF1α and phosphorylated JNK translocate to the nucleus, leading to increased phosphorylated c-Jun and total c-Jun levels. This mechanism promotes the conversion of sensory SCs into the repair phenotype and accelerates the regrowth of sensory axons and recovery of the sensory function.

4.5 Supplementary Information

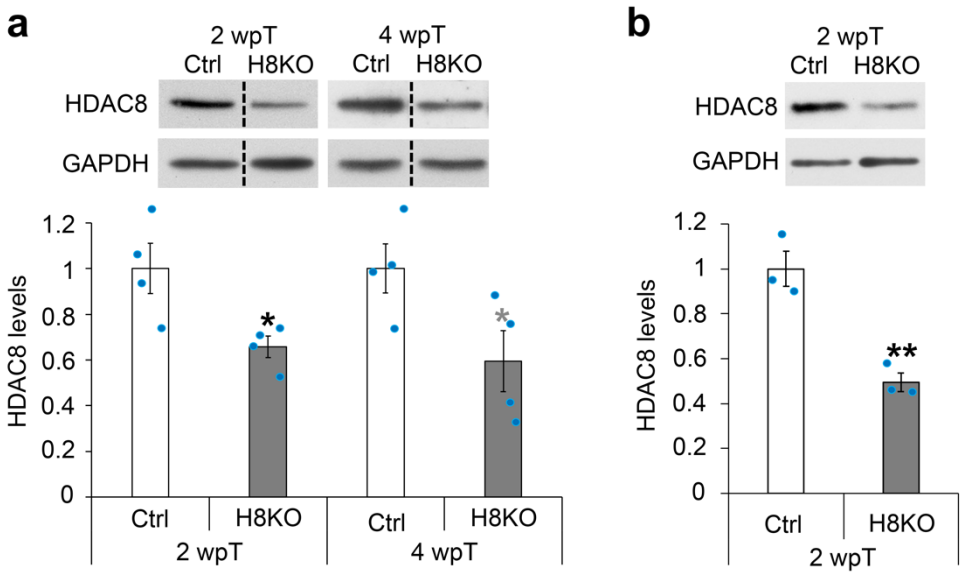

Figure S1. Onset of HDAC8 loss after tamoxifen injections. (**a**, **b**) HDAC8 Western blots on lysates of HDAC8 KO (H8KO) and control (Ctrl) sciatic nerves at 2- and 4-weeks post tamoxifen injections (wpT), and quantification normalized to GAPDH showing efficient HDAC8 recombination at both 2 and 4 wpT. Recombination efficiency is shown in both lines PLPCre-ERT2; *Hdac8* fl/fl (a) and in P0Cre-ERT2; *Hdac8* fl/fl (b) mice compared to their respective control littermates. Unpaired two-tailed (black asterisks) or one-tailed (grey asterisk) Student's t-tests, p values: *<0.05, **<0.01, values=mean, error bars=s.e.m., n=4 animals per group. In (a), dashed lines indicate that samples were run on the same gel but not on consecutive lanes.

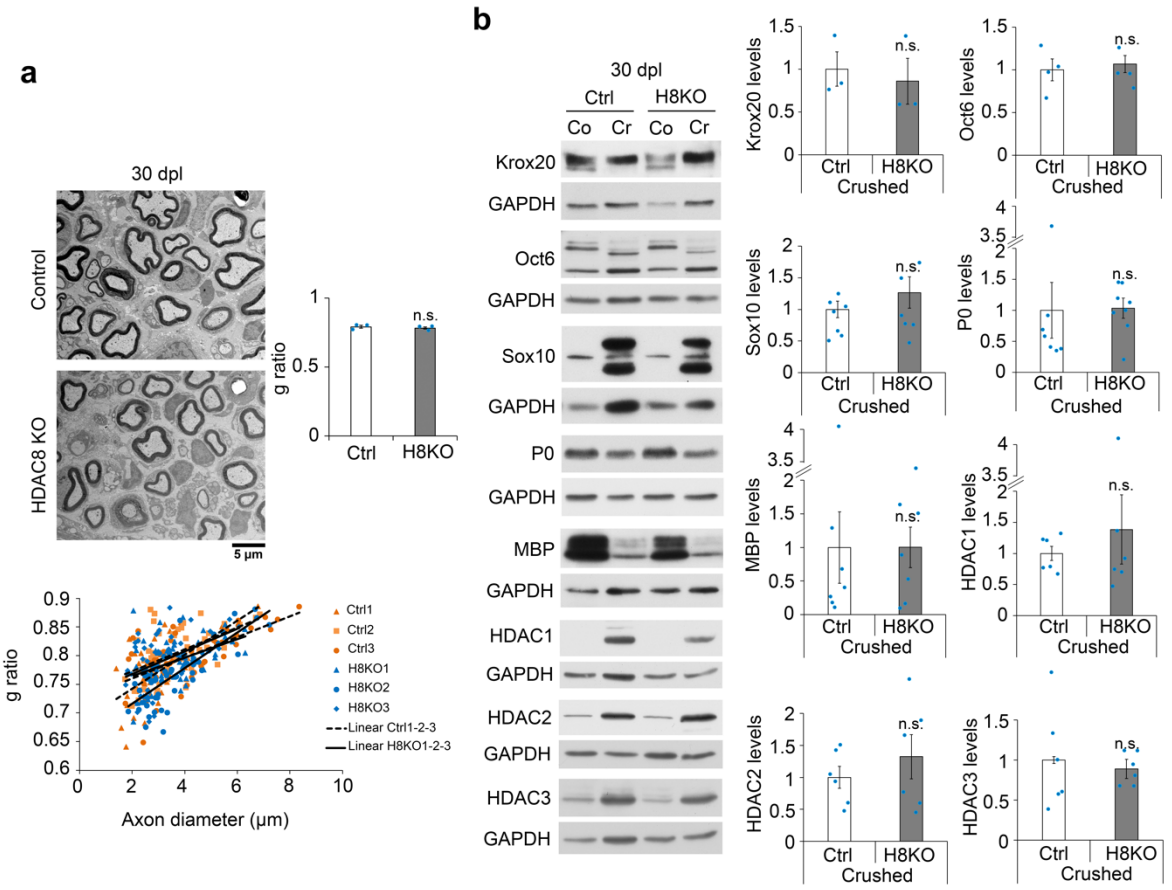

Figure S2. Ablation of HDAC8 does not affect remyelination after injury. (**a**) Electron micrographs of ultrathin cross sections from HDAC8 KO (H8KO) and Control (Ctrl) crushed sciatic nerves at 30 dpl, and quantification of g-ratio (=axon diameter/(axon+myelin) diameter) represented either as average of all counted fibers or plotted against the axon diameter, showing no significant difference of myelin thickness between H8KO and Ctrl nerves. Unpaired one-tailed Student's t-tests, n.s.=non-significant, values=mean, error bars=s.e.m., n=3 animals per group. (**b**) Western blots of Krox20. Oct6, Sox10, P0, MBP, HDAC1, HDAC2 and HDAC3 on lysates of HDAC8 KO (H8KO) and control (Ctrl) sciatic nerves at 30 dpl, and quantification of protein levels in crushed nerves normalized to GAPDH and to contralateral nerves of the same mice, showing no significant difference between the two experimental groups. Unpaired one-tailed Student's t-tests, n.s.=non-significant, values=mean, error bars=s.e.m., n=3 (Krox20), 4 (Oct6), 6 (Sox10, HDAC1, HDAC2, HDAC3), or 7 (P0 and MBP) animals per experimental group.

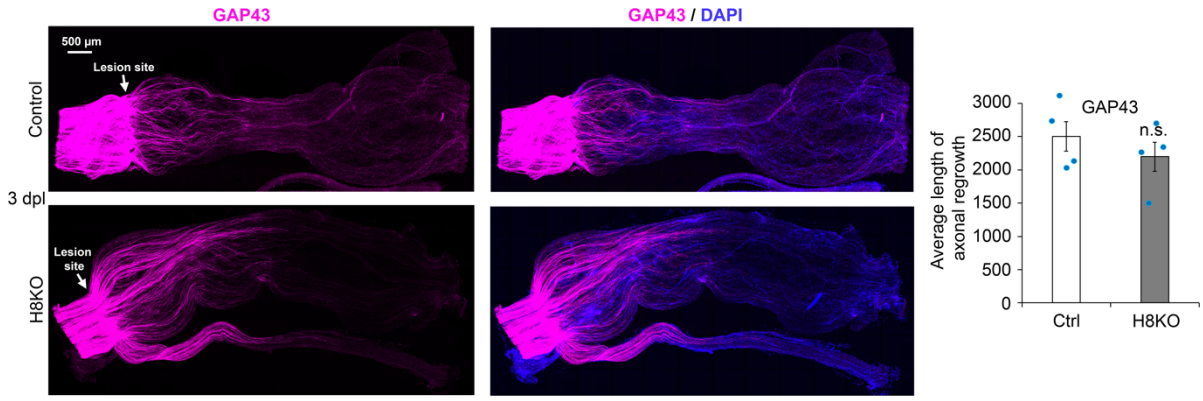

Figure S3. Overall axonal regrowth is not affected by HDAC8 ablation. Whole sciatic nerve immunofluorescence of GAP43 (magenta, general marker of regrowing axons) and DAPI labeling (blue, nuclei) and quantification of axonal regrowth at 3 dpl showing similar regrowth in HDAC8 KO (H8KO) nerves and Control (Ctrl) nerves. Unpaired one-tailed Student's t-tests, n.s.=non-significant, values=mean, error bars=s.e.m., n=4 animals per group, 47 to 79 regrowing axons measured and counted per animal.

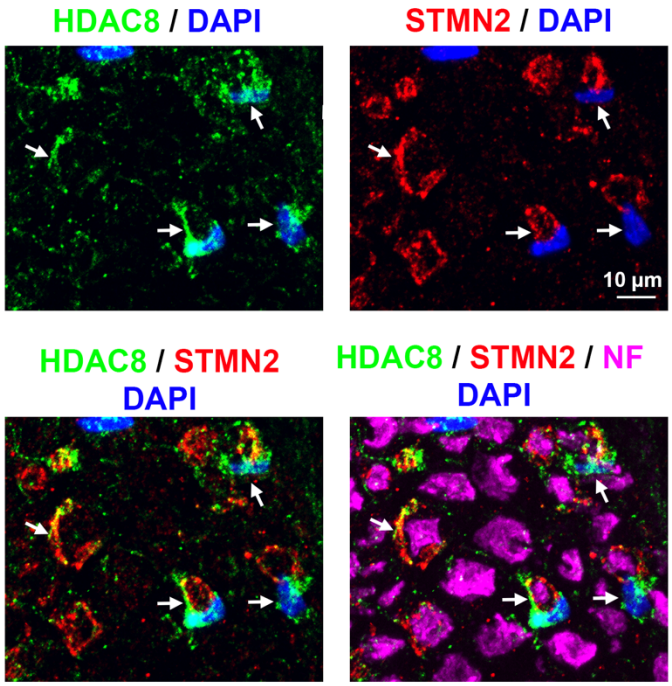

Figure S4. HDAC8 is expressed in sensory SCs. Co-immunofluorescence (z-series projection of confocal stacks) of HDAC8 (green), Stathmin-2 (STMN2, red, marker of regrowing sensory axons) and Neurofilament (NF, magenta, general axonal marker) and DAPI labeling (blue) in sciatic nerve cross-section of WT mice at 1 dpl. Three animals were used and a representative image is shown. White arrows point to HDAC8-positive SCs surrounding Stathmin-2-positive axons.

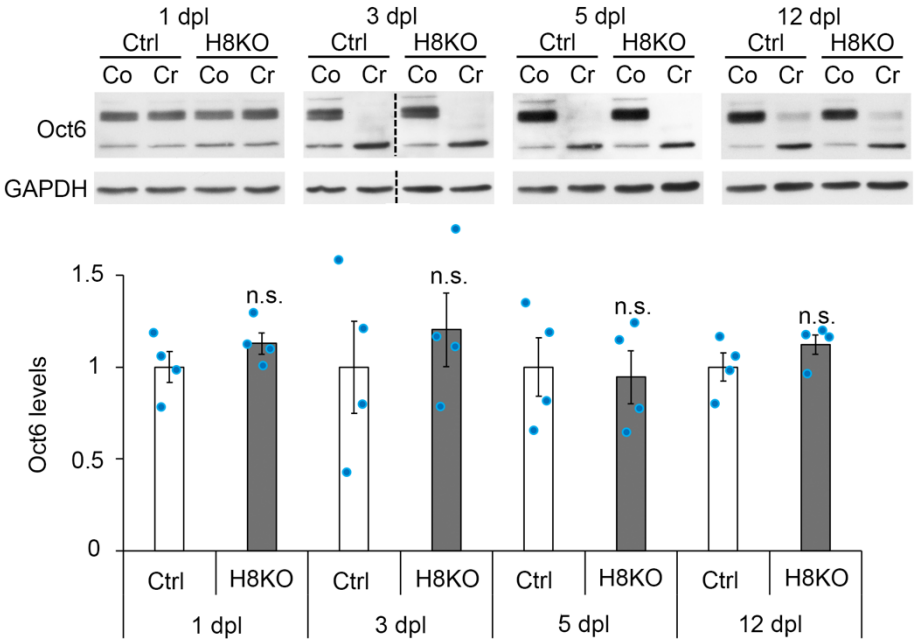

Figure S5. Oct6 levels are not affected by HDAC8 ablation. Oct6 Western blot and quantification normalized to GAPDH at 1, 3, 5 and 12 dpl in lysates of contralateral (Co) and crushed (Cr) mouse sciatic nerves, showing similar Oct6 levels in crushed sciatic nerves of HDAC8 KO (H8KO) and Control (Ctrl) mice. Unpaired one-tailed Student's t-tests, n.s.=non-significant, values=mean, error bars=s.e.m., n= 4 animals per group and per time point. Dashed lines indicate that samples were run on the same gel but not on consecutive lanes.

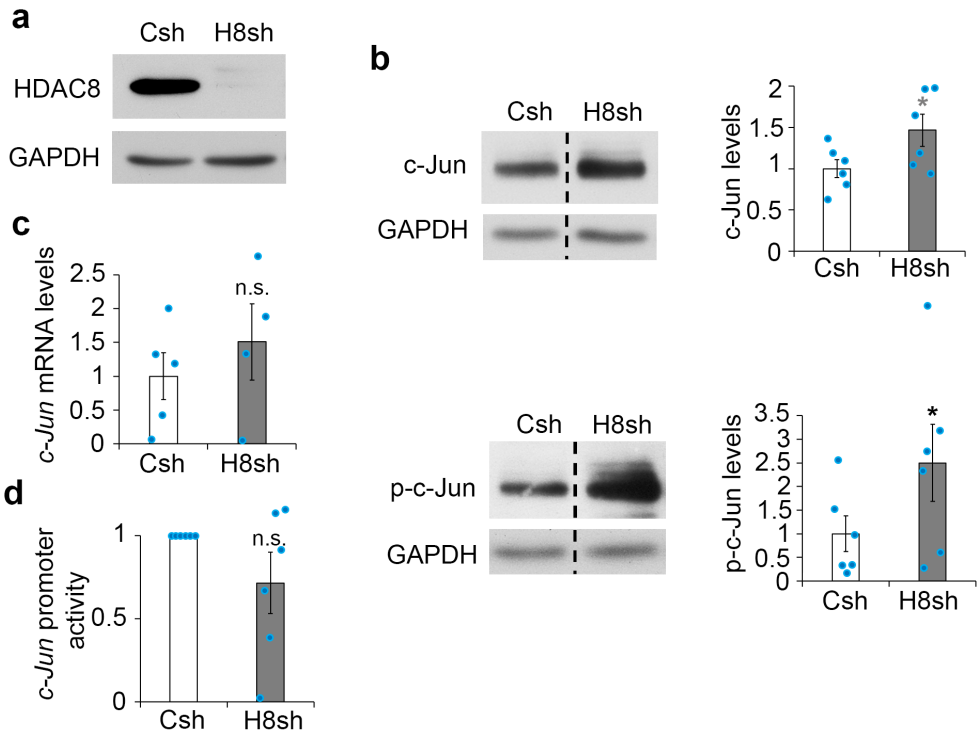

Figure S6. HDAC8-mediated regulation of c-Jun in normoxia. (**a**) Western blot of HDAC8 and GAPDH (loading control) on lysates of rat SCs transduced with a lentivirus carrying a HDAC8-specific shRNA, showing highly efficient HDAC8 knockdown. This was verified multiple times (more than 3 times) in independent experiments and representative images are shown. (**b**, **c**) Western blot of c-Jun and phospho-c-Jun (p-c-Jun) on lysates of rat SCs cultured under conditions mimicking the conversion into the repair phenotype in normoxia and transduced with lentiviruses carrying either a HDAC8-specific shRNA (H8sh) or a control shRNA (Csh), and quantification normalized to GAPDH showing increased c-Jun and p-c-Jun levels in cells were HDAC8 is downregulated. Paired one-tailed (grey asterisk) or two-tailed (black asterisk) Student's t-tests, p value : *<0.05, values=mean, error bars=s.e.m., n= 6 independent experiments per group. Dashed lines indicate that samples were run on the same gel but not on consecutive lanes. (**c**) Quantification *of c-Jun* mRNA levels by qRT-PCR in primary rat SCs cultured as above (b), showing no significant difference *in c-Jun* expression in cells where HDAC8 was downregulated compared to control. Unpaired one-tailed Student's t-tests, n.s.=non-significant, values=mean, error bars=s.e.m., n=4 (H8sh) or 5 (Csh) independent experiments per group. (**d**) Quantification of *c-Jun* promoter activity by luciferase gene reporter assay in cells cultured as above (b), showing similar activity in cells where HDAC8 was downregulated compared to control cells. Paired one-tailed Student's t-tests, n.s.=non-significant, values=mean, error bars=s.e.m., n=6 independent experiments per group.

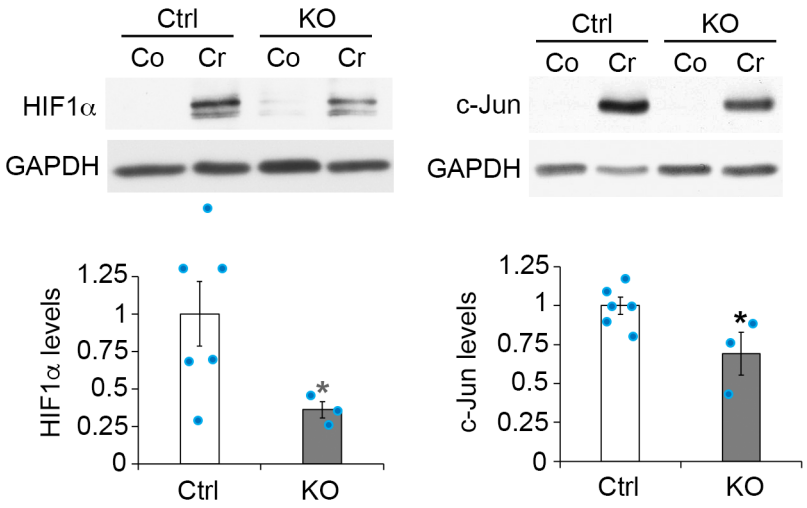

Figure S7. Ablation of HIF1α in SCs leads to decreased c-Jun upregulation after lesion. HIF1α or c-Jun Western blot and quantification normalized to GAPDH at 3 dpl, showing decreased c-Jun levels in crushed sciatic nerves of HIF1α KO mice (KO) compared to Control mice (Ctrl). Unpaired one-tailed (grey asterisk) or two-tailed (black asterisk) Student's t-tests, p value: *<0.05, values=mean, error bars=s.e.m., n=5 (Ctrl) and 3 (KO) animals per group.

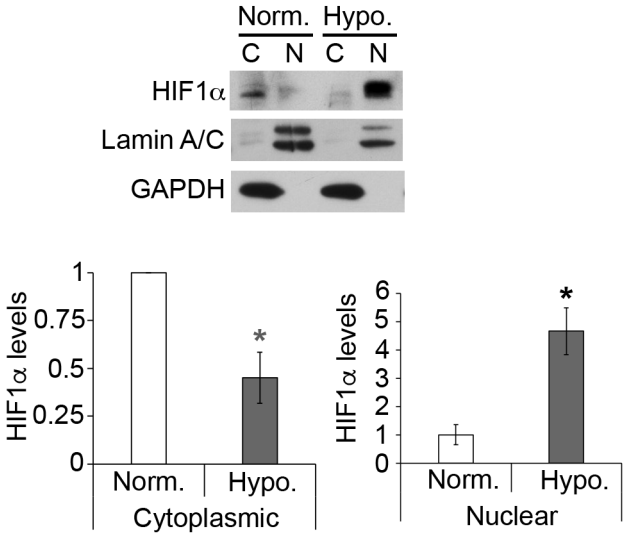

Figure S8. HIF1α upregulation and translocation to nuclear compartment under hypoxia. HIF1α Western blot after subcellular fractionation of cytoplasmic (C) and nuclear (N) fractions of primary rat SCs cultured under normoxia (Norm.) or hypoxia (Hypo., $CoCl_2$ for 16 h) in conditions mimicking the conversion into the repair phenotype. GAPDH and Lamin A/C are used as markers of the cytoplasmic and nuclear fractions, respectively. The graphs represent the quantification of HIF1α levels in normoxia compared to hypoxia in the cytoplasmic and the nuclear fractions and show a decrease of HIF1α in the cytoplasm and a strong increase in the nucleus under hypoxia. Paired (Cytoplasmic) or unpaired (Nuclear) one-tailed (Cytoplasmic) or two-tailed (Nuclear) Student's t-tests, p values: *<0.05, values=mean, error bars=s.e.m., n=3 independent experiments per group.

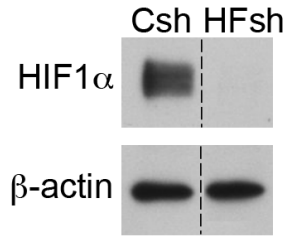

Figure S9. Efficient downregulation of HIF1α by shRNA. HIF1α Western blot on lysates of primary rat SCs transduced with lentiviruses carrying a HIF1α-specific shRNA (HFsh) or a control shRNA (Csh) cultured under hypoxia ($CoCl_2$ for 16 h) in conditions mimicking the conversion into the repair phenotype, showing high efficiency of HIF1α downregulation. This was verified multiple times (more than 3 times) in independent experiments and representative images are shown. The dashed lines indicate that samples were run on the same gel but not on consecutive lanes.

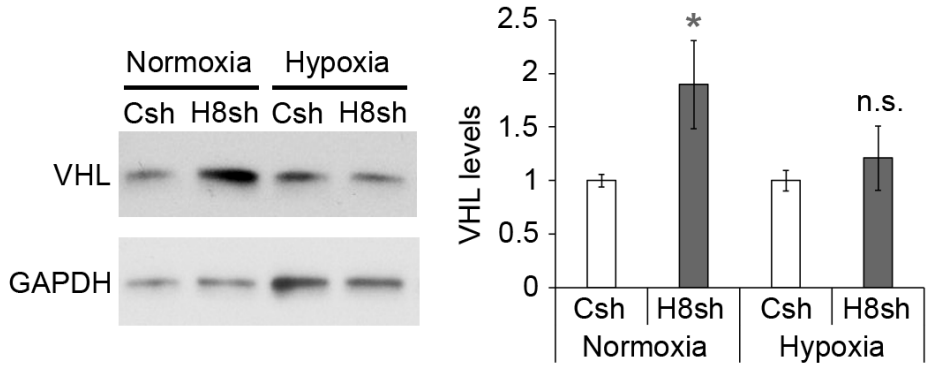

Figure S10. HDAC8 knockdown does not induce VHL downregulation. Western blot of VHL on lysates of rat SCs cultured under conditions mimicking the conversion into the repair phenotype in normoxia or hypoxia ($CoCl_2$, 16 h) and transduced with lentiviruses carrying either a HDAC8-specific shRNA (H8sh) or a control shRNA (Csh), and quantification normalized to GAPDH showing increased VHL levels in normoxia and no difference in hypoxia in cells were HDAC8 is downregulated compared to control cells. Paired one-tailed Student's t-tests, p value: *<0.05, n.s.=non-significant, values=mean, error bars=s.e.m., n=6 independent experiments per group.

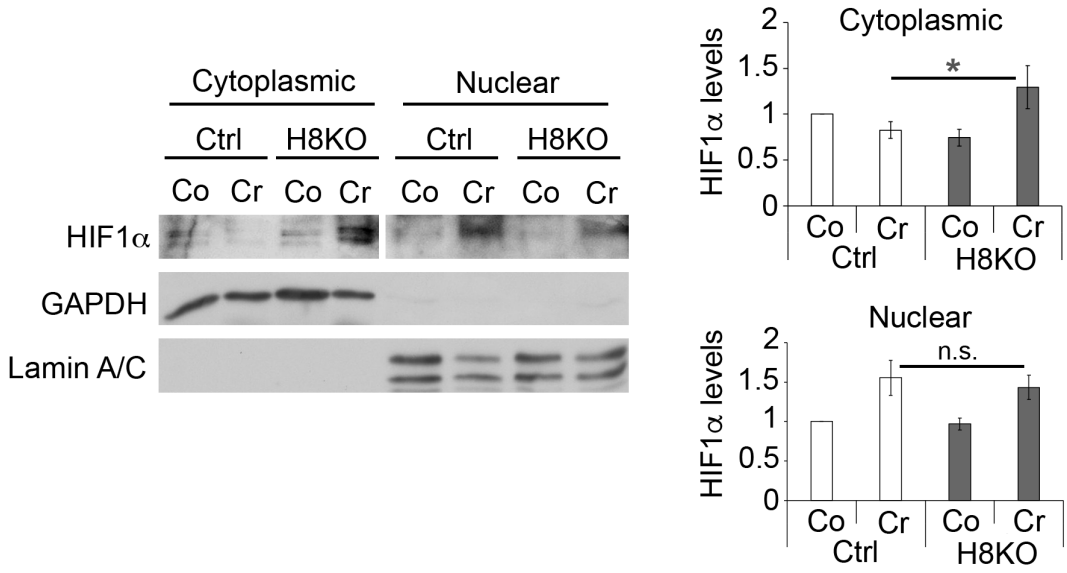

Figure S11. HIF1α levels after lesion are initially increased in the cytoplasmic fraction of HDAC8 KO nerves. HIF1α Western blot after subcellular fractionation of cytoplasmic and nuclear fractions of crushed (Cr) and contralateral (Co) sciatic nerves of HDAC8 KO (H8KO) and control littermate (Ctrl) mice at 1 day post lesion. GAPDH and Lamin A/C are used as markers of the cytoplasmic and nuclear fractions, respectively. The graphs show that HIF1α levels normalized to GAPDH (Cytoplasmic) or Lamin A/C (Nuclear) are increased in the cytoplasmic fraction of crushed HDAC8 KO compared to control nerves, but that levels are similar in the nuclear fraction. The cytoplasmic and nuclear fractions were run on the same gel on consecutive lanes, but the HIF1α images of the cytoplasmic and nuclear fractions are taken from different exposures. Unpaired one-tailed Student's t-tests, p value: *<0.05, n.s.=non-significant, values=mean, error bars=s.e.m., n=3 (H8KO) or 4 (Ctrl) animals per group.

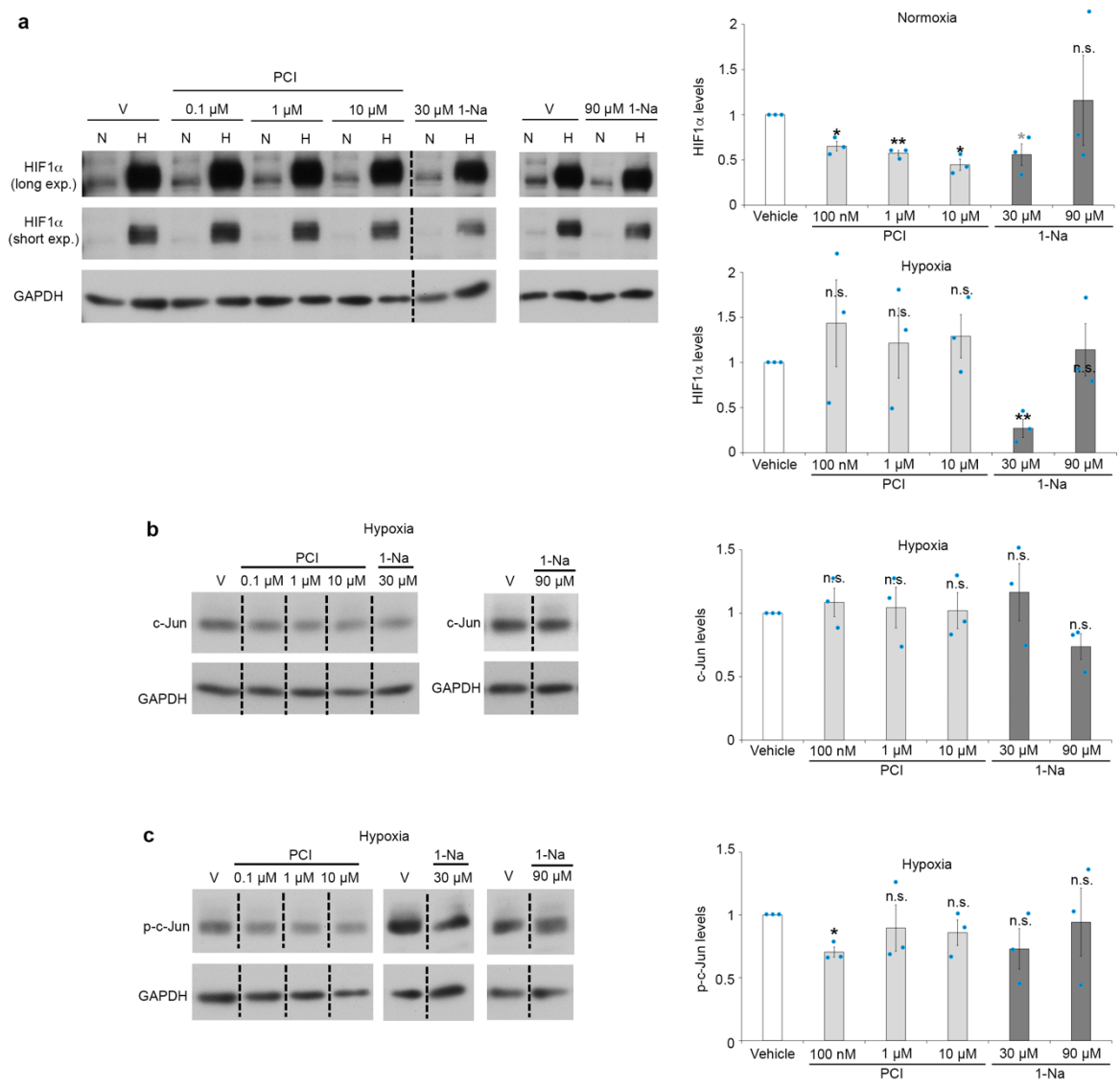

Figure S12. HDAC8 inhibitors do not increase the levels of HIF1α, c-Jun or phospho-c-Jun. Western blots of HIF1α (**a**), c-Jun (**b**) and phospho-c-Jun (p-c-Jun, **c**) in lysates of primary rat SCs cultured under normoxia (N) or hypoxia (H) in conditions mimicking the conversion into the repair phenotype, and incubated for 24 h with two different HDAC8 inhibitors, PCI-34051 and 1-Naphthohydroxamic acid, at different concentrations, or with the vehicle (V). The graphs show the quantification of HIF1α (a), c-Jun (b) and p-c-Jun (c) levels normalized to GAPDH. Dashed lines indicate that samples were run on the same gel but not on consecutive lanes. Paired one-tailed (grey asterisks) or two-tailed (black asterisk) Student's t-tests, p values: *<0.05, **<0.01, n.s.=non-significant, values=mean, error bars=s.e.m., n=3 independent experiments per group.

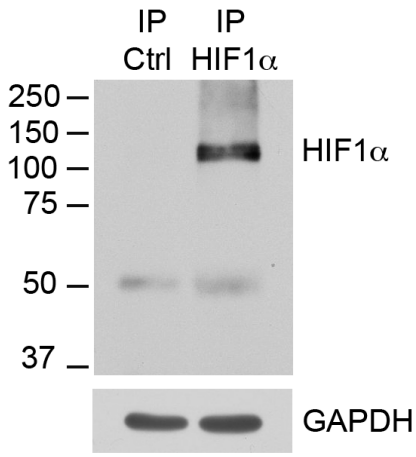

Figure S13. Efficient immunoprecipitation of HIF1α. Immunoprecipitation (IP) of HIF1α or control IP (Ctrl, GFP) and Western blot of HIF1α in lysates of rat SCs cultured under the normoxia in conditions mimicking the conversion into the repair phenotype and incubated with the proteasome inhibitor MG-132 for 8 h. The GAPDH input shows equal amount of lysates used for IP HIF1α and control IP. Three independent experiments have been carried out and representative images are shown.

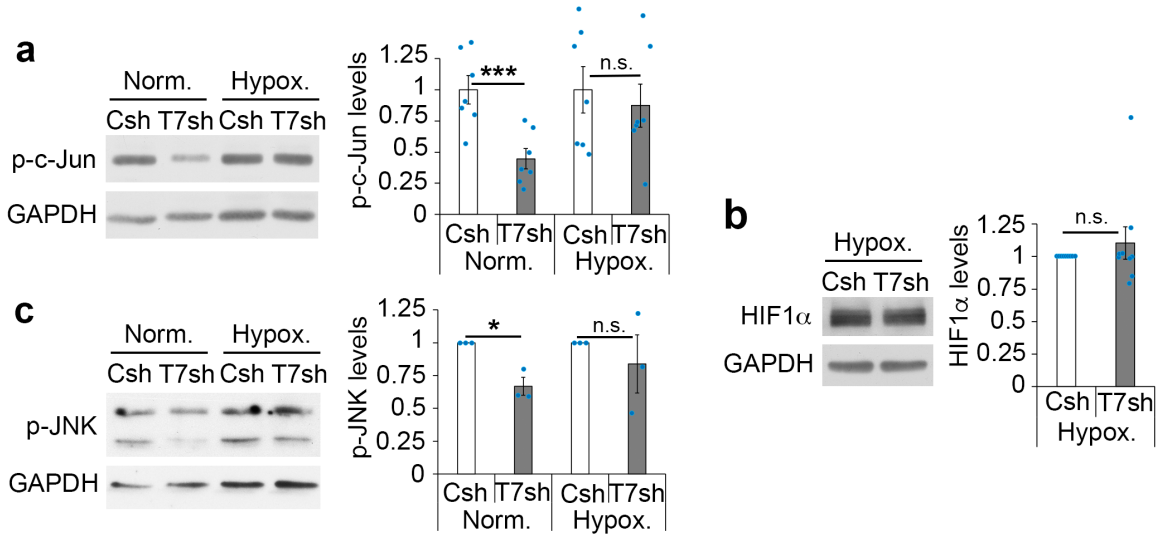

Figure S14. TRAF7 knockdown affects JNK and c-Jun phosphorylation in normoxia. Western blots of phospho-c-Jun (p-c-Jun, a), HIF1α (b) and phospho-JNK (p-JNK, c) in primary rat SCs cultured under normoxia (Norm.) or hypoxia (Hypox.) in conditions mimicking the conversion into the repair phenotype. The graphs show that TRAF7 knockdown leads to decreased levels of p-c-Jun and p-JNK (normalized to GAPDH) in normoxia but does not affect protein levels in hypoxia. Paired two-tailed (black asterisks) or one-tailed Student's t-tests, p values: *<0.05, ***<0.001, n.s.=non significant, values=mean, error bars=s.e.m., n=7 (a), 9 (b) or 3 (c) independent experiments per group.

5 DISCUSSION

While the functions of the class I HDACs HDAC1, HDAC2 and HDAC3 have been extensively studied in different areas of biology and medicine, the functions of HDAC8, the fourth and last member of the class I HDACs, have been comparatively less explored. It is however well established that HDAC8 mutations in humans affecting deacetylase activity can cause subtypes of Cornelia de Lange syndrome, a genetic developmental disorder affecting multiple functions (Kaiser et al., 2014; Sarogni et al., 2020). This syndrome is due to a loss of function of the cohesin complex and HDAC8 has been shown to deacetylate SMC3, a subunit of the cohesin complex, which is required for recycling the complex for subsequent cell divisions (Deardorff et al., 2012). HDAC8 has also been involved in other pathological conditions including cancer, parasitic and viral infections, where it has mainly been shown to contribute to the pathology through its deacetylase activity (Kim et al., 2022; Marek et al., 2015; Yamauchi et al., 2011). Unexpectedly, we found that the deacetylase activity of HDAC8 is not required for its interaction with TRAF7 and subsequent effects on c-Jun phosphorylation and expression levels. Indeed, rat SCs treated with different HDAC8 inhibitors under both normoxic and hypoxic conditions did not upregulate c-Jun phosphorylation and expression levels and no effect on HIF1α stabilization was observed compared to vehicle-treated cells. However, deacetylase-independent functions of HDACs have also been reported. Gupta et al. (2009) were the first to report a deacetylase-independent function of HDAC3, which serves as a specific carrier molecule to bring the phosphorylated from of TR2 (an orphan nuclear receptor) to nuclear bodies (Gupta et al., 2009). Additionally, it has been shown that the interaction between the nuclear receptor corepressor NCOR and HDAC3 is essential to repress the transcription

of lipogenic genes in hepatocytes and that the interaction between NCOR and HDAC3 as well as the transcriptional function of this complex do not require the deacetylase activity of HDAC3. Indeed, deacetylase-dead HDAC3 mutants could repress lipogenic gene expression in HDAC3-depleted mouse liver (Sun et al., 2013). Recently, another deacetylase-independent function of HDAC3 has been discovered in cardiovascular research, where HDAC3 has been shown to maintain cardiac contractility (Ren et al., 2023). Non-deacetylase functions of HDAC8 have also been reported. Indeed, the phosphorylated form of HDAC8 interacts with the telomere protein hEST1B and recruits the chaperon protein Hsp70 to a complex that inhibits the E3-ligase-mediated degradation of hEST1B, thereby stabilizing hEST1B and enhancing telomerase activity (Lee et al., 2006). This study echoes our observations that HDAC8 is involved in the stabilization of a protein, namely HIF1α, and this also in an indirect manner via the stabilization of TRAF7 small isoform. However, in our case HDAC8 acts negatively on HIF1α stabilization, whereas in the study by Lee et al., HDAC8 promotes hEST1B stabilization. However, in our study, HDAC8 acts positively and directly on the stabilization of TRAF7 small isoform. It would be interesting to assess the phosphorylation or other post-translational modifications of HDAC8 in SCs after peripheral nerve injury and investigate if the phosphorylated form of HDAC8 interacts with and stabilizes TRAF7. It is worth pointing out that the discovery of deacetylase-independent functions of HDACs may lead to reconsider the use of HDAC inhibitors in some specific pathological contexts.

In peripheral nerves, the functions of HDAC8 remained however unknown. We found that HDAC8 is upregulated after a sciatic nerve crush lesion in mice, suggesting a potential function in the degeneration and/or regeneration process after lesion. In this study, we thus set out to elucidate the functions of HDAC8 in SCs after a peripheral nerve injury. Ablating HDAC8 specifically in adult SCs

before a sciatic nerve crush lesion surprisingly did not impair regeneration, but instead accelerated it, indicating a negative effect of HDAC8 on the regeneration process and demonstrating that this process is not optimal and can be improved. The negative effect of HDAC8 on SC conversion into repair SCs and, thus on axonal regrowth is similar to our observations regarding the functions of HDAC1/2 in SCs after peripheral nerve injury. Indeed, the ablation of HDAC1/2 promotes the regrowth of axons by upregulating c-Jun expression early after lesion, indicating that HDAC1/2 also have a negative effect on axonal regeneration. However, HDAC1/2 act positively during the remyelination phase after lesion (Brügger et al., 2017; Duman et al., 2020), whereas HDAC8 has no effect on the remyelination process.

Mechanistically, we show here that HDAC8 counteracts hypoxia-induced c-Jun phosphorylation and upregulation in SCs by promoting the degradation of HIF1α and preventing the activation of JNK. Indeed, HIF1α and JNK are known to induce c-Jun phosphorylation and upregulation (Herdegen et al., 1997; Laderoute et al., 2002, 2004; Minet et al., 2001; Tam et al., 2021), and we show here that HIF1α downregulation in primary SCs cultured under hypoxic conditions leads to reduced JNK activation and that JNK inhibition prevents the increase of c-Jun phosphorylation and expression mediated by HDAC8 downregulation. HIF1α degradation in normoxic conditions can be mediated by VHL, which recruits a protein complex with E3 ubiquitin ligase activity that catalyzes HIF1α ubiquitination and thereby targets HIF1α to the proteasome for degradation (Kaelin et al., 2022). VHL-independent regulation of HIF1α degradation has also been reported (Zhang et al., 2020) and we show here that HDAC8-mediated HIF1α degradation in adult SCs is independent of VHL. By mass spectrometry analysis, we identified TRAF7 as a putative binding partner of

HDAC8. We also showed that HDAC8 and TRAF7 are both exclusively or in large majority localized in the cytoplasmic compartment of SCs present in adult mouse sciatic nerves and in primary rat SCs in culture. By co-immunoprecipitation, we found that a short TRAF7 isoform, that had not been studied so far but is described as a predicted isoform in the human NCBI database, interacts with HDAC8 in SCs *in vivo* and in culture and mediates HDAC8-dependent degradation of HIF1α. TRAF7 possesses a RING finger domain with E3 ubiquitin ligase activity that is capable of catalyzing protein ubiquitination and thereby targeting proteins to the proteasome for degradation. The short 50-kDa TRAF7 isoform misses the C-terminal WD40 repeat domains found in the long TRAF7 isoforms. This structural difference confers to the short isoform different functions compared to the long TRAF7 isoforms regarding the activation of JNK. Indeed, TRAF7 is known to promote JNK phosphorylation and subsequent c-Jun phosphorylation by binding to MEKK3 through its WD40 repeat domains (Boowmeester et al., 2004). The short TRAF7 isoform, which misses these domains, does not have this function. Instead, this isoform is stabilized, most likely through its interaction with HDAC8, and induces HIF1α ubiquitination and subsequent HIF1α degradation. Ablation of HDAC8 prevents this mechanism by leading to the downregulation of the short TRAF7 isoform and instead results in increased HIF1α levels and HIF1α -mediated c-Jun phosphorylation and upregulation. In addition, we show that ablation of HDAC8 leads to the upregulation of the long TRAF7 isoform, which potentiates JNK phosphorylation and thereby c-Jun phosphorylation and upregulation. However, it remains unclear whether HIF1α control c-Jun expression directly or indirectly. A consensus points towards an indirect mechanism as no HRE binding sites have been identified on the *c-Jun* promoter. This of course, does not rule out a potential HRE binding site on some, still

undiscovered, *c-Jun* enhancers (Benita et al., 2009; Laderoute et al., 2002; Schödel et al., 2013).

In summary, our study identifies a pathway controlled by HDAC8 that modulates HIF1α stabilization and JNK activation, and subsequent c-Jun phosphorylation and expression specifically in sensory SCs.

This function of HDAC8 is not linked to its deacetylase activity, therefore HDAC8 inhibitors cannot be used to promote the regrowth of sensory axons and sensory function recovery. Instead, HDAC8 should be downregulated, either by using RNA interference or by repressing *Hdac8* gene activation. More work is needed to test whether such treatment strategies can be appropriately timed to promote regeneration. Alternatively, TRAF7 inhibitors or HIF prolyl hydroxylase (PHD) inhibitors that enhance HIF1α stabilization (Ogawa et al., 2023) could also be tested to promote regeneration. Interestingly, the discovery of new models for mammalian regeneration, namely the Murphy Roths Large (MRL) mouse strain, identified cellular oxygen-sensing pathways as possible targets to promote regeneration. Indeed, oxygen-sensing pathways have been conserved from lower organisms and the burst of reactive oxygen species occurring after injury contributes to local tissue hypoxia and acts as signaling molecules for the development of a blastema (Hameed et al., 2015). The MRL mouse strain was originally developed to study lupus erythematosus but its unexpected capability of regenerating large pieces of ear tissues turned out to be of great interest for the regenerative field (Andrews et al.; 1978). The regenerative response of the MRL mouse is not limited to the ear but concerns amputated digits, cartilage, bone, heart, cornea, and peripheral nerve damage (reviewed in DeFrates et al., 2021). Later, HIF1α has been identified as the central mediator of the MRL regenerative response. In the MRL mouse, the basal expression of HIF1α is

abnormally high compared to other mouse strains, both under normoxic condition and after injury (McBreatry et al., 1998). This may confer the retention of a fetal-like metabolism and a progenitor cell population in MRL mouse cells (Naviaux et al., 2009; Zhang et al., 2015). Indeed, compared to the C57B/6 strain, MRL mice rely more on glycolysis for ATP synthesis and HIF1α is known to govern glucose transporters and glycolytic enzyme expression (Heber-Katz, 2017; Naviaux et al., 2009). However, MRL-derived cells do not excessively produce ROS. Additionally, stem cell markers have been identified in cardiomyocytes of MRL mice both before and after injury. These characteristics are independent of the genes associated with lupus erythematosus or any other genes associated with autoimmunity (McBreatry et al., 1998; Naviaux et al., 2009). Compared to non-regenerative mouse strains, several factors implicated in HIF1α ubiquitination and degradation are downregulated in MRL mice, resulting in higher basal expression of HIF1α and HIF1α-target genes. Furthermore, HIF1α inhibition completely abrogated the regenerative properties of MRL mice (Zhang et al., 2015). Therefore, oxygen-sensing pathways have emerged as potential targets to promote regeneration in higher mammals (DeFrates et al., 2021). Indeed, intermittent hypoxia treatment improved respiratory and motor recovery after spinal cord injury as well as axonal regeneration after sensory nerve damage (Cho et al., 2015; Lovett-Barr et al., 2012; Trumbower et al., 2012). Furthermore, the use of the PHD inhibitor DPCA coupled to an injectable hydrogel in non-healing mouse strains resulted in HIF1α upregulation, upregulation of stem cell markers, and complete closure of large size ear hole as well as enhanced bone regeneration compared to vehicle-treated mice (Nagai et al., 2020; Strehin et al., 2013). In the context of spinal cord injury, another PHD inhibitor, FG-4592, improved neuron survival and functional recovery (Wu et al., 2016). These encouraging data thus motivate the use of PHD inhibitors in

mammalian tissue regeneration. Since HIF1α stabilization requires a precise timing, PHD inhibitors should be applied directly on the injury site. This would be best achieved using biomaterials like hydrogels to deliver the molecules on time and locally, avoid unwanted secondary systemic side effects of the drug, and to reduce the therapeutic dose (DeFrates et al., 2021).

Although our study did not identify a beneficial function of HDAC8-TRAF7 binding in SCs for PNS regeneration, we can speculate that by controlling HIF1α stabilization, the interaction of HDAC8 with TRAF7 may have beneficial effects in preventing neoangiogenesis and thereby the growth of tumors (Wicks et al., 2022) such as schwannomas that are more susceptible to develop after a peripheral nerve injury (Helbing et al., 2020). Schwannomas are benign tumors of peripheral nerves that are either sporadic or characteristic of patients suffering from neurofibromatosis type 2. In both cases, they result from inactivating mutations of the *NF2* (merlin) tumor suppressor gene (Rouleau et al., 1993). Most schwannomas arise within ganglia of sensory vestibular, facial, and lower cranial nerves and are very rarely observed in pure motor nerve or along myelinated segments of mixed peripheral nerves (Tryggvason et al., 2012). Indeed, we found that HDAC8 ablation specifically promotes the regrowth of sensory axons and sensory function recovery. We show that HDAC8 is exclusively expressed or expressed at high levels in SCs associated with sensory axons and that ablation of HDAC8 leads to increased levels of c-Jun and phosphorylated c-Jun in SCs. These findings indicate that the conversion into repair SCs is controlled by different mechanisms in sensory and motor SCs and identify HDAC8 as a marker of adult sensory SCs. Furthermore, HDAC8 may prevent the development of Schwannomas in sensory nerves. The role of HDACs in the context of Schwannomas has not been investigated in detail so far. Yet

there are some ongoing clinical trials assessing the efficacy and safety of the pan-HDAC inhibitor AR-42 and of a dual phosphoinositide-3 kinase/HDAC inhibitor CUDC-907 in the context of human neurofibromatosis type 2 and Schwannomas (Welling et al., 2021; Huegel et al., 2022). Notwithstanding of the deacetylase-independent functions of HDAC8 in the context of peripheral nerve injury, the use of HDAC8 inhibitors reduced cell growth and induced apoptosis in human and murine-derived malignant peripheral nerve sheath tumors, indicating that the deacetylase-dependent functions of HDAC8 are potentially tumorigenic in malignant peripheral nerve sheath tumors (Lopez et al., 2015). In addition, the tumorigenic role of HDAC8 activity has also been reported in T-cell-derived leukemia and neuroblastoma cells (Balasubramanian et al., 2008; Oehme et al., 2009). In the future, it would be interesting to study the expression of HDAC8 as well as its potential role in the development of Schwannomas and compare HDAC8 mechanism of action in the context of Schwannomas to its function in repair SCs.

6 OUTLOOK AND FUTURE PERSPECTIVES

A lot of interesting points and questions remain to be investigated regarding the functions of HDAC8 in SCs. The first question concerns the time point at which HDAC8 expression becomes restricted to sensory SCs. Does this occur already at early embryonic stages or in adult SCs? To this end, we could collect sciatic nerves of mouse pups at different time points after birth and perform an immunostaining of HDAC8 together with sensory axon markers. In the same vein, is HDAC8 expression differentially regulated in repair SCs? Indeed, repair SCs do not wrap axons anymore and derive from both myelinating and Remak SCs (Gomez-Sanchez et al., 2017). It would be interesting to investigate if HDAC8 expression remains restricted to sensory SCs-derived repair SCs and if sensory-derived repair SCs specifically remyelinate or re-ensheath sensory axons or, in contrary, if the sensory or motor phenotype of SCs reappear only after having established a contact with an axon, independently of its sensory or motor nature.

The second question concerns the mechanism by which HDAC8 is upregulated in SCs after lesion. Does HDAC8 upregulation result from the loss of axonal contact, is it a cell-intrinsic mechanism or does it occur through the release of a certain factor in the extracellular environment which is sensed by SCs? The same question also concerns the upregulation of HDAC1/2 observed in SCs after injury (Brügger et al., 2017).

Other relevant points and questions were raised by the reviewers. The first one concerns c-Jun and phospho-c-Jun upregulation. Indeed, our study lacks direct evidence of the restriction of c-Jun and phospho-c-Jun to sensory SCs. To this

end, we are carrying out immunostainings on crushed nerves of control and HDAC8 KO mice at 1dpl with c-Jun or phospho-c-Jun together with Stathmin-2, a marker of sensory axons.

To strengthen the sensory function recovery in HDAC8 KO animals, we are also carrying out two additional sensory recovery tests, namely the von Frey test and the Thermal probe test before lesion and from 3dpl to 30dpl. The von Frey test consists of thin calibrated plastic filaments applied to the plantar surface of the hind paw to assess mechanical allodynia in mice and rats, whereas the Thermal probe test quantifies the heat sensitivity threshold in mice (Bradman et al., 2015; Deuis and Vetter, 2016). We also plan to quantify skin reinnervation of mouse paws by staining hind paw skin sections with a pan-neuronal marker. The time point of hind paw skin collection will depend on the results of the von Frey and Thermal probe tests since the stimulus is applied to the hind paw in contrast to the toe pinch test. We are also carrying out HDAC8 and Stathmin-2 immunostainings on cross sections of both the sural branch of the sciatic nerve, which is purely sensory, and on the ventral root, which contains only motor axons, to ensure Stathmin-2 and HDAC8 specificity to sensory axons. A last interesting point to investigate is the eventual restriction of HDAC8 expression to a particular type of sensory axon. Somatosensory neurons are classified in four types: unmyelinated C fibers with a diameter ranging from 0.2 to 1.5 µm, A-delta myelinated sensory fibers with a diameter ranging from 1 to 5 µm, A-beta sensory fibers with a diameter ranging from 6 to 12 µm, and A-alpha sensory fibers with a diameter ranging from 13 to 20 µm (De Hert et al., 2014). Technically, this question will be difficult to answer given the lack of specific markers for the different types of sensory axons. Indeed, some of the markers are also expressed in motor axons or in several types of myelinated or non-myelinated sensory axons (Le Pichon and Chesler, 2014). We can analyse the

expression of HDAC8 in myelinating SCs and peptidergic C fibers by immunostainings of HDAC8 together with Stathmin-2 and either P0 or Isolectin B4, which is a lectin specific to C-fibers. Otherwise, we could carry out immunogold electron microscopy of HDAC8 and measure the calibre of axons interacting with HDAC8-positive SCs. Unfortunately, there is currently no HDAC8 antibody which could be used for this purpose.

In conclusion, we found a potential new sensory SC marker whose effects on HIF1α stabilization are relevant in regenerative biology and cancer biology, knowing the recent evidence highlighting the importance of HIF1α in mammalian regeneration and oncogenesis (reviewed in DeFrates et al., 2021 and in Zhao et al., 2024). We are also the first to our knowledge who brought evidence of the expression of the small isoform of TRAF7 and who identified its function in SC regenerative biology. Lastly, we generated a plasmid coding the small isoform of TRAF7 and we plan to overexpress the small isoform of TRAF7 in rat SCs in the absence of HDAC8. This experiment will allow us to check if the overexpression of the TRAF7 small isoform only is sufficient to revert the increase of HIF1α and c-Jun levels that are observed when HDAC8 is downregulated in SCs in conditions mimicking the conversion into the repair phenotype and under hypoxia.

7 REFERENCES

Abe, N., & Cavalli, V. (2008). Nerve injury signaling. Current opinion in neurobiology, 18(3), 276–283. https://doi.org/10.1016/j.conb.2008.06.005

Adilakshmi, T., Sudol, I., & Tapinos, N. (2012). Combinatorial action of miRNAs regulates transcriptional and post-transcriptional gene silencing following in vivo PNS injury. PloS one, 7(7), e39674. https://doi.org/10.1371/journal.pone.0039674

Akassoglou, K., Kombrinck, K. W., Degen, J. L., & Strickland, S. (2000). Tissue plasminogen activator-mediated fibrinolysis protects against axonal degeneration and demyelination after sciatic nerve injury. The Journal of cell biology, 149(5), 1157–1166. https://doi.org/10.1083/jcb.149.5.1157

Andrews, B. S., Eisenberg, R. A., Theofilopoulos, A. N., Izui, S., Wilson, C. B., McConahey, P. J., Murphy, E. D., Roths, J. B., & Dixon, F. J. (1978). Spontaneous murine lupus-like syndromes. Clinical and immunopathological manifestations in several strains. *The Journal of experimental medicine*, *148*(5), 1198–1215. https://doi.org/10.1084/jem.148.5.1198

Andrews, F. H., Strahl, B. D., & Kutateladze, T. G. (2016). Insights into newly discovered marks and readers of epigenetic information. Nature chemical biology, 12(9), 662–668. https://doi.org/10.1038/nchembio.2149

Angel, P., Hattori, K., Smeal, T., & Karin, M. (1988). The jun proto-oncogene is positively autoregulated by its product, Jun/AP-1. Cell, 55(5), 875–885. https://doi.org/10.1016/0092-8674(88)90143-2

Arthur-Farraj, P. J., Latouche, M., Wilton, D. K., Quintes, S., Chabrol, E., Banerjee, A., Woodhoo, A., Jenkins, B., Rahman, M., Turmaine, M., Wicher, G. K., Mitter, R., Greensmith, L., Behrens, A., Raivich, G., Mirsky, R., & Jessen, K. R. (2012). c-Jun reprograms Schwann cells of injured nerves to generate a repair cell essential for regeneration. Neuron, 75(4), 633–647. https://doi.org/10.1016/j.neuron.2012.06.021

Arthur-Farraj, P. J., Morgan, C. C., Adamowicz, M., Gomez-Sanchez, J. A., Fazal, S. V., Beucher, A., Razzaghi, B., Mirsky, R., Jessen, K. R., & Aitman, T. J. (2017). Changes in the Coding and Non-coding Transcriptome and DNA Methylome that Define the Schwann Cell Repair Phenotype after Nerve Injury. Cell reports, 20(11), 2719–2734. https://doi.org/10.1016/j.celrep.2017.08.064

Arthur-Farraj, P., & Coleman, M. P. (2021). Lessons from Injury: How Nerve Injury Studies Reveal Basic Biological Mechanisms and Therapeutic Opportunities for Peripheral Nerve Diseases. Neurotherapeutics : the journal of the American Society for Experimental NeuroTherapeutics, 18(4), 2200–2221. https://doi.org/10.1007/s13311-021-01125-3

Atanasoski, S., Shumas, S., Dickson, C., Scherer, S. S., & Suter, U. (2001). Differential cyclin D1 requirements of proliferating Schwann cells during development and after injury. Molecular and cellular neurosciences, 18(6), 581–592. https://doi.org/10.1006/mcne.2001.1055

Baba, Y., Nosho, K., Shima, K., Irahara, N., Chan, A. T., Meyerhardt, J. A., Chung, D. C., Giovannucci, E. L., Fuchs, C. S., & Ogino, S. (2010). HIF1A overexpression is associated with poor prognosis in a cohort of 731 colorectal cancers. The American journal of pathology, 176(5), 2292–2301. https://doi.org/10.2353/ajpath.2010.090972

Babetto, E., Wong, K. M., & Beirowski, B. (2020). A glycolytic shift in Schwann cells supports injured axons. Nature neuroscience, 23(10), 1215–1228. https://doi.org/10.1038/s41593-020-0689-4

Balakrishnan, A., Stykel, M. G., Touahri, Y., Stratton, J. A., Biernaskie, J., & Schuurmans, C. (2016). Temporal Analysis of Gene Expression in the Murine Schwann Cell Lineage and the Acutely Injured Postnatal Nerve. PloS one, 11(4), e0153256. https://doi.org/10.1371/journal.pone.0153256

Balasubramanian, S., Ramos, J., Luo, W., Sirisawad, M., Verner, E., & Buggy, J. J. (2008). A novel histone deacetylase 8 (HDAC8)-specific inhibitor PCI-34051 induces apoptosis in T-cell lymphomas. *Leukemia*, *22*(5), 1026–1034. https://doi.org/10.1038/leu.2008.9

Beirowski, B., Babetto, E., Golden, J. P., Chen, Y. J., Yang, K., Gross, R. W., Patti, G. J., & Milbrandt, J. (2014). Metabolic regulator LKB1 is crucial for Schwann cell-mediated axon maintenance. Nature neuroscience, 17(10), 1351–1361. https://doi.org/10.1038/nn.3809

Benita, Y., Kikuchi, H., Smith, A. D., Zhang, M. Q., Chung, D. C., & Xavier, R. J. (2009). An integrative genomics approach identifies Hypoxia Inducible Factor-1 (HIF-1)-target genes that form the core response to hypoxia. *Nucleic acids research*, *37*(14), 4587–4602. https://doi.org/10.1093/nar/gkp425

Benito, C., Davis, C. M., Gomez-Sanchez, J. A., Turmaine, M., Meijer, D., Poli, V., Mirsky, R., & Jessen, K. R. (2017). STAT3 Controls the Long-Term Survival and Phenotype of Repair Schwann Cells during Nerve Regeneration. The Journal of neuroscience : the official journal of the Society for Neuroscience, 37(16), 4255–4269. https://doi.org/10.1523/JNEUROSCI.3481-16.2017

Benninger, Y., Colognato, H., Thurnherr, T., Franklin, R. J., Leone, D. P., Atanasoski, S., Nave, K. A., Ffrench-Constant, C., Suter, U., & Relvas, J. B. (2006). Beta1-integrin signaling mediates premyelinating oligodendrocyte survival but is not required for CNS myelination and remyelination. The Journal of neuroscience : the official journal of the Society for Neuroscience, 26(29), 7665–7673. https://doi.org/10.1523/JNEUROSCI.0444-06.2006

Ben-Yaakov, K., Dagan, S. Y., Segal-Ruder, Y., Shalem, O., Vuppalanchi, D., Willis, D. E., Yudin, D., Rishal, I., Rother, F., Bader, M., Blesch, A., Pilpel, Y., Twiss, J. L., & Fainzilber, M. (2012). Axonal transcription factors signal retrogradely in lesioned peripheral nerve. The EMBO journal, 31(6), 1350–1363. https://doi.org/10.1038/emboj.2011.494

Birchmeier C. (2009). ErbB receptors and the development of the nervous system. Experimental cell research, 315(4), 611–618. https://doi.org/10.1016/j.yexcr.2008.10.035

Biswas, S., & Rao, C. M. (2018). Epigenetic tools (The Writers, The Readers and The Erasers) and their implications in cancer therapy. European journal of pharmacology, 837, 8–24. https://doi.org/10.1016/j.ejphar.2018.08.021

Boerboom, A., Dion, V., Chariot, A., & Franzen, R. (2017). Molecular Mechanisms Involved in Schwann Cell Plasticity. Frontiers in molecular neuroscience, 10, 38. https://doi.org/10.3389/fnmol.2017.00038

Bondurand, N., Girard, M., Pingault, V., Lemort, N., Dubourg, O., & Goossens, M. (2001). Human Connexin 32, a gap junction protein altered in the X-linked form of Charcot-Marie-Tooth disease, is directly regulated by the transcription factor SOX10. Human molecular genetics, 10(24), 2783–2795. https://doi.org/10.1093/hmg/10.24.2783

Bosch-Queralt, M., Fledrich, R., & Stassart, R. M. (2023). Schwann cell functions in peripheral nerve development and repair. Neurobiology of disease, 176, 105952. https://doi.org/10.1016/j.nbd.2022.105952

Bosse F., Hasenpusch-Theil K., Küry P., Müller H. W. (2006). Gene expression profiling reveals that peripheral nerve regeneration is a consequence of both novel injury-dependent and reactivated developmental processes. J. Neurochem. 96, 1441–1457. 10.1111/j.1471-4159.2005.03635.

Bouçanova, F., & Chrast, R. (2020). Metabolic Interaction Between Schwann Cells and Axons Under Physiological and Disease Conditions. Frontiers in cellular neuroscience, 14, 148. https://doi.org/10.3389/fncel.2020.00148

Bouwmeester, T., Bauch, A., Ruffner, H., Angrand, P. O., Bergamini, G., Croughton, K., Cruciat, C., Eberhard, D., Gagneur, J., Ghidelli, S., Hopf, C., Huhse, B., Mangano, R., Michon, A. M., Schirle, M., Schlegl, J., Schwab, M., Stein, M. A., Bauer, A., Casari, G., … Superti-Furga, G. (2004). A physical and functional map of the human TNF-alpha/NF-kappa B signal transduction pathway. Nature cell biology, 6(2), 97–105. https://doi.org/10.1038/ncb1086

Bradman, M. J., Ferrini, F., Salio, C., & Merighi, A. (2015). Practical mechanical threshold estimation in rodents using von Frey hairs/Semmes-Weinstein monofilaments: Towards a rational method. *Journal of neuroscience methods*, *255*, 92–103. https://doi.org/10.1016/j.jneumeth.2015.08.010

Bremer J, O'Connor T, Tiberi C, Rehrauer H, Weis J, Aguzzi A. Ablation of Dicer from murine Schwann cells increases their proliferation while blocking myelination. PLoS One. 2010 Aug 27;5(8):e12450. doi: 10.1371/journal.pone.0012450. PMID: 20805985; PMCID: PMC2929198.

Brennan, A., Dean, C. H., Zhang, A. L., Cass, D. T., Mirsky, R., & Jessen, K. R. (2000). Endothelins control the timing of Schwann cell generation in vitro and in vivo. Developmental biology, 227(2), 545–557. https://doi.org/10.1006/dbio.2000.9887

Brinkmann, B. G., & Quintes, S. (2017). Zeb2: Inhibiting the inhibitors in Schwann cells. Neurogenesis (Austin, Tex.), 4(1), e1271495. https://doi.org/10.1080/23262133.2016.1271495
Britsch, S., Goerich, D. E., Riethmacher, D., Peirano, R. I., Rossner, M., Nave, K. A., Birchmeier, C., & Wegner, M. (2001). The transcription factor Sox10 is a key regulator of peripheral glial development. Genes & development, 15(1), 66–78. https://doi.org/10.1101/gad.186601

Brosius Lutz, A., & Barres, B. A. (2014). Contrasting the glial response to axon injury in the central and peripheral nervous systems. Developmental cell, 28(1), 7–17. https://doi.org/10.1016/j.devcel.2013.12.002

Brügger, V., Engler, S., Pereira, J. A., Ruff, S., Horn, M., Welzl, H., Münger, E., Vaquié, A., Sidiropoulos, P. N., Egger, B., Yotovski, P., Filgueira, L., Somandin, C., Lühmann, T. C., D'Antonio, M., Yamaguchi, T., Matthias, P., Suter, U., & Jacob, C. (2015). HDAC1/2-Dependent P0 Expression Maintains Paranodal and Nodal Integrity Independently of Myelin Stability through Interactions with Neurofascins. PLoS biology, 13(9), e1002258. https://doi.org/10.1371/journal.pbio.1002258

Brügger, V., Duman, M., Bochud, M., Münger, E., Heller, M., Ruff, S., & Jacob, C. (2017). Delaying histone deacetylase response to injury accelerates conversion into repair Schwann cells and nerve regeneration. Nature communications, 8, 14272. https://doi.org/10.1038/ncomms14272

Büttner, R., Schulz, A., Reuter, M., Akula, A. K., Mindos, T., Carlstedt, A., Riecken, L. B., Baader, S. L., Bauer, R., & Morrison, H. (2018). Inflammaging impairs peripheral nerve maintenance and regeneration. Aging cell, 17(6), e12833. https://doi.org/10.1111/acel.12833

Catala, M., & Kubis, N. (2013). Gross anatomy and development of the peripheral nervous system. Handbook of clinical neurology, 115, 29–41. https://doi.org/10.1016/B978-0-444-52902-2.00003-5

Cattin, A. L., Burden, J. J., Van Emmenis, L., Mackenzie, F. E., Hoving, J. J., Garcia Calavia, N., Guo, Y., McLaughlin, M., Rosenberg, L. H., Quereda, V., Jamecna, D., Napoli, I., Parrinello, S., Enver, T., Ruhrberg, C., & Lloyd, A. C. (2015). Macrophage-Induced Blood Vessels Guide Schwann Cell-Mediated Regeneration of Peripheral Nerves. Cell, 162(5), 1127–1139. https://doi.org/10.1016/j.cell.2015.07.021

Cattin, A. L., & Lloyd, A. C. (2016). The multicellular complexity of peripheral nerve regeneration. Current opinion in neurobiology, 39, 38–46. https://doi.org/10.1016/j.conb.2016.04.005

Chang, H. Y., Liu, H. S., Lai, M. D., Tsai, Y. S., Tzai, T. S., Cheng, H. L., & Chow, N. H. (2014). Hypoxia promotes nuclear translocation and transcriptional function in the oncogenic tyrosine kinase RON. Cancer research, 74(16), 4549–4562. https://doi.org/10.1158/0008-5472.CAN-13-3730

Chen, C. Z., Neumann, B., Förster, S., & Franklin, R. J. M. (2021). Schwann cell remyelination of the central nervous system: why does it happen and what are the benefits?. Open biology, 11(1), 200352. https://doi.org/10.1098/rsob.200352

Chen Y, Wang H, Yoon SO, Xu X, Hottiger MO, Svaren J, Nave KA, Kim HA, Olson EN, Lu QR. HDAC-mediated deacetylation of NF-κB is critical for Schwann cell myelination. Nat Neurosci. 2011 Apr;14(4):437-41. doi: 10.1038/nn.2780. Epub 2011 Mar 20. PMID: 21423191; PMCID: PMC3074381.

Chittka, A., Arevalo, J. C., Rodriguez-Guzman, M., Pérez, P., Chao, M. V., & Sendtner, M. (2004). The p75NTR-interacting protein SC1 inhibits cell cycle progression by transcriptional repression of cyclin E. The Journal of cell biology, 164(7), 985–996. https://doi.org/10.1083/jcb.200301106

Cho, Y., Sloutsky, R., Naegle, K. M., & Cavalli, V. (2013). Injury-induced HDAC5 nuclear export is essential for axon regeneration. Cell, 155(4), 894–908. https://doi.org/10.1016/j.cell.2013.10.004

Cho, Y., Shin, J. E., Ewan, E. E., Oh, Y. M., Pita-Thomas, W., & Cavalli, V. (2015). Activating Injury-Responsive Genes with Hypoxia Enhances Axon Regeneration through Neuronal HIF-1α. Neuron, 88(4), 720–734. https://doi.org/10.1016/j.neuron.2015.09.050

Clements, M. P., Byrne, E., Camarillo Guerrero, L. F., Cattin, A. L., Zakka, L., Ashraf, A., Burden, J. J., Khadayate, S., Lloyd, A. C., Marguerat, S., & Parrinello, S. (2017). The Wound Microenvironment Reprograms Schwann Cells to Invasive Mesenchymal-like Cells to Drive Peripheral Nerve Regeneration. Neuron, 96(1), 98–114.e7. https://doi.org/10.1016/j.neuron.2017.09.008

Comerford, K. M., Cummins, E. P., & Taylor, C. T. (2004). c-Jun NH2-terminal kinase activation contributes to hypoxia-inducible factor 1alpha-dependent P-glycoprotein expression in hypoxia. Cancer research, 64(24), 9057–9061. https://doi.org/10.1158/0008-5472.CAN-04-1919

Court, F. A., Sherman, D. L., Pratt, T., Garry, E. M., Ribchester, R. R., Cottrell, D. F., Fleetwood-Walker, S. M., & Brophy, P. J. (2004). Restricted growth of Schwann cells lacking Cajal bands slows conduction in myelinated nerves. Nature, 431(7005), 191–195. https://doi.org/10.1038/nature02841

Cox, J., & Mann, M. (2008). MaxQuant enables high peptide identification rates, individualized p.p.b.-range mass accuracies and proteome-wide protein quantification. Nature biotechnology, 26(12), 1367–1372. https://doi.org/10.1038/nbt.1511

D'Antonio, M., Droggiti, A., Feltri, M. L., Roes, J., Wrabetz, L., Mirsky, R., & Jessen, K. R. (2006). TGFbeta type II receptor signaling controls Schwann cell death and proliferation in developing nerves. The Journal of neuroscience : the official journal of the Society for Neuroscience, 26(33), 8417–8427. https://doi.org/10.1523/JNEUROSCI.1578-06.2006

Deardorff, M. A., Bando, M., Nakato, R., Watrin, E., Itoh, T., Minamino, M., Saitoh, K., Komata, M., Katou, Y., Clark, D., Cole, K. E., De Baere, E., Decroos, C., Di Donato, N., Ernst, S., Francey, L. J., Gyftodimou, Y., Hirashima, K., Hullings, M., Ishikawa, Y., … Shirahige, K. (2012). HDAC8 mutations in Cornelia de Lange syndrome affect the cohesin acetylation cycle. Nature, 489(7415), 313–317. https://doi.org/10.1038/nature11316

DeFrates, K. G., Franco, D., Heber-Katz, E., & Messersmith, P. B. (2021). Unlocking mammalian regeneration through hypoxia inducible factor one alpha signaling. *Biomaterials*, *269*, 120646. https://doi.org/10.1016/j.biomaterials.2020.120646

De Hert, S., De Baerdemaeker, L., & De Maeseneer, M. (2014). What the phlebologist should know about local anesthetics. *Phlebology*, *29*(7), 428–441. https://doi.org/10.1177/0268355513501303

Denarier, E., Forghani, R., Farhadi, H. F., Dib, S., Dionne, N., Friedman, H. C., Lepage, P., Hudson, T. J., Drouin, R., & Peterson, A. (2005). Functional organization of a Schwann cell enhancer. The Journal of neuroscience : the official journal of the Society for Neuroscience, 25(48), 11210–11217. https://doi.org/10.1523/JNEUROSCI.2596-05.2005

Deng, Y., Wu, L. M. N., Bai, S., Zhao, C., Wang, H., Wang, J., Xu, L., Sakabe, M., Zhou, W., Xin, M., & Lu, Q. R. (2017). A reciprocal regulatory loop between TAZ/YAP and G-protein Gαs regulates Schwann cell proliferation and myelination. Nature communications, 8, 15161. https://doi.org/10.1038/ncomms15161

de Ruijter, A. J., van Gennip, A. H., Caron, H. N., Kemp, S., & van Kuilenburg, A. B. (2003). Histone deacetylases (HDACs): characterization of the classical HDAC family. The Biochemical journal, 370(Pt 3), 737–749. https://doi.org/10.1042/BJ2002132

Deuis, J. R., & Vetter, I. (2016). The thermal probe test: A novel behavioral assay to quantify thermal paw withdrawal thresholds in mice. *Temperature (Austin, Tex.)*, *3*(2), 199–207. https://doi.org/10.1080/23328940.2016.1157668

Domènech-Estévez, E., Baloui, H., Meng, X., Zhang, Y., Deinhardt, K., Dupree, J. L., Einheber, S., Chrast, R., & Salzer, J. L. (2016). Akt Regulates Axon Wrapping and Myelin Sheath Thickness in the PNS. The Journal of neuroscience : the official journal of the Society for Neuroscience, 36(16), 4506–4521. https://doi.org/10.1523/JNEUROSCI.3521-15.2016

Diamond, J., Holmes, M., & Coughlin, M. (1992). Endogenous NGF and nerve impulses regulate the collateral sprouting of sensory axons in the skin of the adult rat. The Journal of neuroscience : the

official journal of the Society for Neuroscience, 12(4), 1454–1466. https://doi.org/10.1523/JNEUROSCI.12-04-01454.1992

Dong, Z., Dean, C., Walters, J. E., Mirsky, R., & Jessen, K. R. (1997). Response of Schwann cells to mitogens in vitro is determined by pre-exposure to serum, time in vitro, and developmental age. Glia, 20(3), 219–230.
Duman, M., Jaggi, S., Enz, L. S., Jacob, C., & Schaeren-Wiemers, N. (2022). Theophylline Induces Remyelination and Functional Recovery in a Mouse Model of Peripheral Neuropathy. Biomedicines, 10(6), 1418. https://doi.org/10.3390/biomedicines10061418

Duman, M., Martinez-Moreno, M., Jacob, C., & Tapinos, N. (2020). Functions of histone modifications and histone modifiers in Schwann cells. Glia, 68(8), 1584–1595. https://doi.org/10.1002/glia.23795

Duman, M., Vaquié, A., Nocera, G., Heller, M., Stumpe, M., Siva Sankar, D., Dengjel, J., Meijer, D., Yamaguchi, T., Matthias, P., Zeis, T., Schaeren-Wiemers, N., Hayoz, A., Ruff, S., & Jacob, C. (2020). EEF1A1 deacetylation enables transcriptional activation of remyelination. Nature communications, 11(1), 3420. https://doi.org/10.1038/s41467-020-17243-z

Dun, X. P., & Parkinson, D. B. (2015). Visualizing peripheral nerve regeneration by whole mount staining. PloS one, 10(3), e0119168. https://doi.org/10.1371/journal.pone.0119168

Durst, K. L., Lutterbach, B., Kummalue, T., Friedman, A. D., & Hiebert, S. W. (2003). The inv(16) fusion protein associates with corepressors via a smooth muscle myosin heavy-chain domain. Molecular and cellular biology, 23(2), 607–619. https://doi.org/10.1128/MCB.23.2.607-619.2003
Dyachuk, V., Furlan, A., Shahidi, M. K., Giovenco, M., Kaukua, N., Konstantinidou, C., Pachnis, V., Memic, F., Marklund, U., Müller, T., Birchmeier, C., Fried, K., Ernfors, P., & Adameyko, I. (2014). Neurodevelopment. Parasympathetic neurons originate from nerve-associated peripheral glial progenitors. Science (New York, N.Y.), 345(6192), 82–87. https://doi.org/10.1126/science.1253281

Espinosa-Medina, I., Jevans, B., Boismoreau, F., Chettouh, Z., Enomoto, H., Müller, T., Birchmeier, C., Burns, A. J., & Brunet, J. F. (2017). Dual origin of enteric neurons in vagal Schwann cell precursors and the sympathetic neural crest. Proceedings of the National Academy of Sciences of the United States of America, 114(45), 11980–11985. https://doi.org/10.1073/pnas.1710308114

Fazal, S. V., Gomez-Sanchez, J. A., Wagstaff, L. J., Musner, N., Otto, G., Janz, M., Mirsky, R., & Jessen, K. R. (2017). Graded Elevation of c-Jun in Schwann Cells In Vivo: Gene Dosage Determines Effects on Development, Remyelination, Tumorigenesis, and Hypomyelination. The Journal of neuroscience : the official journal of the Society for Neuroscience, 37(50), 12297–12313. https://doi.org/10.1523/JNEUROSCI.0986-17.2017

Feltri ML, Poitelon Y, Previtali SC. How Schwann Cells Sort Axons: New Concepts. Neuroscientist. 2016 Jun;22(3):252-65. doi: 10.1177/1073858415572361. Epub 2015 Feb 16. PMID: 25686621; PMCID: PMC5181106

Fischer, S., Weishaupt, A., Troppmair, J., & Martini, R. (2008). Increase of MCP-1 (CCL2) in myelin mutant Schwann cells is mediated by MEK-ERK signaling pathway. *Glia*, *56*(8), 836–843. https://doi.org/10.1002/glia.20657

Fledrich, R., Stassart, R. M., & Sereda, M. W. (2012). Murine therapeutic models for Charcot-Marie-Tooth (CMT) disease. British medical bulletin, 102, 89–113. https://doi.org/10.1093/bmb/lds010

Fledrich, R., Stassart, R. M., Klink, A., Rasch, L. M., Prukop, T., Haag, L., Czesnik, D., Kungl, T., Abdelaal, T. A., Keric, N., Stadelmann, C., Brück, W., Nave, K. A., & Sereda, M. W. (2014). Soluble neuregulin-1 modulates disease pathogenesis in rodent models of Charcot-Marie-Tooth disease 1A. Nature medicine, 20(9), 1055–1061. https://doi.org/10.1038/nm.3664

Fledrich, R., Abdelaal, T., Rasch, L., Bansal, V., Schütza, V., Brügger, B., Lüchtenborg, C., Prukop, T., Stenzel, J., Rahman, R. U., Hermes, D., Ewers, D., Möbius, W., Ruhwedel, T., Katona, I., Weis, J., Klein, D., Martini, R., Brück, W., Müller, W. C., … Sereda, M. W. (2018). Targeting myelin lipid metabolism as a potential therapeutic strategy in a model of CMT1A neuropathy. Nature communications, 9(1), 3025. https://doi.org/10.1038/s41467-018-05420-0

Fledrich, R., Akkermann, D., Schütza, V., Abdelaal, T. A., Hermes, D., Schäffner, E., Soto-Bernardini, M. C., Götze, T., Klink, A., Kusch, K., Krueger, M., Kungl, T., Frydrychowicz, C., Möbius, W., Brück, W., Mueller, W. C., Bechmann, I., Sereda, M. W., Schwab, M. H., Nave, K. A., … Stassart, R. M. (2019). NRG1 type I dependent autoparacrine stimulation of Schwann cells in onion bulbs of peripheral neuropathies. Nature communications, 10(1), 1467. https://doi.org/10.1038/s41467-019-09385-6

Fontana, X., Hristova, M., Da Costa, C., Patodia, S., Thei, L., Makwana, M., Spencer-Dene, B., Latouche, M., Mirsky, R., Jessen, K. R., Klein, R., Raivich, G., & Behrens, A. (2012). c-Jun in Schwann cells promotes axonal regeneration and motoneuron survival via paracrine signaling. The Journal of cell biology, 198(1), 127–141. https://doi.org/10.1083/jcb.201205025

Fledrich, R., Kungl, T., Nave, K. A., & Stassart, R. M. (2019). Axo-glial interdependence in peripheral nerve development. Development (Cambridge, England), 146(21), dev151704. https://doi.org/10.1242/dev.151704

Flores, K., Yadav, S. S., Katz, A. A., & Seger, R. (2019). The Nuclear Translocation of Mitogen-Activated Protein Kinases: Molecular Mechanisms and Use as Novel Therapeutic Target. Neuroendocrinology, 108(2), 121–131. https://doi.org/10.1159/000494085

Fricker, F. R., Zhu, N., Tsantoulas, C., Abrahamsen, B., Nassar, M. A., Thakur, M., Garratt, A. N., Birchmeier, C., McMahon, S. B., Wood, J. N., & Bennett, D. L. (2009). Sensory axon-derived neuregulin-1 is required for axoglial signaling and normal sensory function but not for long-term axon maintenance. The Journal of neuroscience : the official journal of the Society for Neuroscience, 29(24), 7667–7678. https://doi.org/10.1523/JNEUROSCI.6053-08.2009

Fricker, F. R., Lago, N., Balarajah, S., Tsantoulas, C., Tanna, S., Zhu, N., Fageiry, S. K., Jenkins, M., Garratt, A. N., Birchmeier, C., & Bennett, D. L. (2011). Axonally derived neuregulin-1 is required for remyelination and regeneration after nerve injury in adulthood. The Journal of neuroscience : the official journal of the Society for Neuroscience, 31(9), 3225–3233. https://doi.org/10.1523/JNEUROSCI.2568-10.2011

Fricker, F. R., Antunes-Martins, A., Galino, J., Paramsothy, R., La Russa, F., Perkins, J., Goldberg, R., Brelstaff, J., Zhu, N., McMahon, S. B., Orengo, C., Garratt, A. N., Birchmeier, C., & Bennett, D. L. (2013). Axonal neuregulin 1 is a rate limiting but not essential factor for nerve remyelination. Brain : a journal of neurology, 136(Pt 7), 2279–2297. https://doi.org/10.1093/brain/awt148

Fridman V, Saporta MA. Mechanisms and Treatments in Demyelinating CMT. Neurotherapeutics. 2021 Oct;18(4):2236-2268. doi: 10.1007/s13311-021-01145-z. Epub 2021 Nov 8. PMID: 34750751; PMCID: PMC8804145.

Fröb, F., & Wegner, M. (2020). The role of chromatin remodeling complexes in Schwann cell development. Glia, 68(8), 1596–1603. https://doi.org/10.1002/glia.23766

Gammill, L. S., & Bronner-Fraser, M. (2003). Neural crest specification: migrating into genomics. Nature reviews. Neuroscience, 4(10), 795–805. https://doi.org/10.1038/nrn1219

Gao, J., Siddoway, B., Huang, Q., & Xia, H. (2009). Inactivation of CREB mediated gene transcription by HDAC8 bound protein phosphatase. Biochemical and biophysical research communications, 379(1), 1–5. https://doi.org/10.1016/j.bbrc.2008.11.135

Gaudet, A. D., Popovich, P. G., & Ramer, M. S. (2011). Wallerian degeneration: gaining perspective on inflammatory events after peripheral nerve injury. Journal of neuroinflammation, 8, 110. https://doi.org/10.1186/1742-2094-8-110

Ghidinelli, M., Poitelon, Y., Shin, Y. K., Ameroso, D., Williamson, C., Ferri, C., Pellegatta, M., Espino, K., Mogha, A., Monk, K., Podini, P., Taveggia, C., Nave, K. A., Wrabetz, L., Park, H. T., & Feltri, M. L. (2017). Laminin 211 inhibits protein kinase A in Schwann cells to modulate neuregulin 1 type III-driven myelination. PLoS biology, 15(6), e2001408. https://doi.org/10.1371/journal.pbio.2001408

Glenn, T. D., & Talbot, W. S. (2013). Signals regulating myelination in peripheral nerves and the Schwann cell response to injury. Current opinion in neurobiology, 23(6), 1041–1048. https://doi.org/10.1016/j.conb.2013.06.010

Glozak, M. A., Sengupta, N., Zhang, X., & Seto, E. (2005). Acetylation and deacetylation of non-histone proteins. Gene, 363, 15–23. https://doi.org/10.1016/j.gene.2005.09.010

Goebbels, S., Oltrogge, J. H., Kemper, R., Heilmann, I., Bormuth, I., Wolfer, S., Wichert, S. P., Möbius, W., Liu, X., Lappe-Siefke, C., Rossner, M. J., Groszer, M., Suter, U., Frahm, J., Boretius, S., & Nave, K. A. (2010). Elevated phosphatidylinositol 3,4,5-trisphosphate in glia triggers cell-autonomous membrane wrapping and myelination. The Journal of neuroscience : the official journal of the Society for Neuroscience, 30(26), 8953–8964. https://doi.org/10.1523/JNEUROSCI.0219-10.2010

Gokey NG, Srinivasan R, Lopez-Anido C, Krueger C, Svaren J. Developmental regulation of microRNA expression in Schwann cells. Mol Cell Biol. 2012 Jan;32(2):558-68. doi: 10.1128/MCB.06270-11. Epub 2011 Nov 7. PMID: 22064487; PMCID: PMC3255778.

Gomez-Sanchez, J. A., Carty, L., Iruarrizaga-Lejarreta, M., Palomo-Irigoyen, M., Varela-Rey, M., Griffith, M., Hantke, J., Macias-Camara, N., Azkargorta, M., Aurrekoetxea, I., De Juan, V. G., Jefferies, H. B., Aspichueta, P., Elortza, F., Aransay, A. M., Martínez-Chantar, M. L., Baas, F., Mato, J. M., Mirsky, R., Woodhoo, A., … Jessen, K. R. (2015). Schwann cell autophagy, myelinophagy, initiates myelin clearance from injured nerves. The Journal of cell biology, 210(1), 153–168. https://doi.org/10.1083/jcb.201503019

Gomez-Sanchez, J. A., Gomis-Coloma, C., Morenilla-Palao, C., Peiro, G., Serra, E., Serrano, M., & Cabedo, H. (2013). Epigenetic induction of the Ink4a/Arf locus prevents Schwann cell overproliferation during nerve regeneration and after tumorigenic challenge. Brain : a journal of neurology, 136(Pt 7), 2262–2278. https://doi.org/10.1093/brain/awt130

Gomez-Sanchez, J. A., Patel, N., Martirena, F., Fazal, S. V., Mutschler, C., & Cabedo, H. (2022). Emerging Role of HDACs in Regeneration and Ageing in the Peripheral Nervous System: Repair Schwann Cells as

Pivotal Targets. International journal of molecular sciences, 23(6), 2996. https://doi.org/10.3390/ijms23062996

Gomez-Sanchez, J. A., Pilch, K. S., van der Lans, M., Fazal, S. V., Benito, C., Wagstaff, L. J., Mirsky, R., & Jessen, K. R. (2017). After Nerve Injury, Lineage Tracing Shows That Myelin and Remak Schwann Cells Elongate Extensively and Branch to Form Repair Schwann Cells, Which Shorten Radically on Remyelination. The Journal of neuroscience : the official journal of the Society for Neuroscience, 37(37), 9086–9099. https://doi.org/10.1523/JNEUROSCI.1453-17.2017

Gomis-Coloma C, Velasco-Aviles S, Gomez-Sanchez JA, Casillas-Bajo A, Backs J, Cabedo H. Class IIa histone deacetylases link cAMP signaling to the myelin transcriptional program of Schwann cells. J Cell Biol. 2018 Apr 2;217(4):1249-1268. doi: 10.1083/jcb.201611150. Epub 2018 Feb 22. PMID: 29472387; PMCID: PMC5881490.

Greer, C. B., Tanaka, Y., Kim, Y. J., Xie, P., Zhang, M. Q., Park, I. H., & Kim, T. H. (2015). Histone Deacetylases Positively Regulate Transcription through the Elongation Machinery. Cell reports, 13(7), 1444–1455. https://doi.org/10.1016/j.celrep.2015.10.013

Groh, J., Weis, J., Zieger, H., Stanley, E. R., Heuer, H., & Martini, R. (2012). Colony-stimulating factor-1 mediates macrophage-related neural damage in a model for Charcot-Marie-Tooth disease type 1X. Brain : a journal of neurology, 135(Pt 1), 88–104. https://doi.org/10.1093/brain/awr283

Grove, M., Kim, H., Santerre, M., Krupka, A. J., Han, S. B., Zhai, J., Cho, J. Y., Park, R., Harris, M., Kim, S., Sawaya, B. E., Kang, S. H., Barbe, M. F., Cho, S. H., Lemay, M. A., & Son, Y. J. (2017). YAP/TAZ initiate and maintain Schwann cell myelination. eLife, 6, e20982. https://doi.org/10.7554/eLife.20982

Grove, M., Lee, H., Zhao, H., & Son, Y. J. (2020). Axon-dependent expression of YAP/TAZ mediates Schwann cell remyelination but not proliferation after nerve injury. eLife, 9, e50138. https://doi.org/10.7554/eLife.50138

Gu, Y., Chen, C., Yi, S., Wang, S., Gong, L., Liu, J., Gu, X., Zhao, Q., & Li, S. (2015). miR-sc8 Inhibits Schwann Cell Proliferation and Migration by Targeting Egfr. PloS one, 10(12), e0145185. https://doi.org/10.1371/journal.pone.0145185

Gupta, P., Ho, P. C., Ha, S. G., Lin, Y. W., & Wei, L. N. (2009). HDAC3 as a molecular chaperone for shuttling phosphorylated TR2 to PML: a novel deacetylase activity-independent function of HDAC3. *PloS one*, *4*(2), e4363. https://doi.org/10.1371/journal.pone.0004363

Hameed, L. S., Berg, D. A., Belnoue, L., Jensen, L. D., Cao, Y., & Simon, A. (2015). Environmental changes in oxygen tension reveal ROS-dependent neurogenesis and regeneration in the adult newt brain. *eLife*, *4*, e08422. https://doi.org/10.7554/eLife.08422

Hantke, J., Carty, L., Wagstaff, L. J., Turmaine, M., Wilton, D. K., Quintes, S., Koltzenburg, M., Baas, F., Mirsky, R., & Jessen, K. R. (2014). c-Jun activation in Schwann cells protects against loss of sensory axons in inherited neuropathy. Brain : a journal of neurology, 137(Pt 11), 2922–2937. https://doi.org/10.1093/brain/awu257

Hanz, S., Perlson, E., Willis, D., Zheng, J. Q., Massarwa, R., Huerta, J. J., Koltzenburg, M., Kohler, M., van-Minnen, J., Twiss, J. L., & Fainzilber, M. (2003). Axoplasmic importins enable retrograde injury signaling in lesioned nerve. Neuron, 40(6), 1095–1104. https://doi.org/10.1016/s0896-6273(03)00770-0

Harrisingh, M. C., Perez-Nadales, E., Parkinson, D. B., Malcolm, D. S., Mudge, A. W., & Lloyd, A. C. (2004). The Ras/Raf/ERK signalling pathway drives Schwann cell dedifferentiation. The EMBO journal, 23(15), 3061–3071. https://doi.org/10.1038/sj.emboj.7600309

Harty, B. L., Coelho, F., Pease-Raissi, S. E., Mogha, A., Ackerman, S. D., Herbert, A. L., Gereau, R. W., 4th, Golden, J. P., Lyons, D. A., Chan, J. R., & Monk, K. R. (2019). Myelinating Schwann cells ensheath multiple axons in the absence of E3 ligase component Fbxw7. Nature communications, 10(1), 2976. https://doi.org/10.1038/s41467-019-10881-y

He, X., Zhang, L., Queme, L. F., Liu, X., Lu, A., Waclaw, R. R., Dong, X., Zhou, W., Kidd, G., Yoon, S. O., Buonanno, A., Rubin, J. B., Xin, M., Nave, K. A., Trapp, B. D., Jankowski, M. P., & Lu, Q. R. (2018). A histone deacetylase 3-dependent pathway delimits peripheral myelin growth and functional regeneration. Nature medicine, 24(3), 338–351. https://doi.org/10.1038/nm.4483

He, Y., Kim, J. Y., Dupree, J., Tewari, A., Melendez-Vasquez, C., Svaren, J., & Casaccia, P. (2010). Yy1 as a molecular link between neuregulin and transcriptional modulation of peripheral myelination. Nature neuroscience, 13(12), 1472–1480. https://doi.org/10.1038/nn.2686

Heber-Katz E. (2017). Oxygen, Metabolism, and Regeneration: Lessons from Mice. *Trends in molecular medicine*, *23*(11), 1024–1036. https://doi.org/10.1016/j.molmed.2017.08.008

Heinen, A., Tzekova, N., Graffmann, N., Torres, K. J., Uhrberg, M., Hartung, H. P., & Küry, P. (2012). Histone methyltransferase enhancer of zeste homolog 2 regulates Schwann cell differentiation. Glia, 60(11), 1696–1708. https://doi.org/10.1002/glia.22388

Helbing, D. L., Schulz, A., & Morrison, H. (2020). Pathomechanisms in schwannoma development and progression. Oncogene, 39(32), 5421–5429. https://doi.org/10.1038/s41388-020-1374-5

Herdegen, T., Skene, P., & Bähr, M. (1997). The c-Jun transcription factor--bipotential mediator of neuronal death, survival and regeneration. Trends in neurosciences, 20(5), 227–231. https://doi.org/10.1016/s0166-2236(96)01000-4

Hertzog, N., & Jacob, C. (2023). Mechanisms and treatment strategies of demyelinating and dysmyelinating Charcot-Marie-Tooth disease. Neural regeneration research, 18(9), 1931–1939. https://doi.org/10.4103/1673-5374.367834

Hildebrand, C., Kocsis, J. D., Berglund, S., & Waxman, S. G. (1985). Myelin sheath remodelling in regenerated rat sciatic nerve. Brain research, 358(1-2), 163–170. https://doi.org/10.1016/0006-8993(85)90960-6

Hodawadekar, S. C., & Marmorstein, R. (2007). Chemistry of acetyl transfer by histone modifying enzymes: structure, mechanism and implications for effector design. Oncogene, 26(37), 5528–5540. https://doi.org/10.1038/sj.onc.1210619

Höke, A., Redett, R., Hameed, H., Jari, R., Zhou, C., Li, Z. B., Griffin, J. W., & Brushart, T. M. (2006). Schwann cells express motor and sensory phenotypes that regulate axon regeneration. The Journal of neuroscience : the official journal of the Society for Neuroscience, 26(38), 9646–9655. https://doi.org/10.1523/JNEUROSCI.1620-06.2006

Hu, X., Hicks, C. W., He, W., Wong, P., Macklin, W. B., Trapp, B. D., & Yan, R. (2006). Bace1 modulates myelination in the central and peripheral nervous system. Nature neuroscience, 9(12), 1520–1525. https://doi.org/10.1038/nn1797

Hu, X., He, W., Diaconu, C., Tang, X., Kidd, G. J., Macklin, W. B., Trapp, B. D., & Yan, R. (2008). Genetic deletion of BACE1 in mice affects remyelination of sciatic nerves. FASEB journal : official publication of the Federation of American Societies for Experimental Biology, 22(8), 2970–2980. https://doi.org/10.1096/fj.08-106666

Hu, X., Hu, J., Dai, L., Trapp, B., & Yan, R. (2015). Axonal and Schwann cell BACE1 is equally required for remyelination of peripheral nerves. The Journal of neuroscience : the official journal of the Society for Neuroscience, 35(9), 3806–3814. https://doi.org/10.1523/JNEUROSCI.5207-14.2015

Huegel, J., Dinh, C. T., Martinelli, M., Bracho, O., Rosario, R., Hardin, H., Estivill, M., Griswold, A., Gultekin, S., Liu, X. Z., & Fernandez-Valle, C. (2022). CUDC907, a dual phosphoinositide-3 kinase/histone deacetylase inhibitor, promotes apoptosis of NF2 Schwannoma cells. *Oncotarget*, *13*, 890–904. https://doi.org/10.18632/oncotarget.28254

Hung, H. A., Sun, G., Keles, S., & Svaren, J. (2015). Dynamic regulation of Schwann cell enhancers after peripheral nerve injury. The Journal of biological chemistry, 290(11), 6937–6950. https://doi.org/10.1074/jbc.M114.622878

Jacob C. (2015). Transcriptional control of neural crest specification into peripheral glia. Glia, 63(11), 1883–1896. https://doi.org/10.1002/glia.22816

Jacob C. (2017). Chromatin-remodeling enzymes in control of Schwann cell development, maintenance and plasticity. Current opinion in neurobiology, 47, 24–30. https://doi.org/10.1016/j.conb.2017.08.007

Jacob, C., Christen, C. N., Pereira, J. A., Somandin, C., Baggiolini, A., Lötscher, P., Ozçelik, M., Tricaud, N., Meijer, D., Yamaguchi, T., Matthias, P., & Suter, U. (2011). HDAC1 and HDAC2 control the transcriptional program of myelination and the survival of Schwann cells. Nature neuroscience, 14(4), 429–436. https://doi.org/10.1038/nn.2762

Jacob, C., Grabner, H., Atanasoski, S., & Suter, U. (2008). Expression and localization of Ski determine cell type-specific TGFbeta signaling effects on the cell cycle. The Journal of cell biology, 182(3), 519–530. https://doi.org/10.1083/jcb.200710161

Jacob, C., Lötscher, P., Engler, S., Baggiolini, A., Varum Tavares, S., Brügger, V., John, N., Büchmann-Møller, S., Snider, P. L., Conway, S. J., Yamaguchi, T., Matthias, P., Sommer, L., Mantei, N., & Suter, U. (2014). HDAC1 and HDAC2 control the specification of neural crest cells into peripheral glia. The Journal of neuroscience : the official journal of the Society for Neuroscience, 34(17), 6112–6122. https://doi.org/10.1523/JNEUROSCI.5212-13.2014

Jaegle M, Ghazvini M, Mandemakers W, Piirsoo M, Driegen S, Levavasseur F, Raghoenath S, Grosveld F, Meijer D. The POU proteins Brn-2 and Oct-6 share important functions in Schwann cell development. Genes Dev. 2003 Jun 1;17(11):1380-91. doi: 10.1101/gad.258203. PMID: 12782656; PMCID: PMC196070.

Jaegle, M., Mandemakers, W., Broos, L., Zwart, R., Karis, A., Visser, P., Grosveld, F., & Meijer, D. (1996). The POU factor Oct-6 and Schwann cell differentiation. Science (New York, N.Y.), 273(5274), 507–510. https://doi.org/10.1126/science.273.5274.507

Jang, S. W., & Svaren, J. (2009). Induction of myelin protein zero by early growth response 2 through upstream and intragenic elements. The Journal of biological chemistry, 284(30), 20111–20120. https://doi.org/10.1074/jbc.M109.022426

Jeanette H, Marziali LN, Bhatia U, Hellman A, Herron J, Kopec AM, Feltri ML, Poitelon Y, Belin S. YAP and TAZ regulate Schwann cell proliferation and differentiation during peripheral nerve regeneration. Glia. 2021 Apr;69(4):1061-1074. doi: 10.1002/glia.23949. Epub 2020 Dec 18. PMID: 33336855; PMCID: PMC7898398.

Jessen, K. R., & Arthur-Farraj, P. (2019). Repair Schwann cell update: Adaptive reprogramming, EMT, and stemness in regenerating nerves. Glia, 67(3), 421–437. https://doi.org/10.1002/glia.23532

Jessen, K. R., & Mirsky, R. (2005). The origin and development of glial cells in peripheral nerves. Nature reviews. Neuroscience, 6(9), 671–682. https://doi.org/10.1038/nrn1746

Jessen, K. R., & Mirsky, R. (2008). Negative regulation of myelination: relevance for development, injury, and demyelinating disease. Glia, 56(14), 1552–1565. https://doi.org/10.1002/glia.20761

Jessen, K. R., Mirsky, R., & Lloyd, A. C. (2015). Schwann Cells: Development and Role in Nerve Repair. Cold Spring Harbor perspectives in biology, 7(7), a020487. https://doi.org/10.1101/cshperspect.a020487

Jessen, K. R., & Mirsky, R. (2016). The repair Schwann cell and its function in regenerating nerves. The Journal of physiology, 594(13), 3521–3531. https://doi.org/10.1113/JP270874

Jessen, K. R., & Mirsky, R. (2019). The Success and Failure of the Schwann Cell Response to Nerve Injury. Frontiers in cellular neuroscience, 13, 33. https://doi.org/10.3389/fncel.2019.00033

Jessen, K. R., & Mirsky, R. (2022). The Role of c-Jun and Autocrine Signaling Loops in the Control of Repair Schwann Cells and Regeneration. Frontiers in cellular neuroscience, 15, 820216. https://doi.org/10.3389/fncel.2021.820216

Jiang, Y., Duan, L. J., & Fong, G. H. (2021). Oxygen-sensing mechanisms in development and tissue repair. Development (Cambridge, England), 148(23), dev200030. https://doi.org/10.1242/dev.200030

Jones, E. A., Jang, S. W., Mager, G. M., Chang, L. W., Srinivasan, R., Gokey, N. G., Ward, R. M., Nagarajan, R., & Svaren, J. (2007). Interactions of Sox10 and Egr2 in myelin gene regulation. Neuron glia biology, 3(4), 377–387. https://doi.org/10.1017/S1740925X08000173

Johnston, A. P., Naska, S., Jones, K., Jinno, H., Kaplan, D. R., & Miller, F. D. (2013). Sox2-mediated regulation of adult neural crest precursors and skin repair. Stem cell reports, 1(1), 38–45. https://doi.org/10.1016/j.stemcr.2013.04.004

Joseph, N. M., Mukouyama, Y. S., Mosher, J. T., Jaegle, M., Crone, S. A., Dormand, E. L., Lee, K. F., Meijer, D., Anderson, D. J., & Morrison, S. J. (2004). Neural crest stem cells undergo multilineage differentiation in developing peripheral nerves to generate endoneurial fibroblasts in addition to

Schwann cells. Development (Cambridge, England), 131(22), 5599–5612. https://doi.org/10.1242/dev.01429

Kadamb, R., Mittal, S., Bansal, N., Batra, H., & Saluja, D. (2013). Sin3: insight into its transcription regulatory functions. European journal of cell biology, 92(8-9), 237–246. https://doi.org/10.1016/j.ejcb.2013.09.001

Kaelin W. G., Jr (2022). Von Hippel-Lindau disease: insights into oxygen sensing, protein degradation, and cancer. The Journal of clinical investigation, 132(18), e162480. https://doi.org/10.1172/JCI162480

Kaeser-Pebernard, S., Vionnet, C., Mari, M., Sankar, D. S., Hu, Z., Roubaty, C., Martínez-Martínez, E., Zhao, H., Spuch-Calvar, M., Petri-Fink, A., Rainer, G., Steinberg, F., Reggiori, F., & Dengjel, J. (2022). mTORC1 controls Golgi architecture and vesicle secretion by phosphorylation of SCYL1. Nature communications, 13(1), 4685. https://doi.org/10.1038/s41467-022-32487-7

Kaiser, F. J., Ansari, M., Braunholz, D., Concepción Gil-Rodríguez, M., Decroos, C., Wilde, J. J., Fincher, C. T., Kaur, M., Bando, M., Amor, D. J., Atwal, P. S., Bahlo, M., Bowman, C. M., Bradley, J. J., Brunner, H. G., Clark, D., Del Campo, M., Di Donato, N., Diakumis, P., Dubbs, H., … Deardorff, M. A. (2014). Loss-of-function HDAC8 mutations cause a phenotypic spectrum of Cornelia de Lange syndrome-like features, ocular hypertelorism, large fontanelle and X-linked inheritance. Human molecular genetics, 23(11), 2888–2900. https://doi.org/10.1093/hmg/ddu002

Kang, H., & Lichtman, J. W. (2013). Motor axon regeneration and muscle reinnervation in young adult and aged animals. The Journal of neuroscience : the official journal of the Society for Neuroscience, 33(50), 19480–19491. https://doi.org/10.1523/JNEUROSCI.4067-13.2013

Kang, H., Tian, L., Mikesh, M., Lichtman, J. W., & Thompson, W. J. (2014). Terminal Schwann cells participate in neuromuscular synapse remodeling during reinnervation following nerve injury. The Journal of neuroscience : the official journal of the Society for Neuroscience, 34(18), 6323–6333. https://doi.org/10.1523/JNEUROSCI.4673-13.2014

Kao SC, Wu H, Xie J, Chang CP, Ranish JA, Graef IA, Crabtree GR. Calcineurin/NFAT signaling is required for neuregulin-regulated Schwann cell differentiation. Science. 2009 Jan 30;323(5914):651-4. doi: 10.1126/science.1166562. PMID: 19179536; PMCID: PMC2790385.

Karhausen, J., Kong, T., Narravula, S., & Colgan, S. P. (2005). Induction of the von Hippel-Lindau tumor suppressor gene by late hypoxia limits HIF-1 expression. Journal of cellular biochemistry, 95(6), 1264–1275. https://doi.org/10.1002/jcb.20489

Kim, J. Y., Cho, H., Yoo, J., Kim, G. W., Jeon, Y. H., Lee, S. W., & Kwon, S. H. (2022). Pathological Role of HDAC8: Cancer and Beyond. Cells, 11(19), 3161. https://doi.org/10.3390/cells11193161

Kim, S., Maynard, J. C., Sasaki, Y., Strickland, A., Sherman, D. L., Brophy, P. J., Burlingame, A. L., & Milbrandt, J. (2016). Schwann Cell O-GlcNAc Glycosylation Is Required for Myelin Maintenance and Axon Integrity. The Journal of neuroscience : the official journal of the Society for Neuroscience, 36(37), 9633–9646. https://doi.org/10.1523/JNEUROSCI.1235-16.2016

Kim, S., Maynard, J. C., Strickland, A., Burlingame, A. L., & Milbrandt, J. (2018). Schwann cell O-GlcNAcylation promotes peripheral nerve remyelination via attenuation of the AP-1 transcription

factor JUN. Proceedings of the National Academy of Sciences of the United States of America, 115(31), 8019–8024. https://doi.org/10.1073/pnas.1805538115

Klein, D., Groh, J., Wettmarshausen, J., & Martini, R. (2014). Nonuniform molecular features of myelinating Schwann cells in models for CMT1: distinct disease patterns are associated with NCAM and c-Jun upregulation. Glia, 62(5), 736–750. https://doi.org/10.1002/glia.22638

Klein, D., & Martini, R. (2016). Myelin and macrophages in the PNS: An intimate relationship in trauma and disease. Brain research, 1641(Pt A), 130–138. https://doi.org/10.1016/j.brainres.2015.11.033

Ko, C. P., & Robitaille, R. (2015). Perisynaptic Schwann Cells at the Neuromuscular Synapse: Adaptable, Multitasking Glial Cells. Cold Spring Harbor perspectives in biology, 7(10), a020503. https://doi.org/10.1101/cshperspect.a020503

Krock, B. L., Skuli, N., & Simon, M. C. (2011). Hypoxia-induced angiogenesis: good and evil. Genes & cancer, 2(12), 1117–1133. https://doi.org/10.1177/1947601911423654

Kubis, H. P., Hanke, N., Scheibe, R. J., & Gros, G. (2005). Accumulation and nuclear import of HIF1 alpha during high and low oxygen concentration in skeletal muscle cells in primary culture. Biochimica et biophysica acta, 1745(2), 187–195. https://doi.org/10.1016/j.bbamcr.2005.05.007

Küffer, A., Lakkaraju, A. K., Mogha, A., Petersen, S. C., Airich, K., Doucerain, C., Marpakwar, R., Bakirci, P., Senatore, A., Monnard, A., Schiavi, C., Nuvolone, M., Grosshans, B., Hornemann, S., Bassilana, F., Monk, K. R., & Aguzzi, A. (2016). The prion protein is an agonistic ligand of the G protein-coupled receptor Adgrg6. Nature, 536(7617), 464–468. https://doi.org/10.1038/nature19312

Kwok, J., O'Shea, M., Hume, D. A., & Lengeling, A. (2017). Jmjd6, a JmjC Dioxygenase with Many Interaction Partners and Pleiotropic Functions. Frontiers in genetics, 8, 32. https://doi.org/10.3389/fgene.2017.00032

La Marca, R., Cerri, F., Horiuchi, K., Bachi, A., Feltri, M. L., Wrabetz, L., Blobel, C. P., Quattrini, A., Salzer, J. L., & Taveggia, C. (2011). TACE (ADAM17) inhibits Schwann cell myelination. Nature neuroscience, 14(7), 857–865. https://doi.org/10.1038/nn.2849

Laderoute, K. R., Calaoagan, J. M., Gustafson-Brown, C., Knapp, A. M., Li, G. C., Mendonca, H. L., Ryan, H. E., Wang, Z., & Johnson, R. S. (2002). The response of c-jun/AP-1 to chronic hypoxia is hypoxia-inducible factor 1 alpha dependent. Molecular and cellular biology, 22(8), 2515–2523. https://doi.org/10.1128/MCB.22.8.2515-2523.2002

Laderoute, K. R., Calaoagan, J. M., Knapp, M., & Johnson, R. S. (2004). Glucose utilization is essential for hypoxia-inducible factor 1 alpha-dependent phosphorylation of c-Jun. Molecular and cellular biology, 24(10), 4128–4137. https://doi.org/10.1128/MCB.24.10.4128-4137.2004

Le, N., Nagarajan, R., Wang, J. Y., Araki, T., Schmidt, R. E., & Milbrandt, J. (2005). Analysis of congenital hypomyelinating Egr2Lo/Lo nerves identifies Sox2 as an inhibitor of Schwann cell differentiation and myelination. Proceedings of the National Academy of Sciences of the United States of America, 102(7), 2596–2601. https://doi.org/10.1073/pnas.0407836102

Leblanc, S. E., Srinivasan, R., Ferri, C., Mager, G. M., Gillian-Daniel, A. L., Wrabetz, L., & Svaren, J. (2005). Regulation of cholesterol/lipid biosynthetic genes by Egr2/Krox20 during peripheral nerve myelination. Journal of neurochemistry, 93(3), 737–748. https://doi.org/10.1111/j.1471-4159.2005.03056.x

Lee, H., Sengupta, N., Villagra, A., Rezai-Zadeh, N., & Seto, E. (2006). Histone deacetylase 8 safeguards the human ever-shorter telomeres 1B (hEST1B) protein from ubiquitin-mediated degradation. Molecular and cellular biology, 26(14), 5259–5269. https://doi.org/10.1128/MCB.01971-05

Leone, D. P., Genoud, S., Atanasoski, S., Grausenburger, R., Berger, P., Metzger, D., Macklin, W. B., Chambon, P., & Suter, U. (2003). Tamoxifen-inducible glia-specific Cre mice for somatic mutagenesis in oligodendrocytes and Schwann cells. Molecular and cellular neurosciences, 22(4), 430–440. https://doi.org/10.1016/s1044-7431(03)00029-0

Le Pichon, C. E., & Chesler, A. T. (2014). The functional and anatomical dissection of somatosensory subpopulations using mouse genetics. *Frontiers in neuroanatomy*, *8*, 21. https://doi.org/10.3389/fnana.2014.00021

Li, H., Yang, H., Liu, Y., Huan, W., Zhang, S., Wu, G., Lu, Q., Wang, Q., & Wang, Y. (2011). The cyclin-dependent kinase inhibitor p27(Kip1) is a positive regulator of Schwann cell differentiation in vitro. Journal of molecular neuroscience : MN, 45(2), 277–283. https://doi.org/10.1007/s12031-011-9518-2

Lin, H. P., Oksuz, I., Hurley, E., Wrabetz, L., & Awatramani, R. (2015). Microprocessor complex subunit DiGeorge syndrome critical region gene 8 (Dgcr8) is required for schwann cell myelination and myelin maintenance. The Journal of biological chemistry, 290(40), 24294–24307. https://doi.org/10.1074/jbc.M115.636407

Lin, W., Sanchez, H. B., Deerinck, T., Morris, J. K., Ellisman, M., & Lee, K. F. (2000). Aberrant development of motor axons and neuromuscular synapses in erbB2-deficient mice. Proceedings of the National Academy of Sciences of the United States of America, 97(3), 1299–1304. https://doi.org/10.1073/pnas.97.3.1299

Lindborg, J. A., Niemi, J. P., Howarth, M. A., Liu, K. W., Moore, C. Z., Mahajan, D., & Zigmond, R. E. (2018). Molecular and cellular identification of the immune response in peripheral ganglia following nerve injury. Journal of neuroinflammation, 15(1), 192. https://doi.org/10.1186/s12974-018-1222-5

Liu, A., Li, J., Marin-Husstege, M., Kageyama, R., Fan, Y., Gelinas, C., & Casaccia-Bonnefil, P. (2006). A molecular insight of Hes5-dependent inhibition of myelin gene expression: old partners and new players. The EMBO journal, 25(20), 4833–4842. https://doi.org/10.1038/sj.emboj.7601352

Lopez, G., Bill, K. L., Bid, H. K., Braggio, D., Constantino, D., Prudner, B., Zewdu, A., Batte, K., Lev, D., & Pollock, R. E. (2015). HDAC8, A Potential Therapeutic Target for the Treatment of Malignant Peripheral Nerve Sheath Tumors (MPNST). *PloS one*, *10*(7), e0133302. https://doi.org/10.1371/journal.pone.0133302

Lopez-Anido, C., Poitelon, Y., Gopinath, C., Moran, J. J., Ma, K. H., Law, W. D., Antonellis, A., Feltri, M. L., & Svaren, J. (2016). Tead1 regulates the expression of Peripheral Myelin Protein 22 during Schwann cell development. Human molecular genetics, 25(14), 3055–3069. https://doi.org/10.1093/hmg/ddw158

Lovett-Barr, M. R., Satriotomo, I., Muir, G. D., Wilkerson, J. E., Hoffman, M. S., Vinit, S., & Mitchell, G. S. (2012). Repetitive intermittent hypoxia induces respiratory and somatic motor recovery after

chronic cervical spinal injury. *The Journal of neuroscience : the official journal of the Society for Neuroscience*, *32*(11), 3591–3600. https://doi.org/10.1523/JNEUROSCI.2908-11.2012

Lu, G., Zhang, M., Wang, J., Zhang, K., Wu, S., & Zhao, X. (2019). Epigenetic regulation of myelination in health and disease. The European journal of neuroscience, 49(11), 1371–1387. https://doi.org/10.1111/ejn.14337

Ma, K. H., Duong, P., Moran, J. J., Junaidi, N., & Svaren, J. (2018). Polycomb repression regulates Schwann cell proliferation and axon regeneration after nerve injury. Glia, 66(11), 2487–2502. https://doi.org/10.1002/glia.23500

Ma, K. H., Hung, H. A., & Svaren, J. (2016). Epigenomic Regulation of Schwann Cell Reprogramming in Peripheral Nerve Injury. The Journal of neuroscience : the official journal of the Society for Neuroscience, 36(35), 9135–9147. https://doi.org/10.1523/JNEUROSCI.1370-16.2016

McBrearty, B. A., Clark, L. D., Zhang, X. M., Blankenhorn, E. P., & Heber-Katz, E. (1998). Genetic analysis of a mammalian wound-healing trait. *Proceedings of the National Academy of Sciences of the United States of America*, *95*(20), 11792–11797. https://doi.org/10.1073/pnas.95.20.11792

Mahar, M., & Cavalli, V. (2018). Intrinsic mechanisms of neuronal axon regeneration. Nature reviews. Neuroscience, 19(6), 323–337. https://doi.org/10.1038/s41583-018-0001-8

Malong, L., Napoli, I., Casal, G., White, I. J., Stierli, S., Vaughan, A., Cattin, A. L., Burden, J. J., Hng, K. I., Bossio, A., Flanagan, A., Zhao, H. T., & Lloyd, A. C. (2023). Characterization of the structure and control of the blood-nerve barrier identifies avenues for therapeutic delivery. Developmental cell, 58(3), 174–191.e8. https://doi.org/10.1016/j.devcel.2023.01.002

Marek, M., Oliveira, G., Pierce, R. J., Jung, M., Sippl, W., & Romier, C. (2015). Drugging the schistosome zinc-dependent HDACs: current progress and future perspectives. Future medicinal chemistry, 7(6), 783–800. https://doi.org/10.4155/fmc.15.25

Martinez-Moreno M, O'Shea TM, Zepecki JP, Olaru A, Ness JK, Langer R, Tapinos N. Regulation of Peripheral Myelination through Transcriptional Buffering of Egr2 by an Antisense Long Non-coding RNA. Cell Rep. 2017 Aug 22;20(8):1950-1963. doi: 10.1016/j.celrep.2017.07.068. PMID: 28834756; PMCID: PMC5800313.

Meijering, E., Jacob, M., Sarria, J. C., Steiner, P., Hirling, H., & Unser, M. (2004). Design and validation of a tool for neurite tracing and analysis in fluorescence microscopy images. Cytometry. Part A : the journal of the International Society for Analytical Cytology, 58(2), 167–176. https://doi.org/10.1002/cyto.a.20022

Michailov, G. V., Sereda, M. W., Brinkmann, B. G., Fischer, T. M., Haug, B., Birchmeier, C., Role, L., Lai, C., Schwab, M. H., & Nave, K. A. (2004). Axonal neuregulin-1 regulates myelin sheath thickness. Science (New York, N.Y.), 304(5671), 700–703. https://doi.org/10.1126/science.1095862

Min, Q., Parkinson, D. B., & Dun, X. P. (2021). Migrating Schwann cells direct axon regeneration within the peripheral nerve bridge. Glia, 69(2), 235–254. https://doi.org/10.1002/glia.23892

Minet, E., Michel, G., Mottet, D., Piret, J. P., Barbieux, A., Raes, M., & Michiels, C. (2001). c-JUN gene induction and AP-1 activity is regulated by a JNK-dependent pathway in hypoxic HepG2 cells. Experimental cell research, 265(1), 114–124. https://doi.org/10.1006/excr.2001.5180

Mirsky, R., Woodhoo, A., Parkinson, D. B., Arthur-Farraj, P., Bhaskaran, A., & Jessen, K. R. (2008). Novel signals controlling embryonic Schwann cell development, myelination and dedifferentiation. Journal of the peripheral nervous system : JPNS, 13(2), 122–135. https://doi.org/10.1111/j.1529-8027.2008.00168.x

Mogha, A., Benesh, A. E., Patra, C., Engel, F. B., Schöneberg, T., Liebscher, I., & Monk, K. R. (2013). Gpr126 functions in Schwann cells to control differentiation and myelination via G-protein activation. The Journal of neuroscience : the official journal of the Society for Neuroscience, 33(46), 17976–17985. https://doi.org/10.1523/JNEUROSCI.1809-13.2013

Mogha, A., Harty, B. L., Carlin, D., Joseph, J., Sanchez, N. E., Suter, U., Piao, X., Cavalli, V., & Monk, K. R. (2016). Gpr126/Adgrg6 Has Schwann Cell Autonomous and Nonautonomous Functions in Peripheral Nerve Injury and Repair. The Journal of neuroscience : the official journal of the Society for Neuroscience, 36(49), 12351–12367. https://doi.org/10.1523/JNEUROSCI.3854-15.2016

Monje, P. V., Soto, J., Bacallao, K., & Wood, P. M. (2010). Schwann cell dedifferentiation is independent of mitogenic signaling and uncoupled to proliferation: role of cAMP and JNK in the maintenance of the differentiated state. The Journal of biological chemistry, 285(40), 31024–31036. https://doi.org/10.1074/jbc.M110.116970

Monk, K. R., Naylor, S. G., Glenn, T. D., Mercurio, S., Perlin, J. R., Dominguez, C., Moens, C. B., & Talbot, W. S. (2009). A G protein-coupled receptor is essential for Schwann cells to initiate myelination. Science (New York, N.Y.), 325(5946), 1402–1405. https://doi.org/10.1126/science.1173474

Monk, K. R., Oshima, K., Jörs, S., Heller, S., & Talbot, W. S. (2011). Gpr126 is essential for peripheral nerve development and myelination in mammals. Development (Cambridge, England), 138(13), 2673–2680. https://doi.org/10.1242/dev.062224

Monk, K. R., Feltri, M. L., & Taveggia, C. (2015). New insights on Schwann cell development. Glia, 63(8), 1376–1393. https://doi.org/10.1002/glia.22852

Morris, J. K., Lin, W., Hauser, C., Marchuk, Y., Getman, D., & Lee, K. F. (1999). Rescue of the cardiac defect in ErbB2 mutant mice reveals essential roles of ErbB2 in peripheral nervous system development. Neuron, 23(2), 273–283. https://doi.org/10.1016/s0896-6273(00)80779-5

Morton PD, Johnstone JT, Ramos AY, Liebl DJ, Bunge MB, Bethea JR. Nuclear factor-κB activation in Schwann cells regulates regeneration and remyelination. Glia. 2012 Apr;60(4):639-50. doi: 10.1002/glia.22297. Epub 2012 Jan 24. PMID: 22275133; PMCID: PMC4120893.

Morton PD, Dellarole A, Theus MH, Walters WM, Berge SS, Bethea JR. Activation of NF-κB in Schwann cells is dispensable for myelination in vivo. J Neurosci. 2013 Jun 12;33(24):9932-6. doi: 10.1523/JNEUROSCI.2483-12.2013. PMID: 23761888; PMCID: PMC3682379.

Mukouyama, Y. S., Gerber, H. P., Ferrara, N., Gu, C., & Anderson, D. J. (2005). Peripheral nerve-derived VEGF promotes arterial differentiation via neuropilin 1-mediated positive feedback. Development (Cambridge, England), 132(5), 941–952. https://doi.org/10.1242/dev.01675

Mueller, M., Wacker, K., Ringelstein, E. B., Hickey, W. F., Imai, Y., & Kiefer, R. (2001). Rapid response of identified resident endoneurial macrophages to nerve injury. The American journal of pathology, 159(6), 2187–2197. https://doi.org/10.1016/S0002-9440(10)63070-2

Mueller, M., Leonhard, C., Wacker, K., Ringelstein, E. B., Okabe, M., Hickey, W. F., & Kiefer, R. (2003). Macrophage response to peripheral nerve injury: the quantitative contribution of resident and hematogenous macrophages. Laboratory investigation; a journal of technical methods and pathology, 83(2), 175–185. https://doi.org/10.1097/01.lab.0000056993.28149.bf

Muppirala, A. N., Limbach, L. E., Bradford, E. F., & Petersen, S. C. (2021). Schwann cell development: From neural crest to myelin sheath. Wiley interdisciplinary reviews. Developmental biology, 10(5), e398. https://doi.org/10.1002/wdev.398

Musti, A. M., Treier, M., & Bohmann, D. (1997). Reduced ubiquitin-dependent degradation of c-Jun after phosphorylation by MAP kinases. Science (New York, N.Y.), 275(5298), 400–402. https://doi.org/10.1126/science.275.5298.400

Murtazina, A., & Adameyko, I. (2023). The peripheral nervous system. Development (Cambridge, England), 150(9), dev201164. https://doi.org/10.1242/dev.201164

Nagai, K., Ideguchi, H., Kajikawa, T., Li, X., Chavakis, T., Cheng, J., Messersmith, P. B., Heber-Katz, E., & Hajishengallis, G. (2020). An injectable hydrogel-formulated inhibitor of prolyl-4-hydroxylase promotes T regulatory cell recruitment and enhances alveolar bone regeneration during resolution of experimental periodontitis. *FASEB journal : official publication of the Federation of American Societies for Experimental Biology*, *34*(10), 13726–13740. https://doi.org/10.1096/fj.202001248R

Napoli, I., Noon, L. A., Ribeiro, S., Kerai, A. P., Parrinello, S., Rosenberg, L. H., Collins, M. J., Harrisingh, M. C., White, I. J., Woodhoo, A., & Lloyd, A. C. (2012). A central role for the ERK-signaling pathway in controlling Schwann cell plasticity and peripheral nerve regeneration in vivo. Neuron, 73(4), 729–742. https://doi.org/10.1016/j.neuron.2011.11.031

Nave, K. A., & Salzer, J. L. (2006). Axonal regulation of myelination by neuregulin 1. Current opinion in neurobiology, 16(5), 492–500. https://doi.org/10.1016/j.conb.2006.08.008

Naviaux, R. K., Le, T. P., Bedelbaeva, K., Leferovich, J., Gourevitch, D., Sachadyn, P., Zhang, X. M., Clark, L., & Heber-Katz, E. (2009). Retained features of embryonic metabolism in the adult MRL mouse. *Molecular genetics and metabolism*, *96*(3), 133–144. https://doi.org/10.1016/j.ymgme.2008.11.164

Nocera, G., & Jacob, C. (2020). Mechanisms of Schwann cell plasticity involved in peripheral nerve repair after injury. Cellular and molecular life sciences : CMLS, 77(20), 3977–3989. https://doi.org/10.1007/s00018-020-03516-9

Norrmén, C., Figlia, G., Lebrun-Julien, F., Pereira, J. A., Trötzmüller, M., Köfeler, H. C., Rantanen, V., Wessig, C., van Deijk, A. L., Smit, A. B., Verheijen, M. H., Rüegg, M. A., Hall, M. N., & Suter, U. (2014). mTORC1 controls PNS myelination along the mTORC1-RXRγ-SREBP-lipid biosynthesis axis in Schwann cells. Cell reports, 9(2), 646–660. https://doi.org/10.1016/j.celrep.2014.09.001

Noseda, R., Belin, S., Piguet, F., Vaccari, I., Scarlino, S., Brambilla, P., Martinelli Boneschi, F., Feltri, M. L., Wrabetz, L., Quattrini, A., Feinstein, E., Huganir, R. L., & Bolino, A. (2013). DDIT4/REDD1/RTP801 is a novel negative regulator of Schwann cell myelination. The Journal of neuroscience : the official journal of the Society for Neuroscience, 33(38), 15295–15305. https://doi.org/10.1523/JNEUROSCI.2408-13.2013

Oehme, I., Deubzer, H. E., Lodrini, M., Milde, T., & Witt, O. (2009). Targeting of HDAC8 and investigational inhibitors in neuroblastoma. *Expert opinion on investigational drugs*, *18*(11), 1605–1617. https://doi.org/10.1517/14728220903241658

Ogawa, C., Tsuchiya, K., & Maeda, K. (2023). Hypoxia-Inducible Factor Prolyl Hydroxylase Inhibitors and Iron Metabolism. International journal of molecular sciences, 24(3), 3037. https://doi.org/10.3390/ijms24033037

Osterloh, J. M., Yang, J., Rooney, T. M., Fox, A. N., Adalbert, R., Powell, E. H., Sheehan, A. E., Avery, M. A., Hackett, R., Logan, M. A., MacDonald, J. M., Ziegenfuss, J. S., Milde, S., Hou, Y. J., Nathan, C., Ding, A., Brown, R. H., Jr, Conforti, L., Coleman, M., Tessier-Lavigne, M., … Freeman, M. R. (2012). dSarm/Sarm1 is required for activation of an injury-induced axon death pathway. Science (New York, N.Y.), 337(6093), 481–484. https://doi.org/10.1126/science.1223899

Painter, M. W., Brosius Lutz, A., Cheng, Y. C., Latremoliere, A., Duong, K., Miller, C. M., Posada, S., Cobos, E. J., Zhang, A. X., Wagers, A. J., Havton, L. A., Barres, B., Omura, T., & Woolf, C. J. (2014). Diminished Schwann cell repair responses underlie age-associated impaired axonal regeneration. Neuron, 83(2), 331–343. https://doi.org/10.1016/j.neuron.2014.06.016

Painter M. W. (2017). Aging Schwann cells: mechanisms, implications, future directions. Current opinion in neurobiology, 47, 203–208. https://doi.org/10.1016/j.conb.2017.10.022

Parfejevs, V., Debbache, J., Shakhova, O., Schaefer, S. M., Glausch, M., Wegner, M., Suter, U., Riekstina, U., Werner, S., & Sommer, L. (2018). Injury-activated glial cells promote wound healing of the adult skin in mice. Nature communications, 9(1), 236. https://doi.org/10.1038/s41467-017-01488-2

Parkinson, D. B., Bhaskaran, A., Droggiti, A., Dickinson, S., D'Antonio, M., Mirsky, R., & Jessen, K. R. (2004). Krox-20 inhibits Jun-NH2-terminal kinase/c-Jun to control Schwann cell proliferation and death. The Journal of cell biology, 164(3), 385–394. https://doi.org/10.1083/jcb.200307132

Parkinson, D. B., Bhaskaran, A., Arthur-Farraj, P., Noon, L. A., Woodhoo, A., Lloyd, A. C., Feltri, M. L., Wrabetz, L., Behrens, A., Mirsky, R., & Jessen, K. R. (2008). c-Jun is a negative regulator of myelination. The Journal of cell biology, 181(4), 625–637. https://doi.org/10.1083/jcb.200803013

Parmantier, E., Lynn, B., Lawson, D., Turmaine, M., Namini, S. S., Chakrabarti, L., McMahon, A. P., Jessen, K. R., & Mirsky, R. (1999). Schwann cell-derived Desert hedgehog controls the development of peripheral nerve sheaths. Neuron, 23(4), 713–724. https://doi.org/10.1016/s0896-6273(01)80030-1

Parrinello, S., Napoli, I., Ribeiro, S., Wingfield Digby, P., Fedorova, M., Parkinson, D. B., Doddrell, R. D., Nakayama, M., Adams, R. H., & Lloyd, A. C. (2010). EphB signaling directs peripheral nerve regeneration through Sox2-dependent Schwann cell sorting. Cell, 143(1), 145–155. https://doi.org/10.1016/j.cell.2010.08.039

Pattaroni, C., & Jacob, C. (2013). Histone methylation in the nervous system: functions and dysfunctions. Molecular neurobiology, 47(2), 740–756. https://doi.org/10.1007/s12035-012-8376-4

Pellegatta M, Taveggia C. The Complex Work of Proteases and Secretases in Wallerian Degeneration: Beyond Neuregulin-1. Front Cell Neurosci. 2019 Mar 20;13:93. doi: 10.3389/fncel.2019.00093. PMID: 30949030; PMCID: PMC6436609.

Pellegatta, M., Canevazzi, P., Forese, M. G., Podini, P., Valenzano, S., Del Carro, U., Quattrini, A., & Taveggia, C. (2022). ADAM17 Regulates $p75^{NTR}$-Mediated Fibrinolysis and Nerve Remyelination. The Journal of neuroscience : the official journal of the Society for Neuroscience, 42(12), 2433–2447. https://doi.org/10.1523/JNEUROSCI.1341-21.2022

Pereira, J. A., Baumann, R., Norrmén, C., Somandin, C., Miehe, M., Jacob, C., Lühmann, T., Hall-Bozic, H., Mantei, N., Meijer, D., & Suter, U. (2010). Dicer in Schwann cells is required for myelination and axonal integrity. The Journal of neuroscience : the official journal of the Society for Neuroscience, 30(19), 6763–6775. https://doi.org/10.1523/JNEUROSCI.0801-10.2010

Perlson, E., Hanz, S., Ben-Yaakov, K., Segal-Ruder, Y., Seger, R., & Fainzilber, M. (2005). Vimentin-dependent spatial translocation of an activated MAP kinase in injured nerve. Neuron, 45(5), 715–726. https://doi.org/10.1016/j.neuron.2005.01.023

Perry, R. B., & Fainzilber, M. (2009). Nuclear transport factors in neuronal function. Seminars in cell & developmental biology, 20(5), 600–606. https://doi.org/10.1016/j.semcdb.2009.04.014

Petersen, S. C., Luo, R., Liebscher, I., Giera, S., Jeong, S. J., Mogha, A., Ghidinelli, M., Feltri, M. L., Schöneberg, T., Piao, X., & Monk, K. R. (2015). The adhesion GPCR GPR126 has distinct, domain-dependent functions in Schwann cell development mediated by interaction with laminin-211. Neuron, 85(4), 755–769. https://doi.org/10.1016/j.neuron.2014.12.057

Poitelon, Y., Lopez-Anido, C., Catignas, K., Berti, C., Palmisano, M., Williamson, C., Ameroso, D., Abiko, K., Hwang, Y., Gregorieff, A., Wrana, J. L., Asmani, M., Zhao, R., Sim, F. J., Wrabetz, L., Svaren, J., & Feltri, M. L. (2016). YAP and TAZ control peripheral myelination and the expression of laminin receptors in Schwann cells. Nature neuroscience, 19(7), 879–887. https://doi.org/10.1038/nn.4316

Pugh, C. W., & Ratcliffe, P. J. (2003). The von Hippel-Lindau tumor suppressor, hypoxia-inducible factor-1 (HIF-1) degradation, and cancer pathogenesis. Seminars in cancer biology, 13(1), 83–89. https://doi.org/10.1016/s1044-579x(02)00103-7

Qian, T. M., Zhao, L. L., Wang, J., Li, P., Qin, J., Liu, Y. S., Yu, B., Ding, F., Gu, X. S., & Zhou, S. L. (2016). miR-148b-3p promotes migration of Schwann cells by targeting cullin-associated and neddylation-dissociated 1. Neural regeneration research, 11(6), 1001–1005. https://doi.org/10.4103/1673-5374.184504

Quadrato, G., & Di Giovanni, S. (2013). Waking up the sleepers: shared transcriptional pathways in axonal regeneration and neurogenesis. Cellular and molecular life sciences : CMLS, 70(6), 993–1007. https://doi.org/10.1007/s00018-012-1099-x

Quintes, S., Brinkmann, B. G., Ebert, M., Fröb, F., Kungl, T., Arlt, F. A., Tarabykin, V., Huylebroeck, D., Meijer, D., Suter, U., Wegner, M., Sereda, M. W., & Nave, K. A. (2016). Zeb2 is essential for Schwann cell differentiation, myelination and nerve repair. Nature neuroscience, 19(8), 1050–1059. https://doi.org/10.1038/nn.4321

Raivich, G., Bohatschek, M., Da Costa, C., Iwata, O., Galiano, M., Hristova, M., Nateri, A. S., Makwana, M., Riera-Sans, L., Wolfer, D. P., Lipp, H. P., Aguzzi, A., Wagner, E. F., & Behrens, A. (2004). The AP-1 transcription factor c-Jun is required for efficient axonal regeneration. Neuron, 43(1), 57–67. https://doi.org/10.1016/j.neuron.2004.06.005

Rasband, M.N., & Macklin, W.B. (2012). Myelin Structure and Biochemistry.

Ren, J., Zeng, Q., Wu, H., Liu, X., Guida, M. C., Huang, W., Zhai, Y., Li, J., Ocorr, K., Bodmer, R., & Tang, M. (2023). Deacetylase-dependent and -independent role of HDAC3 in cardiomyopathy. *Journal of cellular physiology*, *238*(3), 647–658. https://doi.org/10.1002/jcp.30957

Rinwa, P., Calvo-Enrique, L., Zhang, M. D., Nyengaard, J. R., Karlsson, P., & Ernfors, P. (2021). Demise of nociceptive Schwann cells causes nerve retraction and pain hyperalgesia. Pain, 162(6), 1816–1827. https://doi.org/10.1097/j.pain.0000000000002169

Rishal, I., & Fainzilber, M. (2014). Axon-soma communication in neuronal injury. Nature reviews. Neuroscience, 15(1), 32–42. https://doi.org/10.1038/nrn3609

Roberts, S. L., Dun, X. P., Doddrell, R. D. S., Mindos, T., Drake, L. K., Onaitis, M. W., Florio, F., Quattrini, A., Lloyd, A. C., D'Antonio, M., & Parkinson, D. B. (2017). Sox2 expression in Schwann cells inhibits myelination in vivo and induces influx of macrophages to the nerve. Development (Cambridge, England), 144(17), 3114–3125. https://doi.org/10.1242/dev.15065

Rosenberg, L. H., Cattin, A. L., Fontana, X., Harford-Wright, E., Burden, J. J., White, I. J., Smith, J. G., Napoli, I., Quereda, V., Policarpi, C., Freeman, J., Ketteler, R., Riccio, A., & Lloyd, A. C. (2018). HDAC3 Regulates the Transition to the Homeostatic Myelinating Schwann Cell State. Cell reports, 25(10), 2755–2765.e5. https://doi.org/10.1016/j.celrep.2018.11.045

Rouleau, G. A., Merel, P., Lutchman, M., Sanson, M., Zucman, J., Marineau, C., Hoang-Xuan, K., Demczuk, S., Desmaze, C., & Plougastel, B. (1993). Alteration in a new gene encoding a putative membrane-organizing protein causes neuro-fibromatosis type 2. *Nature*, *363*(6429), 515–521. https://doi.org/10.1038/363515a0

Ryu, E. J., Wang, J. Y., Le, N., Baloh, R. H., Gustin, J. A., Schmidt, R. E., & Milbrandt, J. (2007). Misexpression of Pou3f1 results in peripheral nerve hypomyelination and axonal loss. The Journal of neuroscience : the official journal of the Society for Neuroscience, 27(43), 11552–11559. https://doi.org/10.1523/JNEUROSCI.5497-06.2007

Sachs, B. D., Baillie, G. S., McCall, J. R., Passino, M. A., Schachtrup, C., Wallace, D. A., Dunlop, A. J., MacKenzie, K. F., Klussmann, E., Lynch, M. J., Sikorski, S. L., Nuriel, T., Tsigelny, I., Zhang, J., Houslay, M. D., Chao, M. V., & Akassoglou, K. (2007). p75 neurotrophin receptor regulates tissue fibrosis through inhibition of plasminogen activation via a PDE4/cAMP/PKA pathway. The Journal of cell biology, 177(6), 1119–1132. https://doi.org/10.1083/jcb.200701040

Sala, M. A., Chen, C., Zhang, Q., Do-Umehara, H. C., Wu, W., Misharin, A. V., Waypa, G. B., Fang, D., Budinger, G. R. S., Liu, S., Chandel, N. S., Schumacker, P. T., Sznajder, J. I., & Liu, J. (2018). JNK2 up-regulates hypoxia-inducible factors and contributes to hypoxia-induced erythropoiesis and pulmonary hypertension. The Journal of biological chemistry, 293(1), 271–284. https://doi.org/10.1074/jbc.RA117.000440

Salzer J. L. (2015). Schwann cell myelination. Cold Spring Harbor perspectives in biology, 7(8), a020529. https://doi.org/10.1101/cshperspect.a020529

Sarogni, P., Pallotta, M. M., & Musio, A. (2020). Cornelia de Lange syndrome: from molecular diagnosis to therapeutic approach. Journal of medical genetics, 57(5), 289–295. https://doi.org/10.1136/jmedgenet-2019-106277

Senichkin, V. V., Prokhorova, E. A., Zhivotovsky, B., & Kopeina, G. S. (2021). Simple and Efficient Protocol for Subcellular Fractionation of Normal and Apoptotic Cells. Cells, 10(4), 852. https://doi.org/10.3390/cells10040852

Sharghi-Namini, S., Turmaine, M., Meier, C., Sahni, V., Umehara, F., Jessen, K. R., & Mirsky, R. (2006). The structural and functional integrity of peripheral nerves depends on the glial-derived signal desert hedgehog. The Journal of neuroscience : the official journal of the Society for Neuroscience, 26(23), 6364–6376. https://doi.org/10.1523/JNEUROSCI.0157-06.2006

Scapin, C., Ferri, C., Pettinato, E., Zambroni, D., Bianchi, F., Del Carro, U., Belin, S., Caruso, D., Mitro, N., Pellegatta, M., Taveggia, C., Schwab, M. H., Nave, K. A., Feltri, M. L., Wrabetz, L., & D'Antonio, M. (2019). Enhanced axonal neuregulin-1 type-III signaling ameliorates neurophysiology and hypomyelination in a Charcot-Marie-Tooth type 1B mouse model. Human molecular genetics, 28(6), 992–1006. https://doi.org/10.1093/hmg/ddy411

Scudiero, I., Zotti, T., Ferravante, A., Vessichelli, M., Reale, C., Masone, M. C., Leonardi, A., Vito, P., & Stilo, R. (2012). Tumor necrosis factor (TNF) receptor-associated factor 7 is required for TNFα-induced Jun NH2-terminal kinase activation and promotes cell death by regulating polyubiquitination and lysosomal degradation of c-FLIP protein. The Journal of biological chemistry, 287(8), 6053–6061. https://doi.org/10.1074/jbc.M111.300137

Scheib, J. L., & Höke, A. (2016). An attenuated immune response by Schwann cells and macrophages inhibits nerve regeneration in aged rats. Neurobiology of aging, 45, 1–9. https://doi.org/10.1016/j.neurobiolaging.2016.05.004

Schödel, J., Mole, D. R., & Ratcliffe, P. J. (2013). Pan-genomic binding of hypoxia-inducible transcription factors. *Biological chemistry*, *394*(4), 507–517. https://doi.org/10.1515/hsz-2012-0351

Schödel, J., & Ratcliffe, P. J. (2019). Mechanisms of hypoxia signalling: new implications for nephrology. Nature reviews. Nephrology, 15(10), 641–659. https://doi.org/10.1038/s41581-019-0182-z

Seto, E., & Yoshida, M. (2014). Erasers of histone acetylation: the histone deacetylase enzymes. Cold Spring Harbor perspectives in biology, 6(4), a018713. https://doi.org/10.1101/cshperspect.a018713

Shaulian, E., & Karin, M. (2001). AP-1 in cell proliferation and survival. Oncogene, 20(19), 2390–2400. https://doi.org/10.1038/sj.onc.1204383

Sheean ME, McShane E, Cheret C, Walcher J, Müller T, Wulf-Goldenberg A, Hoelper S, Garratt AN, Krüger M, Rajewsky K, Meijer D, Birchmeier W, Lewin GR, Selbach M, Birchmeier C. Activation of MAPK overrides the termination of myelin growth and replaces Nrg1/ErbB3 signals during Schwann cell development and myelination. Genes Dev. 2014 Feb 1;28(3):290-303. doi: 10.1101/gad.230045.113. PMID: 24493648; PMCID: PMC3923970.

Shen, Y., Cheng, Z., Chen, S., Zhang, Y., Chen, Q., & Yi, S. (2022). Dysregulated miR-29a-3p/PMP22 Modulates Schwann Cell Proliferation and Migration During Peripheral Nerve Regeneration. Molecular neurobiology, 59(2), 1058–1072. https://doi.org/10.1007/s12035-021-02589-2

Shin, J. E., Geisler, S., & DiAntonio, A. (2014). Dynamic regulation of SCG10 in regenerating axons after injury. Experimental neurology, 252, 1–11. https://doi.org/10.1016/j.expneurol.2013.11.007

Shukla, S., & Tekwani, B. L. (2020). Histone Deacetylases Inhibitors in Neurodegenerative Diseases, Neuroprotection and Neuronal Differentiation. Frontiers in pharmacology, 11, 537. https://doi.org/10.3389/fphar.2020.00537

Sisakhtnezhad, S., & Matin, M. M. (2012). Transdifferentiation: a cell and molecular reprogramming process. Cell and tissue research, 348(3), 379–396. https://doi.org/10.1007/s00441-012-1403-y

Smith, I. W., Mikesh, M., Lee, Y.i, & Thompson, W. J. (2013). Terminal Schwann cells participate in the competition underlying neuromuscular synapse elimination. The Journal of neuroscience : the official journal of the Society for Neuroscience, 33(45), 17724–17736. https://doi.org/10.1523/JNEUROSCI.3339-13.2013

Sock, E., & Wegner, M. (2019). Transcriptional control of myelination and remyelination. Glia, 67(11), 2153–2165. https://doi.org/10.1002/glia.23636

Sonnenberg-Riethmacher, E., Miehe, M., Stolt, C. C., Goerich, D. E., Wegner, M., & Riethmacher, D. (2001). Development and degeneration of dorsal root ganglia in the absence of the HMG-domain transcription factor Sox10. Mechanisms of development, 109(2), 253–265. https://doi.org/10.1016/s0925-4773(01)00547-0

Spange, S., Wagner, T., Heinzel, T., & Krämer, O. H. (2009). Acetylation of non-histone proteins modulates cellular signalling at multiple levels. The international journal of biochemistry & cell biology, 41(1), 185–198. https://doi.org/10.1016/j.biocel.2008.08.027

Spencer, P. S., Weinberg, H. J., Raine, C. S., & Prineas, J. W. (1975). The perineurial window--a new model of focal demyelination and remyelination. Brain research, 96(2), 323–329. https://doi.org/10.1016/0006-8993(75)90742-8

Srinivasan, R., Sun, G., Keles, S., Jones, E. A., Jang, S. W., Krueger, C., Moran, J. J., & Svaren, J. (2012). Genome-wide analysis of EGR2/SOX10 binding in myelinating peripheral nerve. Nucleic acids research, 40(14), 6449–6460. https://doi.org/10.1093/nar/gks313

Stassart, R. M., Fledrich, R., Velanac, V., Brinkmann, B. G., Schwab, M. H., Meijer, D., Sereda, M. W., & Nave, K. A. (2013). A role for Schwann cell-derived neuregulin-1 in remyelination. Nature neuroscience, 16(1), 48–54. https://doi.org/10.1038/nn.3281

Stassart, R. M., & Woodhoo, A. (2021). Axo-glial interaction in the injured PNS. Developmental neurobiology, 81(5), 490–506. https://doi.org/10.1002/dneu.22771

Strehin, I., Gourevitch, D., Zhang, Y., Heber-Katz, E., & Messersmith, P. B. (2013). Hydrogels Formed by Oxo-ester Mediated Native Chemical Ligation. *Biomaterials science*, *1*(6), 603–613. https://doi.org/10.1039/C3BM00201B

Stewart, H. J., Brennan, A., Rahman, M., Zoidl, G., Mitchell, P. J., Jessen, K. R., & Mirsky, R. (2001). Developmental regulation and overexpression of the transcription factor AP-2, a potential regulator of the timing of Schwann cell generation. The European journal of neuroscience, 14(2), 363–372. https://doi.org/10.1046/j.0953-816x.2001.01650.x

Stierli, S., Napoli, I., White, I. J., Cattin, A. L., Monteza Cabrejos, A., Garcia Calavia, N., Malong, L., Ribeiro, S., Nihouarn, J., Williams, R., Young, K. M., Richardson, W. D., & Lloyd, A. C. (2018). The

regulation of the homeostasis and regeneration of peripheral nerve is distinct from the CNS and independent of a stem cell population. Development (Cambridge, England), 145(24), dev170316. https://doi.org/10.1242/dev.170316

Strahl, B. D., & Allis, C. D. (2000). The language of covalent histone modifications. Nature, 403(6765), 41–45. https://doi.org/10.1038/47412

Sulaiman, O. A., & Gordon, T. (2009). Role of chronic Schwann cell denervation in poor functional recovery after nerve injuries and experimental strategies to combat it. Neurosurgery, 65(4 Suppl), A105–A114. https://doi.org/10.1227/01.NEU.0000358537.30354.63

Sun, Z., Feng, D., Fang, B., Mullican, S. E., You, S. H., Lim, H. W., Everett, L. J., Nabel, C. S., Li, Y., Selvakumaran, V., Won, K. J., & Lazar, M. A. (2013). Deacetylase-independent function of HDAC3 in transcription and metabolism requires nuclear receptor corepressor. *Molecular cell*, *52*(6), 769–782. https://doi.org/10.1016/j.molcel.2013.10.022

Svaren J. (2014). MicroRNA and transcriptional crosstalk in myelinating glia. Neurochemistry international, 77, 50–57. https://doi.org/10.1016/j.neuint.2014.06.010

Tam, S. Y., & Law, H. K. (2021). JNK in Tumor Microenvironment: Present Findings and Challenges in Clinical Translation. Cancers, 13(9), 2196. https://doi.org/10.3390/cancers13092196

Tam, S. Y., Wu, V. W. C., & Law, H. K. W. (2020). JNK Pathway Mediates Low Oxygen Level Induced Epithelial-Mesenchymal Transition and Stemness Maintenance in Colorectal Cancer Cells. Cancers, 12(1), 224. https://doi.org/10.3390/cancers12010224

Taveggia, C., Zanazzi, G., Petrylak, A., Yano, H., Rosenbluth, J., Einheber, S., Xu, X., Esper, R. M., Loeb, J. A., Shrager, P., Chao, M. V., Falls, D. L., Role, L., & Salzer, J. L. (2005). Neuregulin-1 type III determines the ensheathment fate of axons. Neuron, 47(5), 681–694. https://doi.org/10.1016/j.neuron.2005.08.017

Tillerson, J. L., Cohen, A. D., Philhower, J., Miller, G. W., Zigmond, M. J., & Schallert, T. (2001). Forced limb-use effects on the behavioral and neurochemical effects of 6-hydroxydopamine. The Journal of neuroscience : the official journal of the Society for Neuroscience, 21(12), 4427–4435. https://doi.org/10.1523/JNEUROSCI.21-12-04427.2001

Tillerson, J. L., & Miller, G. W. (2003). Grid performance test to measure behavioral impairment in the MPTP-treated-mouse model of parkinsonism. Journal of neuroscience methods, 123(2), 189–200. https://doi.org/10.1016/s0165-0270(02)00360-6

Tofaris GK, Patterson PH, Jessen KR, Mirsky R. Denervated Schwann cells attract macrophages by secretion of leukemia inhibitory factor (LIF) and monocyte chemoattractant protein-1 in a process regulated by interleukin-6 and LIF. J Neurosci. 2002 Aug 1;22(15):6696-703. doi: 10.1523/JNEUROSCI.22-15-06696.2002. PMID: 12151548; PMCID: PMC6758146.

Tomita, K., Kubo, T., Matsuda, K., Fujiwara, T., Yano, K., Winograd, J. M., Tohyama, M., & Hosokawa, K. (2007). The neurotrophin receptor p75NTR in Schwann cells is implicated in remyelination and motor recovery after peripheral nerve injury. Glia, 55(11), 1199–1208. https://doi.org/10.1002/glia.20533

Top, O., Milferstaedt, S. W. L., van Gessel, N., Hoernstein, S. N. W., Özdemir, B., Decker, E. L., & Reski, R. (2021). Expression of a human cDNA in moss results in spliced mRNAs and fragmentary protein isoforms. Communications biology, 4(1), 964. https://doi.org/10.1038/s42003-021-02486-3

Trimarco, A., Forese, M. G., Alfieri, V., Lucente, A., Brambilla, P., Dina, G., Pieragostino, D., Sacchetta, P., Urade, Y., Boizet-Bonhoure, B., Martinelli Boneschi, F., Quattrini, A., & Taveggia, C. (2014). Prostaglandin D2 synthase/GPR44: a signaling axis in PNS myelination. Nature neuroscience, 17(12), 1682–1692. https://doi.org/10.1038/nn.3857

Trumbower, R. D., Jayaraman, A., Mitchell, G. S., & Rymer, W. Z. (2012). Exposure to acute intermittent hypoxia augments somatic motor function in humans with incomplete spinal cord injury. *Neurorehabilitation and neural repair*, *26*(2), 163–172. https://doi.org/10.1177/1545968311412055

Tryggvason, G., Barnett, A., Kim, J., Soken, H., Maley, J., & Hansen, M. R. (2012). Radiographic association of schwannomas with sensory ganglia. *Otology & neurotology : official publication of the American Otological Society, American Neurotology Society [and] European Academy of Otology and Neurotology*, *33*(7), 1276–1282. https://doi.org/10.1097/MAO.0b013e318263d315

Turcotte, S., Desrosiers, R. R., & Beliveau, R. (2004). Hypoxia upregulates von Hippel-Lindau tumor-suppressor protein through RhoA-dependent activity in renal cell carcinoma. American journal of physiology. Renal physiology, 286(2), F338–F348. https://doi.org/10.1152/ajprenal.00254.2003

Tyanova, S., Temu, T., Sinitcyn, P., Carlson, A., Hein, M. Y., Geiger, T., Mann, M., & Cox, J. (2016). The Perseus computational platform for comprehensive analysis of (prote)omics data. Nature methods, 13(9), 731–740. https://doi.org/10.1038/nmeth.3901

Uesaka, T., Nagashimada, M., & Enomoto, H. (2015). Neuronal Differentiation in Schwann Cell Lineage Underlies Postnatal Neurogenesis in the Enteric Nervous System. The Journal of neuroscience : the official journal of the Society for Neuroscience, 35(27), 9879–9888. https://doi.org/10.1523/JNEUROSCI.1239-15.2015

Umehara F, Tate G, Itoh K, Yamaguchi N, Douchi T, Mitsuya T, Osame M. A novel mutation of desert hedgehog in a patient with 46,XY partial gonadal dysgenesis accompanied by minifascicular neuropathy. Am J Hum Genet. 2000 Nov;67(5):1302-5. doi: 10.1016/S0002-9297(07)62958-9. Epub 2000 Oct 2. PMID: 11017805; PMCID: PMC1288570.

Vaquié, A., Sauvain, A., Duman, M., Nocera, G., Egger, B., Meyenhofer, F., Falquet, L., Bartesaghi, L., Chrast, R., Lamy, C. M., Bang, S., Lee, S. R., Jeon, N. L., Ruff, S., & Jacob, C. (2019). Injured Axons Instruct Schwann Cells to Build Constricting Actin Spheres to Accelerate Axonal Disintegration. Cell reports, 27(11), 3152–3166.e7. https://doi.org/10.1016/j.celrep.2019.05.060

Velasco-Aviles, S., Patel, N., Casillas-Bajo, A., Frutos-Rincón, L., Velasco, E., Gallar, J., Arthur-Farraj, P., Gomez-Sanchez, J. A., & Cabedo, H. (2022). A genetic compensatory mechanism regulated by Jun and Mef2d modulates the expression of distinct class IIa Hdacs to ensure peripheral nerve myelination and repair. eLife, 11, e72917. https://doi.org/10.7554/eLife.72917

Viader A, Chang LW, Fahrner T, Nagarajan R, Milbrandt J. MicroRNAs modulate Schwann cell response to nerve injury by reinforcing transcriptional silencing of dedifferentiation-related genes. J Neurosci. 2011 Nov 30;31(48):17358-69. doi: 10.1523/JNEUROSCI.3931-11.2011. PMID: 22131398; PMCID: PMC3388739.

Vogl, M. R., Reiprich, S., Küspert, M., Kosian, T., Schrewe, H., Nave, K. A., & Wegner, M. (2013). Sox10 cooperates with the mediator subunit 12 during terminal differentiation of myelinating glia. The Journal of neuroscience : the official journal of the Society for Neuroscience, 33(15), 6679–6690. https://doi.org/10.1523/JNEUROSCI.5178-12.2013

Wagstaff, L. J., Gomez-Sanchez, J. A., Fazal, S. V., Otto, G. W., Kilpatrick, A. M., Michael, K., Wong, L. Y. N., Ma, K. H., Turmaine, M., Svaren, J., Gordon, T., Arthur-Farraj, P., Velasco-Aviles, S., Cabedo, H., Benito, C., Mirsky, R., & Jessen, K. R. (2021). Failures of nerve regeneration caused by aging or chronic denervation are rescued by restoring Schwann cell c-Jun. eLife, 10, e62232. https://doi.org/10.7554/eLife.62232

Wahlbuhl, M., Reiprich, S., Vogl, M. R., Bösl, M. R., & Wegner, M. (2012). Transcription factor Sox10 orchestrates activity of a neural crest-specific enhancer in the vicinity of its gene. Nucleic acids research, 40(1), 88–101. https://doi.org/10.1093/nar/gkr734

Wang, Z., Zang, C., Cui, K., Schones, D. E., Barski, A., Peng, W., & Zhao, K. (2009). Genome-wide mapping of HATs and HDACs reveals distinct functions in active and inactive genes. Cell, 138(5), 1019–1031. https://doi.org/10.1016/j.cell.2009.06.049

Wakatsuki, S., Yumoto, N., Komatsu, K., Araki, T., & Sehara-Fujisawa, A. (2009). Roles of meltrin-beta/ADAM19 in progression of Schwann cell differentiation and myelination during sciatic nerve regeneration. The Journal of biological chemistry, 284(5), 2957–2966. https://doi.org/10.1074/jbc.M803191200

Waxenbaum, J. A., Reddy, V., & Varacallo, M. (2023). Anatomy, Autonomic Nervous System. In StatPearls. StatPearls Publishing.

Weintraub, A. S., Li, C. H., Zamudio, A. V., Sigova, A. A., Hannett, N. M., Day, D. S., Abraham, B. J., Cohen, M. A., Nabet, B., Buckley, D. L., Guo, Y. E., Hnisz, D., Jaenisch, R., Bradner, J. E., Gray, N. S., & Young, R. A. (2017). YY1 Is a Structural Regulator of Enhancer-Promoter Loops. Cell, 171(7), 1573–1588.e28. https://doi.org/10.1016/j.cell.2017.11.008

Weider, M., Küspert, M., Bischof, M., Vogl, M. R., Hornig, J., Loy, K., Kosian, T., Müller, J., Hillgärtner, S., Tamm, E. R., Metzger, D., & Wegner, M. (2012). Chromatin-remodeling factor Brg1 is required for Schwann cell differentiation and myelination. Developmental cell, 23(1), 193–201. https://doi.org/10.1016/j.devcel.2012.05.017

Welling, D. B., Collier, K. A., Burns, S. S., Oblinger, J. L., Shu, E., Miles-Markley, B. A., Hofmeister, C. C., Makary, M. S., Slone, H. W., Blakeley, J. O., Mansouri, S. A., Neff, B. A., Jackler, R. K., Mortazavi, A., & Chang, L. S. (2021). Early phase clinical studies of AR-42, a histone deacetylase inhibitor, for neurofibromatosis type 2-associated vestibular schwannomas and meningiomas. *Laryngoscope investigative otolaryngology*, *6*(5), 1008–1019. https://doi.org/10.1002/lio2.643

Wilcox MB, Laranjeira SG, Eriksson TM, Jessen KR, Mirsky R, Quick TJ, Phillips JB. Characterising cellular and molecular features of human peripheral nerve degeneration. Acta Neuropathol Commun. 2020 Apr 17;8(1):51. doi: 10.1186/s40478-020-00921-w. PMID: 32303273; PMCID: PMC7164159.

Wolbert, J., Li, X., Heming, M., Mausberg, A. K., Akkermann, D., Frydrychowicz, C., Fledrich, R., Groeneweg, L., Schulz, C., Stettner, M., Alonso Gonzalez, N., Wiendl, H., Stassart, R., & Meyer Zu Hörste, G. (2020). Redefining the heterogeneity of peripheral nerve cells in health and

autoimmunity. Proceedings of the National Academy of Sciences of the United States of America, 117(17), 9466–9476. https://doi.org/10.1073/pnas.1912139117

Woldeyesus, M. T., Britsch, S., Riethmacher, D., Xu, L., Sonnenberg-Riethmacher, E., Abou-Rebyeh, F., Harvey, R., Caroni, P., & Birchmeier, C. (1999). Peripheral nervous system defects in erbB2 mutants following genetic rescue of heart development. Genes & development, 13(19), 2538–2548. https://doi.org/10.1101/gad.13.19.2538

Wolpowitz, D., Mason, T. B., Dietrich, P., Mendelsohn, M., Talmage, D. A., & Role, L. W. (2000). Cysteine-rich domain isoforms of the neuregulin-1 gene are required for maintenance of peripheral synapses. Neuron, 25(1), 79–91. https://doi.org/10.1016/s0896-6273(00)80873-9

Woodhoo, A., Alonso, M. B., Droggiti, A., Turmaine, M., D'Antonio, M., Parkinson, D. B., Wilton, D. K., Al-Shawi, R., Simons, P., Shen, J., Guillemot, F., Radtke, F., Meijer, D., Feltri, M. L., Wrabetz, L., Mirsky, R., & Jessen, K. R. (2009). Notch controls embryonic Schwann cell differentiation, postnatal myelination and adult plasticity. Nature neuroscience, 12(7), 839–847. https://doi.org/10.1038/nn.2323

Wicks, E. E., & Semenza, G. L. (2022). Hypoxia-inducible factors: cancer progression and clinical translation. The Journal of clinical investigation, 132(11), e159839. https://doi.org/10.1172/JCI159839

Wu, X., Briseño, C. G., Grajales-Reyes, G. E., Haldar, M., Iwata, A., Kretzer, N. M., Kc, W., Tussiwand, R., Higashi, Y., Murphy, T. L., & Murphy, K. M. (2016). Transcription factor Zeb2 regulates commitment to plasmacytoid dendritic cell and monocyte fate. Proceedings of the National Academy of Sciences of the United States of America, 113(51), 14775–14780. https://doi.org/10.1073/pnas.1611408114

Wu, Y., Meng, D., You, Y., Sun, R., Fu, M., Yan, Q., Zhang, S., Fang, Z., Bao, J., & Li, Y. (2021). Hypoxia Inducible Factor-1alpha (HIF-1A) plays different roles in Gallbladder Cancer and Normal Gallbladder Tissues. Journal of Cancer, 12(3), 827–839. https://doi.org/10.7150/jca.46749

Wu, K., Zhou, K., Wang, Y., Zhou, Y., Tian, N., Wu, Y., Chen, D., Zhang, D., Wang, X., Xu, H., & Zhang, X. (2016). Stabilization of HIF-1α by FG-4592 promotes functional recovery and neural protection in experimental spinal cord injury. *Brain research*, *1632*, 19–26. https://doi.org/10.1016/j.brainres.2015.12.017

Xu, L. G., Li, L. Y., & Shu, H. B. (2004). TRAF7 potentiates MEKK3-induced AP1 and CHOP activation and induces apoptosis. The Journal of biological chemistry, 279(17), 17278–17282. https://doi.org/10.1074/jbc.C400063200

Yamauchi, Y., Boukari, H., Banerjee, I., Sbalzarini, I. F., Horvath, P., & Helenius, A. (2011). Histone deacetylase 8 is required for centrosome cohesion and influenza A virus entry. PLoS pathogens, 7(10), e1002316. https://doi.org/10.1371/journal.ppat.1002316

Yi, S., Tang, X., Yu, J., Liu, J., Ding, F., & Gu, X. (2017). Microarray and qPCR Analyses of Wallerian Degeneration in Rat Sciatic Nerves. Frontiers in cellular neuroscience, 11, 22. https://doi.org/10.3389/fncel.2017.00022

Yi S, Wang QH, Zhao LL, Qin J, Wang YX, Yu B, Zhou SL. miR-30c promotes Schwann cell remyelination following peripheral nerve injury. Neural Regen Res. 2017 Oct;12(10):1708-1715. doi: 10.4103/1673-5374.217351. PMID: 29171437; PMCID: PMC5696853.

Yi, S., Yuan, Y., Chen, Q., Wang, X., Gong, L., Liu, J., Gu, X., & Li, S. (2016). Regulation of Schwann cell proliferation and migration by miR-1 targeting brain-derived neurotrophic factor after peripheral nerve injury. Scientific reports, 6, 29121. https://doi.org/10.1038/srep29121

Yu, F., White, S. B., Zhao, Q., & Lee, F. S. (2001). HIF-1alpha binding to VHL is regulated by stimulus-sensitive proline hydroxylation. Proceedings of the National Academy of Sciences of the United States of America, 98(17), 9630–9635. https://doi.org/10.1073/pnas.181341498

Yun, B., Anderegg, A., Menichella, D., Wrabetz, L., Feltri, M. L., & Awatramani, R. (2010). MicroRNA-deficient Schwann cells display congenital hypomyelination. The Journal of neuroscience : the official journal of the Society for Neuroscience, 30(22), 7722–7728. https://doi.org/10.1523/JNEUROSCI.0876-10.2010

Zeke, A., Misheva, M., Reményi, A., & Bogoyevitch, M. A. (2016). JNK Signaling: Regulation and Functions Based on Complex Protein-Protein Partnerships. Microbiology and molecular biology reviews : MMBR, 80(3), 793–835. https://doi.org/10.1128/MMBR.00043-14

Zhang, L., Cao, J., Dong, L., & Lin, H. (2020). TiPARP forms nuclear condensates to degrade HIF-1α and suppress tumorigenesis. Proceedings of the National Academy of Sciences of the United States of America, 117(24), 13447–13456. https://doi.org/10.1073/pnas.192181511

Zhang, Y., Strehin, I., Bedelbaeva, K., Gourevitch, D., Clark, L., Leferovich, J., Messersmith, P. B., & Heber-Katz, E. (2015). Drug-induced regeneration in adult mice. *Science translational medicine*, *7*(290), 290ra92. https://doi.org/10.1126/scitranslmed.3010228

Zhang B, Su W, Hu J, Xu J, Askar P, Bao S, Zhou S, Chen G, Gu Y. Transcriptome Analysis of Schwann Cells at Various Stages of Myelination Implicates Chromatin Regulator Sin3A in Control of Myelination Identity. Neurosci Bull. 2022 Jul;38(7):720-740. doi: 10.1007/s12264-022-00850-9. Epub 2022 Apr 10. PMID: 35397705; PMCID: PMC9276879.

Zhao, Y., Xing, C., Deng, Y., Ye, C., & Peng, H. (2023). HIF-1α signaling: Essential roles in tumorigenesis and implications in targeted therapies. *Genes & diseases*, *11*(1), 234–251. https://doi.org/10.1016/j.gendis.2023.02.039

Zorick, T. S., Syroid, D. E., Arroyo, E., Scherer, S. S., & Lemke, G. (1996). The Transcription Factors SCIP and Krox-20 Mark Distinct Stages and Cell Fates in Schwann Cell Differentiation. Molecular and cellular neurosciences, 8(2/3), 129–145. https://doi.org/10.1006/mcne.1996.0052

Zotti, T., Scudiero, I., Vito, P., & Stilo, R. (2017). The Emerging Role of TRAF7 in Tumor Development. Journal of cellular physiology, 232(6), 1233–1238. https://doi.org/10.1002/jcp.25676

8 APPENDIX

8.1 List of Abbreviations

α	Alpha
β	Beta
γ	Gamma
°C	Degree Celsius
∞	infinity symbol
µg	Microgram
µL	Microliter
µm	Micrometer
µM	Micromolar
ABC	Active-beta-catenin
ac	Acetyl group
ADAM17	Alpha-desintegrin and Metalloprotease 17
ADAM19	Alpha-desintegrin and Metalloprotease 19
ADP	Adenosine diphosphate
AGO1	Argonaute protein 1
AGO2	Argonaute protein 2
Akt	Murine thymoma viral oncogene homolog 1
AP-1	Activator protein 1
AP-2α	Activator protein 2 alpha
ApoD	Apolipoprotein D
APS	Ammonium persulfate
Arf	ADP-ribosylation factor
ATP	Adenosine triphosphate
ATF-2	Activating transcription factor 2
ATF-3	Activating transcription factor 3
BACE-1	Beta-secretase 1
BAF	Barrier-to-autointegrated factor
BDNF	Brain-derived neurotrophic factor
BFABP	Brain fatty acid-binding protein
BRG1	Brahma-related gene 1
Brn-2	POU domain, class3, transcription factor 2
BSA	Bovine serum albumine
bSC	Bridge Schwann cell
C	Cytoplasmic
cADPR	Cyclic ADP-ribose
cADPRP	2'-phospho-cyclic ADP-ribose
cAMP	Cyclic adenosine monophosphate
CBP	CREB binding protein

CCL2	C-C motif chemokine ligand 2
cDNA	Complementary DNA
c-Jun	c-Jun proto-oncogene
cKO	Conditionnal knock-out
CMT1A	Charcot-Marie-Tooth disease type 1A
CMT1B	Charcot-Marie-Tooth disease type 1B
CNS	Central Nervous System
Co	Contralateral nerve
Cr	Crushed nerve
CREB	cAMP-response element binding protein
CreERT2	Cre recombinase - estrogen receptor T2
CSF-1	Colony stimulating factor 1
Ctrl	Control
CUDC-907	Fimepinostat
Cx32	Connexin 32
DAPI	4’,6-diamidino-2-phenylindole
(d)dH2O	(double) distilled H2O
dbAMP	dibutyryl cyclic adenosin monophosphate
DDIT4	DNA damage inducible transcript 4
DER 736	Diglycidyl Ether of Poly (propylene glycol)
Dhh	Desert hedgehog
Dlg1	Discs large 1
DLK	Dual leucin zipper kinase
DM	Differentiation medium
DMEM	Dubelcco's Modified Eagle Medium
DMEM/F12	Dubelcco’s Modified Eagle Medium/Ham’s F12 medium
DMSO	Dimethylsulfoxide
DNA	Deoxyribonucleic acid
dNTPs	Deoxynucleotide triphosphates
DPCA	1,4-dihydrophenonthrolin-4-one-3-carboxylic acid
Dpl	Day post lesion
dpT	Day post Tamoxifen
DRG	Dorsal Root Ganglia
dSC	Distal stump Schwann cell
DTT	Dithiothreitol
E	Embyonic day
Edrnb	Endothelin receptor type B
EDTA	Disodium Ethylene Diamine Tetra-Acetate
EC	Endothelial cell
ECM	Extracellular matrix
eEF1A1	Eukaryotic translation elongation factor 1 alpha 1
Erg2-AS	Non-coding RNA antisense to the promoter of Egr2
EGTA	Ethylene-Glycol-Bis[β-Aminoether]N,N´N´,N-Tetra-Acetic Acid

EMT	Epithelial to mesenchymal transition
EphB2	Ephrin B2 receptor
ErbB3	Neuregulin receptor
ERL 4221	3,4-Epoxycyclohexanemethyl 3,4-epoxycyclohexanecarboxylate
ERK1/2	Extracellular signal-regulated kinases 1/2
EZH2	Enhancer of zeste homolog 2
Fabp7	Fatty acid binding protein 7
FACS	Fluorescence Activated Cell Sorting
FAK	Focal adehsion kiase
FBS	Foetal Bovine Serum
Fbxw7	F-box/WD repeat-containing protein 7
FG-4592	Roxadustat
FGF	Fibroblast growth factor
g	Gram
GAP43	Growth associated protein 43
GAPDH	Glyceraldehyde-3-Phosphate Dehydrogenase
GDNF	Glial cell line-derived neurotrophic factor
GFAP	Glial fibrillary acidic protein
GFP	Green fluorescent protein
GNATs	Gcn5-related acetyltransferases
Gpr126	G protein-coupled receptor 126
Gpr44	G protein-coupled receptor 44
GPRC	G-protein-coupled receptor
h	Hour
H3	Histone 3
H4	Histone 4
HAT	Histone acetyltransferase
HDAC1	Histone deacetylase 1
HDAC2	Histone deacetylase 2
HDAC3	Histone deacetylase 3
HDAC4	Histone deacetylase 4
HDAC5	Histone deacetylase 5
HDAC6	Histone deacetylase 6
HDAC7	Histone deacetylase 7
HDAC8	Histone deacetylase 8
HDAC9	Histone deacetylase 9
HDAC10	Histone deacetlylase 10
HDAC11	Histone deacetylase 11
HDM	Histone demethylase
HEK	Human Embryonic Kidney
Hes1	Transcriptional repressor Hairy Enhancer of Split 1
Hes5	Transcriptional repressor Hairy Enhancer of Split 5
hEST1B	Human ever-shorter telomeres 1B

Hey2	Hairy/enhancer-of-split related with YRPW motif protein 2
HIF1α	Hypoxia-inducible factor 1 alpha
HMG	High mobility group
Hsp70	Heat shock protein 70
Hsp90	Heat shock protein 90
Hypo.	Hypoxia
Id2	DNA binding protein inhibitor 2
Id4	DNA binding protein inhibitor 4
IGF	Insulin-like growth factor
IGFBP2	Insulin-like growth factor binding protein 2
IgG	Immunoglobulin G
IL-1α	Interleukin-1 alpha
IP	Immunoprecipitation
iSC	Immature Schwann cell
JIP3	JNK-interacting protein 3
Jmj	Jumonji C domain-containing protein
JMJD2C	Jumonji C domain-containing protein D2C
JMJD3	Jumonji C domain-containing protein D3
JNK	C-Jun N-terminal kinase
JunD	JunD proto-oncogene
K	Lysine
KAT	Histone lysine acetyltransferase
kDa	Kilodalton
KDM	Histone lysine demethylase
KDM3A	Histone demethylase 3A
kg	Kilogram
KMT	Lysin-specific histone methyltransferase
KO	Knock-out
Krox20/Erg2	Early Growth Response 2
L	Liter
L1	L1 adhesion molecule
LB	Luria-Bertani Broth
Let-7	Lethal-7
LIF	Leukemia inhibitory factor
Lin28B	Lin-28 homolog B
lncRNA	Long-noncoding RNA
M	Molar
MAG	Myelin-associated glycoprotein
MAPK	Mitogen-activated protein kinase
MBP	Myelin basic protein
MCP-1	Monocyte chemotactic protein 1
me	Methyl group
me1, me2, me3	Mono, di and trimethylation

MED12	Mediator complex subunit 12
MEK	Mitogen-activated protein kinase
MEKK	MEK Kinase
mg	Milligram
mm	Millimeter
mM	Millimolar
min	Minute
miRNA	Micro RNA
mL	Milliliter
Mpl	Month post lesion
mpT	Month post Tamoxifen
Mpz (P0)	Myelin Protin zero
MRL	Murphy Roths large
mRNA	Messanger RNA
MS	Mass spectrometry
mSC	Myelinating Schwann cell
MSE	Myelinating Schwann cell element
mTOR	Mammalian Target of rapamycin
mV	Millivolt
MYST	MOZ, Ybf2/Sas3, Sas2 and Tip-60)-related histone methylases
N	Nuclear
NAADP	Nicotinic acid adenine dinucleotide phosphate
NAB1/2	NGF1-A (Nerve growth factor-induced protein A) binding factor 1/2
NAD	Nicotinamide adenine dinucleotide
N-cad	N-cadherin
NCAM1	Neural cell adhesion molecule 1
NCOA1	Nuclear receptor coactivator 1
NcoR1	Nuclear receptor corepressor 1
NF2	Neurofribromatosis type 2
NFAT	Nuclear factor of activared T cells
NFATC3/4	Nuclear factor of activated T-cells, cytoplasmic 3/4
NFkB	Nuclear factor kappa-light-chain-enhancer of activated B cells
ng	Nanogram
NGF	Nerve growth factor
NLS	Nuclear localization signal
nM	Nanomolar
NMJ	Neuromuscular junction
NMN	Nicotinamide mononucleotide
NMNAT2	Nicotinamide mononucleotide adenylyltransferase 2
nmSC	Nonmyelinating SC
Norm.	Normoxia
Notch	Neurogenic locus notch homolog protein
NP-40	Nonidet P-40

ns	Non significant
NSA	Nonenyl succinic anhydride
NRG1	Neuregulin 1
NuRD	Nucleosome remodeling and deacetylase
O4	Lipid antigen
Oct6/POU3F1	Octamer-binding transcription factor 6
OE	Overexpression
O-GlcNAc	O-linked N-acetylglucosaminylation
OH-	Hydroxy group
OL	Oligodendrocyte
Olig1	Oligodendrocyte transcription factor 1
OPC	Oligodendrocyte progenitor cell
opti-MEM	optimal minimal essential medium
P	Post natal day
P0	Protein zero
p15Ink4b	Cyclin-dependent kinase 4 inhibitor B
p16Ink4a	Cyclin-dependent kinase inhibitor 2 A
p19Arf	Tumor suppressor ARF
p75NTR	p75 neurotrophin receptor
p75kip2	Cyclin-dependent kinase inhibitor p75
Pax3	Paired box gene 3
Pak1	Cdc42/Rac-activated kinase 1
PBS	Phosphate buffer saline
PCR	Polymerase chain reaction
PDGF	Platelet-derived growth factor
p-c-Jun	Phosphorylated c-Jun
pERK	Phosphorylated ERK
PFA	Paraformaldehyde
PGD2	Prostaglandin D2
PGP9.5	Protein gene product 9.5
PHD	Prolyl hydroxylase
PI3K	Phosphatidyinositol 3-kinase
PIGF	Placenta growth factor
PKCμ	Protein kinase Cμ
PLP	Proteolipid protein
PMP22	Peripheral myelin protein 22-kDa
PMSF	Phenylmethylsulfonyl fluoride
PNS	Peripheral nervous system
ppm	Parts per million
PRC2	Polycomb repressive complex 2
ProMy	Pro-myelinating
PrPc	Cellular prion protein
PRC2	Polycomb repressive complex 2

ProMy	Pro-myelinating
PrPc	Cellular prion protein
PTEN	Phosphatase and tensin homolog
qRT-PCR	Quantitative real-time polymerase chain reaction
R	Arginine
RAGs	Regeneration associated genes
rcf	Relative centrifugal force
RIPA	Radioimmunoprecipitation assay buffer
RNA	Ribonucleic acid
RNase H	Ribonuclease H
Rnasin	Ribonuclease inhibitor
rpm	Rotation per minute
RPMI	Roswell Park Memorial Insititute medium
rSC	Remak Schwann cell
RSC	Rat Schwann cell
RT	Room Temperature
RunX2	Runt-related transcription factor 2
RXRγ	Retinoid X receptor gamma
SARM1	Sterile alpha and toll/interleukin receptor (TIR) motif–containing protein 1
SC	Schwann cell
SC1	Schwann cell factor 1
SCE	Schwann cell specific enhancer
SCG10	Superior cervical ganglion-10 protein (Stathmin 2)
SCP	Schwann cell precursor
SDS	Sodium dodecyl sulfate
SDS-PAGE	Sodium dodecyl-sulfate polyacrylamide gel electrophoresis
sec	Second
sem	Standard error of the mean
Shh	Sonic hedgehog
shRNA	Short hairpin RNA
Sin3a	Suppressor interacting 3a
siRNA	Small interfering RNA
SIRT	Sirtuin
SMAD1	Small worm phenotyp mother against decapentaplegic 1
SMC3	Structural maintenance of chromosomes protein 3
SMOC2	SPARC-related modular calcium-binding protein 2
Sox1	SRY (sex determining region Y) box 1
Sox2	SRY (sex determining region Y) box 2
Sox10	SRY (sex determining region Y) box 10
SPARC	Secreted protein acidic and rich in cysteine
SRC	Steroid receptor coactivator
Srebp	Sterol regulatory element-binding protein
STAT3	Signal transducer and activator of transcription 3

STMN2	Stathmin-2
T3	Triiodothyronine
TAE	Tris-acetate-EDTA buffer
TAZ	Transcriptional co-activator with PDZ binding motif
TBS	Tris-buffered saline
TBST	Tris-buffered saline with 0.1% Tween® 20 detergent
TEAD1	TEA domain transcription factor 1
TEMED	N,N,N',N' -Tetramethylethylenediamine
TGFβ	Transforming growth factor beta
Thy1.1	Thymus cell antigen 1.1
TNFα	Tumor necrosis alpha
TR2	Testicular receptor 2
TRAF7	Tumor necrosis factor TNF receptor associated factor 7
Tris	Tris(hydroxymethyl)aminomethane
UTR	Untranslated region
VEGF	Vascular endothelial growth factor
VEGFA	Vascular endothelial growth factor A
VEGFR1	Vascular endothelial growth factor receptor 1
VHL	Von Hippel-Lindau tumor suppressor
WD	Trp-Asp (W-D) dipeptide
wpT	Week post Tamoxifen
YAP	Yes-associated protein
YY1	Ying and yang 1
Zeb2	Zinc finger E-box-binding homoebox 2

8.2 List of Figures

8.3 List of Tables

9 EIDESSTATTLICHE ERKLÄRUNG

Hiermit erkläre ich, Nadège Blandine Odile HERTZOG, geboren am 23.12.1994 in Porrentry (Schweiz), dass ich meine Dissertation selbstständig und nuch unter Verwendung der angegebenen Hilsmittel angefertig habe. Ich habe keinen anderen Promotionsversuch unternommen.

Ort, Datum Nadège HERTZOG

10 ACKNOWLEDGMENTS

11 CURRICULUM VITAE